TUM School of Engineering and Design
Technical University of Munich

Understanding the anaerobic oxidation of methane in the hyporheic zone of rivers and streams

Tamara Monika Michaelis

Vollständiger Abdruck der von der TUM School of Engineering and Design der Technischen Universität München zur Erlangung des akademischen Grades einer

Doktorin der Naturwissenschaften (Dr. rer. nat.)

genehmigten Dissertation.

Vorsitz: Prof. Dr. Thomas Baumann

Prüfende der Dissertation:
1. Prof. Dr. Florian Einsiedl
2. Prof. Dr. Jan Fleckenstein
3. apl. Prof. Dr. Philippe Schmitt-Kopplin

Die Dissertation wurde am 22.03.2024 bei der Technischen Universität München eingereicht und durch die TUM School of Engineering and Design am 14.08.2024 angenommen.

Abstract

The negative consequences of climate change, such as increased flooding and droughts, the melting of glaciers, and rising sea levels, are already being felt today, and the changes will intensify in the future, not least due to a possible positive climate feedback from natural greenhouse gas (GHG) emissions. However, global budgets of GHG emissions from natural ecosystems are highly uncertain and even less certain is how natural sources of GHGs will respond to climate change. Rivers are one of the most complex and heterogeneous aquatic ecosystems, and they contribute large amounts of the potent greenhouse gas methane (CH_4) to the atmosphere, most of which is microbially produced in the hyporheic zone (HZ) at the top of the riverbed. Many processes of the hyporheic CH_4 cycle, but first and foremost, the anaerobic oxidation of CH_4 to CO_2 (AOM) are poorly understood to date. The aim of this work was, therefore, to improve our understanding of the CH_4 cycle in the HZ as a basis of global GHG budgets and climate models.

The hyporheic CH_4 cycle involves three processes: (i) CH_4 production by anaerobic methanogens in deep anoxic zones; (ii) transport into the overlying water column by diffusion, via plant-mediated transport, and as ebullition, i.e. the spontaneous release of gas bubbles from the sediment; and (iii) CH_4 oxidation to CO_2, which can be coupled to the reduction of various electron acceptors. The data collected in this work contains information on all three parts of the methane cycle, but a particular focus was on further elucidating the anaerobic oxidation of CH_4 coupled to the reduction of nitrate (NO_3^-) or nitrite (NO_2^-). This microbially catalyzed reaction has the potential to reduce CH_4 emissions and simultaneously reduce NO_3^- or NO_2^- to elemental nitrogen and thus, eliminate nitrogen permanently from the aquatic environment.

This work relied on the collection of data at a single study site to gain transferable insights into the processes controlling the CH_4 cycle in the HZ. The site chosen was the river Moosach in southern Germany, near the town of Freising, a small, anthropogenically modified river with a high proportion of fine, organic-rich sediments and low hydrological variability. These conditions were favorable for CH_4 production, which made the HZ of river Moosach interesting for our investigations. The CH_4 cycle was studied by means of extensive field investigations, especially CH_4 concentration and carbon stable isotope measurements, the latter being highly suitable for tracing CH_4 production and consumption processes.

First, we compared CH_4 production and oxidation zones at five distributed sites in the studied river section by measuring high-resolution vertical concentration profiles of CH_4, potential electron acceptors, and other dissolved ions. We combined these measurements with 16S rRNA gene analyses at one of the sites and applied a one-dimensional diffusion-reaction model to explain the observed concentration gradients, particularly those of CH_4 and NO_3^-. The results showed substantial CH_4 production, mainly from CO_2 and hydrogen, and partly

from methanol, as suggested by the stable isotopic composition of CH_4 and the groups of methanogens abundant in the sediment. Only one of the five selected sites showed a clear isotopic enrichment in the upper part of the HZ, which is characteristic of microbial degradation. Here, CH_4 oxidation could have been coupled either to oxygen reduction or denitrification, because both aerobic and NO_3^-/NO_2^--reducing methanotrophs were present in the sediment. However, since the redox zones of oxygen reduction and denitrification were extremely close to each other, the electron acceptor for CH_4 oxidation could not be conclusively clarified with the chosen experimental setup. These results are summarized in the first scientific publication resulting from this work.

Subsequently, a monitoring station was installed at one location in the riverbed of river Moosach for time-resolved sampling of hyporheic pore water and to check whether NO_3^- and/or NO_2^- were electron acceptors for CH_4 oxidation. The station was designed for repeated sampling of pore water through microfilters and was additionally equipped with a custom-built fiber-optic sensor for dissolved oxygen profiling and automated temperature sensors for estimating vertical hyporheic exchange fluxes. Yet, as shown in a second publication, we realized that measurements of CH_4 concentrations and stable carbon isotopes of CH_4 were dependent on the pumping rate during pore-water extraction. This finding has far-reaching implications for many researchers who will work in the HZ in the future and who rely on pore-water extraction to measure dissolved gases. Nevertheless, the combined approach proved to be suitable for a time-resolved assessment of HZ geochemistry. The hyporheic hydrogeochemistry at river Moosach was found to be very stable over time, with strongly reducing redox conditions prevailing just below the sediment–water interface throughout the summer and fall seasons.

The monitoring station was also used to investigate the role of NO_3^- and NO_2^- as electron acceptors for CH_4 oxidation in the HZ in an in situ labeling experiment. In a first experiment of this kind, isotopically labeled CH_4 with and without the addition of NO_3^- was injected into the HZ through microfilters for two weeks each and during those periods, pore water was repeatedly sampled through adjacent filters. The results showed a very high denitrification potential, even if the labeled carbon of the injected CH_4 could not be detected in the CO_2 of the sampled pore water. Nevertheless, an improvement and extension of these experiments promises to yield more insights into the processes of the hyporheic CH_4 cycle in the future.

In order to estimate the magnitude of different transport processes, ebullition from the HZ was monitored for one year, and the gaseous CH_4 emissions were compared to diffusive CH_4 fluxes. Four gas traps were installed in a cross-section at a river bend so that the four sites represented different bed substrates between the fine-grained slip-off slope and the coarse-grained undercut slope. Ebullition exported up to 30 times more CH_4 from the HZ than diffusion. Volume fluxes of up to 1000 ml m^{-2} d^{-1} left the sediment as gas bubbles with CH_4 concentrations of up to 81 %. In this way, most of the CH_4 produced in the HZ escaped oxidation and was released directly into the atmosphere. Ebullition was most active in the central section of the stream. At one location, CH_4 continued to be emitted even in winter, a sign of methanogenesis at cold temperatures. This was discussed in a third publication.

Taken together, these results show high CH_4 production in the HZ of river Moosach. The highly depleted stable carbon isotope composition of CH_4 suggests a large contribution from hydrogenotrophic methanogenesis, but the abundance of certain microbial groups and high ebullition in winter at one site also indicate that methanol could be a substrate for CH_4 produc-

tion. CH_4 was also oxidized at the top of the HZ, as shown by a clear isotopic enrichment in several geochemical profiles. Possible electron acceptors in this redox reaction were oxygen and NO_3^- or NO_2^-. However, due to the steepness of the geochemical gradients, a quantitative separation of aerobic and anaerobic CH_4 oxidation was not possible.

Overall, oxidation could only slightly reduce CH_4 fluxes from the HZ. Although an isotopic enrichment was observed in some profiles, in most cases, CH_4 concentrations decreased towards the top of the HZ at a more or less constant stable isotope composition. Most of the CH_4 was transported into the atmosphere by ebullition and passed the oxidative layer too fast for a reaction. Factors favoring CH_4 emissions were higher temperatures, high organic carbon contents in the HZ, and a fine but permeable bed substrate that ensured anoxic conditions while allowing good exchange with the surface water. Anthropogenic changes to river ecosystems seem to enhance conditions that exacerbate CH_4 emissions, and the interlinked effects of climate change and further river engineering measures are likely to yield a positive feedback to global warming.

This work provided deep insights into the hyporheic CH_4 cycle through large amounts of high-resolution data but also opened new questions and hypotheses for the scientific community. Based on our experience, there could be several ways forward: The introduced monitoring station could be used not only for time-resolved observations in the HZ but also for in situ (isotope) tracer experiments. Such experiments could be extended to various other geochemical turnover processes or different bed substrates. The combination of these data with an integrated hydraulic and geochemical model could deepen our understanding of the CH_4 cycle in the HZ. Last but not least, the design and construction of automated gas traps for ebullition monitoring could significantly advance the quantification of total CH_4 emissions from rivers and streams.

Zusammenfassung

Die negativen Folgen des Klimawandels, wie vermehrte Überschwemmungen und Dürren, das Abschmelzen der Gletscher oder der Anstieg des Meeresspiegels, sind bereits heute spürbar. Diese Veränderungen werden sich in Zukunft noch verstärken, nicht zuletzt, weil Treibhausgasemissionen aus natürlichen Quellen durch die Erderwärmung erhöht werden könnten. Globale Bilanzen der Treibhausgasemissionen aus natürlichen Ökosystemen sind jedoch äußerst unsicher und Rückkopplungseffekte sind noch weniger gut verstanden. Flüsse sind eines der komplexesten und heterogensten aquatischen Ökosysteme und emittieren große Mengen des potenten Treibhausgases Methan (CH_4) in die Atmosphäre. In Flusssystemen entsteht CH_4 größtenteils in der hyporheischen Zone (HZ), die am oberen Rand des Flussbettes liegt und durch Interaktionen von Oberflächen- und Grundwasser geprägt ist. Viele Prozesse des hyporheischen Methankreislaufs, vor allem aber die anaerobe Oxidation von CH_4 zu CO_2 (AOM), sind bisher nur unzureichend verstanden. Ziel dieser Arbeit war es deshalb, als Basis für globale Treibhausgasbilanzierungen und Klima-Modelle ein verbessertes Verständnis des Methankreislaufs in der HZ zu erlangen.

Der hyporheische Methankreislauf schließt drei Prozesse ein: (i) die Methanproduktion durch anaerobe methanogene Archaeen in tiefen anoxischen Zonen; (ii) den Transport in die überliegende Wassersäule durch Diffusion, den Transport durch Pflanzen und die spontane Freisetzung von Gasblasen aus dem Sediment; und (iii) die Methanoxidation zu CO_2, die mit der Reduktion verschiedener Elektronenakzeptoren gekoppelt sein kann. Die im Rahmen dieser Arbeit erhobenen Daten decken alle drei Teilbereiche des Methankreislaufs ab, allerdings lag ein besonderer Fokus auf der weiteren Aufklärung der anaeroben Oxidation von CH_4 in Verbindung mit der Reduktion von Nitrat (NO_3^-) oder Nitrit (NO_2^-). Diese mikrobiell katalysierte Reaktion hat das Potential, Methanemissionen zu verringern und gleichzeitig NO_3^- bzw. NO_2^- zu elementarem Stickstoff zu reduzieren und damit Stickstoff dauerhaft aus der aquatischen Umwelt zu eliminieren.

Diese Arbeit stützt sich auf die Erfassung von Daten an einem einzigen Untersuchungsstandort, um übertragbare Erkenntnisse über die Prozesse des Methankreislaufs in der HZ zu gewinnen. Als Standort wurde die Moosach im Süden Deutschlands, nahe der Stadt Freising, gewählt, ein kleiner, anthropogen veränderter Fluss mit einem hohen Anteil an feinen, stark organischen Ablagerungen und einer geringen hydrologischen Variabilität. Diese Bedingungen waren günstig für die Methanproduktion und machten daher die HZ der Moosach für unsere Untersuchungen interessant. Der Methankreislauf wurde mit Hilfe einer Vielzahl an Feldmessungen, insbesondere Methankonzentrationsmessungen und Analyse der stabilen Kohlenstoffisotope des CH_4, untersucht, wobei sich letztere hervorragend dazu eigneten, Methanproduktions- und Abbauprozesse nachzuvollziehen.

Zunächst wurden hydrochemische Konzentrationsprofile von CH_4, potenziellen Elektronenakzeptoren, und weiteren gelösten Ionen im Sediment der HZ gemessen, um Zonen der Methanproduktion und -oxidation an verschiedenen Standorten im untersuchten Flussabschnitt zu vergleichen. Diese Messungen wurden zudem mit 16S rRNA-Genanalysen an einem der Standorte kombiniert. Ein eindimensionales Diffusions-Reaktions-Modell wurde verwendet, um die Interpretation der Konzentrationsverläufe insbesondere von CH_4 und NO_3^- zu stützen. Die Ergebnisse zeigten eine beträchtliche Methanproduktion, vornehmlich aus CO_2 und Wasserstoff und teilweise aus Methanol, wie die stabile Isotopenzusammensetzung von CH_4 und die Verteilung der CH_4 produzierenden Archaeen im Sediment nahelegen. Nur an einem der fünf ausgewählten Standorte zeigte sich eine deutliche Isotopenanreicherung im oberen Bereich der HZ, die für einen mikrobiellen Abbau charakteristisch ist. Die Methanoxidation könnte in diesem Fall entweder an Sauerstoffreduktion oder Denitrifikation gekoppelt sein, da im Sediment sowohl aerobe, als auch NO_3^-/NO_2^--reduzierende methanotrophe Mikroorganismen gefunden wurden. Da die Redoxzonen der Sauerstoffreduktion und der Denitrifikation aber extrem nahe beieinanderlagen, konnte der Elektronenakzeptor für die Methanoxidation mit dem gewählten experimentellen Aufbau nicht abschließend geklärt werden. Diese Ergebnisse sind in der ersten wissenschaftlichen Veröffentlichung, die aus dieser Arbeit hervorgegangen ist, zusammengefasst.

Für eine anschließende zeitaufgelöste Probenahme von Porenwasser aus der HZ an einem Standort der Moosach und zur Überprüfung, ob NO_3^- und/oder NO_2^- als Elektronenakzeptor für die Methanoxidation genutzt wird, wurde im Flussbett eine Messstation installiert. Die Station wurde für die wiederholte Entnahme von Porenwasserproben durch Mikrofilter entwickelt und zusätzlich mit einem speziell angefertigten faseroptischen Sensor für die Messung des gelösten Sauerstoffs sowie mit automatisierten Temperatursensoren für die Abschätzung der vertikalen hyporheischen Austauschströme ausgestattet. Wie in einer zweiten Publikation beschrieben, stellten wir jedoch fest, dass die Messungen der Methankonzentrationen und der stabilen Kohlenstoffisotope des CH_4 von der Pumprate während der Porenwasserextraktion abhängig waren. Diese Erkenntnis hat weitreichende Folgen für viele Forscher, die in der HZ zukünftig arbeiten werden und die sich bei der Messung gelöster Gase auf die Porenwasserextraktion verlassen. Trotzdem erwies sich der kombinierte Ansatz als geeignet für eine zeitaufgelöste Bewertung der biogeochemischen Prozesse in der HZ. Die hyporheische Hydrogeochemie an der Moosach erwies sich im Laufe der Zeit als sehr stabil, wobei während der gesamten Sommer- und Herbstsaison knapp unterhalb der Sediment-Wasser-Grenzschicht stark reduzierende Redoxbedingungen herrschten.

Die Messstation wurde zudem genutzt, um in einem in situ Markierungsversuch die Rolle von NO_3^- und NO_2^- als Elektronenakzeptoren für die Methanoxidation in der HZ zu untersuchen. In einem erstmalig so durchgeführten Experiment wurde isotopisch markiertes CH_4 mit und ohne Zugabe von NO_3^- über je zwei Wochen durch Mikrofilter in die HZ injiziert und das Porenwasser wiederholt durch benachbarte Filter beprobt. Die Ergebnisse zeigten ein sehr hohes Denitrifikationspotential, auch wenn der markierte Kohlenstoff des injizierten CH_4 im CO_2 des beprobten Porenwassers nicht nachgewiesen werden konnte. Nichtsdestotrotz verspricht eine Verbesserung und Erweiterung dieser Experimente in Zukunft mehr Einblicke in die Prozesse des hyporheischen Methankreislaufs in der HZ zu geben.

Um die Größenordnung verschiedener Transportprozesse abzuschätzen, wurde zudem ein Jahr lang aus der HZ aufsteigendes Gas beprobt und die gasförmigen Methanemissionen wurden mit den diffusiven Methanströmen verglichen. Dafür wurden vier Gasfallen in einem Querschnitt an einer Flussbiegung installiert, so dass die vier Standorte verschiedene Sohlsubstrate zwischen dem feinkörnigen Gleithang und dem grobkörnigen Prallhang repräsentierten. Durch aufsteigende Gasblasen wurde bis zu 30 mal mehr CH_4 aus der HZ exportiert als durch Diffusion, mit Volumenströmen von bis zu 1000 ml m^{-2} d^{-1} und Methankonzentrationen von bis zu 81 %. Auf diese Weise entging der größte Teil des in der HZ produzierten CH_4 der Oxidation und gelangte direkt in die Atmosphäre. Die Gasblasenemissionen waren im zentralen Abschnitt des Flusses am größten. An einer Stelle wurde auch im Winter weiterhin CH_4 emittiert, ein Zeichen für Methanogenese bei kalten Temperaturen. Dies wurde in einer dritten Publikation diskutiert.

Zusammengenommen zeigen diese Ergebnisse eine hohe Methanproduktion in der HZ der Moosach. Die stark abgereicherte stabile Kohlenstoff-Isotopenzusammensetzung des CH_4 deutet auf einen großen Beitrag der hydrogenotrophen Methanogenese hin, aber die Häufigkeit bestimmter mikrobieller Gruppen und hohe Gasemissionen im Winter an einem Standort legen auch nahe, dass Methanol ein Substrat für die Methanproduktion sein könnte. CH_4 wurde in der obersten Schicht der HZ oxidiert, wie eine deutliche Isotopenanreicherung in mehreren geochemischen Profilen zeigt. Mögliche Elektronenakzeptoren bei dieser Redoxreaktion waren Sauerstoff und NO_3^- oder NO_2^-. Aufgrund der Steilheit der geochemischen Gradienten war eine quantitative Trennung von aerober und anaerober Methanoxidation allerdings nicht möglich.

Insgesamt konnte die Oxidation die Methanemissionen aus der HZ nur geringfügig reduzieren. Eine Isotopenanreicherung wurde nur in einigen Profilen festgestellt, während in den meisten Profilen die Methankonzentrationen bei einer konstanten isotopischen Zusammensetzung zur Obergrenze der HZ hin abnahmen. Das meiste CH_4 wurde in Form von Gasblasen in die Atmosphäre transportiert und passierte die oxidative Schicht zu schnell für eine Reaktion. Faktoren, die die Methanemissionen begünstigten, waren erhöhte Temperaturen, stark organische Sedimente in der HZ und ein feines Sohlsubstrat, das bei anoxischen Verhältnissen dennoch durchlässig genug ist, um einen guten Austausch mit dem Oberflächenwasser zu ermöglichen. Anthropogene Veränderungen der Flussökosysteme scheinen hohe Methanemissionen zu begünstigen und die kumulierten Auswirkungen von Klimawandel und dem weiteren Ausbau flussbaulicher Maßnahmen werden wahrscheinlich zu einer positiven Rückkopplung der globalen Erwärmung führen.

Diese Arbeit ermöglichte vertiefte Einblicke in den hyporheischen Methankreislauf durch große Mengen hochauflösender Daten, eröffnete aber auch neue Fragestellungen und Hypothesen für die wissenschaftliche Gemeinschaft. Die hier vorgestellte Messstation kann nicht nur für zeitaufgelöste Beobachtungen in der HZ, sondern auch für in situ (Isotopen)-Tracer Experimente genutzt werden. Solche Experimente könnten auf verschiedene geochemische Umsatzprozesse oder unterschiedliche Sohlsubstrate ausgeweitet werden. Die Kombination dieser Daten mit einem integrierten hydraulischen und geochemischen Modell könnte unser Verständnis des Methankreislaufs in der HZ vertiefen. Nicht zuletzt könnten die Entwicklung und der Bau automatisierter Gasfallen zur Überwachung aufsteigender Methanblasen die Quantifizierung der gesamten Methanemissionen aus Flüssen und Bächen erheblich voranbringen.

Publications

Publication I (Research Article): Chapter 5

Michaelis, T., Wunderlich, A., Coskun, Ö. K., Orsi, W., Baumann, T., & Einsiedl, F. (2022). High-resolution vertical biogeochemical profiles in the hyporheic zone reveal insights into microbial methane cycling. *Biogeosciences*, *19*(18), 4551–4569. https://doi.org/10.5194/bg-19-4551-2022

Author contributions: TM, AW and FE conceptualized the project. TM and AW developed the methodology and performed fieldwork. ÖC and WO contributed the microbiological investigations. TM was responsible for visualization and original draft preparation. Funding acquisition and supervision were performed by FE and TB. TM, AW, WO, TB and FE all participated in writing, reviewing, and editing the paper.

Publication II (Technical Note): Chapter 6

Michaelis, T., Wunderlich, A., Baumann, T., Geist, J., & Einsiedl, F. (2023). Technical note: Testing the effect of different pumping rates on pore-water sampling for ions, stable isotopes, and gas concentrations in the hyporheic zone. *Hydrology and Earth System Sciences*, *27*(20), 3769–3782. https://doi.org/10.5194/hess-27-3769-2023

Author contributions: TM, AW, TB and FE conceptualized the project. TM and AW developed the methodology. TM was responsible for fieldwork, data acquisition and curation, formal analysis, visualization, and original draft preparation. JG and his team supported fieldwork and provided resources. FE and TB acquired funding and supervised the project. TM, AW, TB, JG, and FE all contributed to writing, reviewing, and editing the paper.

Publication III (Research Article): Chapter 7

Michaelis, T., Kaplar, F., Baumann, T., Wunderlich, A., & Einsiedl, F. (2024). High methane ebullition throughout one year in a regulated central European stream. *Scientific Reports*, *14*(1), 5359. https://doi.org/10.1038/s41598-024-54760-z

Author contributions: TM, AW, TB and FE conceptualized the project. TM, FK, and TB developed the methodology. TM and FK were responsible for field work, data acquisition and curation. TM performed formal analysis, visualization, and original draft preparation. FE and TB acquired funding and supervised the project. TM, FK, AW, TB, and FE all contributed in writing, reviewing, and editing the manuscript.

Acknowledgements

This thesis would not have been possible without the ideas, support, and effort of my supervisors, colleagues, friends, and family. First and foremost, I would like to thank my supervisor Prof. Dr. Florian Einsiedl for the opportunity to conduct this research and for his guidance in all phases of my work. I highly appreciate how much time he devoted to my supervision and how deeply he was involved in the project. I also want to express my gratitude to Prof. Dr. Thomas Baumann, who was a second supervisor to me and helped me a lot with many practical aspects of my work, especially in methods development, laboratory analytics, and data analysis.

Furthermore, I would like to thank all the people I have had the pleasure of working with. The open discussions with my co-authors and senior colleagues Dr. Anja Wunderlich, Prof. Dr. William Orsi, and Prof. Dr. Jürgen Geist, who was also my mentor, gave most valuable inputs to my work, not only for the joint publications. Special thanks also goes to the team of Prof. Geist at the Chair of Systems Biology, above all Nico Geveke, who always helped out during my field work in Freising. Many thanks go to my fellow PhD students at the Chair of Hydrogeology. It was so much fun to spend time with you all, not just at work, and I am very grateful for the mutual support we gave each other. Especially Dr. Alejandra Peña Sanchez, Dr. Manuel Gossler, Fabian Böttcher, Felix Schölderle, Theis Winter, and Lea Augustin have contributed a great deal to this work. Many thanks also go to Susanne Thiemann und Jaroslava Obel, who have relieved me of a lot of laboratory work. And last but not least, I want to thank my students Theresa Mond, Felicitas Kaplar, Tobias Lanzl, and Katharina Philipp, all of which contributed data to my research, for their dedicated work during their master and bachelor theses.

I also want to acknowledge the support of my family, who did not only cushion my highs and lows but also gave me a lot of professional support. Particularly my dad contributed to this thesis because he read, reviewed, and discussed everything I wrote during the last three and a half years. I consider myself very lucky to have had this special support from home. My partner Carl May was another strong pillar of support during this time, who was never too tired to discuss the next steps of my work or listen to a presentation I had to practice.

Contents

List of Figures

List of Tables

List of abbreviations

ADCP Acoustic Doppler current profiler

ANME Anaerobic methane oxidizing archaea

ANOVA Analysis of variance

AOM Anaerobic oxidation of methane

BC Boundary condition

CRDS Cavity ring-down spectroscopy

DHR Dynamic harmonic regression

DFT Discrete Fourier transform

DO Dissolved oxygen

DOC Dissolved organic carbon

DZ Denitrification zone

ERF Effective radiative forcing

EPA Environmental protection agency

FID Flame ionization detector

GC Gas chromatograph

gDW Gram dry weight

GHG Greenhouse gas

HZ Hyporheic zone

IC Ion chromatograph

IPCC Intergovernmental Panel on Climate Change

LMM Linear mixed-effects modeling

LOI Loss on ignition

M-DAMO Anaerobic oxidation of methane coupled to metal reduction

MMO Methane monooxygenase

MOZ Methane oxidation zone

MS Mass spectrometer

n-damo, N-DAMO Anaerobic oxidation of methane coupled to nitrate or nitrite reduction

OA-ICOS Off-axis integrated cavity output laser spectroscopy

OC Organic carbon

ORZ Oxygen reduction zone

OTU Operational taxonomic unit

PCR Polymerase chain reaction

Peeper Pore water equilibrium dialysis sampler, in situ equilibrium dialysis sampler

POC Particulate organic carbon

POF Polymeric optical fiber

PTFE Polytetrafluoroethylene

qPCR Quantitative PCR

rRNA Ribosomal RNA

S-DAMO Anaerobic oxidation of methane coupled to sulfate reduction

SRB Sulfate reducing bacteria

SRZ Sulfate reduction zone

SSD, SSE Sum of squared deviations

SSIM Small sample introduction module (for CRDS)

TOC Total organic carbon

UC Unobserved component model

V-SMOW Vienna Standard Mean Ocean Water

V-PDB, VPDB Vienna Pee Dee Belemnite

WFD European Water Framework Directive

1 General introduction

In a reality of globally rising temperatures, rapidly disappearing ice shields, rising ocean levels, and an increased number of extreme events and associated damage, the climate crisis is arguably the biggest challenge of modern times (Ripple et al., 2019). Global warming is driven by elevated atmospheric concentrations of greenhouse gases (GHG), primarily carbon dioxide (CO_2), methane (CH_4), and nitrous oxide (N_2O), which together account for 80 % of total radiative forcing (IPCC, 2021). CH_4 is known to be the second most important GHG and although it is present in the atmosphere in a lower quantity than CO_2, its radiative forcing is 28 times higher considering a time horizon of 100 years (IPCC, 2021). It was also predicted that atmospheric CH_4 concentrations could rise more drastically than CO_2 concentrations under a warming climate, increasing the relative contribution of CH_4 compared to CO_2 to global warming (Yvon-Durocher et al., 2014; Zhu et al., 2020). The rise of atmospheric CH_4 concentrations has accelerated in recent years, which can partly be attributed to an increase in emissions from natural ecosystems (Nisbet et al., 2019; Peng et al., 2022). Freshwaters are the largest natural source of atmospheric CH_4, among which rivers are a significant contributor (IPCC, 2021; Saunois et al., 2020). Rivers, being highly heterogeneous and dynamic, pose a greater challenge in comprehension compared to other freshwater systems, and they account for much of the uncertainty in global CH_4 budgets (Stanley et al., 2016).

At the same time, nutrient cycles have been pushed out of balance through the extensive use of fertilizers and modifications to agricultural systems (Vitousek et al., 2009). Especially the nitrogen cycle has been radically modified, with anthropogenic activities being responsible for half of the global nitrogen fixation (Fowler et al., 2013; Galloway et al., 2008). Effects of surplus nitrogen on aquatic ecosystems are acidification and eutrophication, both associated with a critical loss in biodiversity (Sutton et al., 2011). Rivers are attributed a great denitrification potential: Seitzinger et al. (2006) calculated that $\sim$ 35 Tg N per year can be denitrified in rivers, accounting for the loss of 13 % of total terrestrial nitrogen sources.

Both riverine CH_4 production and denitrification are concentrated in the hyporheic zone (HZ), the realm between surface and groundwater where stream water enters the river bed and a high microbial activity catalyzes diverse geochemical turnover processes. Here, CH_4 is not only microbially produced but also partly consumed. Some sources claim that up to 90 % of CH_4 produced in freshwater environments can be oxidized before escaping to the atmosphere (Bastviken et al., 2008). CH_4 oxidation can be coupled to several reduction reactions, including oxygen (O_2), nitrate (NO_3^-), nitrite (NO_2^-), sulfate (SO_4^{2-}), iron (Fe), or manganese (Mn) reduction (Deutzmann, 2020; He et al., 2018). NO_3^- and NO_2^--dependent anaerobic oxidation of CH_4 (n-damo) has the potential to reduce CH_4 emissions and eliminate surplus nitrogen from streams at the same time.

Knowledge on the role of the n-damo process in the HZ is still limited and its relevance for the global CH_4 and nitrogen budget is far from clear. In addition, it has yet to be shown whether the microorganisms responsible for carbon and nitrogen cycling contribute to a positive climate feedback or play a role in mitigating human impacts on ecosystem degradation and GHG emissions (Cavicchioli et al., 2019; Galloway et al., 2008). This thesis targets this research gap with a large number of in situ measurements from a small stream in southern Germany. The data provide new insights into CH_4 cycling in river beds and help to better assess the importance of the n-damo process in the HZ.

2 Background

2.1 Global methane sources and sinks

With an effective radiative forcing (ERF) of 0.54 (0.43-0.65) W m^{-2}, CH_4 contributes approximately 14 % of total radiative forcing (all GHGs and ozone) according to the Sixths Assessment report of the Intergovernmental Panel on Climate Change (IPCC, 2021). Atmospheric CH_4 concentrations rise annually by 7 ± 3 ppb (2008-2017) with an acceleration in recent years, because sinks cannot balance global emissions (IPCC, 2021; Nisbet et al., 2019). Sinks are mainly chemical reactions in the atmosphere, accounting for 90 % to 99 % of all CH_4 losses, and microbially mediated oxidation in soils and sediments. The rise in atmospheric CH_4 concentrations was with 15.1 ± 0.4 ppb exceptionally high in 2020 despite lower anthropogenic emissions during the Covid-19 pandemic (Peng et al., 2022). This renewed growth could partly be attributed to a lower hydroxyl loss and partly to higher natural emissions, especially from wetlands (Peng et al., 2022). About half of the global CH_4 emissions are anthropogenic, the rest escapes from natural ecosystems (Fig. 2.1). The magnitude of these natural emissions, and even more so their future development, are much more uncertain than for anthropogenic sources (Saunois et al., 2020).

Inland freshwaters including lakes, ponds, reservoirs, streams, and rivers together are the largest source of atmospheric CH_4, greater still than even wetlands, and emit 20 to 30 times more than oceans (considering biogenic emissions) despite their comparably small surface area (Fig. 2.1). Rivers contribute 13 % to 23 % of these freshwater emissions. In a meta study on 358 globally distributed sites, Stanley et al. (2016) deduced that rivers and streams emit 27 Tg CH_4 yr^{-1}. A recent global bottom-up CH_4 budget even estimated 31 Tg CH_4 yr^{-1} at total inland water emissions of 398 ± 79.4 Tg CH_4 yr^{-1}, which is significantly higher compared to the IPCC (2021) estimate (117-212 Tg CH_4 yr^{-1}). CH_4 emission estimates from individual processes (bottom-up) tend to be higher than fluxes calculated from atmospheric measurements (top-down) (Kirschke et al., 2013; Nisbet et al., 2014). Heterogeneity at fine spatial scales and the dynamic character of river ecosystems make representative flux measurements, extrapolation, and bottom-up estimations of total CH_4 emissions from streams extremely difficult (Dean et al., 2018; Stanley et al., 2016).

A powerful method that can support a better distinction between different sources of atmospheric CH_4 is the measurement of the stable carbon isotope composition, a measure for the ratio of ^{13}C to ^{12}C in CH_4, usually expressed in the δ notation relative to the Vienna Pee Dee Belemnite (V-PDB) standard (Sec. 4.3, Eq. 4.1) (Brownlow et al., 2017; Schaefer et al., 2016). Relative contributions of different sources can be separated due to their distinct isotopic signatures in $\delta^{13}C$ of CH_4 (biogenic $\sim$-60 ‰, thermogenic $\sim$-37 ‰, pyrogenic $\sim$-22 ‰) (Schaefer

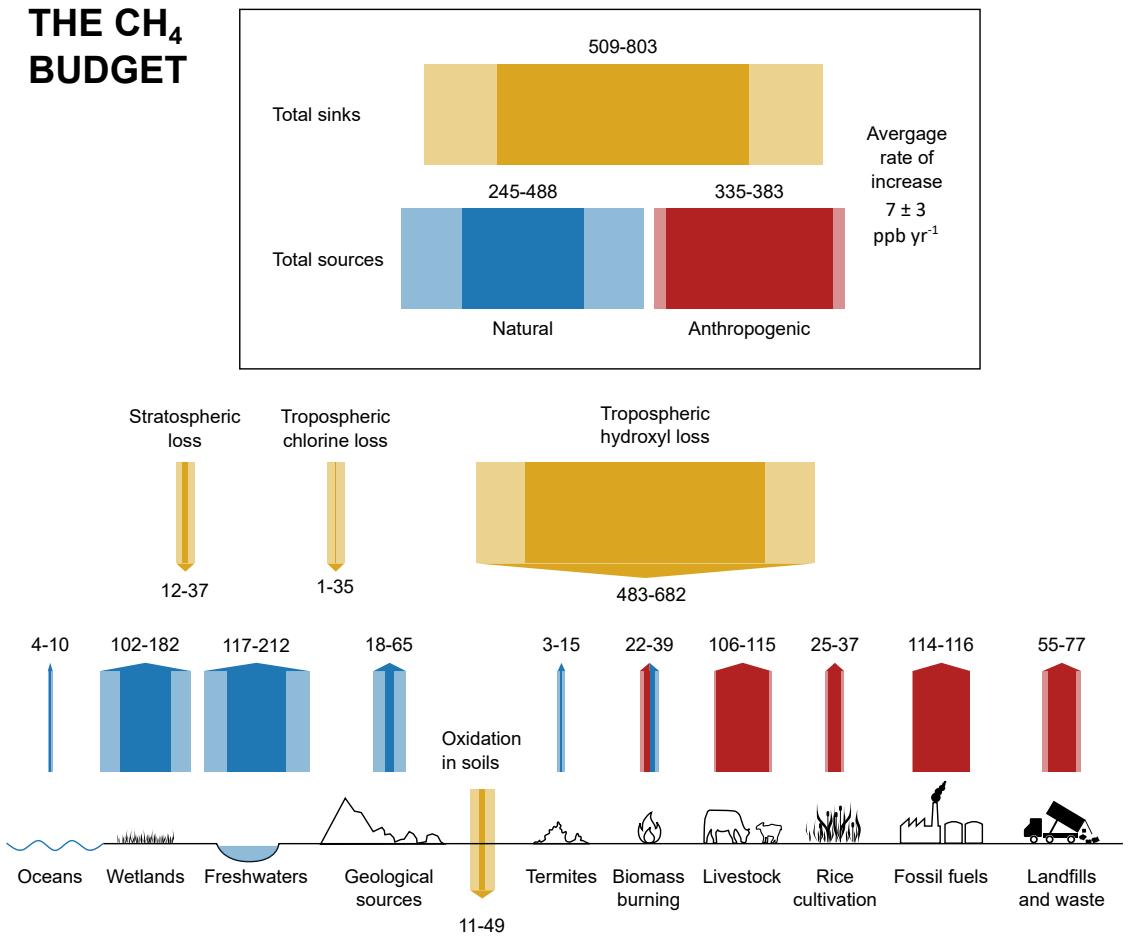

Figure 2.1: **The global CH_4 budget.** Data refer to Mio tonnes of CH_4 per year (Tg CH_4 yr^{-1}) estimated with bottom-up approaches for the time period 2008-2017. Ranges indicate min-max after outlier removal. Adapted from IPCC (2021).

et al., 2016). Recently, an isotopic shift towards lighter $\delta^{13}C$ of atmospheric CH_4 has been observed that might be associated with increased biogenic emissions (Nisbet et al., 2019; Schaefer et al., 2016).

Overall, microbial metabolism is the largest producer of atmospheric CH_4 (Conrad, 2009; Dean et al., 2018) and thus, stimulated microbial activity at higher future temperatures could increase CH_4 production and the relative contribution of CH_4 compared to CO_2 to global warming (Yvon-Durocher et al., 2014). While an increase of CH_4 emissions from wetlands is considered very likely, predictions are contradictory and highly uncertain for soil and aquatic ecosystems (Bodelier & Steenbergh, 2014). Increased microbial activity not only has the potential to fuel CH_4 production, but also to degrade CH_4 at a faster rate (Bastviken et al., 2008; Conrad, 2009; Dean et al., 2018). Oxidation in soils is estimated to consume 11-49 Tg CH_4 yr^{-1}, about 1 % to 10 % of all CH_4 sinks, and oxidation in sediments is said to significantly reduce CH_4 emissions from freshwater ecosystems (Bastviken et al., 2008; Reeburgh, 2007). The need for quantifying whether CH_4 sinks can balance sources under future climate change scenarios has recently been stressed (Dean et al., 2018).

2.2 Pathways of methane production and oxidation in freshwater ecosystems

In light-deprived environments like anoxic sediments, strictly anaerobic methanogens produce microbial CH_4 in the absence of O_2, NO_3^-, and SO_4^{2-} (Deppenmeier, 2002; Lyu et al., 2018). Several studies suggest that methanogenesis is also possible in oxic environments such as the epilimnion of lakes (Bogard et al., 2014; DelSontro et al., 2018; Grossart et al., 2011), but there is a controversy about the relevance of this process (Günthel et al., 2019; Peeters & Hofmann, 2021). All known methanogens are archaea belonging to the Euryarchaeota, more specifically the five taxonomic classes Methanopyri, Methanococci, Methanobacteria, Methanomicrobia, and Thermoplasmata (Offre et al., 2013). Recently discovered novel archaeal lineages related to all types of methanogens have revealed the large extent of diversity of CH_4 producing archaea (Borrel et al., 2014; Lyu et al., 2018). For example, the relatively new lineage Methanomassiliicoccales, phylogenetically related to the Thermoplasmatales, has become known as the seventh order of methanogens (Borrel et al., 2014; Dridi et al., 2012; Paul et al., 2012). Although a number of different methanogenic pathways exist (Deppenmeier, 2002; Offre et al., 2013), only two of them dominate CH_4 emissions from natural environments: Hydrogenotrophic methanogenesis (Eq. 2.1) is estimated to be responsible for around one-third of global CH_4 production and acetoclastic methanogenesis (Eq. 2.2) for two-thirds (Ferry, 2010; Lyu et al., 2018).

$$4H_2 + CO_2 \rightarrow CH_4 + 2H_2O \quad (\Delta G_0' = -138.8 kJ mol^{-1} CH_4) \tag{2.1}$$

$$CH_3COOH \rightarrow CH_4 + CO_2 \quad (\Delta G_0' = -27.6 kJ mol^{-1} CH_4) \tag{2.2}$$

When CH_4 diffuses upwards from deep anoxic sediments, it can be oxidized to CO_2 before it reaches the atmosphere. CH_4 oxidation can occur aerobically or anaerobically, depending

on the abundance and type of methanotrophs, microorganisms capable of catalyzing the respective CH_4 oxidation reactions, and on the availability of suitable electron acceptors. Aerobic CH_4 oxidation (Eq. 2.3) is an exergonic reaction used by microorganisms for energy gain (Plante et al., 2015) and was postulated to offset up to 90 % of CH_4 produced in freshwater environments (Bastviken et al., 2008). The most common CH_4-oxidizing organisms are aerobic methanotrophic bacteria (Nazaries et al., 2013) which are characterized by the use of methane monooxygenase (MMO) enzymes in the first step of their metabolic pathway, the oxidation of CH_4 to methanol (Hakemian & Rosenzweig, 2007; Hanson & Hanson, 1996; Trotsenko & Murrell, 2008). MMO has been found in members of the phylum Proteobacteria, specifically the classes Alphaproteobacteria and Gammaproteobacteria, and more recently in Verrucomicrobia (Dedysh & Knief, 2018; Op den Camp et al., 2009).

$$CH_4 + 2O_2 \rightarrow CO_2 + 2H_2O \quad (\Delta G_0^{'} = -871 kJmol^{-1} CH_4) \tag{2.3}$$

Genes from bacteria of the genus *Candidatus* "Methylomirabilis", belonging to the NC10 phylum, also encode the aerobic CH_4 oxidation pathway, although they are anaerobic methanotrophs with low O_2 tolerance (Eq. 2.4) (Ettwig et al., 2010; Graf et al., 2018; He et al., 2016; Versantvoort et al., 2018). Ettwig et al. (2010) suggested an intra-aerobic pathway in which two nitric oxide molecules (NO) react to dinitrogen (N_2) and O_2 gas. In addition to NC10 bacteria, several other microorganisms have been found to be capable of coupling CH_4 oxidation to denitrification: Archaea belonging to the ANME-2d clade, such as *Candidatus* "Methanoperedens nitroreducens", link NO_3^- reduction to CH_4 oxidation via a pathway commonly known as reverse methanogenesis (Eq. 2.5) (Arshad et al., 2015; Haroon et al., 2013). Oswald et al. (2017) found indications that *Crenothrix*, generally known as an aerobic methanotrophic bacterium, is a facultative anaerobe using NO_3^- as electron acceptor in O_2 depleted environments. Similarly, the gammaproteobacterial methanotroph Methylomonas denitrificans has the ability to reduce NO_3^- to N_2O under O_2 stress (Kits et al., 2015). Also a specific *Methylobacter* species was found to act as faculatative anaerobic methanotroph, that was three times more active under anoxic compared to oxic conditions and could use NO_2^- as electron acceptor (van Grinsven et al., 2020). CH_4 oxidation coupled to denitrification (n-damo) is common in freshwater environments and signs for this process were discovered in lakes (Deutzmann et al., 2014; Einsiedl et al., 2020; Graf et al., 2018; Norði & Thamdrup, 2014; Oswald et al., 2017; Peña Sanchez et al., 2022a), reservoirs (Naqvi et al., 2018; Shen et al., 2020), rivers (Shen et al., 2019a, 2019b), and wetlands (Hu et al., 2014; Shen et al., 2017; Zhang et al., 2018; Zhu et al., 2015).

$$3CH_4 + 8NO_2^- + 8H^+ \rightarrow 3CO_2 + 4N_2 + 10H_2O \quad (\Delta G_0^{'} = -928 kJmol^{-1} CH_4) \tag{2.4}$$

$$CH_4 + 4NO_3^- \rightarrow CO_2 + 4NO_2^- + 2H_2O \quad (\Delta G_0^{'} = -503 kJmol^{-1} CH_4) \tag{2.5}$$

Anaerobic oxidation of CH_4 (AOM) can not only be coupled to denitrification, but also to the reduction of ferric iron (Fe(III)) (Eq. 2.7) and manganese (Mn) (Eq. 2.6), either using soluble Fe^{3+} and Mn^{4+} or metal-oxides (He et al., 2018). The ecological niche for metal-AOM in freshwater ecosystems is highly complex and differs significantly from marine environments

(He et al., 2018). In freshwater environments, metal-dependent AOM has been found in the water column of a ferruginous lake (Crowe et al., 2011), a crude-oil contaminated aquifer (Amos et al., 2012), and in lake sediments characterized by the burial of large quantities of metal-oxides (Norði et al., 2013; Torres et al., 2014) or deep below the methanogenic zone (Sivan et al., 2011). Due to the low bioavailability of metal substrates, the contribution to CH_4 removal from freshwater ecosystems is considered low (Egger et al., 2015; Sivan et al., 2011). Compared to aerobic methanotrophy and n-damo, much less is known about the organisms catalyzing metal-dependent AOM, but several independent studies have suggested the involvement of ANME-2 (Ettwig et al., 2016; Fu et al., 2016; Scheller et al., 2016). Cai et al. (2018) reported the enrichment of the methanotrophic archaeon *Candidatus* "Methanoperedens ferrireducens" (M. ferrireducens) which couples CH_4 oxidation to Fe(III) reduction.

$$\mathrm{CH_4 + 4MnO_2 + 8H^+ \rightarrow CO_2 + 4Mn^{2+} + 6H_2O \quad (\Delta G_0^{'} = -494 kJmol^{-1} CH_4)} \tag{2.6}$$

$$\mathrm{CH_4 + 8Fe(OH)_3 + 16H^+ \rightarrow CO_2 + 8Fe^{2+} + 22H_2O \quad (\Delta G_0^{'} = -81.6 kJmol^{-1} CH_4)} \tag{2.7}$$

SO_4^{2-}-dependent AOM (Eq. 2.8) was first discovered in marine environments (Barnes & Goldberg, 1976; Reeburgh, 1976) and was long thought to be restricted to these due to significantly lower SO_4^{2-} concentrations in freshwater (10-500 µmol L^{-1}) compared to seawater (28 mmol L^{-1}) (Holmer & Storkholm, 2001). But in the last two decades evidence has accumulated that SO_4^{2-}-dependent AOM also occurs in freshwater habitats (Eller et al., 2005; Ng et al., 2020; Norði et al., 2013; Schubert et al., 2011; Segarra et al., 2015; Timmers et al., 2016; van Grinsven et al., 2020). Some of these studies suggest coupling of this process with a cryptic sulfur cycle, that may also involve intermediate-valence sulfur forms and abiotic iron cycling (Ng et al., 2020). SO_4^{2-}-dependent AOM can be catalyzed syntrophically by consortia of methanotrophic ANME archaea (ANME 1, ANME 2a-2c and ANME-3) surrounded by SO_4^{2-} reducing bacteria (SRB) (Boetius et al., 2000; Cui et al., 2015; Scheller et al., 2020). In addition, results of van Grinsven et al. (2020) showed that CH_4 oxidation by *Methylobacter* species was stimulated by SO_4^{2-} addition.

$$\mathrm{CH_4 + SO_4^{2-} + 2H^+ \rightarrow CO_2 + H_2S + 2H_2O \quad (\Delta G_0^{'} = -21 kJmol^{-1} CH_4)} \tag{2.8}$$

The CH_4 cycle in freshwater environments is a rapidly evolving field of research, and recent discoveries have greatly expanded the known variety of CH_4 oxidation pathways. The amount of CH_4 that can be oxidized to CO_2 before reaching the atmosphere matters from a climatological perspective and it is, therefore, necessary to understand and quantify all involved turnover processes under in situ conditions to better constrain how large a CH_4 sink each of the oxidation reactions can be.

2.3 The hyporheic zone and its ecohydrological relevance

In rivers, CH_4 production is concentrated in anoxic sediments of the HZ (Trimmer et al., 2012), the saturated layer of the river bed where stream water enters through hyporheic exchange

flows and a spatially heterogeneous, temporarily dynamic zone known for high biogeochemical activity (Findlay, 1995; Winter et al., 1998). Hyporheic exchange fluxes are the basis of physico-chemical transport processes in the HZ, and control spatio-temporal patterns of dissolved O_2, carbon, and nutrients (Covino, 2017; Krause et al., 2011). Along the flow path of infiltrating surface water, O_2 is consumed first before other terminal electron acceptors become dominant for respiration (Capone & Kiene, 1988; Hancock et al., 2005). In general, O_2 consumption is followed consecutively by zones of denitrification, Mn-, Fe-, and SO_4^{2-} reduction, but overlaps in this redox zonation are common in natural environments (Canfield & Thamdrup, 2009). Significant small-scale heterogeneity allows for the co-occurrence of diverse processes in a multitude of flow paths with different lengths, directions, and velocitiese (Boulton et al., 1998; Sophocleous, 2002). Responsible for the large heterogeneities are fine gradients in hydraulic conductivity and river bed morphology that determine water residence times and contact times between biofilms and carbon or nutrients (Boulton et al., 1998; Findlay, 1995; Sophocleous, 2002).

Carbon is supplied to the HZ by burial of particulate organic matter (POC) after disturbances or with the intrusion of streamwater (Findlay, 1995). Through different pathways of respiration, organic matter is in large parts anaerobically decomposed: Polymers are first depolymerized to monomers and then further degraded by fermentation to simple compounds such as acetate, methylamines, CO_2, and hydrogen (H_2) (Capone & Kiene, 1988; Ferry, 2010). In freshwater systems, three microbial groups degrade organic matter anaerobically: the fermentative group capable of digesting complex molecules, the acetogenic group that further breaks down simpler organic compounds, and methanogens that use mainly acetate, formate, H_2 and CO_2 as substrates (Ferry, 2010; Nazaries et al., 2013).

Theoretically, the HZ can serve as a nitrogen source or sink, depending on biological demand, substrate availability, the O_2 status, and water residence times (Storey et al., 2004; Zarnetske et al., 2011). In reality, surplus nitrogen input from agricultural fertilizers into freshwater systems has become a problem with severe ecological consequences for many stream ecosystems (Sutton et al., 2011). Thus, nitrogen attenuation in the HZ provides an ecosystem service that is more and more relevant for preventing eutrophication of downstream environments. Nitrogen loads are attenuated in the HZ by transformation of reactive nitrogen species to N_2O or N_2 gas via three known pathways: denitrification, anaerobic ammonium (NH_4^+) oxidation (anammox), and n-damo (Trimmer et al., 2012). Denitrification is catalyzed by denitrifiers, mostly facultative anaerobic heterotrophs, for which the HZ provides a perfect habitat, and is therefore typically highly active in the HZ (Kim et al., 2016; Zhou et al., 2014). Anammox describes the chemoautotrophic pathway of NH_4^+ oxidation coupled to NO_2^- reduction which produces N_2 (Trimmer et al., 2012). Anammox activity was found in the HZ in a zone spatially separated from n-damo activity (Shen et al., 2019b). The n-damo process typically occurs in the zone of denitrification, close to the oxic–anoxic interface. The generally steep geochemical gradients and the occurrence of anoxic micro-niches in otherwise oxic environments makes the exact localization and quantification of these respiratory pathways challenging (Raghoebarsing et al., 2006).

Many linkages connect the hyporheic carbon and nitrogen cycles. Denitrification is predominantly heterotrophic and requires a carbon source, a reason why carbon availability correlates negatively with the accumulation of NO_3^- in streams (Trimmer et al., 2012). Eutrophication of

aquatic ecosystems is likely to enhance GHG emissions due to direct (O_2 depletion, increased organic carbon, and availability of nutrients especially for N_2O production) and indirect effects (a shift in primary producer from macrophytes to algae and harmful algal blooms) (Li et al., 2021). On the other hand, the n-damo process has the potential to reduce GHG emissons from the HZ zone by oxidizing CH_4 to CO_2, and at the same time removing NO_3^- from the stream.

However, the ecohydrological significance of the HZ reaches far beyond the riverbed. Accelerated carbon and nutrient cycling in the HZ can have both beneficial and detrimental effects. Removal of bioavailable nitrogen via denitrification for example can prohibit eutrophication of downstream coastal or lake ecosystems (Seitzinger et al., 2006) while substantial GHG production contributes to climate warming (Stanley et al., 2016). A hydraulic ecosystem function of the HZ is flood risk mitigation due to storage of additional water in river bed and banks, attenuation of the discharge peak, and delayed peak arrival (Boulton et al., 1998). Single discharge events have the potential to increase hyporheic O_2 and NO_3^- uptake together with exchange fluxes, especially when hydraulic gradients are reversed from gaining to loosing conditions during an event (Trauth & Fleckenstein, 2017). Not only during floods does the HZ provide physical, biological, and chemical filtration of stream water (Hancock, 2002; Hancock et al., 2005). The HZ is also key for aquatic biodiversity. The top of the riverbed accommodates not only microbiota and macro-zoobenthos but also endangered species such as juvenile freshwater mussels (Denic & Geist, 2015; Geist & Auerswald, 2007). The interstitial pore space provides spawning grounds for diverse fish species, many of which depend on oxygenated conditions for larvae survival (Sternecker & Geist, 2010).

Clogging describes the blockage of interstitial pores with fine deposits. It limits the exchange between streamwater and the HZ (Rode et al., 2015) and reduces substrate quality for a multitude of different aquatic species (Geist & Auerswald, 2007). In a large-scale mesocosm experiment, Wild et al. (2023) showed that addition of fine sediments reduced hatching rates of gravel-spawning fish species by 50 % to 80 %. Hyporheic exchange is also a prerequisite for many other ecosystem functions such as flood-wave retention, stream water filtration, or denitrification. Land-use changes that transform the catchment area from a natural to an anthropogenically modified, agriculturally used landscape are usually associated with increased erosion and thus a higher input of fine material into the rivers (Borrelli et al., 2020; Zhu et al., 2022). Reductions in energy slope and flow velocity by river engineering measures and discharge management can enhance the likelihood of fine accumulations at the riverbed (Auerswald & Geist, 2018). These anthropogenic changes can impair the ecological, chemical, and hydrological functionality of the HZ.

2.4 Drivers of methane cycling in river beds

The hyporheic CH_4 cycle comprises production, consumption, and transport processes (Fig. 2.2). Similar to other freshwater environments, CH_4 production in the HZ takes place in deeper layers where other electron acceptors have been exhausted, and from there the CH_4 is transported up to the top of the streambed, into the water column, or directly to the atmosphere. Yet, conditions in the HZ may differ from lake sediments because the riverbed usually interacts with oxygenated stream water through hyporheic exchange fluxes while lakes are less dynamic and stratification can lead to anoxic bottom waters (Peña Sanchez et al., 2022b). Three main

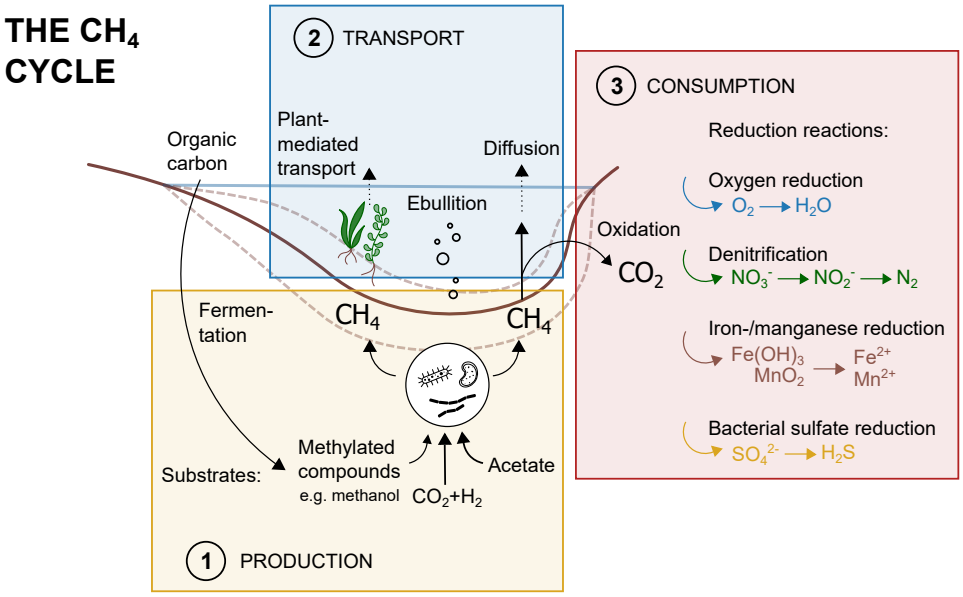

Figure 2.2: **The CH_4 cycle in river beds.** CH_4 is (1) produced by archaea in anaerobic sediments, (2) transported to the atmosphere via diffusion or ebullition and (3) oxidized to CO_2 in a reaction coupled to the reduction of an electron acceptor.

mechanisms transport CH_4 from the methanogenic zone upwards: (i) CH_4 diffuses along the concentration gradient from the CH_4-rich deeper layers of the HZ to the surface water, which constantly looses CH_4 to the atmosphere and therefore, has much lower CH_4 concentrations (Boudreau, 1997). (ii) Plants can bring substantial amounts of CH_4 from their roots to the leaves and into the water column (Sanders et al., 2007). (iii) The quickest and most direct transport pathway is ebullition, the spontaneous release of gas bubbles that can form at very high CH_4 concentrations in the HZ (Maeck et al., 2014).

When CH_4 is transported diffusively, it can be oxidized on it's way with the concomitant reduction of several electron acceptors (Sec. 2.2). Also the transport through plants has been shown to favor CH_4 oxidation, because the surface of submerged macrophytes can be a suitable habitat for methanotrophs (Li et al., 2021). If CH_4 is however transported via ebullition, it is assumed to escape the oxidative layer in the HZ due to the higher travel velocity (Sawakuchi et al., 2016). Studies on CH_4 ebullition in streams disagree on the relative contribution of this transport pathway. While McGinnis et al. (2016) found that ebullition was responsible for 80 % of total CH_4 emissions, Robison et al. (2022) estimated that more CH_4 escaped through diffusive fluxes than as gas bubbles.

Several studies have examined which factors can explain variations of CH_4 production and consumption in the HZ. For example, Shen et al. (2019a) sampled sediment and pore water from seven streams in Southern England for the investigation of potential AOM with different electron acceptors. Using a combination of isotope tracer experiments and phylogenetic analyses in sediment incubations, they found that AOM activity was provoked by the addition of NO_3^- and NO_2^- in all sandy river beds and by SO_4^{2-} and Fe^{3+} in sandy river beds with high CH_4 concentrations, while no AOM activity could be stimulated in gravelly river beds. This is well in line with findings by Shelley et al. (2015) who found 100 times larger CH_4 oxidation capacity in

fine sediment patches compared to coarse gravels. Similarly, Bodmer et al. (2020) measured increases of potential CH_4 production and oxidation rates with decreasing grain diameter.

Next to grain size, a second important control on CH_4 cycling in the HZ is the content of organic matter. Potential CH_4 production and oxidation rates as well as CH_4 emissions increased significantly with rising concentrations of organic carbon in experiments conducted by Bodmer et al. (2020) and Romeijn et al. (2019). A study on 236 streams in the UK recently demonstrated that excess fine sediment delivery was linked to increased organic matter content in river beds, and the combined effect stimulated CH_4 emissions (Zhu et al., 2022).

Further, methanogenic and methanotrophic activity in river sediments have been found to be sensitive to warming (Shelley et al., 2015) with a non-linear temperature response, that was influenced by grain size, organic matter content, and geological origin of stream sediments (Comer-Warner et al., 2018). Direct CH_4 emissions via ebullition from aquatic environments could be described by a non-linear temperature-dependent model (Eq. 7.10) (Aben et al., 2017).

Other driving forces for methanogenesis and methanotrophy in the HZ were hyporheic exchange fluxes (Ng et al., 2020), river hydrological stages (Villa et al., 2020), and shading (Shelley et al., 2017), all of which can be highly variable in both time and space. Anthropogenic land-use changes in the catchment, temperature, and O_2 saturation were shown to influence methanogenic and methanotrophic communities in stream sediments (Nagler et al., 2021). Potential CH_4 production was positively correlated with a high abundance of methanogens, which hardly seems surprising, but interestingly a high abundance of methanotrophs did not increase the CH_4-oxidation potential (Nagler et al., 2021).

3 Aims and scope

Based on the literature review in Ch. 2, CH_4 is produced in the HZ; transported via diffusion, submerged plants, or ebullition; and can be partly oxidized by several reduction reactions. However, opinions on the relative contribution of different transport mechanisms, as well as electron acceptors for CH_4 oxidaiton, diverge. Especially the role of the n-damo process as a CH_4 and NO_3^- sink is less explored. Major uncertainties also remain with regard to the relevance of streams as CH_4 emitters, thus the balance of total CH_4 production and consumption in streams, and how this may develop in the future.

Some parameters are likely to accelerate hyporheic CH_4 cycling such as a large fraction of fines in the bed substrate, high concentrations of organic matter, and a warmer climate (see Sec. 2.4). Yet, many studies rely on incubation experiments to investigate the influence of these parameters. Such studies are designed to isolate the effect of a single parameter and are well suited to do so, but they can only calculate potential CH_4 production and consumption rates and do not determine actual rates in situ. Therefore, the question arises as to how transferable the data from laboratory incubations are to reality. Spatially and temporarily resolved field data exist for lakes (Einsiedl et al., 2020; Peña Sanchez et al., 2022b, 2022a), but are scarce for the HZ of rivers. It is important to strengthen our understanding of conversion processes governing the CH_4 cycle in the HZ with more realistic data from field instead of laboratory investigations.

The following hypotheses arise from the literature review, but need to be tested with solid data from in situ measurements:

- The hyporheic zone of river Moosach is a hotspot of methane cycling, where methane is produced at significant rates as well as oxidized aerobically and anaerobically
- Microbial methane oxidation coupled to nitrate or nitrite reduction (n-damo) not only reduces methane emissions but also enhances the removal of surplus nitrogen from stream ecosystems
- Most of the methane produced in the hyporheic zone is transported upwards by diffusion while ebullitive methane fluxes are of minor importance
- Stream methane emissions are temperature-sensitive and enhanced by fine, organic-rich sediments, and are therefore likely to increase in the future

We aimed at resolving the hyporheic CH_4 cycle with high-resolution data from in situ measurements to test the formulated hypotheses and increase the general understanding of CH_4 cycling in river beds (Fig. 3.1). Special focus was given to the n-damo process. Field investigations

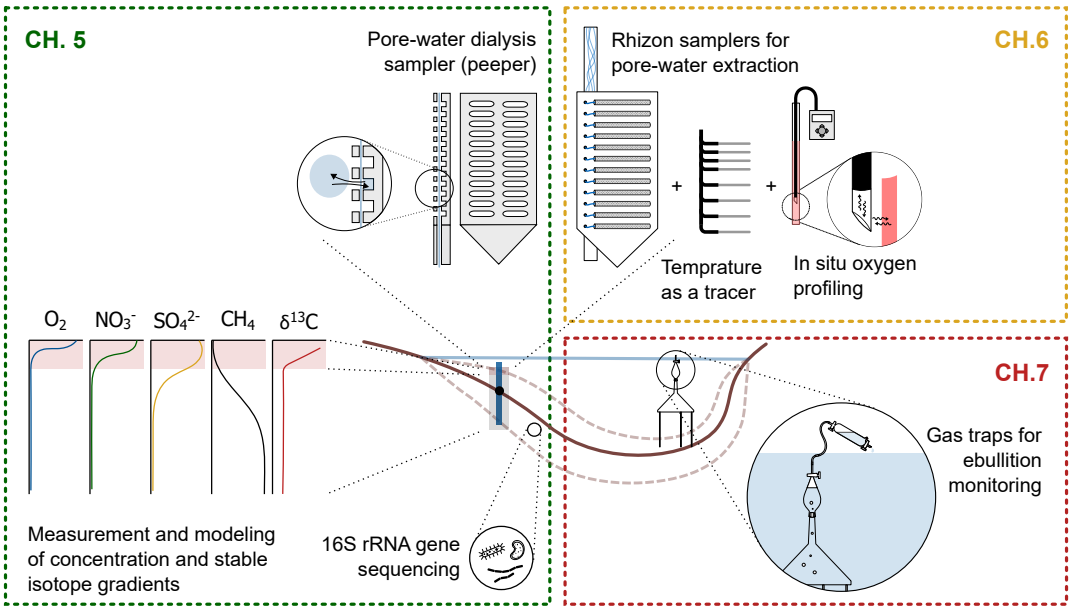

Figure 3.1: **Scope of the thesis.** Ch. 5 describes high-resolution vertical geochemical pore-water profiles interpreted with the help of 16S rRNA gene sequencing and inverse geochemical modeling, Ch. 6 discusses methods for time-resolved HZ investigations, and Ch. 7 focuses on the role of ebullition as a transport pathway of CH_4 to the atmosphere.

targeted spatial patterns of HZ geochemistry and CH_4 distribution, temporal dynamics of CH_4 production and consumption, and the contribution of different transport pathways. For the investigations we chose river Moosach, a small stream in the north of the city of Munich as a test site.

In a first study (Publication I, Ch. 5), we measured high-resolution geochemical profiles at five sites in the HZ of river Moosach. The profiles were interpreted with the help of a simple one-dimensional diffusion-reaction model and additional microbiological analyses. The main goal was to study the spatial and temporal variation of HZ geochemistry and to understand which microbes catalyze which reaction pathways in the CH_4 cycle. We also measured the carbon stable isotope composition of CH_4 (δ^{13}C–CH_4) to identify relevant CH_4 production pathways and locate the CH_4 oxidation zone.

Second, we designed a monitoring station that was permanently installed in the HZ of river Moosach and allowed repeated pore-water sampling, high-resolution dissolved O_2 profiling, and automated temperature measurements for estimating magnitude and direction of hyporheic exchange fluxes (Publication II, Ch. 6). With this device, the same site could be sampled multiple times. The specific aims of this study were first, to advance existing methods for temporarily resolved pore-water sampling from the HZ, and second, to observe the temporal dynamics of hyporheic geochemistry and CH_4 cycling.

As third part of this thesis, we installed gas traps to quantify CH_4 ebullition for a full year and compared ebullitive to estimated diffusive CH_4 fluxes (Publication III, Ch. 7). With this work we wanted to distinguish the importance of the different transport processes. We also used differences in δ^{13}C–CH_4 between gaseous CH_4 and dissolved CH_4 in surface water

to determine the amount of CH_4, that was oxidized. With this we aimed at a data-based assessment of the relevance of CH_4 oxidation in the HZ of river Moosach.

4 Methodological principles

4.1 Study site

Addressing the need for more in situ measurements meant that a substantial part of this thesis would be data acquisition. Aiming at the deduction of general knowledge on the hyporheic CH_4 cycle from field investigations, the decision was taken to focus on a high sampling resolution at a single study site as opposed to measurements in different rivers. Capturing spatial and temporal patterns of CH_4 cycling processes was, due to the large in-stream heterogeneity, only possible with a high sampling effort. We performed measurements of high-resolution vertical geochemical profiles at different places in the stream bed, installed a monitoring station for repeated pore-water extraction, O_2 profiling, and temperature monitoring, and quantified ebullition over the course of a full year, all at one test site.

The selected site was river Moosach (Fig. 4.1), a small stream in the Danube catchment close to the city of Freising that has its origin in several drainage ditches in the north of Munich, and drains into the Isar river after approximately 35 km (Stein, 1987). River Moosach flows along the border of two contrasting geological landscapes with the Munich Gravel Plain in the south east and the Tertiary Hill Country in the north west, and crosses several degraded peatland areas on its way (Auerswald & Geist, 2018). It is a heavily anthropogenically influenced watercourse with a low gradient and little fluctuations in discharge (Pulg et al., 2013). In the upper reaches, the watercourse is mainly fed by groundwater, while in the further course a few side streams supply additional discharge. The groundwater influence results in summer-cool water temperatures especially close to the origin with increasing thermal amplitudes downstream (Kohler et al., 1987; Pulg et al., 2013). The total precipitation area of river Moosach covers 175-185 km^2, but it's actual catchment area is much larger due to the groundwater inflows from the Munich Gravel Plain in the south and was estimated to be around 350 km^2 with a water balance approach (Auerswald & Geist, 2018). Chemically, the stream water is of a calcium-bicarbonate-rich type of originally oligotrophic character and a tendency to be slightly alkaline (pH of $\sim$8) (Kohler et al., 1987).

Today, river Moosach flows in an artificial channel with almost rectangular cross section and is impounded by a series of weirs (Kohler et al., 1987). The river has been cut off from its original headwaters close to the Munich city district *Moosach* after constructions in the 17^{th} century, and is nowadays fed by a network of drainage ditches north of Unterschleißheim. Its course is nearly straight and the river bed has a macrophyte cover of >15 % (Braun et al., 2012). The Moosach is of interest for the present study because the low flow velocity caused by numerous impoundments favors the development of thick fine sediment deposits in which strongly reducing conditions can be expected (Auerswald & Geist, 2018).

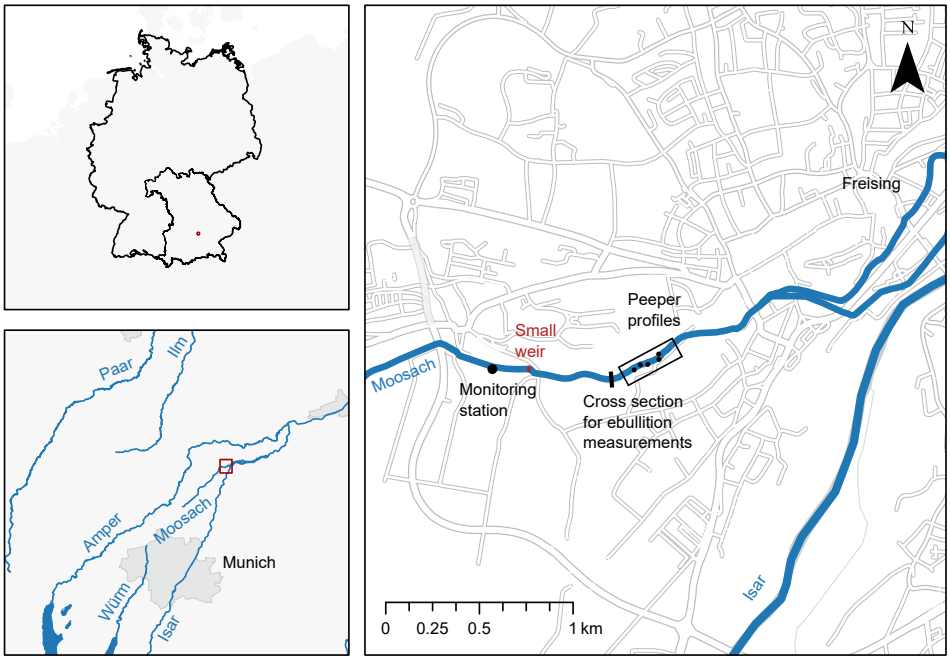

Figure 4.1: **Map of the study area.** Geochemical profiles measured with a pore-water dialysis sampler (peeper) in the eastern part of the study area are discussed in Ch. 5. The monitoring station located upstream in the west of the study area is described in Ch. 6. Data on ebullition monitoring from a cross section in the center of the study area are shown in Ch. 7. Base map retrieved from ArcGIS Vector Tile Server (sources: Esri, HERE, Garmin, FAO, NOAA, USGS, OpenStreetMap contributors, and the GIS User Community).

In the three studies that make up this thesis, three regions of the Moosach River were examined. All sites were located in the middle reach where the energy gradient falls below 0.1 ‰ in some places (Auerswald & Geist, 2018). Vertical geochemical gradients were obtained with a pore-water dialysis sampler (peeper) in the easternmost part of the studied section (Fig. 4.1). A monitoring station was installed approximately 700 m upstream in the headwaters of a small weir. Gas samplers for the quantification of ebullition were installed in a curved cross section further downstream, because river bends usually develop an undercut slope with coarser substrate at the ouside and a slip-off slope with fine material at the inside, and it was therefore possible to compare ebullition from different bed substrates under otherwise equal conditions. The stream was 8-14 m wide and between one and two meters deep at the studied cross sections.

4.2 Measurements of water chemistry, gas analyses, and dissolved oxygen concentrations

Relevant ions and gas concentrations in surface- and pore-water samples were determined with an ion and gas chromatograph, respectively (Fig. 4.2). In chromatography, a sample with a mixture of components is flushed through a column with an adsorbing stationary phase by an eluent or carrier gas (mobile phase) (Worden, 2005). The travel speed of each component varies due to differences in the adhesive forces between the component and the stationary phase of the column. This causes the mixture to be split into its individual parts. A detector at the end of the column produces a measurable signal when a component arrives. Integration over the peak areas in the resulting chromatogram and comparison with standards of known concentrations gives the final concentration of each component. Liquid samples were directly measured with the ion chromatograph. For the measurement of dissolved gases, samples were first equilibrated with a headspace in a gastight vial, concentrations then measured in the headspace gas, and finally the initial concentration in the water sample calculated as a function of water volume, headspace volume, and temperature (EPA, 2001).

Ion chromatography allowed the delineation of denitrification and sulfate reduction zones from geochemical gradients, gas chromatography added information about the location of methanogenic and methanotrophic zones. However, for the allocation of the oxic–anoxic interface, precise measurements of dissolved oxygen (DO) concentrations were needed. First, dissolved O_2 concentrations were measured with a Clark-type microsensor (Revsbech, 1989) in the chambers of peepers by piercing through the membrane covering the peeper. However, the determination of DO concentration in pore-water samples after retrieval of the measurement device from the HZ proved difficult, because contamination with atmospheric O_2 occurred quickly. This reduced the available time for measurements and as a consequence the resolution of the measured profiles (Michaelis et al., 2022). We therefore custom-coated an optical sensor for in situ measurement of DO concentrations after Brandt et al. (2017).

For the production of the sensor, a plexiglas tube was coated at the outside with an optically sensitive dye. The coating served as an optode that measures O_2 partial pressure via fluorescence quenching. O_2 reduces the fluorescence intensity of the photoluminescent dye and accelerates the lifetime decay of the luminescence (Vieweg et al., 2013). When a light pulse

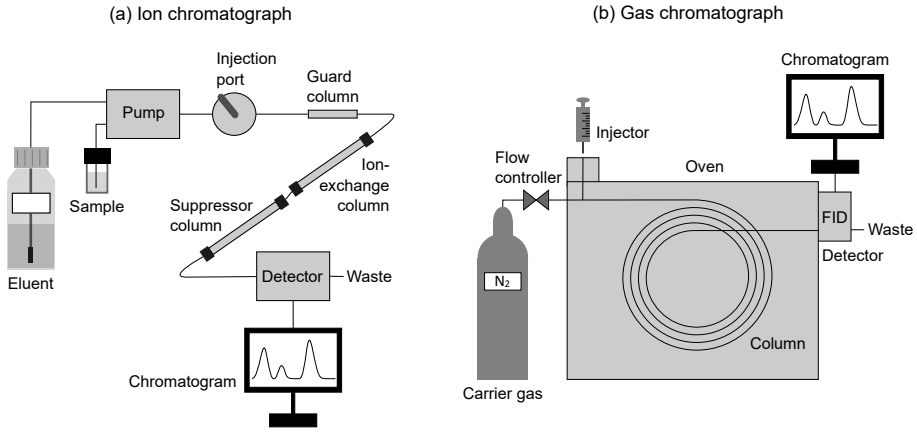

Figure 4.2: **Mechanisms of (a) ion and (b) gas chromatography.** Both of these instruments allow a mixture to be broken down into its components and these components to be quantified. Adapted from Worden (2005).

emitted by an O_2 meter is reflected by the sensor coating, intensity and phase of the optical signal change. The phase-shift between the original and reflected signal is recorded by the O_2 meter and with that measurement O_2 concentration can be calculated based on the two-sided quenching model (App. B, Eq. B.1). This model represents a modification of the Stern-Volmer equation (Stern & Volmer, 1919) adapted to account for heterogeneities in the sensor material (Carraway et al., 1991).

Photoluminescence is temperature dependent, thus temperature measurements in the HZ were necessary for an accurate calculation of DO concentrations. The optode functions without physical contact which enabled measurement of DO concentration from the inside of the plexiglas tube by moving a polymeric optical fiber (POF) through the plexiglas tube without disturbance of the HZ (Brandt et al., 2017). The POF was manufactured with a 45° cutting to redirect the signal excited by the O_2 meter and reflected by the sensor dye perpendicular to the direction of the POF (Fig. 6.1). Further information on sensor calibration and calculation of DO from measured phase shifts can be found in App. B.3.

4.3 The use of stable isotopes for tracing environmental processes

Isotopes are atoms of an element with the same number of protons but different numbers of neutrons, which changes the mass of the element and thereby its stability and reaction rate (Clark & Fritz, 1997; Kendall & Caldwell, 1998; Sidle, 1998). Radioactive isotopes spontaneously disintegrate over time, because a too large difference between the number of protons and neutrons leads to instability, while stable isotopes do not decay (Kendall & Caldwell, 1998). Radioactive and stable isotopes have been widely used as tracers in earth and environmental sciences. The decay of radio-isotopes provides information on the age of a system, which is taken advantage of in hydrological and hydrogeological studies, for example to

identify groundwater sources and their age (Winter & Einsiedl, 2022). But also stable isotopes can be used to track environmental processes because discrimination against a particular isotope, generally the heavier one, in a chemical or biological reaction, known as stable isotope fractionation, alters the stable isotope composition of a substance and makes transport and transformation processes visible (Blair et al., 1985; Clark & Fritz, 1997).

Stable environmental isotopes are defined by the heavy to light ratio R of the two most abundant isotopes of an element, for example the ratio of ^{2}H to ^{1}H for hydrogen, ^{13}C to ^{12}C for carbon, and ^{18}O to ^{16}O for oxygen (Clark & Fritz, 1997). A sample's isotopic composition is usually measured in reference to a standard such as the Vienna Standard Mean Ocean Water (V-SMOW) for water isotopes or the Vienna Pee Dee Belemnite (V-PDB) standard for carbon and is given in per mil (‰) (Eq. 4.1) (Clark & Fritz, 1997; Kendall & Caldwell, 1998). The partitioning of isotopes between the pools of a heavier and a lighter species during fractionation is described by the Rayleigh equation (Eq. 4.2) (Kendall & Caldwell, 1998; Rayleigh, 1896).

$$\delta(‰) = \left(\frac{\mathrm{R_{Sample}}}{\mathrm{R_{Standard}}} - 1 \right) \cdot 10^{3} \tag{4.1}$$

$$\mathrm{R} = \mathrm{R_0} \cdot \mathrm{f}^{(\alpha - 1)} \tag{4.2}$$

where R is the isotope ratio in a reactant, R_0 the initial isotope composition, f the remaining fraction of the reactant, and α the isotope fractionation factor.

Eq. 4.2 is applicable in a fully mixed system with unlimited supply of the reactant and constant α. However, in natural systems α can change during a reaction if the substrate supply is limited (Kendall & Caldwell, 1998). Further, it is usually advisable to consider a range of possible values for α, because the local fractionation factor does not only depend on the transformation process itself, but also environmental conditions (Elsner, 2010). High spatial variance within an ecosytem type is possible (Snover & Quay, 2000), and α has been shown to depend on temperature (Coleman et al., 1981), microbial cell density (Templeton et al., 2006), and the reaction rate (Chanton et al., 2008). Nevertheless, stable isotope fractionation is a powerful tool to trace transport and turnover processes in natural environments.

Stable water isotopes are mostly used in surface and groundwater hydrology. Precipitation has a regionally specific isotopic signature influenced by latitude, altitude, and specific meteoric processes in a region (Stumpp et al., 2014). When the isotope composition of meteoric water is known, this input signal can later be used to trace hydrologic processes (Imig et al., 2023; Reckerth et al., 2017) or groundwater recharge on the catchment scale (Koeniger et al., 2016). Stable isotopes of other elements, like carbon, nitrogen or sulfur, are regularly measured in aquatic ecosystems, for example to explain nutrient dynamics (Peña Sanchez et al., 2022a; Spoelstra et al., 2021; Stoewer et al., 2015), contaminant degradation (Elsner, 2010), or production and consumption of common GHGs such as CH_4 (Einsiedl et al., 2020; Norði & Thamdrup, 2014; Peña Sanchez et al., 2022a). Measurements of the stable carbon isotopes of CH_4 can serve as an indicator of the relative contribution of the various CH_4 formation pathways, as the discrimination against the heavier isotope is different (Conrad, 2009). During CH_4 consumption, the same kinetic isotope effect will lead to a ^{13}C enrichment in the remaining CH_4 pool (Conrad, 2009).

For this work, $\delta^{13}C$–CH_4 and stable water isotopes were measured with laser-based instruments using cavity ring-down spectroscopy (CRDS) or a further development thereof, called off-axis integrated cavity output laser spectroscopy (OA-ICOS), respectively. In short, the measurement principle of CRDS relies on a laser source which emits a light signal into a cavity of highly reflective concave mirrors placed in a vacuum (Wheeler et al., 1998). The laser signal will bounce between the mirrors and decay due to cavity losses. Presence of a sample inside the cavity will influence the shape of this decay which can be recorded by a photo-sensitive detector behind the output mirror. Using the rate of decay instead of the direct attenuation of a light beam transmitted through a sample makes CRDS less sensitive to variations in input signal intensity and allows a more precise resolution than traditional absorption spectroscopy (Wheeler et al., 1998). This enables the distinction between different isotopes of an element and quantification of the stable isotope ratio in a sample.

4.4 Determination of the microbial community distibution

Woese and Fox (1977) first suggested that ribosomal RNA (rRNA) genes were suitable for the comparison of distant taxa due to their ubiquity in cells and their high sequence conservation over time. Today, 16S rRNA gene sequencing is one of the most widely used methods to determine taxonomic distribution in microbial communities (Case et al., 2007). Complexed RNA together with ribosomal proteins make up the ribosome, which sythesizes proteins (Cech, 2000). Peptide bond formation is catalyzed by the rRNA. This fundamental mechanism is equal in all living cellular organisms no matter if archaea, bacteria, or eukaryotes (Voorhees & Ramakrishnan, 2013). The 16S rRNA gene contains highly conserved and highly variable regions, the first of which can serve as priming sites while the latter are versatile enough to distinguish related taxonomic groups (Coenye & Vandamme, 2003; Větrovský & Baldrian, 2013). Universal primers are designed to target a conservative part of the 16S rRNA gene common to most bacteria and archaea (Weisburg et al., 1991) and to amplify the neighboring variable region of the gene in a polymerase chain reaction (PCR) (Devereux & Wilkinson, 2004). The amplification yields amplified conserved fragments of the rRNA gene that is targeted by the chosen PCR primer sequences. These amplified fragments can later be sequenced to gain further information on the microbial community structure. Monitoring the PCR amplification in real-time with SYBR green dye can be used to quantify the total number of 16S rRNA gene copies in a sample, when comparing against a standard curve in quantitative PCR (qPCR) (Jansson & Leser, 2004).

The PCR amplified 16S rRNA gene fragments can be sequenced in high throughput using Illumina paired-end sequencing technology. In this way, a very high number of sequencing runs at a relatively low cost is possible and parts of the full 16S rRNA gene, which in total has approximately 1500 base pairs, can be read millions of times simultaneously (Pichler et al., 2018). As an example, the Illumina MiSeq platform can reach paired reads of up to 300 nucleotides, sequencing with the Illumina MiniSeq platform gives sequence lengths of up to 150 base pairs (Illumina, 2023). The V4-V6 hypervariable regions, each of which starts with a highly conserved sequence to be targeted by a primer, have been shown to be most suitable for representing the complete 16S rRNA gene (Yang et al., 2016). Sequence reads are then clustered into operational taxonomic units (OTUs) that can be compared to a database with

listed taxonomic groups (Johnson et al., 2019). Usually it is assumed that $>95\,\%$ similarity indicates the same genus, $>97\,\%$ similarity the same species (Johnson et al., 2019). This approach cannot reach the same taxonomic accuracy as when sequencing the full 16S gene for three main reaons: new and yet to be discovered groups are underrepresented in the databases; presence of multiple 16S rRNA copies in a single microbial genome can skew abundance estimates; and variability in the 16S sequence from the same species can affect diversity estimates (Case et al., 2007; Větrovský & Baldrian, 2013).

In this thesis, DNA was extracted from sediment samples mainly through mechanical disruption like homogenization with glass beads and repeated freeze-thaw cycles in the presence of a lysis buffer solution (Vuillemin et al., 2019). DNA supernant was then separated from sediment particles using centrifugation and filtration (Vuillemin et al., 2019). A common contaminant in DNA extracted from aquatic sediments, especially if associated with high organic carbon contents, are humic substances (Alm & Stahl, 2004) which had to be removed with a special cleanup kit. For 16S rRNA gene sequencing, a high-throughput approach was applied to reach a high community coverage, targeting the hypervariable V4 region (Pichler et al., 2018). This method allowed us to determine the relative abundance of methanogenic and methanotrophic microorganisms in the HZ of river Moosach and infer which pathways might control CH_4 production and consumption.

4.5 A simple one-dimensional steady-state diffusion-reaction model for geochemical profile interpretation

CH_4 in the HZ is subject not only to microbial turnover, but also to physical transport processes and partitioning between dissolved and gaseous phases. Depicting all of these mechanisms in a combined model is highly complex and would involve the coupling of hydraulic, chemical, and physical models in more than one dimension. No model so far has managed to cover all these complexities (Boano et al., 2014). Because the development and parametrization of such a model was out of scope for this thesis, we chose the simplest possible approximation with a one-dimensional diffusion–reaction model implemented in the software package PROFILE (Berg et al., 1998). PROFILE encodes a one-dimensional representation of molecular diffusion, bioturbation, bioirrigation, and a source/sink term (Eq. 4.3). The latter is clustered into zones of equal production or consumption and estimated as fit parameter in an iterative statistical calculation using piecewise constant functions for R.

$$\frac{\mathrm{d}}{\mathrm{dz}}\left(\varphi(\mathrm{D_S}+\mathrm{D_B})\frac{\mathrm{dC}}{\mathrm{dz}}\right)+\varphi\alpha_\mathrm{i}(\mathrm{c_0}-\mathrm{c(z)})+\mathrm{R}=0 \tag{4.3}$$

where $\mathrm{c(z)}$ is pore-water CH_4 concentration as a function of sediment depth z, $\mathrm{c_0}$ surface water CH_4 concentration, φ total porosity, $\mathrm{D_S}$ molecular diffusivity of CH_4 in the sediment, $\mathrm{D_B}$ biodiffusivity, α_i the irrigation coefficient, and R the rate of net production or consumption.

Eq. 4.3 is discretized numerically with a control volume approach and solved multiple times for different numbers of zones with constant production or consumption rates. The best fit based on a particular set of production/consumption rates is obtained by minimizing the sum of squared deviations (SSE) (Eq. 4.4).

$$\mathrm{SSE} = \sum_{\mathrm{k}=1}^{\mathrm{M}} (\mathrm{c_{mi}} - \bar{\mathrm{c}}_{\mathrm{i}})^2 \tag{4.4}$$

where SSE is the sum of squared deviations, M the number of measured concentrations, $\mathrm{c_{mi}}$ a measured concentration, and $\bar{\mathrm{c}}_{\mathrm{i}}$ the corresponding modeled concentration interpolated to the same depth as $\mathrm{c_{mi}}$.

The statistical procedure aims at finding the simplest production/consumption profile that can still adequately represent a measured concentration gradient and involves two steps. First, a best fit is obtained for an increasing number of production/consumption zones. Each time a zone is added, the hypothesis is put forward that this addition does not significantly improve the fit. This hypothesis is tested by calculating the p-value of the *F* distibution (Eq. 4.5) and rejected if $\mathrm{p} \leq 0.01$. In a second step, adjacent zones are combined, starting with the most similar production rates and continuing stepwise until only one zone is left. Each time two neighbouring zones are lumped, the SSE is calculated. Finally, best fits are compared through the *F* tests. A p-value ≥ 0.01 thereby signals that the fit with more zones is not better than the fit with a reduced number of zones.

$$\mathrm{F} = \frac{\dfrac{\mathrm{SSE_k} - \mathrm{SSE_{k+j}}}{(\mathrm{k}+\mathrm{j}) - \mathrm{k}}}{\dfrac{\mathrm{SSE_{k+j}}}{\mathrm{M} - (\mathrm{k}+\mathrm{j})}} \tag{4.5}$$

where k is the number of zones of the current profile and j is the number of additional or reduced zones. A fit based on k zones is compared to fits based on an increasing number of j zones in the first step (k+1, k+2, k+3, ...), and to a decreasing number of zones in the second (k-1, k-2, ...).

This procedure provides an objective way of identifying production and consumption zones from measured concentration gradients and is therefore well suited to study the CH_4 cycle in aquatic sediments based on vertical geochemical profiles (Jørgensen et al., 2004; Norði & Thamdrup, 2014). However, as stated above, it is a very simplified approach and has several limitations for the application in the HZ. These include the false assumption of steady state, the reduction to one dimension, the lack of an advective flow component, and the disregard of the gas phase. Further, production and consumption zones are strictly separated while in the HZ the occurrence of micro-niches could allow overlaps (Boulton et al., 1998). It is also not possible to couple different reactants with each other, like CH_4 oxidation with O_2, NO_3^-, or SO_4^{2-} reduction. Results produced with this model therefore had to be interpreted with care, taking the uncertainties and limitations into account.

4.6 Heat as a tracer for an estimation of vertical hyporheic exchange fluxes

Temperature measurements are frequently applied to estimate water movement in aquifers or saturated sediments (Anderson, 2005; Constantz, 2008) and have repeatedly proven useful

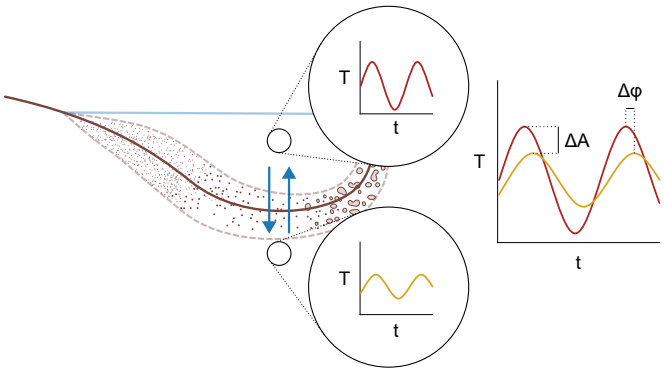

Figure 4.3: **Schematic representation of differences in the diurnal temperature signal of surface and pore water.** Heat transport processes lead to a reduction in amplitude (ΔA) and a delay in phase ($\Delta\varphi$) of the diurnal temperature signal in the surface water. These differences can be used to estimate magnitude and direction of the vertical seepage flux.

for modeling hyporheic exchange fluxes (Bhaskar et al., 2012; Briggs et al., 2012; Schmidt et al., 2014). Heat transport in porous media is governed by two main processes, conduction and convection, as described by the one-dimensional heat transfer equation (Eq. 4.6). These heat transport mechanisms lead to an amplitude dampening (ΔA) and phase delay ($\Delta\varphi$) in the diurnal temperature signal of pore water when compared to surface water (Fig. 4.3) (Constantz, 2008). These differences can be used to estimate the flux between two temperature sensors in different depths (Hatch et al., 2006; Keery et al., 2007).

$$\frac{\partial \mathrm{T}}{\partial \mathrm{t}} = \frac{\lambda_\mathrm{e}}{\rho \mathrm{c}} \frac{\partial^2 \mathrm{T}}{\partial \mathrm{z}^2} - \mathrm{q} \frac{\rho_\mathrm{w} \mathrm{c}_\mathrm{w}}{\rho \mathrm{c}} \frac{\partial \mathrm{T}}{\partial \mathrm{z}} \tag{4.6}$$

where T is temperature, t time, z depth, λ_e effective thermal conductivity of the saturated sediment, q steady vertical seepage flux per unit area, positive in the z direction, ρ and c are density and specific heat capacity of the sediment, and ρ_w and c_w density and specific heat capacity of water.

Stallman (1965) proposed an analytical solution for Eq. 4.6 with two boundary conditions: a sinusoidal temperature signal with constant amplitude at the top of the model domain, and a constant and uniform seepage flux in z direction. On this basis, Hatch et al. (2006) and Keery et al. (2007) developed analytical solutions that allow calculation of vertical hyporheic fluxes from amplitude dampening and phase change in the temperature signal of sensor pairs in different depths. These were implemented in the software package VFLUX (Gordon et al., 2012) which allows automated evaluation of temperature data from several depth-distributed sensors.

In VFLUX, the seasonal component from a non-stationary temperature time series is first extracted with Dynamic Harmonic Regression (DHR) (Young et al., 1999). DHR is a special case of an Unobserved Component (UC) model which accounts for a trend, cyclical, seasonal, and irregular component. Cyclical and seasonal components are defined as a sum of trigonometric functions. The DHR is a non-stationary form of the Discrete Fourier Transform (DFT) and uses Kalman filtration and a fixed interval smoothing algorithm for the extraction of the seasonal component from a time series with temporally variable amplitudes and phases (Young et al.,

1999). ΔA and $\Delta\varphi$ from the filtered time series are then used to estimate vertical hyporheic flux rates based on the methods described by Hatch et al. (2006) and Keery et al. (2007).

5 Publication I

High-resolution vertical biogeochemical profiles in the hyporheic zone reveal insights into microbial methane cycling

This chapter was published as: Michaelis, T., Wunderlich, A., Coskun, Ö. K., Orsi, W., Baumann, T., & Einsiedl, F. (2022). High-resolution vertical biogeochemical profiles in the hyporheic zone reveal insights into microbial methane cycling. *Biogeosciences*, *19*(18), 4551–4569. https://doi.org/10.5194/bg-19-4551-2022

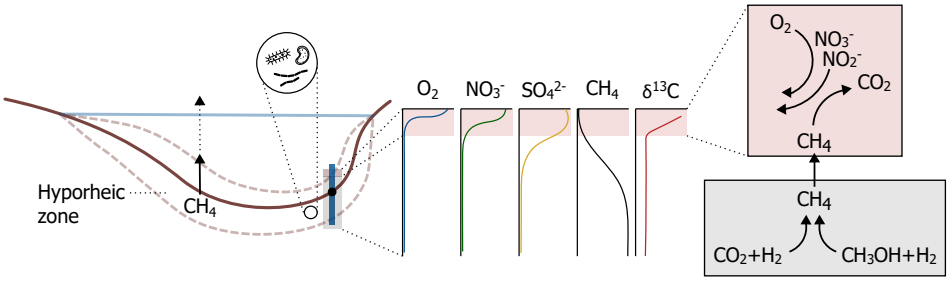

Abstract. Facing the challenges of climate change, policy making relies on sound greenhouse gas (GHG) budgets. Rivers and streams emit large quantities of the potent GHG methane (CH_4), but their global impact on atmospheric CH_4 concentrations is highly uncertain. In situ data from the hyporheic zone (HZ), where most CH_4 is produced and some of it can be oxidized to CO_2, are lacking for an accurate description of CH_4 production and consumption in streams. To address this, we recorded high-resolution depth-resolved geochemical profiles at five different locations in the stream bed of the river Moosach, southern Germany. Specifically, we measured pore-water concentrations and stable carbon isotopes ($\delta^{13}C$) of dissolved CH_4 as well as relevant electron acceptors for oxidation with a 1 cm vertical depth resolution. Findings were interpreted with the help of a numerical model, and 16S rRNA gene analyses added information on the microbial community at one of the locations. Our data confirm with pore-water CH_4 concentrations of up to 1000 µmol L^{-1} that large quantities of CH_4 are produced in the HZ. Stable isotope measurements of CH_4 suggest that hydrogenotrophic methanogenesis represents a dominant pathway for CH_4 production in the HZ of the river Moosach, while a relatively high abundance of a novel group of methanogenic archaea, the *Candidatus* "Methanomethyliales" (phylum *Candidatus*

"Verstraetearchaeota"), indicate that CH_4 production through H_2-dependent methylotrophic methanogenesis might also be an important CH_4 source. Combined isotopic and modeling results clearly implied CH_4 oxidation processes at one of the sampled locations, but due to the steep chemical gradients and the close proximity of the oxygen and nitrate reduction zones no single electron acceptor for this process could be identified. Nevertheless, the numerical modeling results showed potential not only for aerobic CH_4 oxidation, but also for anaerobic oxidation of CH_4 coupled to denitrification. In addition, the nitrate–methane transition zone was characterized by an increased relative abundance of microbial groups (Crenothrix, NC10) known to mediate nitrate and nitrite-dependent methane oxidation in the hyporheic zone. This study demonstrates substantial CH_4 production in hyporheic sediments, a potential for aerobic and anaerobic CH_4 oxidation, and underlines the high spatiotemporal variability in this habitat.

5.1 Introduction

At the United Nations Climate Change Conference 2021 (COP26) in Glasgow over 100 countries signed the Global Methane Pledge, an agreement to reduce CH_4 emissions by 30 % by 2030 compared to 2020 levels (European Commission and United States of America, 2021). CH_4 has been estimated to account for 20 % of Earth's warming (Kirschke et al., 2013), and atmospheric methane concentrations have increased with a significant acceleration in recent years (Nisbet et al., 2019). The largest source of uncertainty in global CH_4 budgets are natural emissions (Saunois et al., 2020). Although rivers and streams represent only a small fraction of surface waters, they contribute considerable amounts of CH_4 to atmospheric concentrations (Saunois et al., 2020). Based on the evaluation of 385 globally distributed sites, rivers and streams are expected to emit 27 Tg CH_4 yr^{-1} (Stanley et al., 2016) which is equal to 756 Tg CO_2 equivalents (IPCC, 2013) and constitutes approximately 17 % of freshwater emissions and 7 % of all natural sources (Saunois et al., 2020).

In rivers and streams CH_4 production is a microbially driven process concentrated in anaerobic sediments of the hyporheic zone (HZ) (Trimmer et al., 2012). The HZ represents a spatially and temporarily dynamic saturated subsurface layer where stream water enters a river's bed and banks and is a zone known for high biogeochemical activity (Findlay, 1995; Winter et al., 1998). Hyporheic exchange delivers electron acceptors such as oxygen (O_2), nitrate (NO_3^-), and sulfate (SO_4^{2-}), as well as nutrients and organic carbon (OC) to the HZ, where microbially mediated transformation reactions take place (Boano et al., 2014). After dissolved O_2 is consumed, other terminal electron acceptors become dominant in consecutive zones of denitrification; mangangese (Mn), iron (Fe) and SO_4^{2-} reduction; and finally, CH_4 production (methanogenesis) (Canfield & Thamdrup, 2009).

CH_4 is produced by methanogens, strictly anaerobic archaea that thrive where the environment is deprived of light; NO_3^-; and SO_4^{2-} (Deppenmeier, 2002). Two metabolic pathways dominate CH_4 production in natural environments, hydrogenotrophic and acetoclastic methanogenesis (Conrad, 2005). Diffusing upwards from anaerobic sediments, CH_4 can be oxidized to CO_2 by methanotrophic microorganisms before reaching the atmosphere. The most abundant methanotrophs are aerobic methanotrophic Proteobacteria (Nazaries et al., 2013), but when the environment is depleted in O_2, other electron acceptors such as NO_3^- and NO_2^- can be utilized in anaerobic oxidation of methane (AOM). Archaea from the ANME-2d clade like *Candidatus*

"Methanoperedens nitroreducens" (*M. nitroreducens*) couple NO_3^- reduction with CH_4 oxidation (Arshad et al., 2015; Haroon et al., 2013). Bacteria of the genus *Candidatus* "Methylomirabilis" of the NC10 phylum use NO_2^- as an electron acceptor (Ettwig et al., 2010). Oswald et al. (2017) and Kits et al. (2015) found indications that *Crenothrix* and *Methylomonas denitrificans* are facultative anaerobic methanotrophs consuming NO_3^- in O_2-depleted environments. Methane oxidation coupled to denitrification has been shown to occur in many freshwater environments including lakes (Deutzmann et al., 2014; Einsiedl et al., 2020; Norði & Thamdrup, 2014; Oswald et al., 2017; Peña Sanchez et al., 2022b), reservoirs (Naqvi et al., 2018) and wetlands (Hu et al., 2014; Shen et al., 2017; Zhang et al., 2018). AOM can also be coupled to the reduction of sulfate (S-DAMO, sulfate-dependent anaerobic methane oxidation) and the metals Fe and Mn (M-DAMO) (Beal et al., 2009). Evidence has accumulated that S-DAMO occurs in freshwater habitats (Ng et al., 2020; Norði et al., 2013; Segarra et al., 2015; van Grinsven et al., 2020) despite the low energy yield and typically low SO_4^{2-} concentrations.

Several recent studies have addressed the question as to which predictors best explain the spatiotemporal variability in methanogenesis and CH_4 oxidation in rivers and streams. For example, Shen et al. (2019a) compared potential AOM activity in different river sediments under laboratory conditions and found that the addition of NO_3^-, NO_2^-, SO_4^{2-} and Fe^{3+} could provoke AOM activity in sandy river beds, while no AOM could be stimulated in gravelly river beds. This is in line with findings by Shelley et al. (2015) and Bodmer et al. (2020), who measured increasing CH_4 production and oxidation capacity with decreasing grain diameter. Other parameters stimulating CH_4 production and oxidation in streams are high organic carbon contents (Bednařík et al., 2019; Bodmer et al., 2020; Romeijn et al., 2019) and shading (Shelley et al., 2017). Further, methanogenic and methanotrophic activity in river sediments has been found to increase with rising temperature (Comer-Warner et al., 2018; Shelley et al., 2015).

While all these studies quantified potential CH_4 production and oxidation rates in laboratory incubation experiments, only a few studies have measured vertical geochemical gradients on site to investigate the depth distribution of redox zones in stream beds in the context of CH_4 cycling. Exceptions are for example the work of Villa et al. (2020), who measured vertical profiles of CH_4, CO_2 and N_2O at different beach positions and water stages to examine the relation of hyporheic exchange and greenhouse gas (GHG) emissions, and Ng et al. (2020), who showed that S-DAMO could reduce CH_4 concentrations in a wetland-stream system by interpreting vertical geochemical profiles with a multicomponent reactive transport model. Yet, spatial patterns of methanogenic and CH_4 oxidation zones in the HZ remain largely unexplored. Therefore, more field data are required to accurately describe how much CH_4 is produced and consumed in streams, and under which conditions.

Attempting to fill this knowledge gap, we measured high-resolution depth-resolved geochemical profiles at different locations in a stream bed to study the spatial patterns of CH_4 production and oxidation and to investigate the potential for AOM. As our study site we chose the HZ of a stream dominated by fine, organic-rich sediments that has a high potential to form and emit substantial amounts of CH_4. To support the interpretation of vertical concentration profiles of O_2, NO_3^-, NO_2^-, SO_4^{2-} and CH_4 we measured stable carbon-isotopes of CH_4. In addition, quantitative polymerase chain reaction (qPCR) and sequencing of 16S rRNA genes were performed on a sediment core at one of the locations. The one-dimensional numerical

modeling software PROFILE (Berg et al., 1998) was used to support the interpretation of the measured geochemical profiles.

5.2 Materials and methods

5.2.1 Site characterization and determination of sediment properties

Five different sites in the hyporheic zone of the river Moosach in southern Germany were chosen for the sampling campaigns in 2020 and 2021. The river Moosach is a groundwater-fed stream with a topographic catchment area of 175 km^2 which originates in two moor drainage ditches north of the city of Munich and runs along the border of two contrasting geological landscapes, the Tertiary Hill Country on the left and the Munich gravel plain on the right bank (Auerswald & Geist, 2018; Pulg et al., 2013). The river water can be characterized as a calcium-magnesium-bicarbonate type with elevated concentrations of chloride. Stream water chemistry is further characterized in Sec. A.1 of the Supplement. Upstream of the points of measurement, the river crosses the "Freisinger Moos", a heavily drained lowland moor area (Zehlius-Eckert et al., 2003). Human activities like damming, diversions and straightening measures have significantly altered the natural course and hydrological behavior of the Moosach since the Middle Ages (Pulg et al., 2013). The discharge is controlled by weirs and check dams leading to stable hydrologic conditions.

Impoundments nowadays constitute about one-third of the river's length, leading to a decreased gradient, flow velocity and shear stress (Pulg et al., 2013). The river Moosach is subject to colmation and siltation: 51 % of the gravel bed is covered with fine deposits (Auerswald & Geist, 2018). Auerswald and Geist (2018) performed an extensive study on the composition of these fine deposits in the river Moosach and found that on average 46 % were carbonates dominated by calcite, 38 % were silicates and 16 % were organic matter. Macrophytes cover approximately 15 % of the riverbed which decreases average flow velocity due to increased hydraulic roughness (Braun et al., 2012). Braun et al. (2012) found average flow velocities above ground of 0.11 and 0.16 $m\,s^{-1}$ in cross sections with and without macrophytes, respectively.

The sampling sites are situated in the middle section of the river where the energy slope drops below the average of 1.3 ‰ to as low as 0.1 ‰ in some places and where fine deposits predominate (Auerswald & Geist, 2018). Stream water temperatures as recorded at a monitoring station of the Bavarian State Office of the Environment (2023) 4.5 km downstream of the sampling sites are on average between 6.2 °C in January and 16.3 °C in July. The annual mean discharge of the Moosach is 2.46 $m^3\,s^{-1}$; low-flow conditions generally prevail between July and September, and high-flow events are more common in winter and spring. Detailed information on stream discharge and surface water temperatures during the sampling period is given in Fig. A.1 in the Supplement.

A schematic map of the five sampling locations and their placement in the river cross section is given in Fig. 5.1a and b. At this section, the river Moosach is typically 10-12 m wide with a maximum water depth of approximately 1.3-1.4 m. On each site, a geochemical pore-water profile was recorded as described in Sec. 5.2.2, and sediment grain size distributions were determined. Additionally, basic chemical parameters of the surface water (temperature,

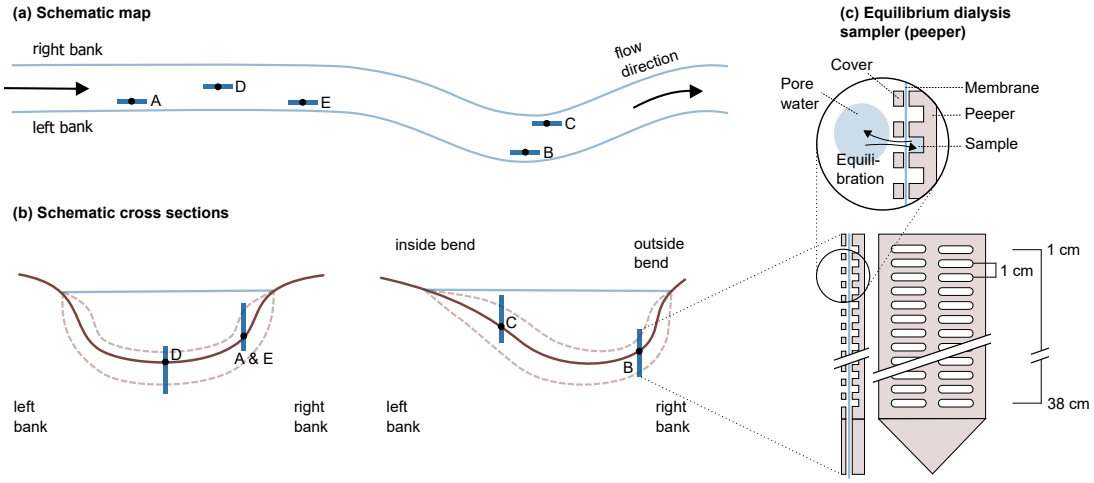

Figure 5.1: **Schematic representation of the five sampling sites along the river (a) and across the riverbed (b).** In panel (c), the sampler is schematically drawn, modified after Teasdale et al. (1995) (top: detail, bottom left: side view, bottom right: front view; for clarity, only 12 of the 38 chambers are illustrated).

dissolved oxygen concentration, pH and electrical conductivity) were measured on each sampling day. For location C, an additional sediment core was taken for microbiological analyses.

Detailed information on sampling periods, surface water chemistry and sedimentary composition of each sampling site is given in Sec. A.1. In short, at each site a high-resolution geochemical profile was measured with an equilibrium dialysis sampler (peeper) which remained in the sediment for at least 3 weeks. Sediment composition was analyzed with sieve-slurry analyses following the DIN EN ISO 17892-4 standard (Fig. A.2). With 65-75 % silt and clay, the most fine-grained material was found on the right banks at locations A and E. On the outside bend of the right bank (location B), a clear stratification was found with gravel between 0-11 cm depth and sandy silt below. Deposits at location C consisted of 60-63 % silt and clay. At location D, central in the river, sand had the main fraction with 66-79 %.

5.2.2 Pore-water sampling with a sediment peeper

High-resolution geochemical depth profiles were obtained at each sampling site with an in situ equilibrium dialysis sampler (peeper) as described by Hesslein (1976) (see Fig. 5.1c). The body of the peeper was equipped with two rows of 38 chambers with a spatial depth resolution of 1 cm. All chambers were filled with deionized water, covered with a semi-permeable polysulfone membrane with a pore diameter of 0.2 µm (Pall Corporation, Dreieich, Germany), and fixed with a Plexiglas cover and plastic screws. At each sampling site, the peeper was pushed manually into the stream bed until most chambers were buried in the sediment and only the uppermost chambers had contact with river water. To minimize flow disturbance, peepers were oriented longitudinally to the flow direction as indicated in Fig. 5.1a.

An equilibrium between the water in the chambers and the surrounding pore water was obtained by diffusion of dissolved molecules through the membrane during a time period of at least 3

weeks. This exceeds the recommended equilibration time of a minimum of 2 weeks (Teasdale et al., 1995). The extended equilibration time was chosen to allow for recovery of natural geochemical gradients after the disruption caused by placing the peeper. Pore-water samples represent an average of pore-water concentrations during the sampling period and diurnal or other short-term temporal fluctuations during this time cannot be detected.

For sampling, the peeper was removed from the sediment and cleaned with deionized water. The first column of chambers was used for oxygen measurements and withdrawal of samples for determination of ion concentrations, and the second column was used for CH_4 concentration measurements and analyses of stable carbon isotopes of CH_4. A Clark-type microsensor (Unisense A/S, Aarhus, Denmark) was pierced through the membrane for immediate measurements of dissolved O_2 in the field. The O_2 measurements were conducted on site within 10 min after removal of the peeper from the sediments to avoid contamination with atmospheric O_2. Liquid samples were then drawn from the same chambers with 5 ml syringes.

The 10 ml glass vials for CH_4 concentration measurements and stable carbon isotope analysis (δ^{13}C–CH_4) were prepared in the laboratory with 20 µl 10 M NaOH, sealed with rubber butyl stoppers and flushed for at least 2 min with synthetic air (O_2, N_2) to remove background atmospheric CH_4. Immediately before sample injection, a small needle was pushed through the stoppers to allow pressure exchange. Subsequently, with a syringe and needle samples were injected slowly along the side of the vial to avoid degassing. Both needles were removed directly after sample injection. To avoid CH_4 losses to the atmosphere through the membrane, sampling was conducted quickly within 15 min after removal from the sediment. Nevertheless, small amounts of CH_4 could diffuse out through the membrane or escape during sample injection and thus, measured CH_4 concentrations might be slightly underestimated. Samples for ion concentrations were collected in 1.5 ml glass vials and prepared with 10 µl 0.5 M NaOH for anion analysis (Cl^-, NO_3^-, NO_2^-, SO_4^{2-}) or 10 µl 1 M HNO_3 for cation analysis (NH_4^+). All samples were withdrawn within 45 min after removal of the peeper. The samples were transported to the laboratory in a cooler and stored refrigerated prior to analysis.

5.2.3 Chemical and isotopic analyses

Anion and cation measurements

Anion and cation concentrations were determined using ion chromatography, specifically a system of two Dionex ICS-1100 (Thermo Fisher Scientific, Dreieich, Germany) equipped with Dionex IonPac^{TM} AS9-HC and CS12A columns for anion and cation separation, respectively. Measurements were performed in triplicates and evaluated on the basis of seven concentration standards (Merck KGaA, Darmstadt, Germany). Concentrations are given as mean values of the triplicates. Analytical uncertainty was $<$10 % and detection limits were 0.020 mmol L^{-1} for Cl^-, 0.012 mmol L^{-1} for NO_3^-, 0.007 mmol L^{-1} for NO_2^-, 0.008 mmol L^{-1} for SO_4^{2-} and 0.005 mmol L^{-1} for NH_4^+.

CH_4 concentrations and δ^{13}C measurements of CH_4

Methods for CH_4 sampling and concentration measurements are further developments of standards introduced by the EPA (2001). Sample vials were equilibrated in a water bath at 30 °C for at least 2 h before measurements of headspace CH_4 concentrations with a TRACE

1300 Gas Chromatograph (GC) (Thermo Fisher Scientific, Dreieich, Germany). The GC was equipped with a TG-5MS column and flame ionization detector (FID) and calibrated with three standards (Rießner Gase GmbH, Lichtenfels, Germany). Triplicate measurements were performed through manual injection of 250 µL headspace gas. Total CH_4 concentrations in the water and gas phase of the sample vials were calculated with Henry's law according to the equilibrium headspace method first described by Kampbell and Vandegrift (1998).

The same sample vials were used for measuring $^{12}C/^{13}C$ ratios of CH_4 with cavity ring-down spectroscopy (CRDS), specifically the G2201-i gas analyzer with a Small Sample Introduction Module (SSIM) (Picarro Inc., Santa Clara, CA, USA) calibrated with two standards (Airgas, Plumsteadville, PA, USA). Reliable results could only be obtained for headspace CH_4 concentrations > 30 ppm. This threshold concentration was found in previous experiments (Sec. A.2). Due to the small available gas volume in the headspace of approximately 7 mL, dilution with synthetic air was necessary and CH_4 concentrations in the analyzer decreased while repeating measurements. Values were only adopted when at least two of three measurements were above the threshold concentration. The standard δ notation is used for representing the results according to Eq. 5.1 relative to the VPDB (Vienna Pee Dee Belemnite) standard.

$$\delta(‰) = \left(\frac{\mathrm{R_{Sample}}}{\mathrm{R_{Standard}}} - 1 \right) \cdot 10^3 \tag{5.1}$$

5.2.4 Inverse modeling of concentration gradients

The one-dimensional numerical modeling software PROFILE, introduced by Berg et al. (1998), was used to support the interpretation of measured geochemical profiles. The software provides an objective procedure for finding the simplest production–consumption profile which accurately represents the measured concentration gradients. For this, concentration profiles are divided into different zones with constant production–consumption rates. Then, several best-fit results are produced by minimizing the sum of squared deviations (SSD), each representing a different number of these zones. Finally, best fits are compared using statistical *F* testing for finding the lowest number of zones which best describe the data.

The model assumes concentration gradients to represent a steady state (Berg et al., 1998), which neglects the fact that reaction rates in the HZ show temporal variability (Marzadri et al., 2012). However, the pore-water samples obtained with the sediment peeper represent a time-averaged state during the total sampling period of at least 3 weeks. The relative contribution of short-term fluctuations decreases with the length of the averaged time. Therefore, as a first approximation we assume that after 3 weeks this dynamic component is small particularly in the deeper HZ and can be neglected.

Boundary conditions (BCs) were set as follows: for O_2, NO_3^- and SO_4^{2-} a fixed concentration was set at the top, and a zero-flux BC was set at the bottom of the profile; for CH_4 a fixed concentration and zero-flux BC were set at the top of the profile, similar to what was used by Norði and Thamdrup (2014). Positive production rates were only allowed for SO_4^{2-} and CH_4 while for O_2 and NO_3^- only negative rates (consumption) were permitted. Bioturbation and irrigation were neglected. Molecular diffusion coefficients in water D^0 ($m^2\,s^{-1}$) were calculated based on Boudreau (1997) as a function of the average water temperature during

the equilibration period. Sediment diffusion coefficients D_S were determined as a function of D^0 based on an empirical relation (Iversen & Jørgensen, 1993). More details and calculated diffusion coefficients D^0 and D_S are given in Sec. A.3.

5.2.5 DNA extraction, qPCR and 16S rRNA gene sequencing

At location C, an additional sediment core was taken for depth-resolved microbiological analyses via DNA extraction, quantitative PCR and 16S rRNA gene sequencing. For this, a coring tube with an inner diameter of 42 cm was cut open lengthwise, cleaned with ethanol and distilled water and closed again with tape. The core was taken by manually pushing the tube into the sediment right next to the peeper, pulling it out and transferring it to the laboratory. There, the tape was removed for opening the tube and allowing access to the sediment core. The sediment was split into 10 subsamples with a resolution of 2 cm in the upper 12 cm depth and 3 cm below. All samples were immediately frozen and stored at -22 °C until further analysis.

For each sampled depth, we performed four biological replicates of DNA extraction. Total DNA was extracted from 0.5 g of sediment as previously described (Vuillemin et al., 2019). DNA templates were diluted to 1:100 in ultrapure PCR water (Roche, Germany) and used in qPCR amplifications with updated 16S rRNA gene primer pair 515F (5'- GTG YCA GCM GCC GCG GTA A -3') and 806R (5'- GGA CTA CNV GGG TWT CTA AT -3') to increase our coverage of archaea and marine clades and run as previously described (Pichler et al., 2018). All qPCR reactions were set up in 20 µL volumes with 4 µL of DNA template, 20 µL SsoAdvanced Universal SYBR Green Supermix (Bio-Rad, Feldkirchen, Germany), 4.8 µL nuclease-free H_2O (Roche, Germany), 0.4 µL primers (10 µM; biomers.net) and 0.4 µL $MgCl_2$ and carried out on a CFX Connect qPCR machine for gene quantification. For 16S rRNA genes, we ran 40 PCR cycles of two steps corresponding to denaturation at 95 °C for 15 s, annealing and extension at 55 °C for 30 s. All qPCR reactions were set up in 20 µL volumes with 4 µL of DNA template and performed as previously described (Coskun et al., 2019). Gel-purified amplicons of the 16S rRNA genes were quantified in triplicate using a Quant-iT dsDNA reagent (Life Technologies, Carlsbad, CA, USA) and used as a standard. An epMotion 5070 automated liquid handler (Eppendorf, Hamburg, Germany) was used to set up all qPCR reactions and to prepare the standard curve dilution series spanning from 10^7 to 10^1 gene copies. Reaction efficiency values in all qPCR assays were between 90 % and 110 % with R^2 values > 0.95 for the standards.

For 16S rRNA gene library preparation, qPCR runs were performed with barcoded primer pair 515F and 806R as described previously (Pichler et al., 2018). In brief, 16S rRNA gene amplicons were purified from 1.5 % agarose gels using the QIAquick Gel Extraction Kit (Qiagen, Hilden, Germany), quantified with the Qubit dsDNA HS Assay Kit (Thermo Fisher Scientific, Dreieich, Germany), normalized to 1 nM solutions and pooled. Library preparation was carried out according to the MiniSeq System Denature and Dilute Libraries Guide (Illumina, San Diego, CA, USA). Sequencing was performed on the Illumina MiniSeq platform at the GeoBio-Center$^{\mathrm{LMU}}$. We used USEARCH version 10.0.240 for MiniSeq read trimming and assembly, OTU (operational taxonomic unit) picking and 97 % sequence identity clustering (Edgar, 2013), which, as we showed previously, captures an accurate diversity represented within mock communities sequenced on the same platform (Pichler et al., 2018). OTU representative sequences were identified by BLASTn (nucleotide-nucleotide basic local alignment search tool)

searches against SILVA database version 132 (Quast et al., 2012). To identify contaminants, 16S rRNA genes from extraction blanks and dust samples from the lab were also sequenced in triplicate (Pichler et al., 2018). These 16S rRNA gene sequences were used to identify any contaminating bacteria (e.g. *Acinetobacter*, *Bacillus*, *Staphylococcus*) and selectively curate the OTU table.

5.3 Results and discussion

5.3.1 Concentration profiles show steep geochemical gradients and the formation of a complex redox zonation

The geochemical profiles obtained in the HZ of the river Moosach are shown in Fig. 5.2. The total depth of the profiles depended on how deep the peeper was pushed into the ground and varied between 27 cm and 38 cm. Above the sediment–water interface, in-stream concentrations were 270-300 µmol L^{-1} for dissolved O_2, 280-380 µmol L^{-1} for NO_3^-, 240-360 µmol L^{-1} for SO_4^{2-} and 1270-1650 µmol L^{-1} for Cl^-. Surface water concentrations as measured on the day of sampling are displayed as vertical beams above the sediment–water interface in Fig. 5.2.

Land use in the catchment is predominantly agriculture, and leaching of fertilizers presumably adds NO_3^- to river and groundwater, but values stayed clearly below the threshold of the EU Nitrates Directive of 50 mg L^{-1} (806 µmol L^{-1}). SO_4^{2-} concentrations in the surface water were strikingly high for a freshwater river, especially in spring. Groundwater in the quaternary aquifer, the groundwater body hydraulically connected to the river, showed SO_4^{2-} concentrations between 448 and 573 µmol L^{-1} during 2007-2020 as measured in an observation well approximately 1.6 km southwest of the sampling sites (Bavarian State Office of the Environment, 2023). Peat can contain substantial amounts of carbon-bonded sulfur and pyritic sulfides (Casagrande et al., 1977; Spratt Jr et al., 1987), and SO_4^{2-} can be released due to pyrite and organic matter oxidation (Vermaat et al., 2016), likely so in the drained moor areas in the foothills of the Munich gravel plain that the river Moosach crosses. In an agricultural watershed sulfur fertilizers can also be a source of elevated SO_4^{2-} concentrations in shallow aquifers (Spoelstra et al., 2021).

Below the sediment–water interface dissolved O_2 concentrations decreased within a few centimeters in all sampled profiles and remained at $<$10 µmol L^{-1} deeper down with only a few exceptions. Steep O_2 gradients and anoxic conditions just below this narrow aerobic zone were to be expected because the river Moosach is strongly altered by human engineering including controlled discharge conditions; a very low gradient; slow flow velocities; and deposits of fine, organic-rich materials. In profile B, O_2 concentrations were higher compared to all other sites (20-80 µmol L^{-1} below 3 cm depth). This may be due to higher surface water influxes in the coarser gravelly sediment as opposed to the fine deposits found at the other sites. However, even at 10-20 cm depth, where CH_4 concentrations peaked in a sedimentary layer dominated by silt, O_2 was present at concentrations between 20 and 60 µmol L^{-1}. These high O_2 concentrations appear to be rather implausible in this zone where CH_4 is produced through methanogenesis, a strictly anaerobic process. An explanation could, however, be a contamination with atmospheric O_2 during field measurements. Similarly, profile D shows anomalies in the O_2 data with concentration peaks at 23-26 cm, 30 cm and 33 cm depth.

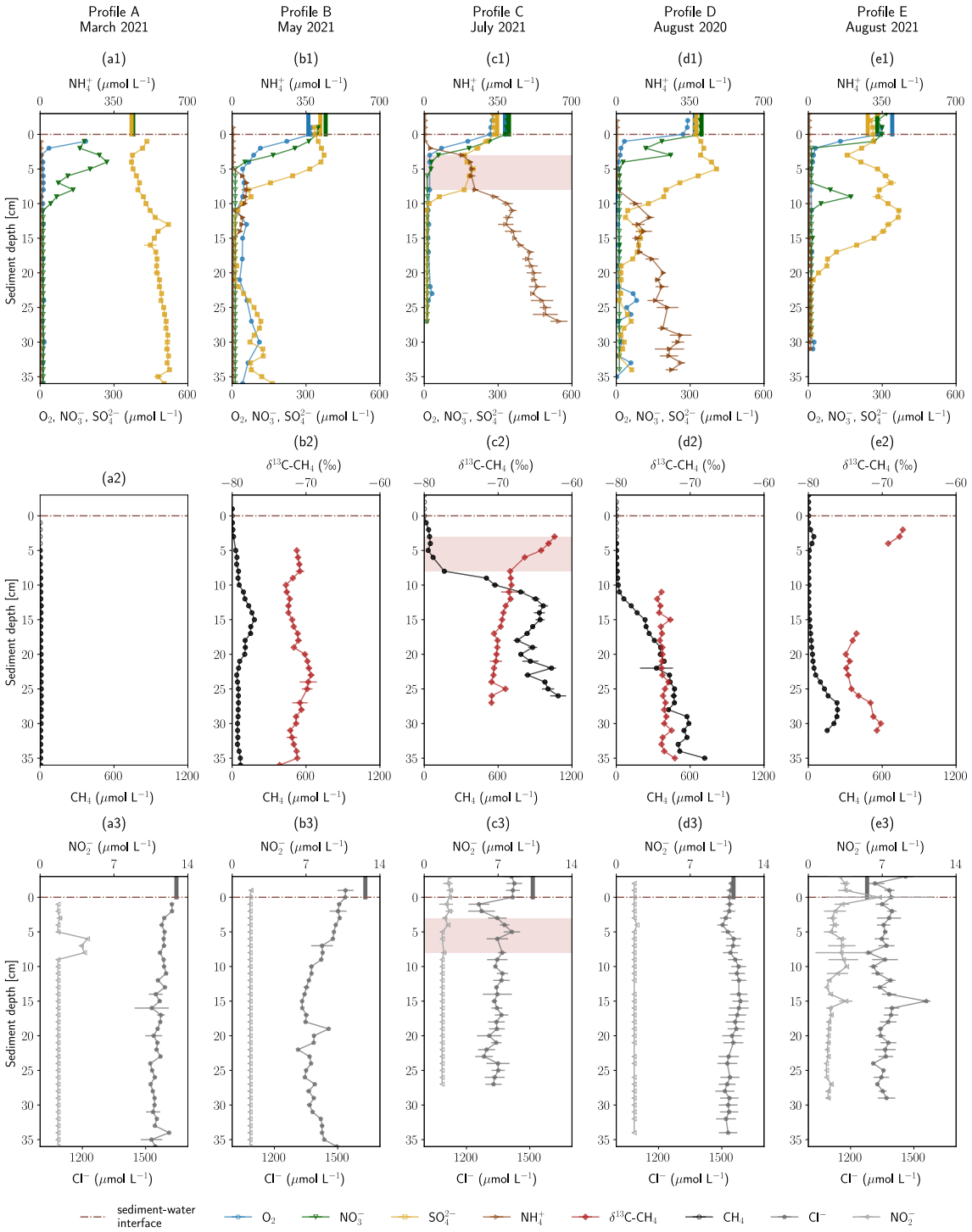

Figure 5.2: **Depth-resolved profiles of hyporheic pore-water geochemistry at five sampling sites.** Panels (a1) to (e1) show O_2, NO_3^-, NH_4^+ and SO_4^{2-} concentrations. Panels (a2) to (e2) show CH_4 concentrations and δ^{13}C–CH_4 values. Panels (a3) to (e3) show NO_2^- and Cl^- concentrations. Empty markers indicate values outside the range of used standards. Error bars show standard deviations of independent measurements (n=3). Vertical lines above the sediment–water interface are concentrations measured in the surface water at the sampling date. Red background color highlights an enrichment in δ^{13}C–CH_4. Profiles are ordered by season.

These may also be attributed to measurement artifacts since they are located deep in the methanogenic zone where strictly anoxic conditions generally prevail.

Similar to dissolved O_2, NO_3^- concentrations decreased from 280-380 µmol L^{-1} in river water to concentrations of $<$12 µmol L^{-1} (detection limit) within a few centimeters. In contrast, the conservative tracer Cl^- did not disappear in a comparable manner, which may demonstrate that microbial consumption and not dilution or mixing was responsible for the development of these steep chemical gradients. A peak of NO_2^- in profile A exactly where the NO_3^- gradient is located (6-8 cm) indicates bacterial NO_3^- reduction to NO_2^-, possibly as an intermediate in denitrification (Fig. 5.2a3). In profiles B-E O_2 reduction and denitrification zones were very close and both gradients overlapped. Oxygen reduction and denitrification zones seem to be only millimeters wide, similar to what was described for other freshwater sediments in the literature (Raghoebarsing et al., 2006). In profile D a peak between 8-10 cm depth with a maximum of 173 µmol L^{-1} stands out that coincides with a reduction in SO_4^{2-} concentrations.

SO_4^{2-} concentration profiles showed some distinctive features. In profiles A and B, concentrations slightly increased towards the bottom of the profile. This could be connected to the intrusion of upwelling, reduced groundwater with a higher SO_4^{2-} concentration compared to surface water. Rising Cl^- concentrations in the lower third of profile B support this interpretation, since they reach 1491 µmol L^{-1}, a value very similar to groundwater Cl^- concentrations of 1440-1495 µmol L^{-1} in recent years (2016-2020) (Bavarian State Office of the Environment). Further, in profiles B and D, SO_4^{2-} concentrations increased in the upper parts of the profiles in 0-3 cm and 0-5 cm depth, respectively, and also in profile E between 3-7 cm and 9-11 cm depth. Here, a biogeochemical source, for example re-oxidation of H_2S traveling upwards from more reduced zones, could explain the observed trends. Below, in 3-11 cm (profile B), 5-11 cm (profile C) and 12-22 cm depth (profile E), concentrations declined, potentially through bacterial SO_4^{2-} reduction. This interpretation is supported by a sulfidic smell during sampling. Interestingly, in profile C SO_4^{2-} concentrations decreased significantly not only between 8-11 cm but also between 0-3 cm depth, concurrently with decreases in O_2 and NO_3^- concentrations. One possible interpretation is a dilution effect at the clogged sediment surface, as also suggested by simultaneous decreases in Cl^- (Fig. 5.2c3) and Ca^{2+} (data not shown) concentrations. But the data could also show the co-occurrence of oxic and anoxic micro-niches in close proximity, a situation that has also been described previously (Storey et al., 1999; Triska et al., 1993).

NH_4^+ concentrations in most profiles (C-E) consistently increased with sediment depth. While maximal concentrations in profiles C and D were 116 µmol L^{-1} and 308 µmol L^{-1}, respectively, in profile C values reached a level of $>$1000 µmol L^{-1}. During biodegradation of organic matter, NH_4^+ is released when nitrogenous compounds are transformed through ammonification (Ladd & Jackson, 1982). Increases with depth show progressive decomposition, and high NH_4^+ concentrations can be seen as a proxy for a high content of microbially degraded organic matter in the sediment. Thus, organic carbon content seems to be significantly lower in location E compared to C and D. In location A, NH_4^+ concentrations even stayed below the detection limit ($<$5 µmol L^{-1}). Profile B has elevated NH_4^+ concentrations in 6-14 cm depth and values below the detection limit elsewhere.

Similar to NH_4^+ concentrations, CH_4 concentrations generally increased with depth and were highest in profile C, followed by profile D. In profile A, where NH_4^+ concentrations were lowest compared to all other profiles, CH_4 concentrations stayed below 10 µmol L^{-1}. More complex

were the observed CH_4 gradients in profiles B and D. In profile B, CH_4 peaked at a concentration of 180 µmol L^{-1} in a sediment depth of 15 cm. Below, from 23 cm onwards, concentrations decreased and stayed around 50 µmol L^{-1}. CH_4 concentrations of profile E revealed a small peak (44 µmol L^{-1}) at 3 cm depth, showed very low concentrations of $<$10 µmol L^{-1} between 5-15 cm and rose again up to 237 µmol L^{-1} at a depth of 28 cm.

Generally, a tendency of increasing CH_4 concentrations with higher surface water temperatures can be observed. Profiles A and B, measured in spring, showed significantly lower CH_4 concentrations than those sampled in summer. However, comparing profiles C, D and E, all measured in summer, substantial differences in total CH_4 concentrations are eye-catching. By far the highest CH_4 concentrations were measured in July 2021 (T_M = 16.6 °C for profile C, Tab. A.2) although surface water temperatures were slightly lower than in August 2020 (T_M = 17.1 °C for profile D). Pore-water CH_4 concentrations did not exceed CH_4 saturation concentrations of at least 2.1 mmol L^{-1} (calculated using PHREEQC (Parkhurst and Appelo, 2013) for the mean surface water temperature during the sampling periods and respective water depths at each site) with only one exception. In profile C, a CH_4 concentration of 19.8 mmol L^{-1} was measured in 27 cm depth (not displayed in Fig. 5.2, since it is far out of the axes' range), which exceeds the saturation concentration by far and implies direct contact with a gas bubble. In addition, it must be mentioned that bubble formation is also possible at lower CH_4 partial pressures if microstructures are present or if CH_4 production occurs in small-scale local hotspots. In comparison, profile E, measured in August 2021, exhibits low concentrations despite the summer temperatures (T_M = 15.8 °C). Varying organic matter contents at the three sites might explain these differences and seems to be a determining parameter for total CH_4 production, as inferred from differences in NH_4^+ concentrations. When complex organic molecules are degraded by microbes, NH_4^+ is not only released, but also educts for methanogenesis like H_2, CO_2, acetate and methylated compounds like methanol (Capone and Kiene, 1988). The degradation of organic carbon is therefore a driver of methanogenesis, and we see a correlation between CH_4 and NH_4^+ concentrations (see Fig. A.4). This finding is also consistent with previous reports from stream sediment incubations (Bednařík et al., 2019; Bodmer et al., 2020; Romeijn et al., 2019).

Cl^- can be viewed as a conservative tracer. As mentioned above, one irregularity is a sudden concentration decrease in the first centimeters of profile C. This could show the effect of clogging because fine deposits fill the pore space and reduce hyporheic exchange. Interesting is also that Cl^- concentrations decrease in the middle section of profile B. Cl^- concentrations in profiles A, D and E do not exhibit any trends, fluctuations are highest in profile E.

5.3.2 Explaining redox zones with sediment heterogeneities and hyporheic exchange fluxes

Observed concentration profiles at the different stream sites showed distinct characteristics and were very heterogeneous. The divergence of the profiles becomes particularly clear when comparing profiles A and E that show hardly any similarities although they were sampled at two very similar sites. In March, where river water is well oxygenated with average surface water temperatures of 7.5 °C (profile A), SO_4^{2-} concentrations were high ($>$ 300 µmol L^{-1}) throughout the profile and almost no CH_4 was produced. In August (profile E), clear gradients in SO_4^{2-}

and CH_4 concentrations together with nearly constant Cl^- concentrations point towards a high activity of SRB (sulfate-reducing bacteria) and methanogens. As mentioned earlier, higher stream water temperatures in summer (profile E) could be the reason for higher microbial activity compared to early spring (profile A). However, the influence of temperature on GHG emissions from rivers has been discussed controversially. Increasing GHG production with rising temperatures was observed in laboratory incubations of river sediments (Comer-Warner et al., 2018; Shelley et al., 2015) while Silvennoinen et al. (2008) found that 55 % of all CH_4 emissions from the Temmesjoki River were released during winter time.

In our data, temperature alone may not explain the differences between the two profiles A and E. Concentration gradients in profile E do not follow the generally known redox zonation (Canfield & Thamdrup, 2009). The assumption that stream water enters the HZ at the sediment–water interface and that electron acceptors are consumed successively can explain neither the complex SO_4^{2-} dynamics nor the deep NO_3^- peak. A possible reason could be surface water entering the sediment bank from the side, maybe in a sandier layer, such that sample depths represent different and varying flow path lengths of hyporheic fluxes. This is further illustrated in Fig. 5.3e. Stream water entering the bank from the side could be an additional reason (besides cold temperatures and potentially low organic matter degradation) for low CH_4 levels in profile A (Fig. 5.3a). Figure 5.3 schematically shows the hypothesized sedimentary characteristics and potential hyporheic fluxes at all five sampling sites.

Sediment stratification and resulting hyporheic fluxes can also help in understanding profile B. In the top section, as would be expected, O_2, NO_3^- and SO_4^{2-} are consumed consecutively, and CH_4 concentrations rise, but below 15 cm depth, we see the reverse trends. A lens of fine material in an otherwise gravelly sediment would be a plausible explanation for this observation (Fig. 5.3b). In fact, very fine sediment was found below 11 cm depth, with gravel above, but the sediment core did not cover the lowest part of the profile (Sec. A.1). Hyporheic flow velocities outside the fine lens would be faster than inside, and thus, although path lengths at the bottom are longer, contact times have been shorter than in the central part of the profile. This would mean that we see the methanogenic zone in the central part and the sulfate reduction zone at the bottom of profile B, depending on the available time for reactions along the flow path.

Also profile C deviated from the commonly assumed redox zonation. Bacterial SO_4^{2-} reduction appeared to occur concurrently with O_2 reduction and denitrification, possibly in co-occurring oxic and anoxic zones (Storey et al., 1999). Alternatively, this may be caused by dilution effects in the upper centimeters of the profile. Also unexpected were stagnating SO_4^{2-} concentrations with a slightly convex concentration gradient between 3-8 cm depth. There might be an additional SO_4^{2-} source, maybe recycling of reduced sulfur species from deeper zones or some cryptic sulfur cycling as has been suggested in the context of S-DAMO in freshwater environments (Ng et al., 2020; Norði et al., 2013). But also here, heterogeneous flow paths, for example due to wood and plant parts, could affect measured profiles such that water travel times do not linearly increase with depth.

The profile most clearly following the thermodynamic sequence was profile D. Here, O_2 was consumed first, followed by NO_3^- and SO_4^{2-}. Only after all other electron acceptors were consumed, CH_4 concentrations began to rise with depth.

When discussing the influence of hyporheic fluxes on redox zonation, it needs to be noted that not only spatial heterogeneities but also temporal dynamics may play a key role. For example,

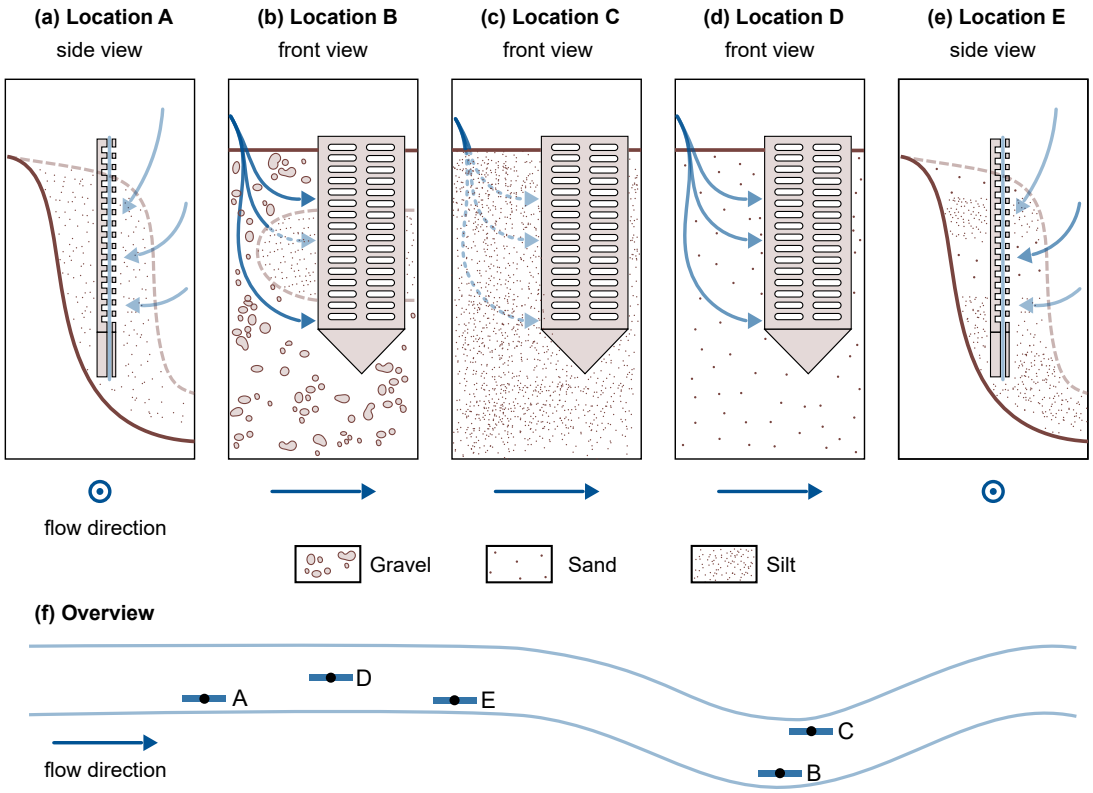

Figure 5.3: **Schematic representation of potential hyporheic flow paths (blue arrows) at the five sampling sites.** For locations A and E, a side view was chosen, and for locations B, C and D a front view was used. Where the front view is shown, flow direction in the river is from left to right, and where the side view is shown, flow direction is out of the drawing plane. The color strength of the arrows corresponds to the expected magnitude of hyporheic fluxes. The sediment composition is schematically indicated. Quantitative data on the sediment composition at the five locations can be found in Sec. A.1.

extreme events can alter the chemistry of infiltrating surface water, as well as hyporheic flow path lengths and residence times, thus impacting hyporheic geochemistry in multiple ways (Zimmer & Lautz, 2014). In this study in particular, location C might have been impacted by two high-flow events during the sampling period. Further, seasonal changes in river-groundwater mixing can potentially impact redox conditions and microbial populations (Danczak et al., 2016). However, fine sediments have been shown to reduce hyporheic exchange (Sunjidmaa et al., 2022). The combination of very fine deposits and stable, controlled hydrologic conditions is expected to limit hyporheic exchange and may also temper temporal dynamics in the HZ of the river Moosach.

5.3.3 Stable carbon isotopes of CH_4 reveal the importance of hydrogenotrophic methanogenesis and the roles of diffusive versus biotic processes in reducing CH_4 concentrations beneath the sediment surface

Figure 5.2 also shows δ^{13}C–CH_4 values for Profiles B-E in panels a2 to e2. CH_4 concentrations at location A were too low for isotopic analyses. In profile B, δ^{13}C–CH_4 values were on average -74 ‰. δ^{13}C–CH_4 values were very similar, but slightly shifted in a range of $<$3 ‰ with an increasing trend (top to bottom) between 5-8 cm and 10-23 cm depth and a decreasing trend between 8-12 cm and 23-31 cm depth. These variations were too small to be taken as an indication for any microbially mediated processes and could be explained by diffusion controlled isotope fractionation.

In profile C on the other hand, two sections are clearly evident (see Fig. 5.2c2). From bottom to top, between 27 cm and 8 cm depth, δ^{13}C–CH_4 values increased almost linearly from -71 ‰ to -69 ‰; then the slope changed abruptly and an isotopic enrichment from -69 ‰ to -62 ‰ can be seen between a sediment depth of 8 cm and 3 cm. Isotopically lighter $^{12}CH_4$ is transported and consumed faster than heavier $^{13}CH_4$, which leads to an isotopic enrichment of the remaining CH_4 pool in the heavier $^{13}CH_4$ (Whiticar et al., 1986). This isotopic shift towards heavier isotopes from 8 cm to 3 cm combined with decreasing CH_4 concentrations, therefore, clearly indicates microbial CH_4 consumption. Interestingly, the measured O_2 gradient lied above this zone (0-3 cm depth), while denitrification potentially occurred in exactly this depth (0-5 cm), and SO_4^{2-} concentrations stagnated around 176 µmol L^{-1} in 3-8 cm depth. Inverse modeling and the microbial community distribution at location C may help in interpreting the details of CH_4 oxidation as outlined in detail below (Sec. 5.3.4 and 5.3.5). The zone of $^{13}CH_4$ enrichment in profile C, where CH_4 oxidation is inferred, is highlighted by a red background color in Fig. 5.2 & 5.4 to visually help in differentiating this zone from the rest of the profile. The slight isotopic enrichment of δ^{13}C–CH_4 of a few per mil below, between 27 cm and 8 cm depth, is likely affected by diffusion-controlled stable isotope fractionation. It is striking that CH_4 concentrations steeply decrease already between 12 cm and 8 cm depth, beneath the zone of strong $^{13}CH_4$ enrichment. Apparently, microbial consumption only impacts the upper part of the gradient, while diffusive transport shapes the lower part of the gradient.

In profile D, δ^{13}C–CH_4 values were on average -71 ‰, and the isotopic composition stayed nearly constant. At least above 10 cm depth, where CH_4 concentrations were high enough for repeated isotope measurements, results suggest that microbial CH_4 oxidation did not play a key role in removing CH_4 from the HZ at location D. In profile E, reliable δ^{13}C–CH_4 values

could only be obtained in 2-4 cm and 17-21 cm depth. In the upper zone, values lay between -67 ‰ and -69 ‰, and in the lower zone, they were between -71 ‰ and -75 ‰, with a tendency towards less negative values in the lowest part of the profile. Since differences between isotope values at the top and the bottom were within a few per mil and there is a large data gap between 5-16 cm, data interpretations are difficult. The slightly heavier carbon isotopes of CH_4 at the top of the profile may be an indication for aerobic or anaerobic oxidation, but there is no additional evidence for this interpretation.

A kinetic isotope effect also occurs during CH_4 production and is larger for hydrogenotrophic than for acetoclastic methanogenesis (Krzycki et al., 1987). Here, δ^{13}C–CH_4 values in the methanogenic zone were consistently lower than -60 ‰, which is characteristic for hydrogenotrophic methanogenesis (Whiticar, 1999). This fits well to findings of Bednařík et al. (2019) and Mach et al. (2015), who found that hydrogenotrophic methanogenesis was the dominant CH_4 production pathway in the HZ of the Elbe and Sitka rivers.

At all sampling sites CH_4 concentrations decreased towards the sediment surface, but in most of the profiles, where δ^{13}C–CH_4 data were available, this was not accompanied by a significant enrichment in the heavier $^{13}CH_4$. Diffusive processes in these cases appear to be responsible for reducing CH_4 concentrations between the methanogenic zone and the upper part of the riverbed. At the sediment–water interface only very low CH_4 concentrations were found in all profiles (A-E), pointing towards small diffusive fluxes across the sediment–water interface. This finding is surprising because we expected high CH_4 concentrations and large fluxes to the water column and towards the atmosphere. However, it must be noted that we looked at diffusive CH_4 fluxes within the HZ and did not cover the possible generation and transport of gas bubbles. The contribution of these bubbles to total CH_4 fluxes across the sediment–water interface at the river Moosach remains unknown, but ebullition might be a significant contributor to CH_4 effluxes as suggested in the literature (DelSontro et al., 2010; McGinnis et al., 2016).

As explained above, isotopic evidence indicated a significant contribution of microbial CH_4 consumption to a reduction in diffusive CH_4 fluxes only in profile C. In all other profiles, it is possible either that CH_4 is oxidized at rates too low to alter its isotopic composition or that CH_4 oxidation takes place close to the sediment–water interface where CH_4 concentrations were too low for the isotope measurements. In both cases, this implies a limited relevance for the reduction in diffusive CH_4 fluxes. To gain further insights into aerobic and anaerobic CH_4 oxidation, the modeling software PROFILE was applied (Sec. 5.3.5). One reason for the observed methane oxidation processes in location C could be an increased supply of O_2 and NO_3^- during the two high-flow events in the sampling period.

5.3.4 Inverse modeling of concentration gradients as a basis for discussing aerobic versus anaerobic oxidation of CH_4

Figure 5.4 shows the results of inverse concentration gradient modeling with the software tool PROFILE. Overall, the modeled and measured concentrations agreed well to each other, especially for CH_4 and SO_4^{2-}. In the more complex CH_4 and SO_4^{2-} profiles, often several consumption zones were detected. Deviations of modeled from measured data were more pronounced for O_2 gradients in profiles B and D, as well as for the NO_3^- gradient in profile E. Here, the model could not capture the data well, potentially because higher concentration

values and outliers in deeper sediment depths might have biased the fit in the upper gradient, resulting in broader oxygen reduction and denitrification zones.

In the PROFILE software, vertical transport can be attributed to diffusion, bioturbation and irrigation. However, exchange flows control riverbed biogeochemistry and solute transport in the HZ (Bardini et al., 2012, 2013). As a result, the disregard of advective solute transport with hyporheic exchange flows may lead to an underestimation of O_2, NO_3^- and SO_4^{2-} reduction rates, since entering surface water increases the availability of educts for geochemical reactions. Where pore-water movement is slow, O_2 uptake is proportional to the rate of solute influx (Rutherford et al., 1993, 1995). On the other hand, CH_4-rich pore water is diluted with stream water, and modeled CH_4 oxidation rates may, therefore, rather be overestimated. Yet, hydraulic conductivities as calculated using the empirical formula of Beyer (1964) are relatively low ($<8{\cdot}10^{-5}\,m\,s^{-1}$) in the fine-grained deposits of the river Moosach (Tab. A.4) which reduces the influence of the advective component in locations A, C and E. The model is applied to find the depths of reactive production and consumption zones. Calculated reaction rates are used to compare profiles, but due to the limitations described above, absolute values should not be overinterpreted.

Depth-integrated modeled O_2 consumption rates were in the range 0.10-0.41 $mmol\,m^{-2}\,d^{-1}$. NO_3^- reduction rates were found to be between 0.18 and 0.29 $mmol\,m^{-2}\,d^{-1}$ in profiles C, D and E, while only 0.08 $mmol\,m^{-2}\,d^{-1}$ of NO_3^- was consumed in profile B in a much narrower DZ (denitrification zone). Using PROFILE for the interpretation of concentration gradients in a microcosm study, Norði and Thamdrup (2014) found rates of 11.4 $mmol\,m^{-2}\,d^{-1}$ for O_2 and 0.9 $mmol\,m^{-2}\,d^{-1}$ for NO_3^- uptake, which is about 30-100 times higher for O_2 and 3-12 times higher for NO_3^- than simulated here. In their work both O_2 and NO_3^- were consumed completely within millimeters building much steeper gradients than observed in this study. Modeled ORZs (oxygen reduction zones) in profiles C and E were 4.5 cm and 3.5 cm wide; in profiles B and D they were even 7 cm, in the latter two cases partly due to poor fits. Additionally, as mentioned above, an underestimation of modeled O_2 and NO_3^- uptake rates is likely, since the model does not include advective hyporheic exchange fluxes. In profile C, stream water can easily enter the sandy stream bed, and flow velocities are expected to be higher than close to the banks; O_2 uptake and denitrification are supposed to be much larger than suggested by the diffusive model.

In profile B a single SRZ (sulfate reduction zone) was found in 6-12 cm depth, whereas SO_4^{2-} reduction takes place in several depth ranges in profiles C-E. Total modeled SO_4^{2-} consumption ranged from 0.06 $mmol\,m^{-2}\,d^{-1}$ (profile D) to 0.43 $mmol\,m^{-2}\,d^{-1}$ (profile E). This is in line with modeling results of Norði et al. (2013), who found 0.2 $mmol\,m^{-2}\,d^{-1}$ sulfate reduction in a freshwater lake sediment. Yet, directly measured rates were 10 times higher in their study, showing a discrepancy between modeled and measured values. Jørgensen et al. (2001) found SO_4^{2-} reduction rates of 0.65-1.43 $mmol\,m^{-2}\,d^{-1}$ in the Black Sea using the same model. In profiles B and D SRZs were located beneath the ORZ and DZ, as would be expected, but in profiles C and E the uppermost SRZ overlapped with the ORZ and DZ. For profile C, the concurrent decrease in O_2, NO_3^- and SO_4^{2-} has already been discussed in Sec. 5.3.1 (anaerobic micro-niches or dilution effects at a clogged sediment surface). For profile E, NO_3^- is completely consumed between 1-2 cm depth in a very narrow DZ, and SO_4^{2-} concentrations start to decrease from 1 cm onwards, most likely right after NO_3^- has been removed from

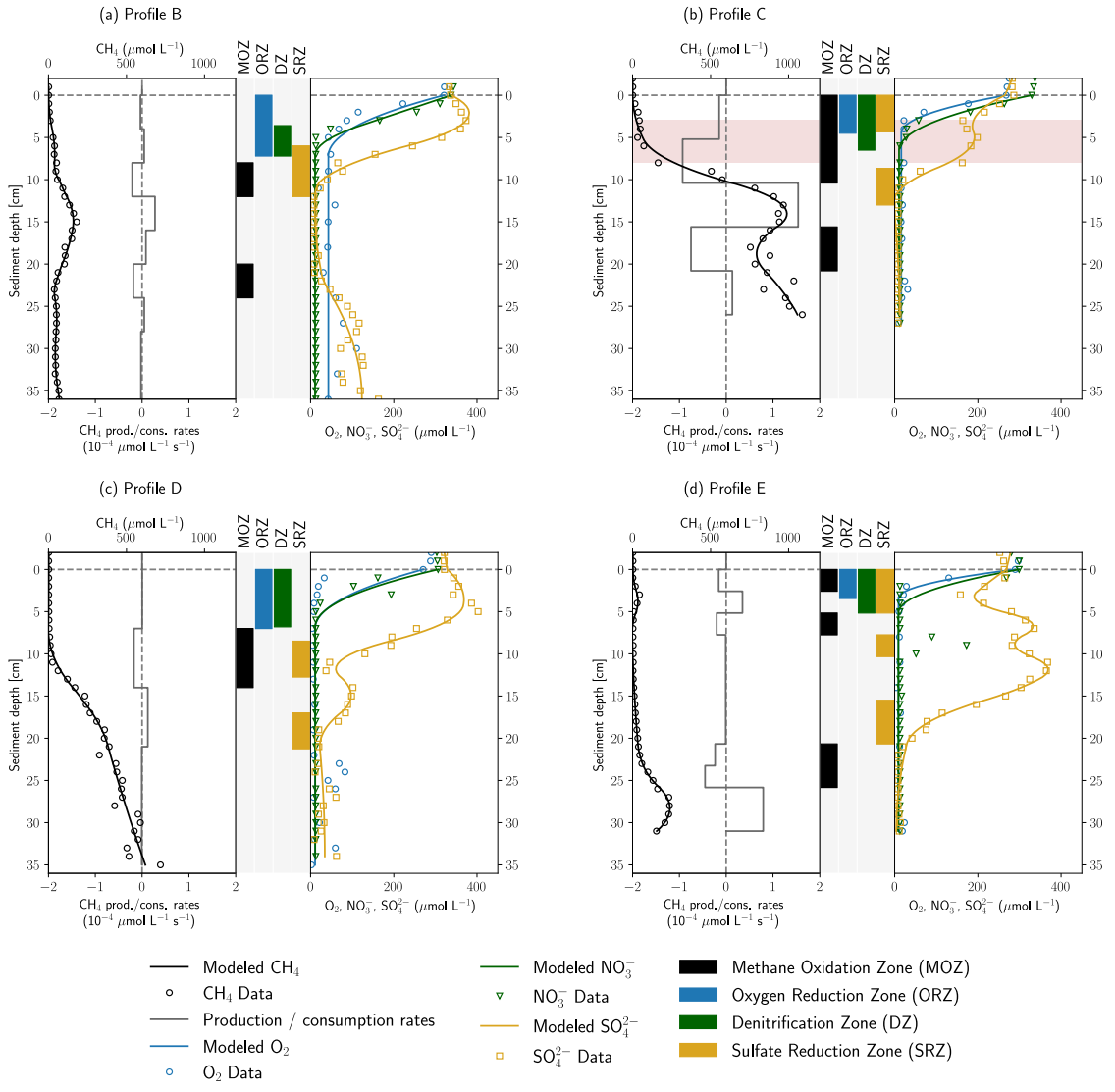

Figure 5.4: **Results of concentration gradient modeling using the PROFILE software for profiles B-E.** In panels (a)-(d), the left side shows modeled and measured CH_4 concentrations as well as modeled CH_4 production and consumption rates. In the center, the depth ranges of MOZ, ORZ, DZ and SRZ are highlighted. Zones with very low consumption rates ($<5{\cdot}10^{-6}$ µmol L^{-1} s^{-1}) were not identified. On the right, measured and modeled O_2, NO_3^- and SO_4^{2-} concentrations are shown. Rates are not displayed for electron acceptors for reasons of clarity. Red background color in panel (b) highlights an enrichment in $\delta^{13}C$–CH_4.

the system. The model did not capture these very steep gradients precisely because data resolution was too coarse. Likewise, the sudden NO_3^- peak in 9 cm depth in profile E was not recognized because too few data points in the peak were available.

MOZs (methane oxidation zones) were found in every profile even where δ^{13}C–CH_4 values were stable, but rates were generally low ($<2{\cdot}10^{-4}$ µmol L^{-1} s^{-1}). For example, in profiles B and E, CH_4 was modeled to be consumed on both sides of the peaks in 3 cm and 15 cm depth, at rates of 0.06-0.07 mmol m^{-2} d^{-1} and 0.04-0.05 mmol m^{-2} d^{-1}, respectively. It is not surprising that these small consumption rates did not change the isotopic composition of CH_4. A single MOZ was found in profile D in 7-14 cm depth with a depth-integrated rate of 0.11 mmol m^{-2} d^{-1}. In profile C, 0.42 mmol CH_4 m^{-2} d^{-1} were simulated to be oxidized between 0.0-10.4 cm depth but with a 6 times higher rate below the ORZ (5.2-10.4 cm). This upper MOZ falls together with the observed enrichment in δ^{13}C–CH_4 between 3-8 cm depth.

The model was applied to help in identifying the electron acceptors responsible for CH_4 oxidation. This involves checking for overlaps between the MOZ and ORZ, DZ and SRZ. In profiles A and D, the MOZ only overlaps the SRZ combined with very low modeled oxidation rates. Profiles C and E show overlaps of all zones in the uppermost centimeters where δ^{13}C–CH_4 measurements were not available due to low CH_4 concentrations. Here, aerobic methane oxidation could potentially take place. In profile C, the modeled oxidation rate increased significantly below the ORZ and intersected with the DZ in the upper and the SRZ in the lowest part. This could point towards AOM coupled to denitrification or bacterial sulfate reduction in anoxic micro-niches, but since gradients were very steep and trace oxygen might also have been present, the delineation of the relevant electron acceptor is not possible. The higher CH_4 oxidation rate in the presence of NO_3^- compared to O_2 in profile C, if valid, may show a situation in the HZ of the river Moosach similar to sediments of Lake Constance. Measurements of Deutzmann et al. (2014) showed that N-DAMO was the major CH_4 sink although the community of aerobic methanotrophs would have been capable of oxidizing the entire methane flux. Limiting for aerobic oxidation was the available CH_4 after passing through the denitrification zone where most of it was already oxidized. Nonetheless, it is also possible that aerobic methane oxidation has a greater influence than suggested by the model. Either way, both aerobic and anaerobic CH_4 oxidation have the potential to reduce GHG emissions at location C.

Both profiles C and E have an additional MOZ deeper down where all electron acceptors were already consumed. In profile C it looks like the slope changes in the lower part of the profile are due to an overfitting of the model to fluctuating concentrations within the methanogenic zone. In profile D however, the deepest MOZ is located where CH_4 oxidation would be expected because of a clear slope change in the CH_4 concentration gradient. Potential electron acceptors could be SO_4^{2-}, which is present only a few centimeters above; Fe or Mn-oxides; or perhaps trace amounts of O_2.

5.3.5 Microbial communities at location C

The relative abundance of 16S rRNA gene sequences with similarity to known methanogenic microbial groups increased with sediment depth into the methane zone (Fig. 5.5a). In the shallower depths (0-4 cm) the methanogenic microbial community was dominated by the

Methanomassiliicoccales and Methanofastidiosales, whereas at the bottom of the profile (16-21 cm) *Candidatus* "Methanomethyliales" and Methanomassiliicoccales dominated the methanogenic microbial community (Fig. 5.5b). The Methanomassiliicoccales and *Candidatus* "Methanomethyliales" both exhibit metabolic pathways in the genome indicative of H_2-dependent methylotrophic methanogenesis (Berghuis et al., 2019; Vanwonterghem et al., 2016). In saline or sulfate-rich environments, where methylated compounds like trimethyl amine or dimethyl sulfide are available as non-competitive substrates, this pathway can be of high importance (Conrad, 2020), but it is less considered in freshwater environments. However, Methanomassiliicoccales have been linked to CH_4 production from methanol in freshwater wetlands (Narrowe et al., 2019). Methanol can be derived from pectin, which is contained in terrestrial plants (Conrad, 2005), and thus, the combination of a high relative abundance of Methanomassiliicoccales combined with a high input of allochthonous plant material found in the sediment cores render this production pathway possible. The strong depletion in δ^{13}C–CH_4 in the methanogenic zone supports the potential for CH_4 production from methanol. Carbon fractionation factors related to CH_4 production from methanol (ε_C = 68-77) are similar to those of hydrogenotrophic methanogenesis (ε_C = 55-58) and much higher than for acetoclastic methanogenesis (ε_C = 24-27) or CH_4 production from other methylated compounds (Whiticar, 1999). *Candidatus* "Methanomethyliales" is a newly discovered group of methanogenic archaea branching within *Candidatus* "Verstraetearchaeota" (Berghuis et al., 2019; Vanwonterghem et al., 2016). The increased relative abundance of *Candidatus* "Methanomethyliales" in our sediment core within the methane zone is the first clear piece of evidence that these novel methanogenic archaea could be important for CH_4 production in the HZ.

Above the methane zone, there is an increased relative abundance of both aerobic and anaerobic CH_4 oxidizing microbial groups (Fig. 5.5d and e). The aerobic groups affiliated with Methylomonaceae (Gammaproteobacteria) and Methyloligellaceae (Alphaproteobacteria) dominated at depths above 12 cm (Fig. 5.5d) and are known to be involved in aerobic CH_4 oxidation (Takeuchi et al., 2019).

The anaerobic methanotrophs had the closest affiliation to *Candidatus* "Methylomirabilis" and *Crenothrix*. Both are involved in different steps of coupling CH_4 oxidation to the reduction of NO_3^- and NO_2^- (Ettwig et al., 2010; Oswald et al., 2017). The results indicate that anaerobic and aerobic CH_4 oxidizers can somehow inhabit the same sediment depths in the HZ, a finding that has been observed in paddy soil previously (Vaksmaa et al., 2017). *Crenothrix* is known to be a facultative anaerobe, which can explain their presence in oxic environments, but O_2 was shown to have a detrimental effect on members of the *Candidatus* "Methylomirabilis" like *Candidatus* "Methylomirabilis oxyfera" (Luesken et al., 2012). Their high abundance in the uppermost centimeters of the sediment is, therefore, surprising. Yet, the close proximity and co-existence of aerobic and anaerobic CH_4 oxidizers fits well to the observed steep and partly overlapping gradients. The mixed distribution of strict anaerobes together with aerobes and facultative aerobes within the HZ could be due to mixing and turbidity at the stream bottom, which might resuspend and distribute sediments to different zones.

The presence of 16S rRNA gene sequences affiliated with the bacterial groups *Candidatus* "Brocadia" and *Candidatus* "Anammoximicrobium", which are known to perform anaerobic oxidation of ammonium (anammox) (Wu et al., 2020), may show that anammox via nitrite reduction was also ongoing. Because the anammox bacteria overlapped with anaerobic CH_4-

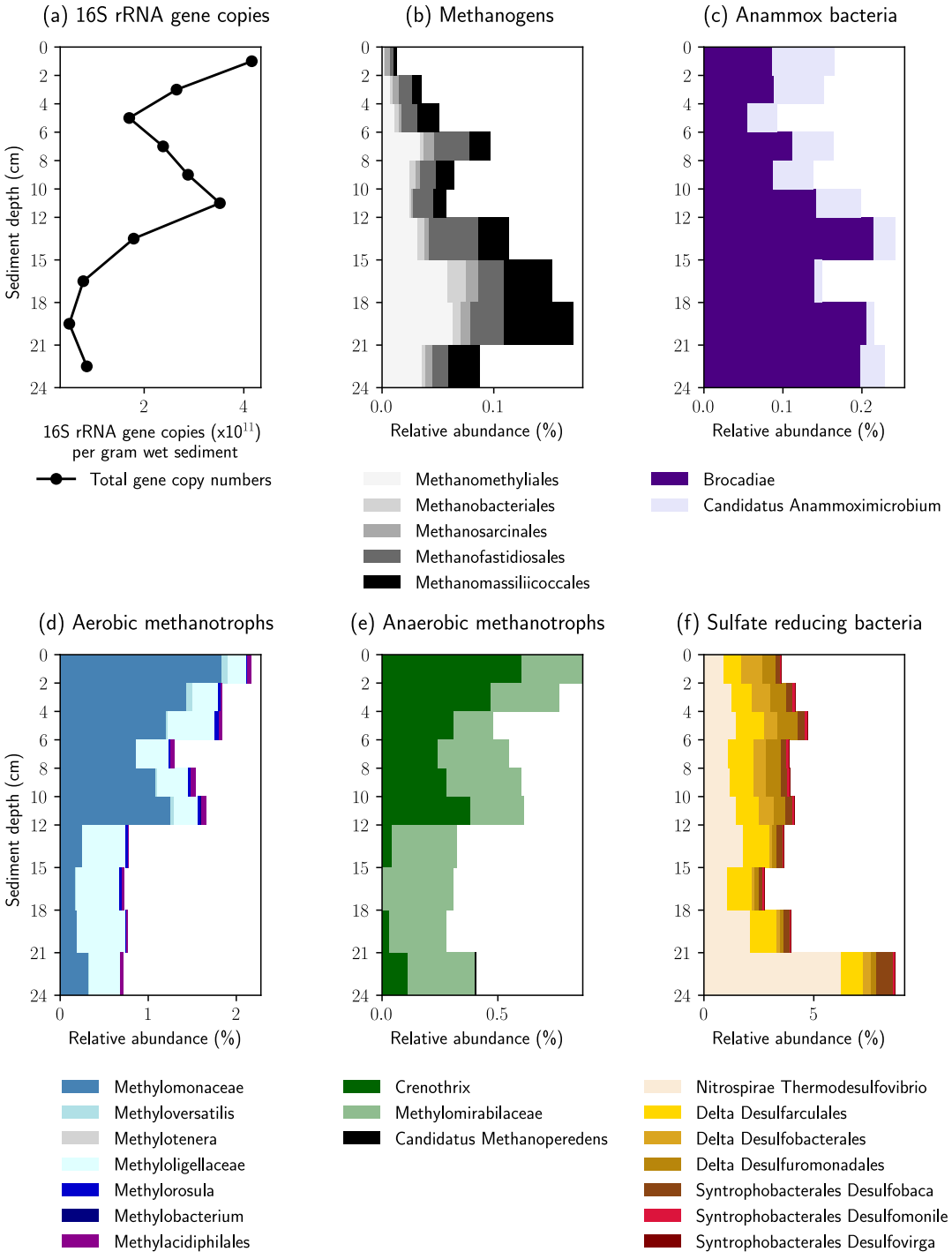

Figure 5.5: **Relative abundance of key microbial groups detected in the 16S rRNA gene sequencing datasets.** The histograms display the relative abundance (percentage of total reads) assigned to each group displayed. Note the increase in relative abundance of methanogenic groups below 12 cm, whereas the relative abundance of methane oxidizing groups increases above 12 cm.

oxidizing bacteria (*Candidatus* "Methylomirabilis" and *Crenothrix*) in the vertical profile, our results might show that, similar to anoxic lake bottom water (Einsiedl et al., 2020), a coupling of anammox with NO_2^--dependent CH_4 oxidation (N-DAMO) is possible in the anoxic sediments of the HZ. This may represent a mechanism whereby N_2 is released and nitrogen is eliminated from the HZ. Based on the low abundance of ANME archaea we postulate that S-DAMO is unlikely to be a relevant process within the HZ of the river Moosach. This is also in line with earlier findings by Shen et al. (2019a), who found that NO_3^- and NO_2^- could trigger AOM in all sandy river sediments in their study, while SO_4^{2-} and Fe were only effective in a few examples.

5.4 Conclusions

Measurements and interpretation of geochemical profiles and stable isotopes (δ^{13}C–CH_4) at five different sampling sites in the river Moosach showed a predominant source of dissolved CH_4 and a potential for AOM. Based on our field study we confirm previous findings that large quantities of CH_4 are produced in river sediments, which can contribute to global warming. CH_4 was produced in all sampled locations, but CH_4 concentrations varied drastically between profiles. Much more CH_4 was produced in summer, especially in areas with fine, organic-rich sediments like inside bends of curved river sections. These findings suggest that the main influencing factors for CH_4 production in the HZ are temperature, organic carbon content and sediment composition. The uniqueness of the measured profiles underlines the high spatiotemporal variability in the hyporheic zone. Therefore, deriving general conclusions from point measurements is highly problematic, and the representativeness of the available data should be critically questioned in future research on CH_4 emissions from rivers.

Based on measured δ^{13}C values and the microbial community found in location C, we consider hydrogenotrophic and H_2-dependent methylotrophic methanogenesis as relevant CH_4 production pathways. CH_4 concentrations at the sediment surface have been found to be low, and δ^{13}C–CH_4 values were almost constant over the sampled sediment depth in most of the measured profiles, indicating a diffusion-limited transport of this GHG towards and across the sediment–water interface. However, in one of the profiles, an isotopic shift in δ^{13}C–CH_4 to less negative values linked with decreasing CH_4 concentrations implied biological methane oxidation. Both microbiological and modeling methods showed the potential for anaerobic methane oxidation coupled with denitrification (N-DAMO). Yet, chemical gradients were very steep so that aerobic and anaerobic redox zones were in too close proximity to find a clear evidence for N-DAMO within the HZ of the river Moosach. Nevertheless, our results clearly show the removal of nitrogen and decreasing CH_4 concentrations towards the sediment–water interface. Both processes are crucial in improving the quality of river water and in reducing GHG emissions to the atmosphere.

Author contributions

TM, AW and FE conceptualized the project. TM and AW developed the methodology and performed fieldwork. ÖC and WO contributed the microbiological investigations. TM was responsible for visualization and original draft preparation. Funding acquisition and supervision

were performed by FE and TB. TM, AW, WO, TB and FE all participated in writing, reviewing and editing the paper.

Acknowledgements

We thank Tobias Lanzl for support during the field campaign as well as Susanne Thiemann and Jaroslava Obel for their help with analytics in the laboratory. We also want to thank Dr. Friedhelm Pfeiffer for critical reading and reviewing. Further, we want to acknowledge the good cooperation with the team of the Chair of Aquatic Systems Biology (Technical University of Munich, TUM).

Review statement

This paper was edited by Steven Bouillon and reviewed by Carsten J. Schubert and one anonymous referee.

6 Publication II

Technical note: Testing the effect of different pumping rates on pore-water sampling for ions, stable isotopes, and gas concentrations in the hyporheic zone

This chapter was published as: Michaelis, T., Wunderlich, A., Baumann, T., Geist, J., & Einsiedl, F. (2023). Technical note: Testing the effect of different pumping rates on pore-water sampling for ions, stable isotopes, and gas concentrations in the hyporheic zone. *Hydrology and Earth System Sciences*, *27*(20), 3769–3782. https://doi.org/10.5194/hess-27-3769-2023

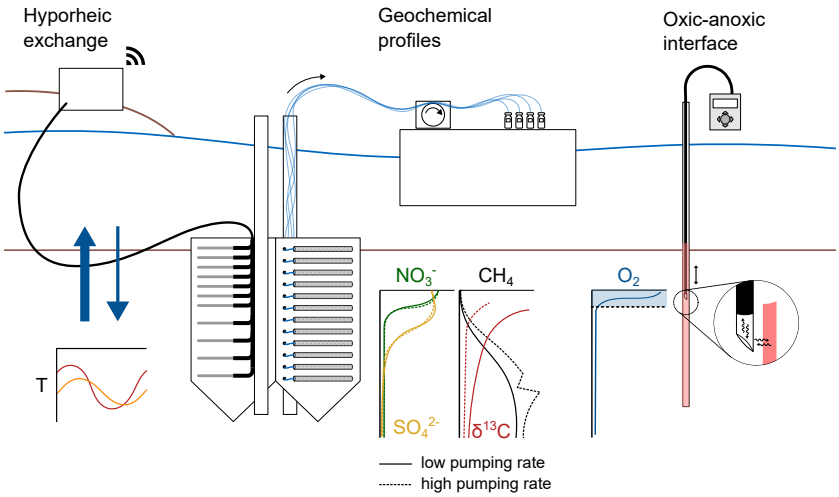

Abstract. The hyporheic zone (HZ) is of major importance for carbon and nutrient cycling as well as for the ecological health of stream ecosystems, but it is also a hot spot of greenhouse gas production. Biogeochemical observations in this ecotone are complicated by a very high spatial heterogeneity and temporal dynamics. It is especially difficult to monitor changes in gas concentrations over time because this requires pore-water extraction, which may negatively affect the quality of gas analyses through gas losses or other sampling artifacts. In this field study, we wanted to test the effect of different pumping rates on gas measurements and installed Rhizon samplers for repeated pore-water extraction in the HZ of a small stream. Pore-water sampling at different pumping rates was combined with an optical sensor unit for

in situ measurements of dissolved oxygen and a depth-resolved temperature monitoring system. While Rhizon samplers were found to be highly suitable for pore-water sampling of dissolved solutes, measured gas concentrations, here CH_4, showed a strong dependency of the pumping rate during sample extraction, and an isotopic shift in gas samples became evident. This was presumably caused by a different behavior of water and gas phase in the pore space. The manufactured oxygen sensor could locate the oxic–anoxic interface with very high precision. This is ecologically important and allows us to distinguish between aerobic and anaerobic processes. Temperature data could not only be used to estimate vertical hyporheic exchange but also depicted sedimentation and erosion processes. Overall, the combined approach was found to be a promising and effective tool to acquire time-resolved data for the quantification of biogeochemical processes in the HZ with high spatial resolution.

6.1 Introduction

The hyporheic zone (HZ) is the interstitial habitat below streams and rivers, adjacent to and influenced by the stream water above and the groundwater below (Peralta-Maraver et al., 2018). The importance of this zone for stream ecosystems has long been recognized (Boulton et al., 1998) and is emphasized until today (Lewandowski et al., 2019). Ecosystem functions of the HZ include rapid carbon and nutrient recycling (Findlay, 1995; Sophocleous, 2002), physical, chemical, and biological filtration of streamwater (Hancock et al., 2005), and flood wave retention (Boulton et al., 1998). The HZ also serves as a habitat for microbiota and macro-zoobenthos (Hendricks, 1993; Robertson & Wood, 2010), provides spawning grounds for fish (Malcolm et al., 2005; Smialek et al., 2021; Sternecker & Geist, 2010), and is important as a juvenile habitat for endangered freshwater mussels (Auerswald & Geist, 2018; Denic & Geist, 2015). On the other hand, as a result of the high microbial activity, greenhouse gas (GHG) production can be substantial in the HZ (Stanley et al., 2016; Trimmer et al., 2012), making many rivers net methane (CH_4), nitrous oxide (N_2O) and carbon dioxide (CO_2) emitters (Romeijn et al., 2019; Saunois et al., 2020).

Therefore, a deep understanding of the processes in the HZ is essential in many disciplines (Krause et al., 2011). High spatiotemporal heterogeneity is making data acquisition for model development and calibration a challenge (Braun et al., 2012). The HZ is a complex system, influenced by many interrelated factors, and more observations are needed to better describe the hydrological, geochemical, and ecological functioning of this dynamic zone.

Well-known approaches to investigating HZ biogeochemistry are direct sediment sampling or pore-water sampling from sediment cores. Water samples can be extracted from cores by centrifugation (Emerson et al., 1980), squeezing (Bender et al., 1987) or pressurization (Jahnke, 1988). However, coring, transportation, and water extraction may disturb the sample and significantly deteriorate sample quality. Sediment sampling also disturbs the sampling site, limits spatial resolution, and can change geochemical gradients through the introduction of bypass flow along boreholes and sampling devices. These issues are critical in the HZ, where geochemical gradients are often steep. Pore-water equilibrium dialysis samplers (peepers), as first described by Hesslein (1976), can be used to obtain pore-water concentration profiles without coring at a high vertical resolution (e.g. Michaelis et al., 2022). A disadvantage is that samples represent an average over the sampling period of (usually) several weeks,

making it impossible to observe short-term temporal dynamics typical of the HZ (Boano et al., 2014). Further, both sampling from sediment cores or peepers is not suitable for long-term observations due to perturbation during sampling and the necessity to sample at slightly different positions.

For in situ measurements, microsensors have been developed which can be driven into the sediment to record dissolved O_2 or HS^- concentrations, pH, and redox potential with a vertical resolution in the millimeter range (Boetius & Wenzhöfer, 2009). These sensors have been employed at the sea floor (e. g. Vonnahme et al., 2020), but they are not suitable for rivers or streams with high flow velocities or coarse-grained sediments due to their high fragility. In addition, sensors and additional instrumentation for precise handling are very expensive.

Several methods have been developed and applied for direct pore-water extraction from the HZ. For example, USGS MINIPOINTS consist of several steel drive points with different lengths for the extraction of pore water from several depths (Duff et al., 1998). In a similar way, depth-resolved hyporheic pore-water sampling has been realized with multi-level piezometers, a set of tubes with different types of screens at the tips (Krause et al., 2012; Rivett et al., 2008; Schaper et al., 2018), or with fixed PVC or silicon tubes attached to syringes (Casas-Mulet et al., 2021; Geist & Auerswald, 2007). Rhizon samplers (microfilter tubes), typically applied for soil moisture measurements in the unsaturated zone, have also occasionally been used for pore-water extraction: Rhizon samplers were used for pore-water extraction from sediment cores by Shotbolt (2010), in combination with an in situ chamber in the Wadden sea by Seeberg-Elverfeldt et al. (2005), and to sample pore-water from lake sediment microcosms by Song et al. (2003). From each of these systems, samples can either be extracted with syringes or peristaltic pumps (Knapp et al., 2017; Seeberg-Elverfeldt et al., 2005).

However, these methods have rarely been used for gas analyses in hyporheic pore water. A vacuum can lead to outgassing, and, therefore, when pulling out the samples, gas contents may be affected. Suitable pumping rates for pore-water extraction have been evaluated from chloride gradients, and rates $< 4.0\,\mathrm{ml\,min^{-1}}$ were found to be acceptable (Duff et al., 1998). But the effect of pumping rates on gas concentrations has never been tested. Especially in fine-grained bed substrates, where the pressure in the extraction system to maintain these flow rates has to be much lower than ambient pressure, degassing effects are no longer negligible. Gas concentrations will reflect the low pressure in the extraction system, which is very hard to measure. In this study, we wanted to test this hypothesis and installed a monitoring station at a site with fine-grained deposits close to the riverbank where high methane (CH_4) concentrations were to be expected. Fifteen Rhizon samplers were installed with a 3 cm vertical distance for repeated pore-water sampling. Three different pumping rates for pore-water sampling were tested and the results were compared to geochemical profiles observed with a peeper that was installed very close to the Rhizon samplers.

The sampling station was amended with a custom-coated fiber-optic oxygen sensor unit based on the description of Brandt et al. (2017) for a precise allocation of the oxic–anoxic interface. Air contamination during sample extraction from sediment cores, peeper chambers, or other types of in situ samplers is likely and problematic for studying anoxic processes. An in situ sensor was therefore essential for the assessment of CH_4 in the HZ. As a third component, temperature monitoring at 14 different depths was used for an estimation of hyporheic exchange. Flux rates were calculated with analytical models introduced by Hatch et al. (2006) and Keery et al. (2007)

using the software package VFLUX (Gordon et al., 2012). The temperature data were also needed for evaluating raw data of the O_2 sensor.

6.2 Methods

6.2.1 Study site and station design

The study was conducted at the Moosach River in southern Germany, close to the city of Freising. The river has a catchment area of 175 km^2 and is characterized by a low gradient and a high fraction of fines in the streambed (Auerswald & Geist, 2018). The Moosach River is characterized by very uniform flow conditions due to regulations of the water level by weirs. This lack of dynamics is also considered one of the reasons for its stable streambed material with high rates of fine sediment deposition (Auerswald & Geist, 2018). The area where the sampling site was situated lies upstream of a weir that keeps the headwater level nearly constant at almost all discharge conditions. The sampling station was installed on the right bank of the river in a low-flow zone with fine, organic-rich deposits. The grain size distribution of the deposits consisted of 3 % gravel, 27 % sand, and 70 % silt with a porosity of 81.5 % (Sec. B.1 in the Supplement). The organic matter content was 21 %. High CH_4 production was expected due to the high content of fines and organic matter (Bodmer et al., 2020). Water depth at the site was approximately 0.6 m.

The monitoring station was installed on March 15$^{\mathrm{th}}$, 2021. For installation, a protective casing was manually pushed into the streambed, the interior of the casing was cleared of sediment to allow the sampler to be inserted without damaging the filter tubes or temperature sensors, and finally the protective casing was removed and the sampler left to settle in. After installation, we observed heavy sedimentation and during the summer months, mainly between July and September, major macrophyte growth. The first sampling campaign was done 2 weeks after installation, when disturbances caused by the installation had been wearing off. Ten more sampling campaigns were performed in 2021 and three in 2022 (Sec. B.2, Tab. B.1 in the Supplement).

The sampling station comprised 15 Rhizon samplers for depth-resolved pore-water sampling (Sec. 6.2.2), a self-manufactured oxygen sensor (Sec. 6.2.4), and 14 temperature sensors (Sec. 6.2.5). Fig. 6.1 shows all components of the sampling station. Rhizon samplers and temperature sensors were fixed horizontally on opposite sides of a Plexiglas (PMMA) panel. The panel was inserted longitudinally to the flow direction in order to keep disturbances to river flow and horizontal hyporheic fluxes to a minimum. Rhizon samplers faced towards the main channel while temperature sensors faced towards the riverbank. A swimming raft allowed access to the tubes connected to the Rhizon samplers to guarantee sampling without sediment disruption. Temperature sensors were connected to data loggers installed on land next to the river. A fiber-optic measurement system for O_2 concentration was placed right next to the sampling station. With the custom-made optical sensor, an oxygen meter, and an optical fiber, O_2 saturation could be measured with a depth resolution of 1 cm.

Clogging of the Rhizon samplers with a pore size of 0.12-0.18 µm occurred only once shortly after initial installation at three samplers above the sediment–water interface due to biofilm

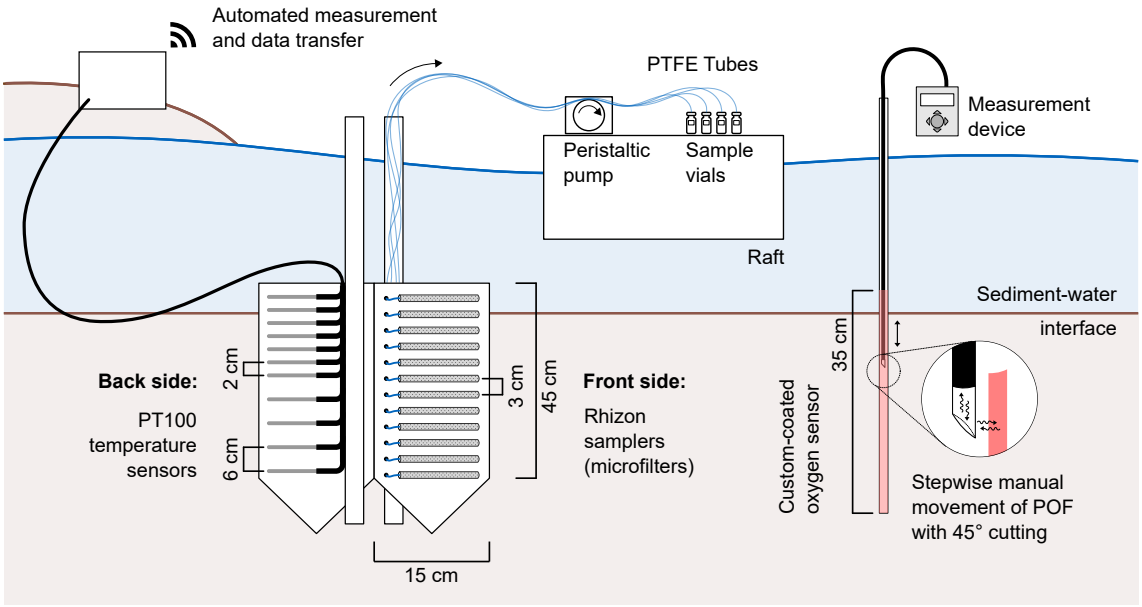

Figure 6.1: **Design of the monitoring station at the Moosach River, Freising, Germany.** For reasons of clarity, the schematic figure does not show all sensors.

growth. After replacing the top three samplers, this problem did not reoccur. No problems with clogging occurred at the samplers within the sediment. To avoid potential clogging, 2 ml of pore water still in the sampling tubes after each sampling campaign was backwashed.

Pore-water sampling with Rhizon samplers

Our sampling station was equipped with 15 Rhizon samplers with a pore diameter of 0.12-0.18 µm and a filter length of 5 cm (Rhizosphere, Wageningen, The Netherlands). The samplers were fixed horizontally with 3 cm distances. Polytetrafluorethylene (PTFE) tubes with a 1.32 mm inner diameter (Cole-Parmer, St. Neots, UK) were connected to the samplers to lead pore-water samples to the water surface. The material was chosen for its low gas permeability.

Samples were extracted simultaneously from all 15 Rhizon samplers with two ISM 1089 Ismatec Ecoline peristaltic pumps (VWR International, Darmstadt, Germany) with eight cassettes each and gastight Viton peristaltic tubing with an inner diameter of 0.51 mm (Cole-Parmer GmbH, Wertheim, Germany). Three pumping rates were tested in 2022: 0.09 mL min^{-1} on May 30$^{\text{th}}$, 0.19 mL min^{-1} on May 3$^{\text{rd}}$, and 0.38 mL min^{-1} on May 31$^{\text{st}}$. Prior to sampling, 4 ml of pore water was taken for pre-rinsing to exchange at least the tube volume of 3.8 ml without increasing the sampling volume too much. Stream temperature conditions were similar on all sampling days; discharge was 0.09 m^3 s^{-1} (4.8 %) higher at the end of May compared to the beginning of the month (Fig. 6.2). It should be mentioned that the application of a vacuum results in degassing. As the actual pressure conditions cannot be measured, this change in the sample cannot be fully quantified. Calculations indicate that the effect is more pronounced at higher gas concentrations and affects not only the gases but also the pH value and the concentration of bicarbonate.

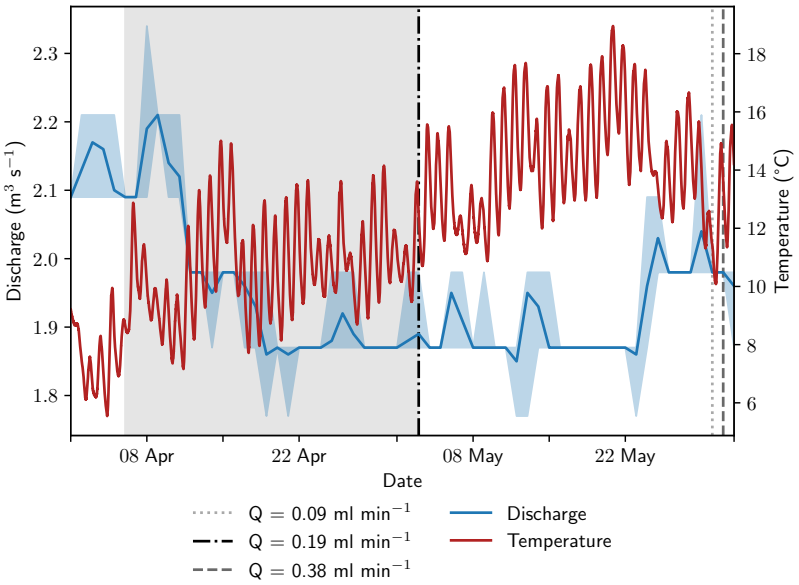

Figure 6.2: **Discharge and stream temperatures during the sampling period.** Discharge data from a monitoring station approximately 5 km downstream was retrieved from the Bavarian State Office of the Environment (2023). The span between minimum and maximum discharge is shaded in light blue, average stream discharge is shown as a blue line. The equilibration period of the peeper is highlighted with grey background color. Vertical lines show sampling dates at the monitoring station and are coded to the sampling rates.

Samples for stable water isotopes and anion and cation analyses were collected in 1.5 mL glass vials without headspace. For gas analyses, 10 mL glass vials were crimped gastight with butyl rubber stoppers and flushed with synthetic air (O_2, N_2). Right before sampling, 3 mL synthetic air was removed from the enclosed vials. Rubber stoppers were then pierced with needles connected to the peristaltic tubing and 3 mL of sample were pumped directly into the vial, providing a completely gastight, pressure-compensated sampling technique. Samples for gas analyses were fixated with 20 µL 10 M NaOH (Carl Roth, Karlsruhe, Germany). For sulfide measurements, 15 mL Falcon tubes were prepared with 1 mL 1 M zinc acetate (Carl Roth, Karlsruhe, Germany). A sample of 4 mL was injected slowly from below to allow precipitation of ZnS before air contact. All samples were transported in a cooler and stored refrigerated prior to analysis.

Pore-water sampling with a peeper

As a second pore-water sampling method, a pore-water dialysis sampler (peeper) was used. The body of the peeper was equipped with two columns of 38 chambers, each being filled with deionized water and covered with a semipermeable membrane (pore diameter 0.2 µm) (Pall Corporation, Dreieich, Germany). Over a period of 1 month, between 3 April and 3 May, an equilibrium between the water in the chambers and the surrounding pore water was obtained. Immediately after removing the peeper from the sediment, the water from the chambers was extracted with syringes and injected into vials. Due to the low amount of available sample

volume (on average 3 mL per chamber), pore-water analysis was restricted to anion, cation, and CH_4 concentrations along with the stable carbon isotope ratio ($\delta^{13}C$) of CH_4. Samples for anion and cation analysis were stored in 1.5 mL glass vials. Samples were fixated with 10 µL 0.5 M NaOH (anions) and 10 µL 1 M HCl (cations) to cope with long analysis times due to the large number of samples. Vial preparation for gas analyses, including fixation, flushing, and sealing, was similar to the sampling method described in Sec. 6.2.1. During sample injection, two syringes were used: one for the sample and one to allow pressure exchange. Both needles were removed directly after sampling.

Dissolved O_2 concentrations were measured in the field immediately after retrieval of the peeper from the sediment and its cleaning with deionized water. A Clark-type microsensor (Unisense, Aarhus, Denmark) was pierced through the membrane for the measurements (Revsbech, 1989). A time constraint on this technique is contamination with atmospheric O_2, which can diffuse quickly through the membrane under air contact. Thus, O_2 measurements had to be conducted as rapidly as possible and only selected chambers were tested to avoid artifacts.

6.2.2 Analytical methods for pore-water analysis

Anion and cation concentrations were measured with a system of two ICS-1100 ion chromatographs (Thermo Fisher Scientific) equipped with Dionex IonPacTM AS9-HC and CS12A columns, respectively. All results represent an average of triplicate measurements and were evaluated based on seven calibration standards (Merck, Darmstadt, Germany) reaching an analytical uncertainty of < 10 %. Detection limits were 0.039 mmol L^{-1} for Ca^{2+}, 0.032 mmol L^{-1} for Mg^{2+}, 0.020 mmol L^{-1} for Cl^-, 0.012 mmol L^{-1} for NO_3^-, 0.007 mmol L^{-1} for NO_2^-, and 0.008 mmol L^{-1} for SO_4^{2-}.

Stable water isotopes were measured in the same vials which had been used for cation analysis or in completely filled 1.5 mL glass vials that had been sampled separately. Only samples without acid or a base addition for fixation could be used. Fixation was necessary for peeper samples and Rhizon samples for the median pumping rate of 0.19 mL min^{-1} (same sampling date) due to the high number of samples and long expected analysis times. Samples were analyzed with the IWA-45EP isotopic water analyzer (Los Gatos Research, San Jose, USA) calibrated with three standards (USGS Reston Stable Isotope Laboratory, Reston, USA) with an analytical error of < 0.1 ‰ for $\delta^{18}O$ and < 1 ‰ for δ^2H. Results are expressed in the δ notation relative to the V-SMOW standard. Deuterium excess was calculated as $d = \delta^2H - 8 \cdot \delta^{18}O$ (Dansgaard, 1964).

Methane concentrations were measured according to a procedure introduced by the US Environmental Protection Agency EPA (2001) adapted for small sample volumes. Before analysis, vials were left for equilibration at 30 °C for at least 2 hrs. Headspace CH_4 concentrations were measured with a Trace 1300 gas chromatograph (GC) (Thermo Fisher Scientific, Dreieich, Germany) with a TG-5MS column and flame-ionization detector (FID), calibrated with three concentration standards (Rießner Gase, Lichtenfels, Germany). Samples were measured in triplicates of 250 µL manual headspace gas injection. Calculations of total concentrations before equilibration with the headspace were based on Henry's law as previously described (EPA, 2001; Kampbell & Vandegrift, 1998).

The vials for CH_4 concentration measurements were also used for isotopic analyses with a G2201-i gas analyzer (Picarro, Santa Clara, USA) for $^{12}C/^{13}C$ ratios in CH_4 with an analytical uncertainty of < 0.16 ‰. Headspace vials were directly connected to the Small Sample Introduction Module (SSIM) with needles. Dilution of the samples with synthetic air and repressurization of the glass vials was necessary for repeated measurements due to the small sample and headspace volume. Reliable results could not be obtained at headspace CH_4 concentrations of < 30 ppm (Michaelis et al., 2022). Results are represented in the δ notation relative to the V-PDB standard.

Sulfide samples were reactivated in the laboratory by adding 50 µL 49 % H_2SO_4 to dissolve the ZnS precipitate directly before analysis with the 1.14779.001 Spectroquant sulfide test for the Spectroquant Prove 100 photometer (Merck, Darmstadt, Germany). Sulfide concentrations were found to be below the detection limit of 0.02 mg L^{-1} during several sampling campaigns and were therefore excluded from subsequent sampling and analyses. This may be indicative of very low sulfide concentrations in the HZ, but an issue with sampling or analytical methods cannot be ruled out.

6.2.3 Statistical analyses

CH_4 concentration, $\delta^{13}C$–CH_4, $\delta^{18}O$–H_2O, $\delta^{2}H$–H_2O, Ca^{2+}, Mg^{2+}, and Cl^{-} concentration data from peeper and Rhizon measurements at different pumping rates were tested for statistically significant differences. First, data sets were checked for normal distribution with the Shapiro–Wilk test and a visual inspection of box plots. Levene's test was used for assessing the homogeneity of variance. Since the requirements for *t* tests and the one-directional ANOVA test (normal distribution of all data sets and, for ANOVA, homogeneity of variances) were not met for all data sets, nonparametric tests were chosen. The Mann–Whitney *U* test was applied for pairwise comparisons and the Kruskall–Wallis *H* test for assessing differences in more than two data sets, comparing all sampling techniques for each parameter. Independent *t* tests were used for pairwise comparisons where both data sets were normally distributed. All assessments were implemented in Python (version 3.8.3) using the scipy.stats package (version 1.5.1).

6.2.4 Dissolved oxygen profiling

Measuring O_2 concentrations in extracted samples had two major disadvantages: sample contamination with atmospheric O_2 during extraction could not be securely excluded and the vertical resolution of 3 cm between the Rhizon samplers was too low to depict the steep O_2 gradient. Therefore, a system for in situ oxygen profiling was constructed and installed.

Following the example of Brandt et al. (2017), an optode for optical O_2 measurements was manufactured by coating a Plexiglas tube with an oxygen-sensitive dye. To produce the sensing element, a sensor cocktail was prepared by dissolving 20 mg of platinum tetrakis-(pentafluorophenyl)porphyrin (PtTFPP) (Porphyrin Systems, Lübeck, Germany) and 2 g polystyrene in 10 mL toluene. The sensor cocktail was filled into a glass tube with a punched Viton septum (diameter 4.5 mm) at the lower end where the PMMA tube with an outer diameter of 5 mm (inner diameter of 3 mm) fits tightly. The PMMA tube was then pulled through the sensor

solution with a stepper motor at 0.25 cm s^{-1} and left to dry for at least 12 hrs yielding a thin oxygen-sensitive coating on the outside of the tube. Measurements were performed with the Fibox 4 trace oxygen meter (PreSens, Regensburg, Germany) connected to a polymeric optical fiber (POF) with an outer diameter of 2.7 mm. The tip of the POF was equipped with a 45 ° cutting to allow signal transfer orthogonal to the fiber (see Fig. 6.1).

In contrast to the work of Brandt et al. (2017), the sensor was not connected to an automated motor unit for data recording due to the low stability of the long Plexiglas tube ($>$ 75 cm above the sediment–water interface at a water depth of 60 cm) and the risk of water-level changes at high flow. Instead, measurements were performed manually by pulling up the POF in 1 cm steps as marked on the cable. At each depth, at least three measurements were done at a rate of 1 Hz. For each depth, mean and standard deviation of repeated measurements were calculated.

For calibration, distilled water with seven different O_2 concentrations was prepared by stripping with N_2 or He gas for different amounts of time. Each sensor was installed in a flow-through cell which was flushed with the deoxygenated water. Dissolved O_2 concentration in the flow-through cell was in parallel measured with a microsensor (Unisense, Aarhus, Denmark). For temperature control, the flow-through cell was placed in a column connected to a WCR-P22 thermo-controlled water bath (Witeg, Wertheim, Germany). Calibration was conducted at 20 °C. For each sensor, temperature dependence at 0 % and 100 % air saturation (a. s.) was evaluated with five and four temperatures between 5 °C and 30 °C, respectively. Details on calibration results and the calculation of dissolved O_2 concentrations from measured phase angles can be found in Sec. B.3.

6.2.5 Vertical hyporheic exchange estimation using temperature measurements

Temperature was measured in 14 different depths to trace hyporheic exchange fluxes at the sampling site. The four-wire PT100 sensors (Omega Engineering, Norwalk, USA) with an accuracy of $\pm$ 0.03 °C were calibrated in a WCR-P22 water bath (Witeg, Wertheim, Germany) with an accuracy of $\pm$ 0.1 °C at seven different temperatures between 0 °C and 30 °C before installation in the field. During calibration, sensor recordings were compared to the average temperature considering all sensors yielding a constant correction factor for each sensor.

On site, the sensors were installed with a 2 cm depth resolution for the first 15 cm and a 6 cm resolution below. Another sensor was placed approximately 20 cm below the water surface in the water column. The sensors were fixed on the back side (facing the riverbank) of the panel holding the Rhizon samplers. The 14 sensors were connected to four PT104A loggers (Omega Engineering, Deckenpfronn, Germany) and a Raspberry Pi-based control unit for automated data acquisition every 5 min.

Due to the long installation time, four out of 14 sensors stopped functioning properly, two additional sensors were excluded from analysis due to data gaps of $>$ 24 hrs. Data processing included the removal of outliers $<$ 0 °C or $>$ 30 °C, interpolation over data gaps $<$ 24 hrs, and resampling to equally spaced 5 min intervals.

Vertical hyporheic exchange rates were estimated using the software package VFLUX (Gordon et al., 2012). The software implements analytical solutions (Hatch et al., 2006; Keery et al.,

Table 6.1: Parameters for vertical hyporheic exchange estimation using the software package VFLUX.

Parameter	Description	Value	Source
n	Total porosity	81.5 %	Measurements (Sec. A.1)
β	Thermal dispersivity	0.001 m	Hatch et al. (2006)
λ	Thermal conductivity	0.60 $W\,m^{-1}\,K^{-1}$	Measurements (Sec. A.1); Dalla Santa et al. (2020)
c_s	Volumetric heat capacity of the sediment	0.55 $MJ\,m^{-3}\,K^{-1}$	Dalla Santa et al. (2020)
c_w	Volumetric heat capacity of water	4.18 $MJ\,m^{-3}\,K^{-1}$	Gordon et al. (2012)

2007) to the one-dimensional heat transfer equation for steady fluid flow through a homogeneous porous medium (Stallman, 1965). These solutions use amplitude and phase change in the sinusoidal diurnal signal of a pair of two temperature sensors in different depths for the calculation of the advective flow component. VFLUX first obtains the diurnal oscillation signal by filtering the data using dynamic harmonic regression (DHR) (Young et al., 1999). Then, differences in amplitude and phase are extracted for each periodic cycle. The software calculates vertical flux rates for each specified sensor pair in meters per second based on both amplitude and phase change for each of the methods described by Hatch et al. (2006) and Keery et al. (2007). Sediment-specific input parameters for the calculations are summarized in Tab. 6.1.

6.3 Results

6.3.1 Comparison of pore-water sampling techniques

Geochemical profiles measured in pore-water samples from peeper and Rhizon samplers showed high agreement, especially for stable water isotopes and ions. Figure 6.3 shows depth profiles measured with a peeper and the Rhizon samplers at three different pumping rates. Rhizon sampling at different pumping rates was conducted in May. NO_3^- and SO_4^{2-} concentrations were very similar for all profiles showing steep gradients in close proximity to the sediment–water interface. The low number of samples above the detection limit, together with the steep geochemical gradients, was not sufficient for statistical evaluation. Ca^{2+}, Mg^{2+}, and Cl^- concentrations were on average 5-7 % lower in the peeper data compared to Rhizon samples, but different pumping rates did not have an effect on average concentrations (Sec. B.4, Fig. B.6).

Average CH_4 concentrations in Rhizon samples deviated by -30 % (lowest pumping rate) to +100 % (highest pumping rate) from peeper samples. While the CH_4 concentration profiles recorded with the peeper showed a smooth gradient, profiles from Rhizon measurements showed large concentration differences in consecutive depths. Average measured concentrations were significantly different not only between peeper and Rhizon samples but also for different pumping rates (Fig. B.5).

To analyze if isotope fractionation processes influence the measurements of dissolved solutes and gases, stable water isotopes ($\delta^{18}O$ and δ^2H) were measured in water samples and stable

Table 6.2: Stable water isotopes (δ^2H & δ^{18}O) and deuterium excess *d* in pore water and surface water.

Sample type	Date	Pumping rate	δ^{18}O	δ^2H	d
Pore-water average	30$^{\text{th}}$ May 2022	0.09 mL min^{-1}	-9.296 ‰	-67.658 ‰	6.710 ‰
	31$^{\text{st}}$ May 2022	0.38 mL min^{-1}	-9.282 ‰	-67.555 ‰	6.701 ‰
Surface Water	30$^{\text{th}}$ May 2022		-9.186 ‰	-67.196 ‰	6.292 ‰
	31$^{\text{st}}$ May 2022		-9.183 ‰	-67.273 ‰	6.191 ‰

carbon isotopes (δ^{13}C) in methane. Water isotopes were only measured at the highest and lowest pumping rate. Results were found to be similar with no significant differences based on the *t* test (Sec. B.4). Table 6.2 shows water isotopes from pore water samples and surface water samples. Deuterium excess in the sediment was 0.5 ‰ higher in pore-water compared to surface water samples. This is below the analytical precision for δ^2H measurements of 1 ‰.

With an average of -71.2 ‰ CH_4 had a significantly lighter isotopic composition in peeper samples compared to samples extracted with Rhizon samplers (averages between -65.9 ‰ and -69.2 ‰). The stable carbon isotopic composition of CH_4 was with -65.9 ‰ the heaviest at the lowest pumping rate. Homogeneity of variances was neither given in CH_4 concentration nor stable isotope data. Standard deviation of CH_4 concentrations increased with increasing pumping rate (420 µmol L^{-1} at the lowest pumping rate, 678 µmol L^{-1} at the medium pumping rate, and 1119 µmol L^{-1} at the highest pumping rate) but was more similar for isotopic data. When comparing all four data sets with the Kruskall-Wallis *H* test, differences were significant for both CH_4 concentrations ($p = 0.01$) and stable isotopes ($p = 0.0003$).

In addition, the hyporheic geochemistry of the study site was described in detail with 11 sampling campaigns between April and September 2021 (Sec. B.2). Geochemical gradients were found to be very steep, with oxygen reduction and denitrification zones in close proximity or even partly overlapping. A substantial amount of CH_4 was produced in the deep anoxic layers of the HZ. Ion and gas concentrations were stable over time with only gradual changes between spring and summer. The most pronounced changes were sedimentation events which moved the location of the sediment–water interface upwards. The anoxic, reduced conditions in deeper layers stayed unchanged throughout the sampling period in 2021. CH_4 concentration profiles measured with a peeper in September 2021 and in May 2022 showed almost exactly the same gradients.

6.3.2 Locating the oxic–anoxic interface

The fiber-optic sensor unit based on the description of Brandt et al. (2017) was tested against a microsensor in the chambers of the peeper (Fig. 6.4). The fiber-optic system was able to locate the oxic–anoxic interface precisely. All three repeated measurements showed good agreement at a high resolution of 1 cm. However, the lowest O_2 concentration (20 µmol L^{-1}) measured with the microsensor was higher than dissolved O_2 concentrations observed with the fiber-optic system below the oxic–anoxic interface. In O_2 saturated conditions, absolute values for calculated O_2 concentrations from the fiber-optic system showed high variance. Due to the flat shape of the calibration model in near-saturated conditions (see Sec. B.3, Fig. B.4),

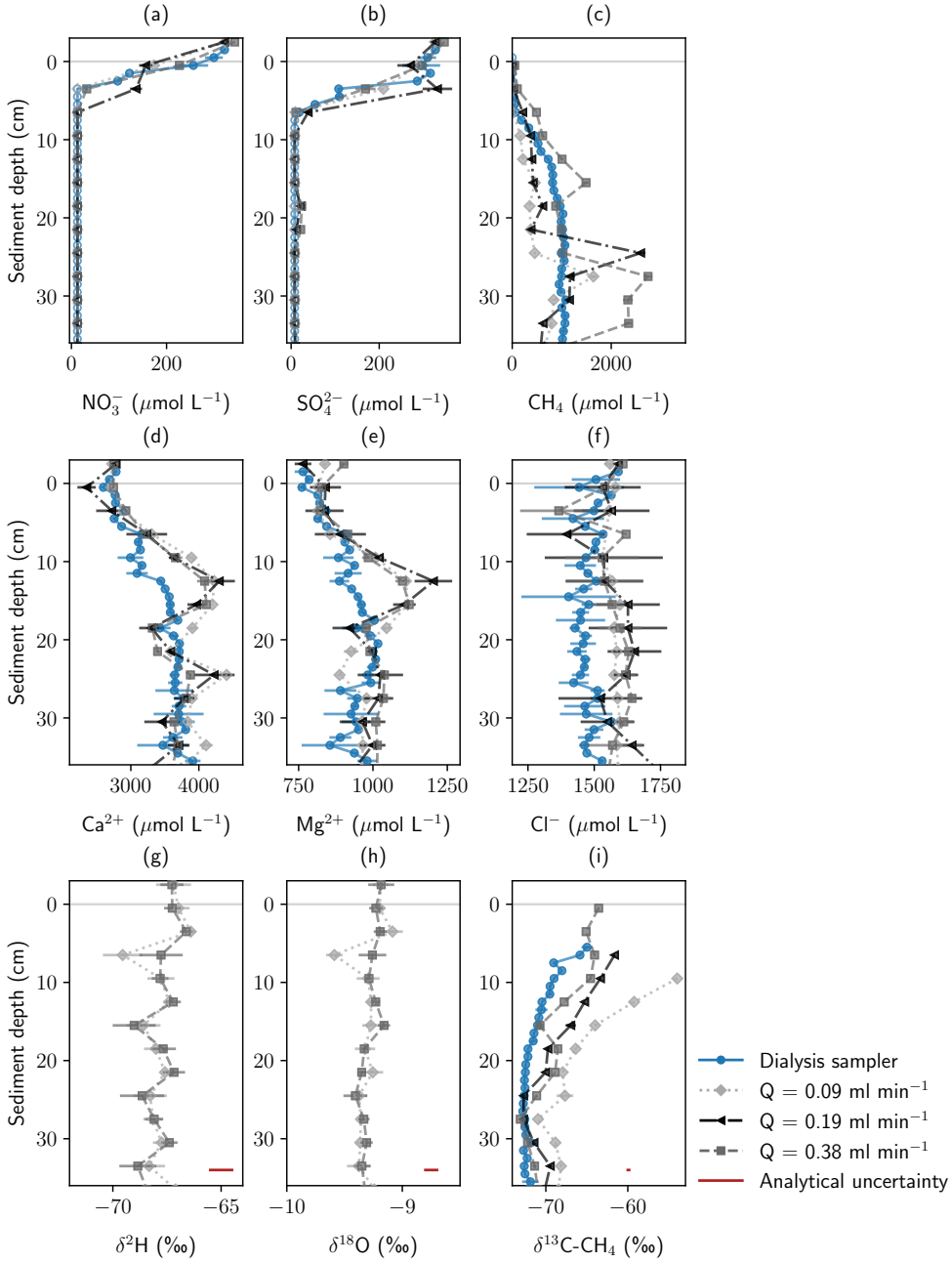

Figure 6.3: **Concentration and stable isotope profiles measured with a pore-water dialysis sampler and Rhizon samplers from the monitoring station at three different pumping rates.** All samples were extracted in May 2022. Panels show (a) NO_3^-, (b) SO_4^{2-}, (c) CH_4, (d) Ca^{2+}, (e) Mg^{2+}, and (f) Cl^- concentrations; (g, h) stable water isotopes; and (i) stable carbon isotopes in CH_4. Error bars show standard deviation of repeated measurements. In addition, analytical uncertainty of the measurement devices is shown for isotope data.

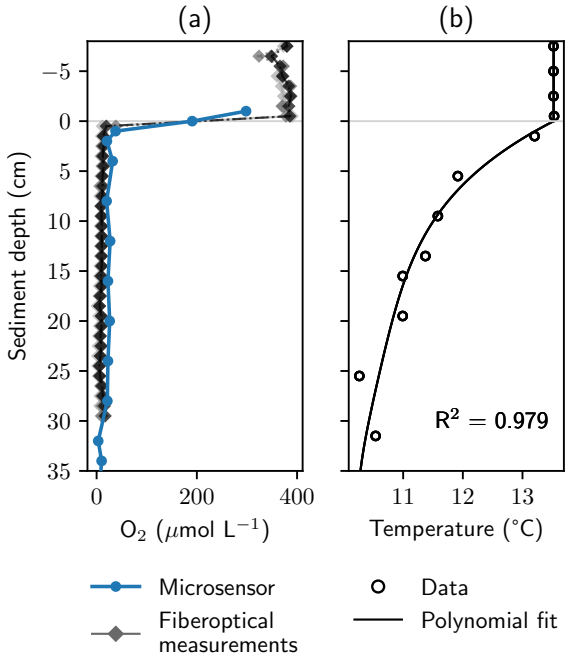

Figure 6.4: **Oxygen and temperature gradients at the study site.** Panel (a) shows dissolved O_2 profiles measured with a microsensor in the chambers of a peeper and with a manufactured in situ fiber-optic sensor. Saturated values measured with the fiber-optic system were normalized to avoid unrealistically high values. Panel (b) shows temperature measurements and a fourth-order polynomial fit, which was used to calculate O_2 concentrations from measured phase angles.

signal noise led to larger errors than in the anoxic zone. Oversaturated values were normalized to avoid unrealistically high values (Eq. B.4).

6.3.3 Assessing vertical hyporheic exchange

Temperature data were continuously recorded between April and August 2022. Pronounced amplitude dampening and time lag of the diurnal signal could be extracted with DHR and subsequently used for flux calculations (Fig. 6.5). Six sensors had to be excluded from the data set due to low data quality or larger data gaps, leaving a total of eight sensors for the evaluation. Sensor pairs for flux calculation were chosen not to be neighbouring, but every other sensor, for example sensor 1 and 3, sensor 2 and 4, sensor 3 and 5. Here, results based on the amplitude method described by Hatch et al. (2006) with the parameters from Tab. 6.1 are shown. Fluxes simulated with the phase method and with analytical solutions derived by Keery et al. (2007) are discussed in Sec. B.5.

Flux rates calculated with the upper three sensors showed peaks of a downward flux of up to $1 \cdot 10^{-5}\,\mathrm{m\,s^{-1}}$ ($85\,\mathrm{cm\,d^{-1}}$) in April and May 2022. Flux rates calculated between the lower five sensors showed mainly upward-directed flow. Average flux rates at 10 cm, 12 cm, and 18 cm depth were $-1.6 \cdot 10^{-7}\,\mathrm{m\,s^{-1}}$ ($-1.4\,\mathrm{cm\,d^{-1}}$), $-2.6 \cdot 10^{-7}\,\mathrm{m\,s^{-1}}$ ($-2.2\,\mathrm{cm\,d^{-1}}$), and $-4.9 \cdot 10^{-7}\,\mathrm{m\,s^{-1}}$ ($-4.2\,\mathrm{cm\,d^{-1}}$), respectively. This is shown in detail in Sec. B.5, Fig. B.8, where

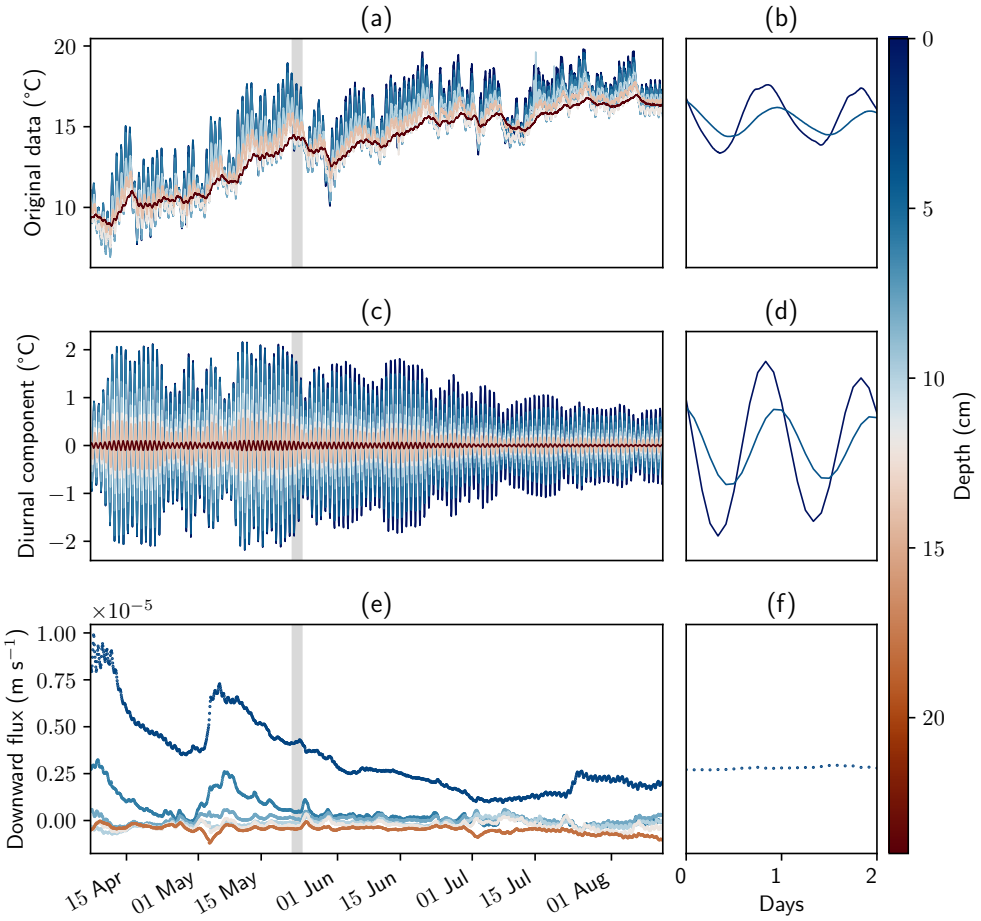

Figure 6.5: **Temperature measurements, filtered data, and calculated fluxes.** Panels (a), (c), and (e) show the complete measurement period and all sensors. Panels (b), (d), and (f) show sensors in the surface water and at 10 cm depth for a time window of two days. Panels (a) and (b) show original data. Filtered data and fluxes were calculated with the software package VFLUX and the amplitude method described by Hatch et al. (2006) using the parameters from Tab. 6.1.

fluxes calculated for 3 cm and 6 cm depth were excluded from the plot. Based on these values, mean water transit times in the 40 cm stretch from the bottom to the top of the geochemical profiles would be between 9 to 29 days.

6.4 Discussion

Our results showed an excellent agreement for ion concentration and stable water isotope measurements in pore-water samples for the two different methods used, and equally good agreement for different pumping rates when using Rhizon samplers and peristaltic pumps. The only exceptions were Cl^- concentrations, which were consistently higher at the monitoring station compared to the peeper, and Mg^{2+} at medium and high pumping rates (Fig. B.6). This indicates high suitability of Rhizon samplers for repeated pore-water extraction at one specific site to study temporal dynamics in nutrient cycling. Certainly, Rhizons could also be used to

trace the fate of contaminants, as long as the pore diameter of the filter allows the contaminant molecule to pass and the contaminant is fully dissolved in water. For concentration and isotope analyses of dissolved gases, here CH_4, we found a lower agreement between pore-water samples extracted by Rhizons and peepers. Gas concentrations and variance increased with increasing pumping rates when using Rhizon samplers. On average, concentrations were lower compared to dialysis measurements.

Based on the data from 2021, which showed a very stable geochemical system, rapid changes in stream geochemistry between the sampling days at the beginning and end of May 2022 are not expected. The stream temperature was very similar on all sampling days, and river discharge was only 4.8 % higher at the end of the month (Fig. 6.2). Ebullition occurred sporadically, but no larger, sudden gas releases were observed at the sampling site, neither in 2021 nor during recent field campaigns. Therefore, a rapid change in gas concentrations in the sediment seems to be very unlikely and the observed changes in CH_4 concentrations and stable isotopic composition in CH_4 are most likely caused by the changes in pumping rate and not by varying hydrological or geochemical conditions at the sampling site.

Of course, actual changes in gas content and composition between sampling days would explain the measured differences. If these are not triggered by temperature changes or discharge peaks, they could be caused by physical stress or a sudden ebullition event. However, these events seem rather unlikely considering the stagnating geochemistry in 2021 and the rather remote location of the sampling site without public access. The possibility that water is sampled from different parts of the pore space at different pumping rates seems more convincing. Pressure gradients around the samplers will change if the pumping rate is increased.

Another possible explanation for the observed differences in CH_4 concentrations and carbon stable isotopic composition may be differing behaviors of water and gas phases in the interstitial pore space. Rising air bubbles were sporadically observed at the sampling site and entrapped gas was found in sediment cores. During sample extraction, gas was seen to travel upwards through the tubes. These gas bubbles might become trapped in front of the microfilters at low pumping rates because pressure gradients may not be sufficient for the extraction of gas bubbles from the sediment. At higher pumping rates, bubbles seem to get mobilized from a larger distance, potentially further away than liquid pore-water samples. Additionally, a greater vacuum at higher pumping rates may cause increased outgassing and, thus, the creation of additional gas bubbles. Since the tubes were directly connected to the sampling vials, bubbles were not lost, but the gas and water phases were both contained in the sample vial. This could explain the large scatter and high concentration peaks observed at higher pumping rates. Most likely a combination of this effect and the extraction of sample from different parts of the pore space is responsible for the observed differences in gas samples at different pumping rates.

The dependence of CH_4 concentrations on the pumping rate complicates data interpretation because it is unknown from which part of the pore space the gas and water phases were extracted and it is difficult to define a ”correct” pumping rate where the gas and water phases are extracted from the same pore space. One also has to consider the trade-off between low pumping rates (low pressure gradient, little degassing) and corresponding sampling times (contact with air, sampling artifacts). Thus, gas measurements in pore-water samples extracted with Rhizon samplers are bound to have significant bias, especially if gas bubbles are present in the system.

Yet, dialysis does not include the gas phase in pore-water measurements at all, and it is questionable if it represents CH_4 distribution accurately. Bubbles can't enter the chambers of the peeper and therefore, cannot be directly sampled. Contact with the gas bubbles over extended time periods might however increase dissolved CH_4 concentration in the water sample. An effect could be a smoothed concentration gradient with slightly elevated concentrations. In addition, peepers integrate over several weeks while direct pore-water extraction can capture a specific moment in time. Hence, dialysis may not be a better solution for representing the distribution of gaseous and dissolved CH_4 in the sediment.

Other techniques for pore-water extraction such as multi-level piezometers or USGS MINIPOINTS were not tested in this study but may have similar advantages and disadvantages to Rhizon samplers. They allow time-resolved measurements and are hypothesized to be better suited for measuring effect and the distribution of gas in sediments than dialysis samplers. But if, as suspected, changes in negative pressure at different pumping rates lead to a different behavior of the gas and water phases in the pore space, this effect is likely to occur whenever samples are directly extracted from the pore space, no matter with which device. Larger pore diameters could increase the suitability for gas sampling, but we would still recommend testing the effect of different pumping rates when working with gas analyses in this type of fine-grained environment.

While sampling had a negligible effect on isotope fractionation for stable water isotopes, measured as proxies for the liquid phase, $\delta^{13}C$ values of CH_4 showed significant differences in the four measured profiles, showing an isotope fractionation towards heavier carbon isotopes at low pumping rates. At high concentrations ($>$ 950 µmol L^{-1}), $\delta^{13}C$ of CH_4 was found to be similar for sampling with Rhizon samplers and peepers (-72.0 $\pm$1.1 ‰). Below 950 µmol L^{-1}, a steep nonlinear increase in $\delta^{13}C$ was observed with decreasing CH_4 concentrations (Fig. 6.6). The higher stable carbon isotope composition at low concentrations can either be caused by microbial CH_4 degradation (Whiticar & Faber, 1986) or by an isotope fractionation effect during sampling, for example due to diffusion through the tubes or losses at the peristaltic pump. CH_4 escaping through leakages or diffusion would lead to a greater loss of the lighter $^{12}CH_4$ compared to $^{13}CH_4$, and an enriched remaining CH_4 pool (Li et al., 2022). This effect is expected to be more pronounced at low concentrations. Effects of microbial degradation would be expected to be in a similar range for peeper and Rhizon-derived profiles; thus $\delta^{13}C$ values exceeding maximum $\delta^{13}C$ in peeper samples by up to 10 ‰ imply fractionation during sample extraction.

This is true for a very fine-grained sampling site with a high content of organic matter and the occurrence of gas bubbles. In this type of system, the extraction of pore water requires high negative pressures at the interface between sampler and saturated sediment to overcome capillary forces in the sediment. The predominance of gas in the pore space complicates the sampling procedure and data interpretation. In sandy or gravelly riverbeds, lower suction rates are sufficient for pore-water extraction and CH_4 is likely to be present at lower concentrations and, thus, probably completely dissolved in the water phase. In these systems, the problems observed here may not be of relevance. Nevertheless, we find it important to emphasize the potential problems of using Rhizons for gas sampling because this has not been addressed previously in the literature and because Rhizons might be increasingly used in the future, when the interest in the HZ as an important source of GHG rises.

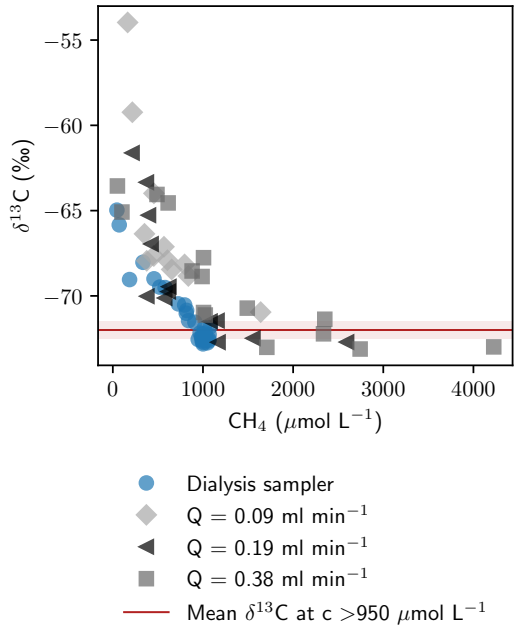

Figure 6.6: **Relation of CH_4 concentrations and isotopic composition.** The average $\pm$ standard deviation of δ^{13}C–CH_4 for all data points with concentrations $>950\,\mu mol\,L^{-1}$ (-72.0 $\pm$1.1 ‰) is shown in red.

Dissolved O_2 concentrations measured in peeper chambers were elevated compared to in situ measurements and we did not find an affordable way to measure dissolved O_2 concentrations in extracted pore-water samples without contamination with atmospheric air. Considering the steep geochemical gradients, the employed sampling resolution of 3 cm would not have been sufficient to precisely locate the oxic–anoxic interface. For the assessment of CH_4 in a case like this, there is a necessity for in situ measurements. The sensor developed by Brandt et al. (2017) was a low-cost effective tool and a great addition to the monitoring station. Temperature sensors that were necessary for the evaluation of the O_2 sensor's raw data could also be used for a continuous monitoring of the sampling site. The data were used to describe the site as an upwelling system, which is important information for the interpretation of geochemical profiles and, in addition, could visualize sedimentation and erosion processes. The measurements could further help to improve geochemical transport models if applied because diffusion coefficients are temperature dependent. However, the installation of the sensors must be done carefully to ensure a long service life. At our field site, several sensors stopped functioning properly, most likely due to problems at soldered joints and connectors or due to humidity and water intrusion.

The combination of pore-water sampling, in situ oxygen profiling, and temperature monitoring allowed a precise characterization of the functioning of the HZ with high spatiotemporal resolution, and the three methods were found to complement each other very well. The combination could, for example, be very useful for studying the effect of floods and droughts on stream ecosystems in terms of nutrient cycling and GHG emission pulses, although additional

fastenings may be necessary to ensure stability during floods. So far, as to our knowledge, the effect of drying and first flush events on riverine GHG emissions has not been studied, and the described setup would be well suited to tracing the hydrological and geochemical changes in the HZ during such events. The setup could also be used for tracer experiments, since Rhizon samplers cannot only be used for pore-water extraction but also for water injection. This could, for example, benefit the understanding of hyporheic flow patterns or the calculation of mean residence times and carbon or nutrient turnover rates.

6.5 Conclusions

In this study, we tested three methods for resolving temporal dynamics in HZ geochemistry. Rhizon samplers were found to be suitable for the extraction of water samples and the measurement of dissolved solutes with a high vertical resolution. However, suitability for gas analyses was reduced, as indicated by a dependency of CH_4 concentration on the pumping rate and a fractionation towards heavier isotopes during sampling. This finding might be most pronounced in fine-grained systems with gas inclusions in the sediment, and sampling with Rhizon samplers for gas analyses might be more suitable for rivers with coarser bed substrate and higher hydraulic conductivity, where the gas is expected to be completely dissolved in the water phase. A fiber-optic O_2 sensor was manufactured, calibrated, and tested in combination with the monitoring station. Although absolute O_2 concentrations in saturated and near-saturated conditions could only be determined with relatively high uncertainty, the system was very well suited for precisely locating the oxic–anoxic interface. This parameter is highly relevant for aquatic ecology and the sensor has proven a useful, low-cost solution for HZ monitoring. The station was complemented with temperature sensors which could be used to detect sediment dynamics and estimate hyporheic fluxes. Combining the three methods has several advantages over sampling pore water alone. Knowledge of the exact location of the oxic–anoxic interface and data on temperature and sediment dynamics between point samplings enable a better interpretation of geochemical profiles and deeper insights into the dynamics of HZ geochemistry.

Author contributions

TM, AW, TB and FE conceptualized the project. TM and AW developed the methodology. TM was responsible for fieldwork, data acquisition and curation, formal analysis, visualization, and original draft preparation. JG and his team supported fieldwork and provided resources. FE and TB acquired funding and supervised the project. TM, AW, TB, JG, and FE all contributed to writing, reviewing, and editing the paper.

Acknowledgements

First and foremost we would like to thank Theresa Mond for her great work during the field campaigns in 2021. We would also like to acknowledge the team of the Chair of Aquatic Systems Biology for support during fieldwork and the provision of technical equipment, power

access, and space. Our thanks also go to the Chair and Testing Office for Foundation Engineering, Soil Mechanics, Rock Mechanics and Tunneling (mainly Gerhard Bräu) for loss on ignition (LOI) measurements. Further, we are greatful to the Chair of Engineering Geology, who made lab space and technical equipment for sediment analyses available. In addition, we would like to thank Kai Zosseder und Daniel Bohnsack for guidance in thermal conductivity measurements and Manuel Gossler for valuable input on temperature measurements and modeling. We thank Theresa Mond and Sophia Klausner for their essential support during the installation of the monitoring station, Jaroslava Obel for her help with laboratory analytics, and Friedhelm Pfeiffer for critical reading and reviewing of the manuscript.

Review statement

This paper was edited by Alberto Guadagnini and reviewed by two anonymous referees.

7 Publication III

High methane ebullition throughout one year in a regulated central European stream

This chapter was submitted as: Michaelis, T., Kaplar, F., Baumann, T., Wunderlich, A., & Einsiedl, F. (2024). High methane ebullition throughout one year in a regulated central European stream. *Scientific Reports*, *14*(1), 5359. https://doi.org/10.1038/s41598-024-54760-z

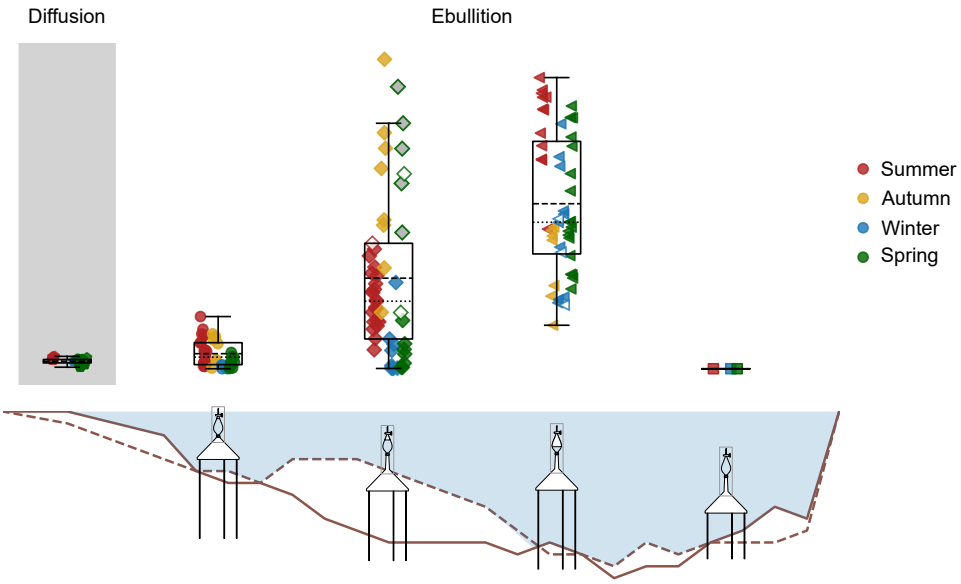

Abstract. Ebullition transports large amounts of the potent greenhouse gas methane (CH_4) from aquatic sediments to the atmosphere. River beds are a main source of biogenic CH_4, but emission estimates and the relative contribution of ebullition as a transport pathway are poorly constrained. This study meets a need for more direct measurements with a whole-year data set on CH_4 ebullition from a small stream in southern Germany. Four gas traps were installed in a cross section in a river bend, representing different bed substrates between undercut and slip-off slope. For a comparison, diffusive fluxes were estimated from concentration gradients in the sediment and from measurements of dissolved CH_4 in the surface water. The data revealed highest activity with gas fluxes above 1000 ml m^{-2} d^{-1} in the center of the stream, sustained ebullition during winter, and a larger contribution of ebullitive compared to diffusive CH_4 fluxes. Increased gas fluxes from the center of the river may be connected to greater exchange with the surface water, thus increased carbon and

nutrient supply, and a higher sediment permeability for gas bubbles. By using stable isotope fractionation, we estimated that 12-44 % of the CH_4 transported diffusively was oxidized. Predictors like temperature, air pressure, discharge, or precipitation could not or only poorly explain temporal variations of ebullitive CH_4 fluxes.

7.1 Introduction

Climate change is no longer a mere scientific phenomenon, but has impacted landscapes, ecosystems and societies around the globe (Ripple et al., 2022), forcing political action worldwide. To design effective mitigation strategies and adaptation measures, sound carbon budgets and feedback models are essential. To date, greenhouse gas (GHG) emissions from natural aquatic environments are poorly constrained and potential feedback to a warming climate is discussed controversially (IPCC, 2021).

Rivers are one of the largest sources of uncertainty in global methane (CH_4) budgets (Saunois et al., 2020) due to high spatiotemporal heterogeneity and a low number of direct measurements (Stanley et al., 2016). Yet, rivers and streams have repeatedly been shown to contribute large amounts of this potent GHG to the atmosphere (Bange et al., 2019; Borges et al., 2015; Campeau & Del Giorgio, 2014), and future emissions may rise further due to warming (Comer-Warner et al., 2018; Zhu et al., 2020), higher fine sediment inputs (Zhu et al., 2022), or increased eutrophication (Li et al., 2021). A major transport pathway of CH_4 from aquatic environments to the atmosphere, accounting for 50 % to 90 % of CH_4 emissions from lakes (Saunois et al., 2020), is ebullition, the spontaneous release of gas bubbles from anoxic sediments. In addition, Rocher-Ros et al. (2023) recently suggested that about half of the global CH_4 emissions from rivers were emitted via ebullition. However, the contribution of ebullition to riverine CH_4 emissions is currently still highly uncertain due to a lack of data especially from mid to high latitudes (Rosentreter et al., 2021).

In the context of ebullitive CH_4 emissions from rivers, recent literature has mainly focused on reservoir impoundments (Linkhorst et al., 2020, 2021; Miller et al., 2017; Wilkinson et al., 2019), leaving the relevance of free flowing sections in small streams as GHG emitters less explored. However, headwater streams represent the largest part of most river networks (Bishop et al., 2008), and several studies suggested an overproportional importance of these environments: McGinnis et al. (2016), as one of the first, demonstrated the potential significance of small streams, showing CH_4 emission rates comparable to tropical reservoirs; Castro-Morales et al. (2022) measured 2-7 times higher CH_4 partial pressure in tributaries compared to main channels; and Zhang et al. (2020) found an exponential decrease of ebullitive CH_4 fluxes with Strahler stream order.

Ebullition is a highly dynamic process and episodic variations may be overseen in short-term observations (Maeck et al., 2014). Nevertheless, sampling campaigns are often conducted within few days or weeks (e.g. Maeck et al., 2013), or are restricted to spring, summer and autumn for their favorable sampling conditions (e.g. McGinnis et al., 2016; Robison et al., 2021), leaving a lack of winter data from study sites in temperate climates. To the best of our knowledge, only few studies have conducted whole-year investigations on ebullitive CH_4 emissions from streams (e.g. DelSontro et al., 2010; Wilkinson et al., 2015).

This study was designed to collect a comprehensive data set of direct measurements of CH_4 ebullition from an anthropogenically impacted small stream and to quantify the GHG emissions throughout the year. Earlier studies have already identified river Moosach in southern Germany as an interesting study site for ebullition due to high CH_4 concentrations in the pore-water, a high abundance of methanogens in the hyporheic zone (HZ) (Michaelis et al., 2022), and the detection of gas bubbles in sediment cores (Michaelis et al., 2023). For the present study, bubble traps were installed at four sites in a cross-section located in a river bend, representing different substrates between slip-off slope, central section, and undercut slope (Fig. 7.1). Measurements of ebullition volumes, CH_4 and CO_2 concentrations, together with the stable carbon isotopic composition of CH_4 ($\delta^{13}C$–CH_4) in the gas bubbles were conducted for 12 months to capture temporal variability of all four seasons. $\delta^{13}C$–CH_4 data are well suited to study conversion processes in the CH_4 cycle (Einsiedl et al., 2020; Michaelis et al., 2022; Peña Sanchez et al., 2022b). Ebullitive CH_4 transport was further compared to estimates of diffusive fluxes across the sediment–water and the water–air interface, calculated from vertical CH_4 concentration profiles in the streambed and dissolved CH_4 concentrations in the surface water, respectively.

7.2 Materials and methods

7.2.1 Study site and general set-up

The study was conducted at River Moosach, a small stream in the south of Germany which drains a catchment area of 175 km^2, including larger peatlands of the Munich Gravel Plain and the Tertiary Hill Country. The river's course and hydrology have been altered by engineering measures like straightening and the construction of dams and dikes (Pulg et al., 2013). Nowadays, the river has a very low gradient, in the central section as low as 0.1 ‰, which leads to an increased accumulation of fines (Auerswald & Geist, 2018). The organic matter content of the fine fraction was found to be high with an average of 16 % (Auerswald & Geist, 2018).

To compare ebullitive GHG fluxes from different substrates, a cross section in a river bend was selected. In river turns or meanders, typically a secondary current erodes the outside curve, leading to an undercut slope, and deposits fine bed material at the inside bend, shaping a convex slip-off slope. Incremental differences between the fine deposits of the slip-off slope and the coarser bed substrate at the undercut slope can be studied in these conditions, at equal site characteristics otherwise.

Four bubble traps were permanently installed and sampled over a period of 12 months (Fig. 7.1). Bubble traps consisted of inverted funnels with an opening diameter of 42 cm, topped with an inverted glass separation funnel with stopcock for gas storage (Fig. C.1 in the Supplement). Trapping and storage funnels were connected through a rubber stopper with a bore hole reducing the diameter to 14.6 mm. This was meant to hamper convective exchange and thus, reduce transfer of GHGs from the stored gas into the surface water. Bubble traps A (left bank, slip-off slope), B (center left), and D (right bank, undercut slope) were installed on June 8th 2022. Macrophytes grew at sites A and B during July 2022. Therefore, a fourth trap (C, center right) was later installed (July 25th 2022) after discharge and flow velocity measurements to represent the main flow section with highest flow velocities centrally in the river (Fig. 7.1). All

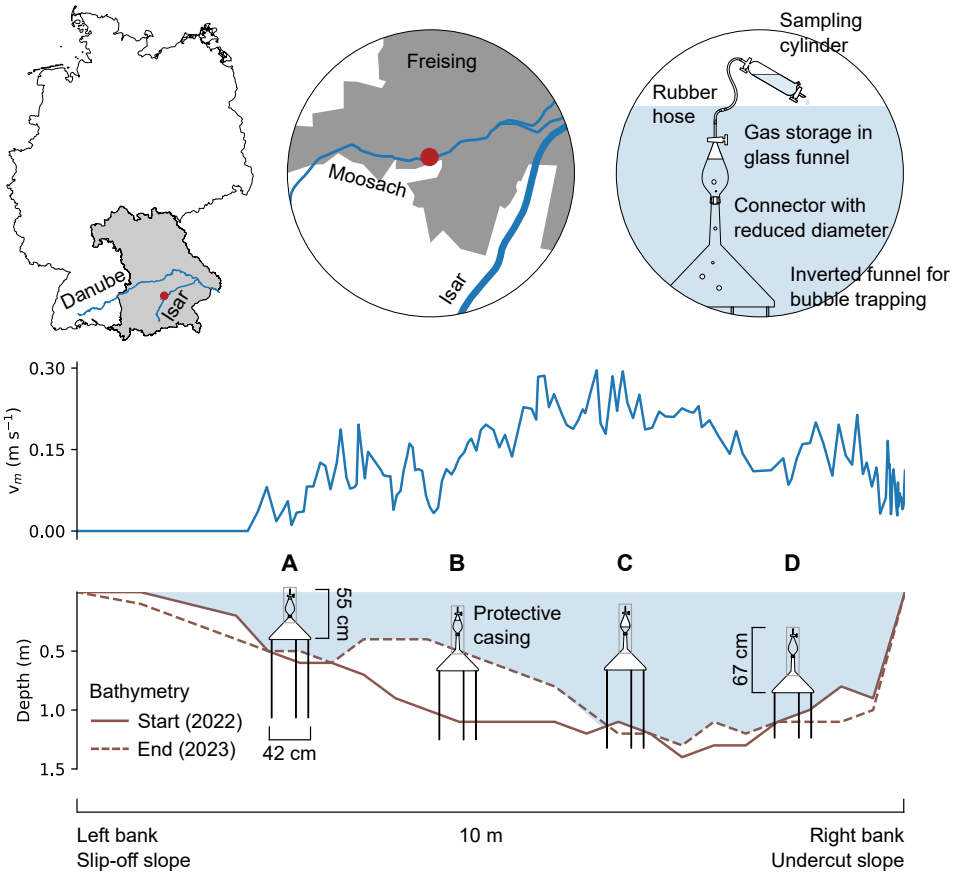

Figure 7.1: **Experimental set-up.** A map of the study area is provided in left and center of the top row. The map was compiled with ArcGIS Pro (version 3.0.3). In the middle row, average flow velocity v_m across the stream width is displayed as measured on June 28th, 2022. The cross section with four gas traps is displayed at the bottom. Bathymetry was measured at installation (2022) and removal (2023) of the gas traps. Heavy sedimentation covered parts of sampler B after a period of high flow in spring 2023. A detail in the top right schematically shows the sampling procedure.

bubble traps were installed approximately 10 to 20 cm above the streambed, such that they were fully submerged during almost all flow conditions. The traps were not designed floating, but provided with legs for fixation in the sediment to avoid tilting with the current, movement in space, or disturbance by animals and people.

7.2.2 Bathymetry and sediment characterization

The river bathymetry was measured at the days of installation and removal of the gas traps. An echosounder (Deeper, Vilnius, Lithuania) was moved across the river in 0.5 m steps and stream depth was recorded at each interval. Heavy sedimentation occurred at site B after a flooding event in spring 2023 and sampler B was half buried in the deposits after the event (Fig. 7.1).

For sediment characterization, two sediment cores were taken a little downstream of each bubble trap by manually pushing a liner with 6 cm inner diameter into the sediment. Porosity was measured by weighting sediment cores with a known volume before and after drying at 105 °C. Grain size distribution curves were created by sieving with decreasing mesh diameters and sedimentation experiments according to the German norm DIN EN ISO 17892-4. Loss on ignition (LOI) was determined by annealing dried and grinded sediment samples in a furnace at 550 °C to constant mass as described in the norm DIN EN 17685-1.

7.2.3 Flow velocity measurements

Flow velocity measurements were conducted for a relative comparison of the four sites. A velocity distribution over the studied cross section was measured with an Acoustic Doppler Current Profiler (ADCP) (SonTek, Yellow Springs, USA) on June 28$^{\mathrm{th}}$, 2022 (Fig. 7.1). The integrated discharge was with 1.25 $\pm$ 0.06 $m^3\,s^{-1}$ (mean $\pm$ standard deviation, n = 5) 34 % lower than the average discharge on that day at an official monitoring station 4.5 km downstream (1.68 $m^3\,s^{-1}$) (Bavarian State Office of the Environment, 2023). Macrophytes covered parts of the cross section during ADCP measurements which may have lead to inaccuracies in the bottom delineation and thus, to an underestimation of the cross sectional area. On the other hand, the official monitoring station was located downstream of the studied cross section behind the confluence with a small diversion creek and thus, there could also be a systematic difference between the two locations.

7.2.4 Sampling design

Bubble traps were sampled in intervals of 3 to 20 days, depending on expected gas volumes and weather conditions. In total, 158 samples were taken on 66 separate days and analyzed for gas concentrations and carbon stable isotopes of CH_4 (δ^{13}C–CH_4). Care was taken not to disturb the sediment during sampling, because extreme ebullition was observed once the sediment was physically stressed. Thus, sampling was carried out from an inflatable dinghy with minimal contact to the bubble traps. For extracting gas from the traps, a sampling cylinder with two glass stopcocks and a septum, pre-filled with de-ionized water, was connected to the inverted glass funnel for gas storage with a water-filled gas-tight rubber-hose (Fig. 7.1 and C.1).

By letting water out at the bottom end of the sampling cylinder, gas stored in the bubble trap was sucked into the cylinder. Small amounts of gas up to max. 16 ml (depending on size and filling level of the sampling cylinder) were lost in the rubber hose. Subsequently, all stopcocks were closed and the sampling cylinders were transported to the laboratory for further analysis.

For measurement of dissolved CH_4 concentrations in surface water, sampling cylinders were completely filled with stream water. Samples were taken centrally in the cross section approximately 5-10 cm below the water table. In the laboratory, a nitrogen (N_2) headspace of 10-20 % was created and the sample fixated with NaOH to ensure a pH $>$ 12 and to prohibit microbial turnover.

In addition, geochemical depth-profiles with a 1 cm vertical resolution were measured in the streambed at the beginning of the sampling period at three of the four sites. Three pore-water equilibrium dialysis samplers (peepers) were installed in June 2022, two meter downstream of bubble traps A, B, and D. For a more detailed description of the sampling method see Michaelis et al. (2022). For sampling, peepers were removed from the sediment, cleaned with de-ionized water, and samples withdrawn quickly from the chambers. Samples for CH_4 analyses were taken first in 10 ml glass vials previously flushed with synthetic air (80 % N_2, 20 % O_2), closed with a rubber-butyl stopper, and prepared with 20 µL 10 M NaOH. A second needle was inserted during sample injection for pressure release while care was taken to reduce turbulence and avoid degassing by slowly filling vials along the walls. For anion- and cation analyses, samples were taken in 1.5 ml glass vials fixated with 10 µL 0.5 M NaOH and 1 M HCl, respectively. All pore-water samples were transported to the laboratory and stored refrigerated until further analysis.

7.2.5 Laboratory analytics

Gas sampling cylinders for ebullition measurements were first weighted. Gas volumes were determined as weight difference of the completely water-filled gas cylinder and the cylinder with the gas sample. Before further measurements, sampling cylinders were left in the laboratory over night ($>$12 hrs) for gas equilibration between water phase and headspace at room temperature. Temperature was measured when extracting gas from the cylinder.

CH_4 concentrations were measured with the Trace 1300 gas chromatograph with flame-ionization detector (GC-FID) equipped with a TG-5MS column and calibrated with three standards (Rießner Gase, Lichtenfels, Germany). 250 µL of gas were manually injected three times for each sample. CH_4 concentrations in pore-water could be measured directly, but CH_4 contents in gas bubbles exceeded the calibrated range of the instrument by far, making a 1:100 dilution necessary. An underestimation of measured concentrations by 4.8 % was quantified with 10 dilutions of a gas concentration standard, each measured in triplicates, and samples were corrected with this factor before further data processing. After dilution and manual injection, concentrations could be obtained with an uncertainty of 5.3 % (relative uncertainty based on 2*SD of all 10 standard dilutions and repeated measurements). All samples were diluted and measured twice to detect and avoid gross errors.

The stable carbon isotope ratio ($\delta^{13}C$) of CH_4 was measured in triplicates with a G2201-i gas analyzer with an analytical uncertainty of $<$ 0.16 ‰ (Picarro, Santa Clara, USA), calibrated with two standards (Airgas, Plumsteadville, USA). Ebullition samples were further diluted to

meet the measurement range specified for the instrument and gas bags with the dilutions were connected to a small sample introduction module (SSIM). For pore-water samples from peeper profiles, vials were directly connected to the SSIM with a needle. Due to the small sample volumes, re-pressurization of the sampling vials with the carrier gas was necessary between repeated measurements.

The high gas volumes and large shares of GHG in ebullition samples allowed analysis of CO_2 and N_2 contents with a GC Micro Box (SLS Micro Technology, Germany). The instrument was calibrated with two standards (Linde AG, Unterschleißheim, Germany), achieving a relative uncertainty of $< 20\,\%$.

7.2.6 Data processing and calculation of ebullitive fluxes

CH_4 concentrations in pore-water samples from peepers were determined with the headspace equilibration method (EPA, 2001; Kampbell & Vandegrift, 1998) adapted for small sample volumes as described previously (Michaelis et al., 2022). Also for ebullition samples it was necessary to determine how the headspace gas composition in the sampling cylinder had changed before the measurements due to partitioning of the gas components between gas and water phases. Initial CH_4 and CO_2 contents before equilibration were inversely modeled from the measured headspace composition after equilibration using an optimization procedure and the chemical modeling software PHREEQC (version 3.7.3) (Parkhurst & Appelo, 2013). The geochemical modeling approach was chosen because it enabled consideration of the lime-carbonic acid balance, which strongly influences CO_2 solubility, and because it took into account how the presence of CH_4 and CO_2 mutually affected the bubble pressure. It was therefore superior to a component-wise calculation with Henry's law.

Input parameters for each PHREEQC run were gas pressure, temperature in the laboratory during measurements, and a best guess of the gas composition before equilibration. Optimal values for the initial CH_4 and CO_2 contents were determined by minimizing the sum of squared errors of the measured and modeled final gas composition after equilibration using the python package scipy.optimize (version 1.11.2). Pressure was set to the atmospheric pressure on the sampling day (DWD, 2023). The calculations were based on the assumption of a full equilibrium between water and gas phases in the sampling cylinder, which can be expected due to a storage time of > 12 hours and shaking. An uncertainty is that changes in pressure due to warming of the sample in the laboratory could not be considered. However, the sensitivity of the inverse modeling method to changes in gas pressure was found to be very low. In 10 random samples, pressure changes by $\pm 20\,\%$ only changed final gas contents by $< 1\,\%$.

Gas content c was converted from percent to mol L^{-1} using the molar volume of 22.4 L mol^{-1} and a temperature correction for the surface water temperature on the sampling day T_{SW} in °C according to Eq. 7.1 (EPA, 2001). Flux F in mol m^{-2} d^{-1} was then calculated by dividing the product of gas content c (mol L^{-1}) and gas volume V_{HS} (L) by the area A of the inverted funnel (0.14 m^2) and the time difference Δt (days) since the last sampling (Eq. 7.2). Volume fluxes were similarly calculated by dividing measured gas volume (V_{HS}) by area and time interval.

$$c(\mathrm{mol/L}) = \frac{c(\%)}{100} \cdot \frac{273}{22.4(273 + T_{SW})} \tag{7.1}$$

$$F = \frac{c \cdot V_{HS}}{A \cdot \Delta t} \tag{7.2}$$

To address the question of how much CH_4 can escape from and how much CO_2, N_2, and O_2 can enter a gas bubble during transport through the water column, we modeled the gas exchange of a pure CH_4 bubble with the single bubble dissolution (SiBu) model (version 1.2.6c) (Greinert & McGinnis, 2009). Gas contents in the bubble after passing the water column were estimated for a small (volume V = 0.004 L; diameter d = 2 mm) and large (V = 0.52 L; d = 10 mm) CH_4 bubble, a water depth of 1.3 m, and dissolved gas concentrations in the surface water of 0.26 mmol L^{-1} for O_2 (measured), $5.2 \cdot 10^{-4}$ mmol L^{-1} for CH_4 (measured), and 0.15 mmol L^{-1} for CO_2 (calculated based on carbonate concentration and a measured pH of 7.9). In addition, we tested how large the gas exchange would be if a medium sized pure CH_4 bubble with a volume of 0.02 L (d = 3.4 mm) reached an equilibrium with river Moosach's surface water (1.3 mmol L^{-1} Na^+, 2.5 mmol L^{-1} Ca^{2+}, 0.9 mmol L^{-1} Mg^{2+}, 1.5 mmol L^{-1} Cl^-, 0.3 mmol L^{-1} NO_3^-, 0.3 mmol L^{-1} SO_4^{2-}, and 11.7 mmol L^{-1} HCO_3^-) with PHREEQC (Parkhurst & Appelo, 2013).

7.2.7 Modeling diffusive fluxes across the sediment–water interface

Fluxes across the sediment–water interface were modeled from measured concentration gradients of CH_4 in pore water. A one-dimensional representation of the steady-state diffusion–reaction equation accounting for molecular diffusion, bioturbation, bioirrigation, and a source/sink term (Eq. 7.3) was solved numerically with the software package PROFILE (version 1.0) (Berg et al., 1998).

$$\frac{d}{dz}\left(\varphi(D_S + D_B)\frac{dC}{dz}\right) + \varphi\alpha_i(c_{sw} - c(z)) + R = 0 \tag{7.3}$$

where c(z) is pore-water CH_4 concentration as a function of sediment depth z, c_{sw} surface water CH_4 concentration, φ total porosity, D_S molecular diffusivity of CH_4 in the sediment, D_B biodiffusivity, α_i the irrigation coefficient, and R the rate of net production or consumption. c_{sw} and φ were taken from measurements, D_B was assumed to be zero, and R estimated section-wise as model fit parameter with a statistical optimization procedure (Berg et al., 1998). D_S was calculated as a function of the molecular diffusivity in water D_0 and porosity φ (Iversen & Jørgensen, 1993). D_0 for a water temperature of 17.0 °C, measured on the sampling day of the geochemical profiles, was calculated to be $1.49 \cdot 10^{-5}$ $cm^2\,s^{-1}$ based on Boudreau (1997). Boundary conditions were a fixed concentration at the top (c_{sw}) and bottom of the profile.

Equation 7.3 does not incorporate an advective flow component and thus cannot take hyporheic exchange into account. The bioirrigation term was used to consider different hyporheic exchange rates between sites. Bioirrigation coefficient α_i was calculated as a function of depth z as suggested by Martin and Sayles (1987) (Eq. 7.4).

$$\alpha_i(z) = \alpha_{i,0} \cdot \exp(-\alpha_{i,1} x) \tag{7.4}$$

Values for parameters $\alpha_{i,0}$ and $\alpha_{i,1}$ were chosen in ranges reported previously (Martin & Banta, 1992; Martin & Sayles, 1987) such that they represent largest exchange with the surface water

in the central river section (site B, $\alpha_{i,0}$ = 170 yr^{-1} and $\alpha_{i,1}$ = 0.4 cm^{-1}), medium exchange at the slip-off slope (site A, $\alpha_{i,0}$ = 12 yr^{-1} and $\alpha_{i,1}$ = 0.2 cm^{-1}) and very low exchange at the consolidated undercut slope (site D, $\alpha_{i,0}$ = 7 yr^{-1} and $\alpha_{i,1}$ = 1 cm^{-1}). Below 10 cm at the center and slip-off slope, or below 5 cm at the undercut slope, α_i was set to zero.

It is worth to be mentioned that the model assumes steady-state conditions. Therefore, short-term dynamics cannot be represented. Since pore-water concentrations measured with dialysis average over a measurement period of several weeks, short-term temporal variations are neither reflected in the data, which makes a quasi steady-state assumption applicable for a first approximation. Nevertheless, interpretation of the modeling results must take these limitations into account.

7.2.8 Estimation of diffusive fluxes across the water–air interface

The magnitude of diffusive CH_4 fluxes across the water–air interface was estimated based on dissolved CH_4 concentrations in surface water c_{sw} using Eq. 7.5 (Raymond et al., 2012; Wanninkhof et al., 2009).

$$F_{CH_4} = k \cdot (c_{sw} - c_{air}) \tag{7.5}$$

where c_{sw} is the average measured surface water CH_4 concentration, c_{air} the background CH_4 concentration in the atmosphere, and k the gas transfer velocity in m d^{-1}. Values for c_{air} were obtained from the NOAA Global Monitoring Laboratory (NOAA, 2023). An atmospheric CH_4 concentration of 1997 ppbv, average of April to June 2021 at the Hohenpeißenberg monitoring station (NOAA, 2023), was the most recent estimate available to represent the sampling season and study area. k was calculated according to Eq. 7.6 (Raymond et al., 2012; Robison et al., 2022).

$$k = \left(\frac{SC_{CH_4}}{600}\right)^{1/2} / k_{600} \tag{7.6}$$

where SC_{CH_4} is the Schmidt number of CH_4, and k_{600} the gas transfer rate standardized for a Schmidt number of 600. Following Raymond et al. (2012), we used Eq. 7.7 for calculating the Schmidt number of CH_4 as a function of surface water temperature T_{sw} (°C), and Eq. 7.8 for the estimation of k_{600}.

$$SC_{CH_4} = 1824 - 98.12 \cdot T_{sw} + 2.413 \cdot T_{sw}^2 - 0.0241 \cdot T_{sw}^3 \tag{7.7}$$

$$k_{600} = (v_m \cdot S)^{0.89} \cdot D^{0.54} \cdot 5037 \tag{7.8}$$

where v_m is the average stream velocity in m s^{-1} calculated as v_m=Q/A with a cross-sectional area A of approximately 10 m^2, S the channel slope of 0.15 ‰ (Auerswald & Geist, 2018), and D the water depth of the stream of 1.3 m at the studied cross section. Daily averaged data for discharge Q (m^3 s^{-1}) was available from the Bavarian State Office of the Environment (2023). Due to an increase in background CH_4 concentrations since 2021 and lower actual discharge than recorded at the official monitoring site (see Sec. 7.2.3) the estimates for diffusive fluxes across the water–air interface have a tendency to be over- rather than underestimated.

7.2.9 Estimation of methane oxidation based on stable isotope ratios

CH_4 that is transported diffusively through the HZ can be oxidized microbially to CO_2 before reaching the water column. Oxidation of CH_4 under aerobic and anaerobic conditions leads to an isotopic enrichment in $\delta^{13}C$–CH_4 due to a preferential consumption of lighter isotopes (Whiticar et al., 1986). We used differences in isotopic composition between CH_4 in gas bubbles and dissolved CH_4 in surface water to estimate the fraction of CH_4 oxidized, assuming that gas bubbles represent the source CH_4 before oxidation (Sawakuchi et al., 2016). The fraction oxidized was calculated for an open system at steady state according to Eq. 7.9 (Happell et al., 1994; Sawakuchi et al., 2016).

$$f_{ox} = \frac{\delta_{sw} - \delta_b}{(\alpha - 1) \cdot 1000} \tag{7.9}$$

where f_{ox} is the fraction of CH_4 oxidized, δ_{sw} and δ_b are the average $\delta^{13}C$–CH_4 values in surface water and gas bubbles, respectively, and α the stable isotope fractionation factor. Isotopic carbon fractionation of CH_4 is influenced by transport, here diffusion, and CH_4 oxidation ($\alpha = \alpha_{ox} - \alpha_{diff}$) (Preuss et al., 2013). A wide range of carbon isotope fractionation factors for CH_4 oxidation (α_{ox}) between 1.003 and 1.039 has been reported, introducing considerable uncertainty into the quantification of CH_4 oxidation (Happell et al., 1994; Templeton et al., 2006). Stable isotope fractionation factors are not related to the methanotrophic strain or enzymatic pathway (Feisthauer et al., 2011), but are strongly temperature dependent (Coleman et al., 1981). As we have not determined a site specific stable isotope fractionation factor for CH_4 oxidation, values for α_{ox} were taken from an environment similar to our study site and corrected by 0.00039 °C^{-1} (Chanton et al., 2008) for a median temperature of 12 °C (median of measured values between 8 and 16 °C). Preuss et al. (2013) reported α_{ox} = 1.031 for saturated soils at 4 °C and α_{diff} = 1.001, giving a final α of 1.027 after temperature correction. This value is similar to what has been reported for marine sediments (1.026 to 1.027 at 15 °C) (Kinnaman et al., 2007). To account for parameter uncertainty we also tested values in the range between 1.017 and 1.037.

7.2.10 Regression analysis

CH_4 fluxes were plotted against several environmental parameters which were named in the literature as potentially affecting CH_4 ebullition from streams. Temperature was measured at a monitoring station approximately 630 m upstream of the study site (Michaelis et al., 2023). Daily averaged values for discharge and precipitation were retrieved from the Bavarian State Office of the Environment (2023), air pressure drop was calculated from data made available by the German Weather Service DWD (2023). For each independent variable except for air pressure, an average over the sampling period was calculated and plotted against ebullitive CH_4 flux. To correlate the largest pressure drop with CH_4 flux, the minimum difference between consecutive air pressure values during a sampling interval was extracted from daily air pressure data. For discharge, precipitation, and air pressure drop, Pearson correlation coefficients were calculated to detect linear correlations. The Pearson correlation coefficient r lies between -1 and 1, with values close to zero indicating no correlation, and values close to -1 or 1 a strong negative or positive correlation, respectively. In addition, linear mixed-effects modeling (LMM)

was performed with the python package statsmodels (version 0.14.1). For surface water and sediment temperature in 20 cm depth, the modified Arrhenius model (Eq. 7.10; Kadlec and Reddy, 2001) was fitted as prior employed by Aben et al. (2017) in the context of temperature dependence of CH_4 ebullition.

$$E_T = E_{20} \cdot \theta_s^{(T-20)} \tag{7.10}$$

where E_T is the ebullition rate in mmol m^{-2} d^{-1} at temperature T (°C), E_{20} the ebullition rate at 20 °C, and θ_s a dimensionless system temperature coefficient. The best fit for E_{20} and θ_s was determined with the scipy.optimize package (version 1.11.2) in python (version 3.11.4).

7.3 Results

7.3.1 Sediment characteristics

Sediment characteristics between the undercut and the slip-off slope were found to differ in the top layer, but were very similar below a depth of approximately 10 cm (Fig. 7.2). The slip-off slope (site A) was found to have homogeneous fine-grained bed substrate down to at least 30 cm depth, mainly consisting of fine sands and coarse to middle grained silt and an organic carbon content of 14.6 % (Tab. C.1 in the Supplement). Similar material was found throughout the cross section below the top layer. Moving towards the undercut slope, the top layer was inceasingly coarse grained with 87 % sand at the center left (site B), 14 % gravel, 63 % sand at the center right (site C), and 41 % gravel, 33 % sand at the right bank (undercut slope, site D). LOI was highest at site C with 26.6 %, and lowest at site D with 5.0 % (above 9 cm depth) to 9.9 % (below 9 cm). Porosity was substantially lower at site D (59.9 %) compared to the rest of the cross-section (76.5 % to 81.0 %).

7.3.2 Vertical pore-water gradients

Vertical pore-water gradients revealed highest CH_4 concentrations between 241 and 447 µmol L^{-1} at the undercut slope (site D) between 12 to 23 cm depth (Fig. 7.3). Centrally in the river (site B), CH_4 concentrations were lowest with a maximum of 190 µmol L^{-1}. At sites B and D, CH_4 concentrations increased close to the sediment layer boundary. Concentrations in the homogeneous deposits at the slip-off slope (site A) increased almost linearly between 1 and 20 cm depth.

$\delta^{13}C$–CH_4 gradients decreased by 0.2 to 0.3 ‰ per cm with depth at sites A and B, with values at site B being isotopically enriched by approximately 5 ‰ compared to site A. From 2 to 4 cm depth, a slope change in $\delta^{13}C$–CH_4 was found at site B, showing a pronounced isotopic enrichment by 1.9 ‰ cm^{-1} towards the top of the streambed, from -68.0 ‰ in 4 cm to -64.3 ‰ in 2 cm depth. The $\delta^{13}C$–CH_4 profile measured at site C differed in shape from the other two observations. $\delta^{13}C$–CH_4 was found to be more negative in the top section with an average of -71.5 ‰ between 6 to 14 cm depth compared to the bottom of the profile with an average of -67.2 ‰ from 19 to 33 cm depth.

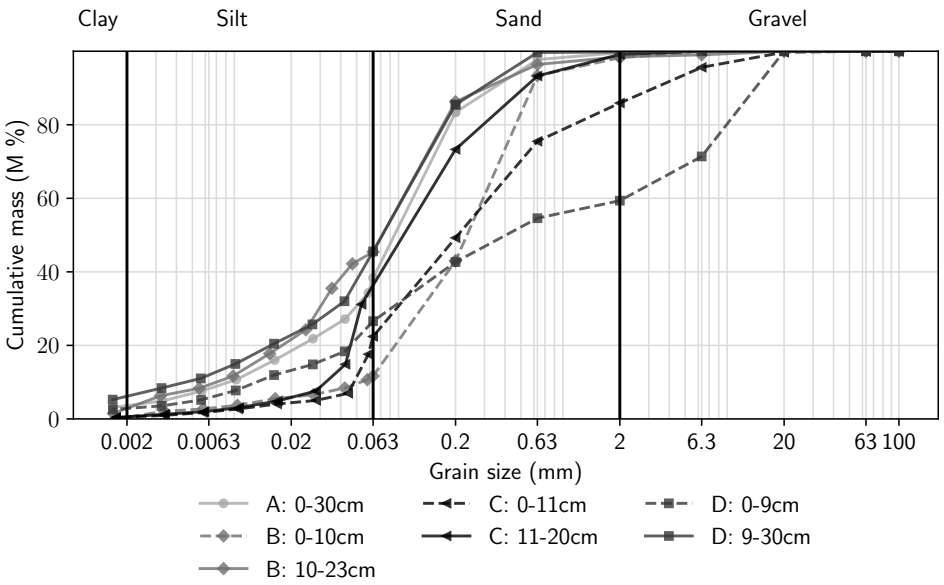

Figure 7.2: **Grain size distribution at the four sampling sites.** Sediment cores were taken downstream of each gas trap. Site A represents the slip-off slope, sites B and C the center of the stream, and site D the undercut slope.

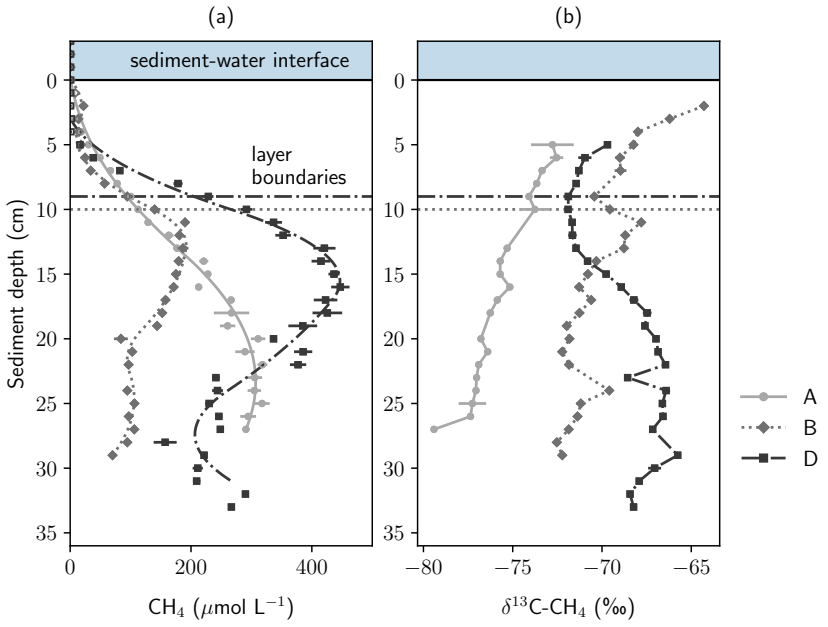

Figure 7.3: **Sediment CH_4 concentrations and stable carbon isotopic composition of CH_4 in pore water.** Site A represents the slip-off slope, site B the center, and site D the undercut slope. In panel (a), markers represent measured data and lines modeled CH_4 concentrations. Lines in panel (b) connect measured values.

More information on the geochemistry of the three sites, in particular dissolved O_2, anion, and cation measurements, are presented in Fig. C.2 in the Supplement.

7.3.3 Ebullition

Ebullition was observed at all four sites, although only small volume fluxes $< 8\,mL\,m^{-2}\,d^{-1}$ were detected at site D (Fig. 7.4). A data summary for the full year is provided in Tab. 7.1 and season-specific descriptive statistics are compiled in Tab. C.2 in the Supplement. During summer, volume fluxes were highest at site C with an average of $802\,mL\,m^{-2}\,d^{-1}$, followed by a period in autumn where higher gas volumes were emitted at site B ($651\,mL\,m^{-2}\,d^{-1}$ at site B compared to $374\,mL\,m^{-2}\,d^{-1}$ at site C). Later during winter, volume fluxes at site C increased again to an average of $464\,mL\,m^{-2}\,d^{-1}$ while all other sites had low fluxes of less than $35\,mL\,m^{-2}\,d^{-1}$ until end of February. Ebullition increased again in May at sites A and B. At site B, volume fluxes went up to a maximum of $1068\,mL\,m^{-2}\,d^{-1}$. These spring values at site B were influenced by sedimentation which buried the bottom of the gas trap after a spring flood in mid May (around May 12th).

CH_4 contents of up to 81 % were found in the gas bubbles, while CO_2 contents remained below 5 % with the exception of two outlier values at site B that were removed from Fig. 7.4. Outliers occurred on February 22nd and April 18th, when modeling of measured contents of $<$1 % resulted in final contents of 8 % and 18 %, respectively. CH_4 contents were positively correlated with volume fluxes and generally higher at sites with higher gas emissions (Fig. C.3). From June to September 2022, CH_4 contents at site A were on average 23 % with volume fluxes between 67 and $319\,mL\,m^{-2}\,d^{-1}$, at site B 44 % with volume fluxes between 116 and $592\,mL\,m^{-2}\,d^{-1}$, and at site C 73 % with volume fluxes between 420 and $994\,mL\,m^{-2}\,d^{-1}$. At site D, gas volumes were generally too low to obtain reliable gas composition or stable isotope measurements. Further, holding times in the storage funnel had to be long in order to reach a sufficient amount of gas for sampling which decreased credibility of measured gas contents and fluxes at site D.

Calculated GHG fluxes were below $2\,mmol\,m^{-2}\,d^{-1}$ for CO_2, but reached values of up to $31\,mmol\,m^{-2}\,d^{-1}$ for CH_4. Considering the full year, CH_4 fluxes were highest in the central section of the river with a total of $963\,mmol\,CH_4\,m^{-2}\,yr^{-1}$ at site C and $492\,mmol\,CH_4\,m^{-2}\,yr^{-1}$ at site B, followed by the slip-off slope ($67\,mmol\,CH_4\,m^{-2}\,yr^{-1}$ at site A). Values were calculated as sum of all measured fluxes at one site and scaled to represent a sampling period of 365 days.

Stable carbon isotopes of CH_4 in gas bubbles stayed most of the year below -64 ‰ (Fig. 7.4). An exception was July 2022 when $\delta^{13}C$–CH_4 at site A increased up to -47.9 ‰. Only one value for $\delta^{13}C$–CH_4 at site D could be obtained which was -52.5 ‰. $\delta^{13}C$–CH_4 values at site B were on average -3.5 ‰ more negative than at site C when comparing values measured on equal sampling days. The average $\delta^{13}C$–CH_4 at site B was -69.7 ‰ and at site C -66.5 ‰. $\delta^{13}C$–CH_4 at site A was more variable than at sites B and C throughout the year.

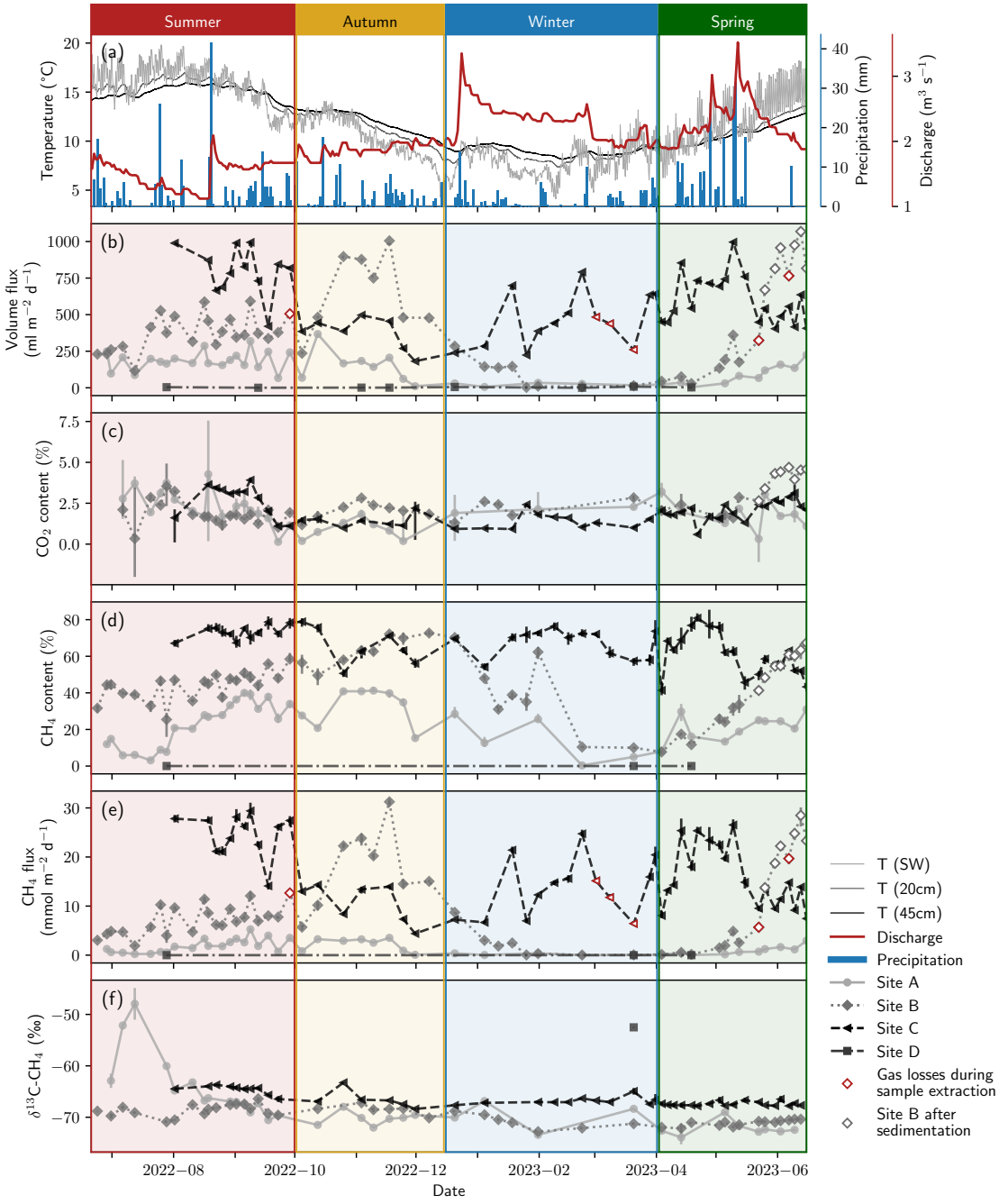

Figure 7.4: **Summary of ebullition measurements.** Panel (a) shows precipitation, discharge, surface water temperature, and the temperature in 20 cm and 45 cm depth. Gas volume fluxes are displayed in panel (b). Panel (c) shows CO_2 (GC Micro Box) and panel (d) CH_4 (GC-FID) contents in the gas samples. Two outliers in the CO_2 data were removed from the data set of site B (see text). Panel (e) depicts CH_4 fluxes, and panel (f) stable carbon isotopes of CH_4. Error bars indicate the range of minimum and maximum measured values for gas contents and the standard deviation of repeated measurements for $\delta^{13}C$–CH_4. For an easier description, the data was grouped into seasons which were chosen based on visual inspection of the data to represent specific seasonal patterns (summer: 15-06-2022 to 01-10-2022, autumn: 01-10-2022 to 15-12-2022, winter: 15-12-2022 to 01-04-2023, spring: 01-04-2023 to 15-06-2023).

Table 7.1: Data summary. This table shows the main statistical values for the full year period. For ebullition, season-specific data is presented in Tab. C.2 in the Supplement. For pore-water measurements, one data set represents all values measured in a vertical profile from 1 cm depth onwards.

Data type	Parameter	Site	n	min	max	mean	SD
Ebullition	Volume flux (mL m^{-2} d^{-1})	A	43	3.8	367.4	138.2	91.3
		B	53	2.8	1068.4	409.0	288.4
		C	51	181.4	996.0	581.0	217.6
		D	8	0.0	7.6	2.8	2.7
	CH_4 content (%)	A	43	0.4	41.3	23.4	11.8
		B	53	7.7	72.7	44.9	16.4
		C	51	41.4	80.9	66.1	10.1
		D	3	0.01	0.02	0.02	0.01
	CH_4 flux (mmol m^{-2} d^{-1})	A	43	0.004	5.3	1.5	1.4
		B	53	0.03	31.2	9.1	8.1
		C	51	4.4	29.4	16.7	7.1
		D	3	$1 \cdot 10^{-5}$	$5 \cdot 10^{-5}$	$3 \cdot 10^{-5}$	$2 \cdot 10^{-5}$
	$\delta^{13}C$–CH_4 (‰)	A	34	-73.9	-47.9	-67.9	5.6
		B	44	-72.8	-66.4	-69.7	1.6
		C	45	-68.4	-63.4	-66.5	1.4
		D	1	-	-	-52.5	-
Diffusive CH_4 flux (mmol m^{-2} d^{-1})	Across air–water interface	-	11	0.21	1.04	0.69	0.24
	Across sediment–water interface	-	3	0.03	0.11	0.06	0.04
Pore-water profiles	CH_4 conc. (µmol L^{-1})	A	27	1.1	318.2	178.6	115.5
		B	28	8.5	190.0	100.6	60.2
		D	33	0.8	447.2	246.9	144.2
	$\delta^{13}C$–CH_4 (‰)	A	20	-79.4	-72.5	-75.6	1.8
		B	26	-72.5	-64.3	-70.0	2.0
		D	28	-71.9	-65.8	-68.8	2.1

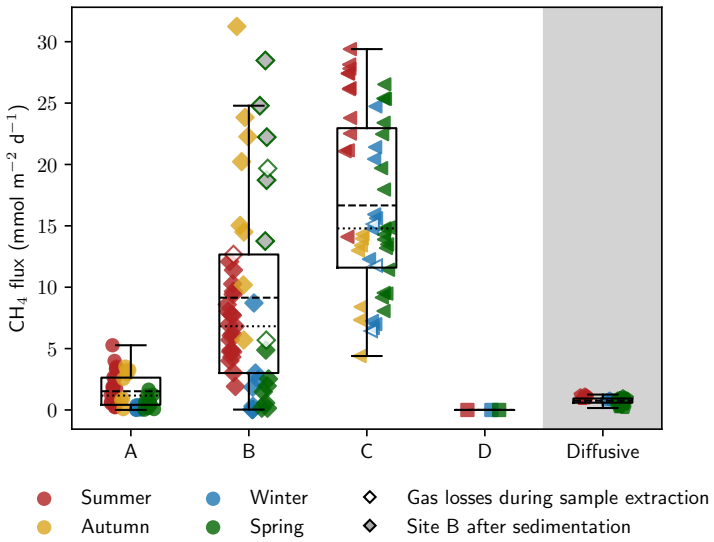

Figure 7.5: **Boxplots showing site-specific differences in CH_4 fluxes and a comparison with diffusive fluxes across the water–air interface.** Non-filled markers indicate that gas losses occurred during sampling. At site B, gray filling indicates that the gas trap was influenced by sedimentation (spring 2023).

7.3.4 Diffusive fluxes and oxidation

Diffusive CH_4 fluxes across the sediment–water interface were modeled to be 0.04 mmol m^{-2} d^{-1} at site A, 0.11 mmol m^{-2} d^{-1} at site B, and 0.03 mmol m^{-2} d^{-1} at site D. Diffusive CH_4 fluxes across the water–air interface calculated from dissolved CH_4 concentrations in the surface water were higher with an average of 0.69 ± 0.24 mmol m^{-2} d^{-1} and a range between 0.21 and 1.04 mmol m^{-2} d^{-1} (Fig. 7.5). Based on the assumptions mentioned in Sec. 7.2.9 and with a stable isotope fractionation factor of α = 1.027, we calculated that a fraction of 15.9 % to 27.8 % of this diffusively transported CH_4 was oxidized. Lower and higher estimates represent different end member values of δ^{13}C–CH_4 in the gas phase (δ_b = -69.7 ‰, average δ^{13}C–CH_4 at site C, or -66.5 ‰ at site B in Eq. 7.9, respectively). Using the same end members for δ^{13}C–CH_4 and a range of values for α from 1.017 to 1.037 to account for parameter uncertainties, between 44.1 % and 11.6 % of the CH_4 transported diffusively was oxidized.

7.4 Discussion

Gas bubbles were composed of mostly CH_4, some CO_2, and residual N_2. On its way through the water column, a pure CH_4 bubble with an initial volume of 0.004-0.52 L would loose 1.7-10.6 % CH_4 and gain up to 6.9 % N_2 and up to 3.2 % O_2 (estimated with the SiBu model; Greinert and McGinnis, 2009). After equilibration with the surface water, a pure CH_4 bubble of 0.02 L would reach 7.5 % CH_4, 20 % O_2, 72 % N_2, and 0.1 % CO_2 (modeled with PHREEQC; Parkhurst and Appelo, 2013). These calculations show that exchange processes in the water column cannot explain the final measured gas composition. The measured N_2 contents exceeded the values that can occur due to exchange processes during transport and even if an equilibrium were

reached, the measured CO_2 contents of up to 5 % could not be achieved. If the gas exchange with the surface water is limited, the gas composition reflects the conditions at the site of bubble formation (Langenegger et al., 2019). Similar to what has been observed earlier (Chanton et al., 1989), CH_4 contents were positively correlated with volume flux (Fig. C.3 in the Supplement) and N_2 contents followed a reverse pattern. Thus, at higher CH_4 production rates, more CH_4 and less N_2 was found in the gas samples. At very low volume fluxes, the increased surface to volume ratio of the gas sample in the storage funnel and the longer holding times may have further decreased the CH_4 content by allowing larger exchange with the surface water before sampling. Interestingly, CH_4 and CO_2 contents were not correlated (Fig. C.2). Since the CO_2 contents in the gas samples exceeded the amount that can enter the bubble during exchange with the surface water, CO_2 must have been microbially produced in the HZ together with CH_4. However, CH_4 and CO_2 production did not seem to follow the same seasonal fluctuations.

Year-round, CH_4 ebullition was highest at the central section of the river bed, represented by sites B and C (Fig. 7.5). Our initial hypothesis was that highest ebullitive CH_4 fluxes were to be expected at the undercut slope (site A), because sediment incubation studies suggested increasing methanogenic potential with decreasing grain size (Bodmer et al., 2020; Shelley et al., 2015), and because higher ebullition rates have been connected to shallow waters (Natchimuthu et al., 2016; Wik et al., 2016). However, increased microbial turnover due to higher hyporheic exchange and an increased permeability for gas bubbles in the river's center may explain the observations. Fischer et al. (2005) measured 2.9 to 5.5 times higher microbial activity in the central river section compared to nearshore habitats. Higher flow velocities in the central channel and a lower penetration resistance of the bed substrate foster the exchange between interstitial and surface water and thus allow better supply of carbon and nutrients from the surface water (Auerswald & Geist, 2018). An increased carbon supply in the center of the river is supported by very high organic carbon contents at site C (26.6 %). In addition, leaf litter and wood were detected in sediment cores from the central streambed.

The interpretation that higher permeability fosters methanogenesis is only valid as long as anoxic conditions prevail, which is unlikely in gravelly river beds where dissolved O_2 and other electron acceptors can travel deep into the HZ and prohibit the production of CH_4. But once the fine fraction is high enough to ensure anoxic conditions, additional fine material seems to decelerate carbon supply by reducing hyporheic exchange. Flow velocities were lower at the slip-off slope compared to the other sites, so that less allochthonous plant material was transported there, resulting in slower burial of POC with settling sediments. This is in line with intermediate LOI values at site A (14.6 %). At the coarse-grained but consolidated undercut slope, plant material could not enter the streambed due to the hard crust atop, as shown by low LOI values (5 % and 9 %). Surprising in this context was only the low LOI in the top layer of site B (center left) with only 6 %. Yet, vertical concentration profiles suggest that the methanogenic zone was located below 10 cm depth, where carbon contents were again much higher (13.3 %). The accordance of high sediment organic matter content and high ebullitive CH_4 fluxes is in line with results from incubation studies (Bednařík et al., 2019; Romeijn et al., 2019).

Higher permeability not only increases carbon and nutrient supply, but also creates pathways for transport of gases to the top of the sediment. We measured highest sediment porosity at the most productive site. But not only the total pore space, but also the size distribution of the pores matters for ebullitive CH_4 emissions (Liu et al., 2018). In contrast to a presumably small

average pore diameter at the homogeneous, fine-grained slip-off slope (site A), leaf litter and wood potentially formed preferential paths for the escape of gas bubbles. Lower pore-water CH_4 concentrations centrally in the river bed support the hypothesis that CH_4 produced in this area was quickly transported out of the system, removing CH_4 from the pore-water. Where the top layer was consolidated (site D), gas could not escape and the pore-water was more enriched in CH_4. Dissolved CH_4 concentrations in the HZ were below the theoretical threshold for bubble formation of 1.9 mmol L^{-1}, which was estimated for in situ conditions with PHREEQC. However, nucleation can occur earlier than predicted by theory due to the catalytic effect of surfaces (Lubetkin, 2003). In sediments, CH_4 bubbles form where the local production rate exceeds the diffusive transport away from the source (Liu et al., 2018). We assume that the hetero surface effect and highly localized CH_4 production can explain the formation of bubbles in the HZ of river Moosach and that at higher production rates bubbles emerge faster and less CH_4 is distributed in the pore space by diffusion.

With regard to the time dimension, ebullition was observed to vary seasonally rather than short-term or randomly. During summer, autumn, and winter periods each sampler showed relatively stable ebullition rates with similar CH_4 contents. Seasonal changes were most pronounced at site B. After intermediate fluxes during summer, ebullition increased drastically during autumn, and then declined during winter. The autumn increase could be connected to the end of the vegetation period. Macrophyte roots may have left paths for gas bubbles when dead plants were transported away by the current. After stored gas was released during that period, almost no GHGs escaped until mid-May, when a temperature increase re-activated microbial activity to produce biogenic CH_4. Extreme ebullition at site B during spring 2023 may not be comparable with earlier values, because parts of the gas trap were covered in sediment after a discharge peak earlier in the year (see Fig. 7.1). Fluxes reported after this event need to be interpreted cautiously and we have therefore shown them with white markers in Fig. 7.4 and grey-filled markers in Fig. 7.5.

The sustained high CH_4 ebullition during winter at site C is especially interesting in comparison with this seasonal behavior of site B prior to being covered. While ebullitive fluxes at B stagnated at very low rates during winter, they even increased at C despite the cold water temperatures. A sudden release of gas produced during summer seems unlikely here, because fluxes would be expected to drop after this event if no new CH_4 is produced in the methanogenic zone. We speculate that only active methanogenesis during the winter period may explain the high gas volumes and bubble CH_4 contents during winter and early spring seasons at site C. This is surprising since CH_4 ebullition has been shown to be a highly temperature-dependent process (Aben et al., 2017). However, some strains of methanogens are known to inhabit cold environments in high altitudes and latitudes (Barret et al., 2022; Zhang et al., 2008). The consistent difference in $\delta^{13}C$–CH_4 of 3.5 ‰ between sites B and C indicates that the proportions of methane-forming pathways are different in the two stream sections, possibly due to the availability of different substrates. Methanol-derived methanogenesis, a cold-adapted production pathway used by psychrophilic methanogens (Cao et al., 2014; Jia et al., 2021; Zhang et al., 2008), could have played a larger role at site C than in the rest of the river bed. The methylotrophic methanogens *Candidatus* "Methanomethyliales" (phylum *Candidatus* "Verstraeteaechaeota") and Methanomassiliicoccales, the latter associated with CH_4 production

from methanol in freshwater wetlands (Narrowe et al., 2019), have been detected in the bed of river Moosach (Michaelis et al., 2022) which may support this hypothesis.

Values of δ^{13}C–CH_4 not only showed differences between the sites but also changes over time. At site A, an isotopic shift towards heavier isotopes occurred concurrently with the main plant growth period in July. Two mechanisms could have caused this effect. Microbial oxidation can increase the content of ^{13}C in the remaining CH_4 due to preferential consumption of the lighter isotope ^{12}C, but CH_4 transported as gas bubbles is assumed to escape oxidation due to the high transport velocity. More likely, the shift in CH_4 isotopic composition reflects a change in the main methanogenic pathway, for example a higher contribution of acetoclastic methanogenesis during this period. Acetoclastic methanogenesis is associated with less negative δ^{13}C–CH_4 (-50 ‰ to -60 ‰) than hydrogenotrophic methanogenesis (-60 ‰ to -110 ‰) or methane production from methanol (Whiticar, 1999). Plant growth during that time of the year could have influenced the availability of substrates or the isotopic composition of the substrates.

To explain the observed seasonal dynamics, we have tested how well the modified Arrhenius model can describe the relation of ebullition and temperature, and if a linear correlation between CH_4 flux and discharge, precipitation, or air pressure drop can be found with Pearson correlation coefficients (Fig. 7.6). A strong non-linear temperature-dependence of ebullitive CH_4 fluxes from aquatic ecosystems to the atmosphere has been observed earlier (Aben et al., 2017). Other studies suggested that CH_4 ebullition from streams can be flow-dependent (McGinnis et al., 2016) and that air-pressure drops, for example during storms, can induce ebullition, while high pressure inhibits ebullition (Mattson & Likens, 1990; Natchimuthu et al., 2016).

For our data, no or only low correlation was found for air pressure drop and precipitation ($|r| \leq 0.30$). Discharge showed a statistically significant moderate negative correlation (r between -0.31 and -0.37). Similarly, LMM of the full data set with site as a random factor was statistically significant for temperature ($p_{T(SW)} = 0.013$; $p_{T(20cm)} = 0.001$) and discharge ($p < 0.001$) but not for precipitation (p = 0.285) or pressure drop (p = 0.808). There was a linear negative correlation between temperature and discharge because discharge during the winter is generally higher at river Moosach than during summer. The increased CH_4 fluxes at lower discharge may therefore be either season or flow dependent. To summarize, precipitation and air pressure drop do not seem to be good predictors for CH_4 emissions while temperature and discharge appear to have a potentially interrelated influence on CH_4 ebullition.

The modified Arrhenius model only yielded a very poor fit with generally low R^2 values and could not well describe the relation between CH_4 ebullition and temperature. The poor quality of fit indicates that the model is not well suited to describe the temperature-depenence of CH_4 ebullition and that temperature alone is insufficient to predict the amount of CH_4 released to the atmosphere. Other factors, especially site characteristics and sediment properties, must be considered when extrapolating from point measurements. Pronounced differences in volume fluxes and CH_4 contents were found between the sites, and four sites were insufficient for a sound statistical evaluation or extrapolation. For example, fluxes at site D were year-round way below all other sites, and winter fluxes at site C were on average 7 times larger than summer fluxes at site A. Overall, spatial heterogeneity in CH_4 ebullition was considerably larger than temporal variability which is in line with some other studies (Koschorreck et al., 2023; Robison et al., 2021). For future sampling campaigns, we would, therefore, recommend to focus on the

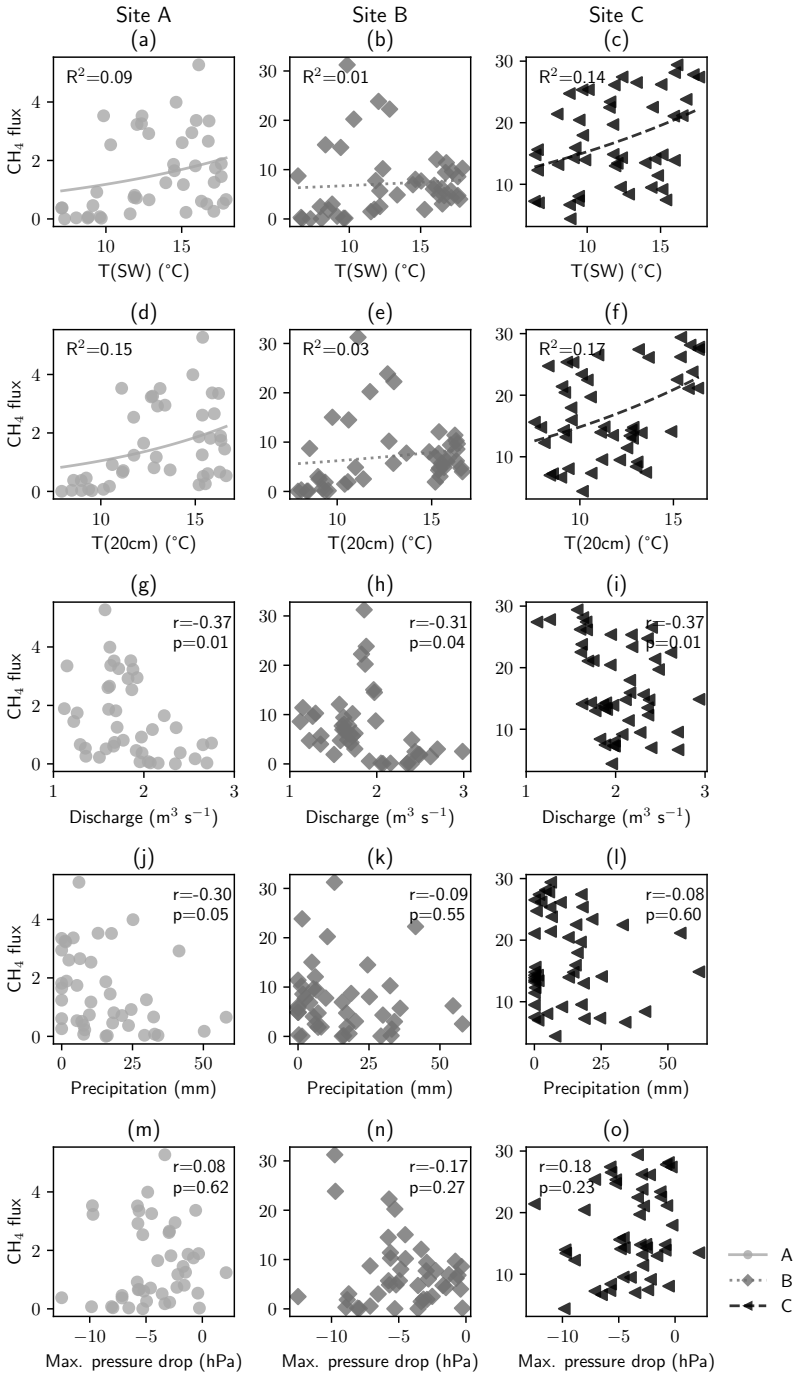

Figure 7.6: **Regression analysis of methane fluxes and relevant parameters.** Precipitation represents the sum, all other parameters the average during the gas collection time. For surface water and sediment temperature, the modified Arrhenius model was fitted. For discharge, precipitation, and air pressure drop, Pearson correlation coefficients were calculated to test for linear regression. Correlations were statistically significant ($p < 0.05$) only for discharge. There was also a statistically significant correlation between temperature (both T_{SW} and T_{20cm}) and CH_4 flux at sites A and C (Pearson correlation). At site B, high spring fluxes were not considered due to the reduced comparability after a sedimentation event, which partly buried the gas trap.

representation of as many sampling sites as possible, as opposed to monitoring one site over a longer time. A large number of field sites, where both diffusive gase transport and ebullition effects are monitored, and a solid bed substrate characterization are necessary for reliable budgeting.

Estimated diffusive fluxes across the sediment–water interface between 0.03 and 0.11 mmol $m^{-2}\,d^{-1}$ were lower than the average 0.69 mmol $m^{-2}\,d^{-1}$ calculated for fluxes across the water–air interface. The first could be underestimated, because a stronger exchange with surface water may exist than the model could represent without an advective flow component. This advective flow would dilute CH_4 concentrations at the top of the streambed and transport this CH_4 into the surface water. Also the assumption of steady state is a drawback of the applied model and could lead to an underestimation of the actual diffusive fluxes across the sediment–water interface. Another reason for the lower fluxes across the sediment–water interface compared to the water–air interface could be the supply of CH_4 to the surface water from rising gas bubbles. Overall, we consider CH_4 flux estimates across the water–air interface as more reliable for total CH_4 emissions than flux estimates across the sediment–water interface and therefore, only consider the first in the following comparison.

Ebullitive CH_4 fluxes were up to 30 times larger than diffusive fluxes. This is in line with global estimations for lakes (Saunois et al., 2020), but contradicts what has been described for rivers recently (Robison et al., 2022). In fact, ebullitive CH_4 fluxes measured in this study were higher than in many other stream systems. Stanley et al. (2016) reported average CH_4 ebullition fluxes of 1.96 mmol $m^{-2}\,d^{-1}$ (ranging from 0.0 to 9.4 mmol $m^{-2}\,d^{-1}$), and Robison et al. (2021) 1.00 ± 0.23 mmol $m^{-2}\,d^{-1}$ (ranging from 0.01 to 1.79 mmol $m^{-2}\,d^{-1}$). Ebullition in river Moosach reached rates typically found in tropical reservoirs, similar to what was measured by McGinnis et al. (2016) (21.3 mmol $m^{-2}\,d^{-1}$). On a global scale, a linear relation between diffusive and ebullitive CH_4 fluxes has recently been used for estimating total riverine CH_4 emissions, leading to roughly equal contributions of both processes (Rocher-Ros et al., 2023). Our data challenges the assumption that it is possible to infer ebullition rates from diffusive flux estimates. It needs to be said that Rocher-Ros et al. (2023) had very robust data on diffusive CH_4 fluxes but had to rely on very scarce data on CH_4 ebullition for this global estimate ($>$ 24000 measurements of dissolved CH_4 concentrations plus $>$ 8000 direct measurements of diffusive CH_4 fluxes versus only 630 observations of ebullition). Obviously, the data available on CH_4 ebullition is insufficient, especially considering the high spatiotemporal variability of this process, as also documented in the present manuscript.

Reasons for the untypically high ebullition rates we measured could be the very low gradient and the large amount of fine deposits in the stream. Both are related to anthropogenic alterations like the construction of a series of dams (Auerswald & Geist, 2018). The controlled discharge conditions prohibit larger disruptions of the streambed and therefore allow stable methanogenic communities to establish. An additional input of carbon and nutrients not only from the nearby peatlands, but also from agricultural fields around the river may further foster turnover rates in the HZ, particularly after heavy precipitation events and floods. Crop lands have been shown to significantly raise erosion rates (Borrelli et al., 2020). One might therefore speculate that human influence could have an enhancing effect on CH_4 emissions from small streams. We did not specifically test for anthropogenic effects on CH_4 ebullition and their magnitude remains an open question for future research. But if indeed land-use changes and anthropogenic

alterations of river Moosach's course and hydrology have enhanced the CH_4 emission potential, renaturation measures at river Moosach could be beneficial from a climatological perspective.

Stream sediments have repeatedly shown a potential for aerobic as well as anerobic oxidation of CH_4 (Bodmer et al., 2020; Shelley et al., 2015; Shen et al., 2019a). CH_4 oxidation would be expected in a narrow zone at the oxic–anoxic interface if CH_4 is transported diffusively (Raghoebarsing et al., 2006). However, if CH_4 mainly escapes to the atmosphere in the form of gas bubbles, it most likely escapes microbial oxidation. In river Moosach, a potential for CH_4 oxidation coupled to O_2 reduction and denitrification was found earlier (Michaelis et al., 2022). In this study, we calculated that up to 44 % of the CH_4 transported diffusively was oxidized, but again it should be mentioned that the diffusive pathway was of minor importance. Of the three geochemical profiles, only site B showed a clear isotopic enrichment in δ^{13}C–CH_4 together with a decline in CH_4 concentrations towards the top of the streambed (Fig. 7.3). At site D, a decrease in dissolved CH_4 concentrations combined with an enrichment in δ^{13}C–CH_4 below 15 cm depth could either be caused by CH_4 oxidation or mixing processes. As dissolved O_2, NO_3^-, and SO_4^{2-} were all consumed above 9 cm (Fig. C.2), oxidation seems rather unlikely. However, we cannot exclude that trace amounts of dissolved O_2 triggered CH_4 oxidation. Also iron and manganese remain as potential electron acceptors although their environmental relevance is often limited by their usually low bioavailability (Egger et al., 2015). On the other hand, a concurrent decrease in NH_4^+ concentrations below 15 cm depth suggests a lower availability of reactive carbon because NH_4^+ is released during organic matter decomposition (Ladd & Jackson, 1982). A combination of lower methanogenesis rates and a shift in the relative contribution of different production pathways, which are linked to different δ^{13}C–CH_4 values, are alternative explanations of the observations. Reduced carbon supply compared to the other sites due to the consolidation of the top layer is a likely reason. In the shallow, well-mixed stream, there is also no significant CH_4 oxidation potential in the water column as would be expected in deep lakes (Einsiedl et al., 2020; Peña Sanchez et al., 2022b). For our study site, where fine sediment dominates the river bed, we can therefore conclude that CH_4 oxidation is not too relevant as a CH_4 sink.

7.5 Conclusions

Ebullition was monitored at four sites in one cross section of a small stream over the course of a full year. Spatial heterogeneity of the HZ was large and CH_4 fluxes differed strongly between sites. Ebullitive CH_4 fluxes were up to 30 times larger than diffusive CH_4 fluxes. Year-round, the central section of the river bed emitted most CH_4 as gas bubbles. Reasons are probably a good supply of carbon and nutrients due to a higher potential for exchange with the surface water, and a higher permeability of the sediment for gas bubbles. Gas fluxes varied with the four seasons rather than in short term or random intervals. At one site, a sustained high ebullitive CH_4 flux during winter demonstrated CH_4 production in the HZ even at cold water temperatures down to $< 8\,^{\circ}$C. In comparison with diffusive fluxes, ebullition transported up to 30 times more CH_4 to the atmosphere and just 12 % to 44 % of the CH_4 transported diffusively was oxidized.

Author contributions

TM, AW, TB and FE conceptualized the project. TM, FK, and TB developed the methodology. TM and FK were responsible for field work, data acquisition and curation. TM performed formal analysis, visualization, and original draft preparation. FE and TB acquired funding and supervised the project. TM, AW, TB, and FE all contributed in writing, reviewing and editing the manuscript.

Acknowledgements

First of all, we would like to thank Katharina Philipp for her crucial help during installation, sampling, and laboratory analyses. We would also like to acknowledge that Aurelio Andy and Adrian Seeholzer later helped sampling the gas traps. We thank Peter Berg for advise in the application of the modeling software PROFILE and how to adapt it to our case study. Further, we want to acknowledge Jürgen Geist and the Team of the Chair of Aquatic Systems Biology for supporting this study and especially our field work at all times. We are grateful to the Chair and Testing Office for Foundation Engineering, Soil Mechanics, Rock Mechanics and Tunneling, mainly Gerhard Bräu, for Loss On Ignition (LOI) measurements. We thank the Chair of Hydraulic and Water Resources Engineering, the Chair of Hydromechanics, and the Chair of Hydrology and River Basin Management for the lending and explanation of the measuring equipment for discharge and flow velocity measurements. In addition, we are thankful to the Chair of Engineering Geology that made lab space and technical equipment for sediment analyses available. And finally, we would like to thank Jaroslava Obel for her help with analytics in the laboratory.

Data availability

The datasets generated and analysed during the current study have been uploaded to a figshare repository and can be accessed under https://doi.org/10.6084/m9.figshare.24298354.

8 An in situ labeling experiment to test the potential of the n-damo process in the hyporheic zone

8.1 Motivation and concept

Carbon stable isotope fractionation towards the top of the stream bed and isotopically enriched stream water compared to pore water or gas bubbles in the sediment were signs of CH_4 consumption in the HZ. In the sediment, microorganisms capable of aerobic CH_4 oxidation as well as AOM coupled to denitrification were present. However, due to the sharp incline and close proximity of dissolved O_2 and NO_3^- concentrations, both rapidly decreasing few centimeters below the sediment–water interface, it was not possible to separate oxic from anoxic CH_4 oxidation solely based on geochemical pore-water profiles. This is discussed in more detail in Sec. 9.2. Microbially catalyzed redox reactions such as CH_4 oxidation coupled to the reduction of different electron acceptors are commonly studied in laboratory incubations (Bodmer et al., 2020; Comer-Warner et al., 2018; Romeijn et al., 2019; Shen et al., 2019a) but it is questionable to what extent the results can be transferred to real environmental conditions. Therefore, we conceptualized an isotope tracer experiment within the HZ to further clarify the role of NO_3^- and NO_2^- as electron acceptors for CH_4 oxidation under in situ conditions.

CH_4 with isotopically labeled carbon was injected into the streambed to see whether CH_4 is microbially oxidized to CO_2 in the HZ and if the presence of NO_3^- changes anything in the reactive behavior of CH_4. If CH_4 is oxidized to CO_2 in situ at a sufficient rate, the labeled carbon of the injected CH_4 should be recovered in dissolved CO_2 in pore-water samples (Fig. 8.1a). Isotopically labeled CH_4 and NO_3^- were injected through microfilter tubes in a step-function: two weeks of CH_4 injection without NO_3^-; followed by a one-week break to restore natural conditions; and two weeks of CH_4 injection with NO_3^- addition. Dissolved O_2 concentrations were monitored directly in front of the sampling and injection ports to test whether it was possible to maintain fully anoxic conditions during the experiment. Two conservative tracers (Cl^- and ^{18}O-labeled water) were added to identify the flow paths and calculate the recovery rates of the injection fluid in samples. In addition, two sediment cores were taken for microbiological analyses: one before and one directly after the experiment. Changes to the microbial community can show which taxonomic groups actively grew due to the injection of CH_4 and NO_3^- to the HZ.

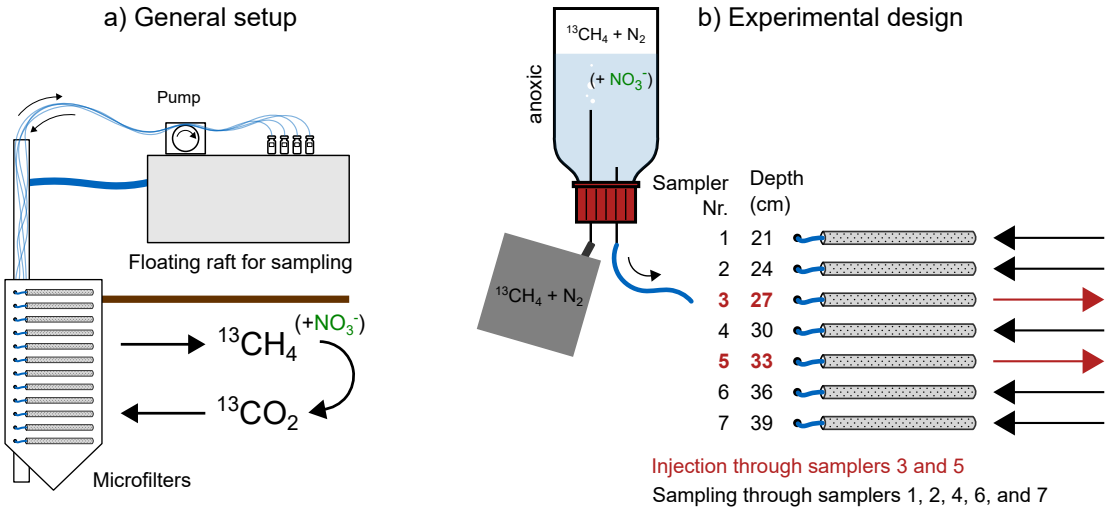

Figure 8.1: **Concept and set-up of the in situ labeling experiment.** Panel (a) shows the general set-up of the experiment, panel (b) explains the experimental design. For the first two weeks of the experiment, only conservative tracers and ^{13}C-labeled CH_4 were injected, in the last two weeks the tracers, $^{13}CH_4$, and NO_3^-.

8.2 Methods

8.2.1 Experimental set-up and preparation of the injection liquid

Quaternary groundwater from a well close to the experimental site with similar hydro-chemistry to river Moosach's interstitial water was isotopically labeled to have a $\delta^{18}O$–H_2O of 113 $\pm$ 2 ‰ (n = 4); run through an anion exchange filter with AG 1-X8 Resin (BioRad, Feldkirchen, Germany) to remove potential electron acceptors for CH_4 oxidation and enrich Cl^- to 105 $\pm$ 2 mg L^{-1}; sterile filtered into autoclaved 1 L glass bottles closed with rubber butyl stoppers; and flushed with argon gas for more than 30 min to remove traces of O_2. This water was then amended with labeled CH_4 (R_{CH4} = 0.15 $\pm$ 0.01; $\delta^{13}C$–CH_4 = 336 $\pm$ 105 ‰; VWR International, Darmstadt, Germany) by creating a headspace of 40 % CH_4 and 60 % N_2. 413 µmol L^{-1} (19 mg L^{-1}) NO_3^- were added to two out of four injection bottles.

The experiment was conducted at the monitoring station described in Ch. 6. For injection, two bottles were placed upside down in a rack on the floating raft next to the monitoring station (Fig. 8.1b). A gasbag filled with 40 % labeled CH_4 and 60 % N_2 was connected to the bottle through a needle. A second needle was pierced through the rubber stopper and then connected to the gastight tubing associated with the permanently installed Rhizon samplers (pore diameter 0.12-0.18 µm, filter length 5 cm; Rhizosphere, Wageningen, The Netherlands). Before connecting the bottles to the tubing, pore water was withdrawn until the tube volume was exchanged twice and the tubes were completely filled with anoxic pore water. The pump was then reversed to inject the prepared liquid into the HZ. While the injection bottles were emptying, gas from the connected gas bag was slowly sucked into the headspace.

The prepared water was continuously injected with an ISM 1089 Ismatec Ecoline peristaltic pump (VWR International, Darmstadt, Germany) at a rate of 0.06 mL min^{-1}. The injection liquid with only CH_4 amendments was injected for two weeks through filters in 27 cm and 33 cm depth (Fig. 8.1b). After a week's break, the experiment was repeated with the two bottles containing CH_4 and NO_3^-. Before, during, and after the injection periods, pore water was extracted through the remaining Rhizon filters for analyses of R_{CH4}, R_{CO2}, stable water isotopes, and anions. Sampling was conducted with peristaltic pumps at a rate of 0.29 mL min^{-1} and at all ports simultaneously. The injection was interrupted in the meantime to avoid short circuits.

8.2.2 Analytical methods

Samples for gas analyses were taken in 20 mL glass vials closed with 0.76 mm thick Viton septums and aluminium seals. Vials were prepared by flushing with N_2 for eliminating background CH_4 and CO_2. After removing 6 mL of gas, vials were connected to the gastight peristaltic tubing with a needle and filled with 6 mL of sample to re-establish atmospheric pressure. Gas measurements were run on a GC coupled to a mass spectrometer of the type GCMS-QP2020 NX (Shimadzu, Kyōto, Japan) with N_2 as carrier gas. Concentrations of $^{12}CH_4$, $^{13}CH_4$, $^{12}CO_2$, and $^{13}CO_2$ were evaluated based on three calibration standards (Rießner Gase GmbH, Lichtenfels, Germany). The stable carbon isotope ratio R was calculated as quotient of the heavy to the lighter isotope concentration (Eq. 8.1).

$$\mathrm{R} = \frac{[^{13}\mathrm{C}]}{[^{12}\mathrm{C}]} \tag{8.1}$$

where R is the stable carbon isotope ratio, [^{13}C] the concentration of the heavier $^{13}CH_4$ or $^{13}CO_2$, and [^{12}C] the concentration of the lighter $^{12}CH_4$ or $^{12}CO_2$.

Pore-water samples for measurements of stable water isotopes and ions were taken in 1.5 mL glass vials and analyzed as described in Sec. 6.2.2 with an IWA-45EP isotopic water analyzer (Los Gatos Research, San Jose, USA) and a system of two ICS-1100 ion chromatographs (Thermo Fisher Scientific), respectively. Dissolved O_2 concentrations in the HZ during the experiment were monitored with the fiber-optic sensor described in Sec. 6.2.4 (Brandt et al., 2017), which was placed few centimeters in front of the Rhizon filters. Directly after each sample extraction, one dissolved O_2 profile was recorded with a 1 cm vertical resolution. The calculation of dissolved O_2 concentrations from measured phase angles was based on the method and calibration shown in Sec. B.3.

8.2.3 Sediment coring and 16S rRNA analyses

A first core for DNA extraction, qPCR, and 16S rRNA sequencing was taken before the experiment behind the plexiglas plane that held the Rhizon samplers to avoid disturbances before the start of the injection. A second core was taken after the last pore-water extraction directly in front of the filters. The distance between both cores was less than 20 cm. Each core was transported to the laboratory and stored refrigerated until subsampling on the next day. Subsamples were retrieved by cutting the core liner lengthwise and removing sediment

material with a spatula cleaned with ethanol. All subsamples were immediately frozen and stored at $<$-20 °C.

Geomicrobiological analyses were done in duplicates according to the protocol described in Sec. 5.2.5. In short, DNA was extracted from 0.5 g of sediment based on the method developed by Vuillemin et al. (2019) and diluted 1:10 in ultrapure PCR water (Roche, Germany). DNA samples were amplified in qPCR reactions with barcoded 16S rRNA gene primer pair 515F (5'- GTG YCA GCM GCC GCG GTA A -3') and 806R (5'- GGA CTA CNV GGG TWT CTA AT -3') (Pichler et al., 2018). For sequencing, the 16S rRNA gene library was prepared from qPCR amplicons, that were extracted from 1.5 % agarose gels with the QIAquick Gel Extraction Kit (Qiagen, Hilden, Germany), quantified with the Qubit dsDNA Assay Kit (Thermo Fisher Scientific, Dreieich, Germany), normalized to 1 nM solutions, and pooled. Sequencing was performed at the GeoBio-Center$^{\mathrm{LMU}}$ on the Illumina MiniSeq platform. Operational taxonomic units (OTUs) were identified with USEARCH version 10.0.240 for MiniSeq based on 97 % sequence identity clustering (Edgar, 2013). OTUs were then compared to taxonomic units of the SILVA database version 132 with the BLASTn search algorithm (Quast et al., 2012).

8.2.4 Data evaluation

From the tracer measurements (Cl^- and $H_2^{18}O$), the ratio of recovered injection water in each sample was calculated with an (isotope) mixing model (Phillips and Gregg, 2001, Eq. 8.2).

$$\mathrm{fA} = \frac{\delta\mathrm{M} - \delta\mathrm{B}}{\delta\mathrm{A} - \delta\mathrm{B}} \tag{8.2}$$

where fA is the fraction of component A in a sample, δM the stable isotope composition of the mixture, and δA and δB the stable isotope composition of component A and B, respectively. Mixing was calculated from Cl^- concentrations with the same formula, replacing the δ value by the measured concentration. End members A and B were the $\delta^{18}O$–H_2O or Cl^- concentration of the injection liquid and mean background isotope ratio/concentration in the HZ, respectively. The recovery rates from Cl^- concentrations were very similar to those obtained from the $H_2^{18}O$ tracer and therefore, are not displayed in Fig. 8.2.

For NO_3^-, the expected concentration under the assumption of conservative transport with the pore water was calculated based on the tracer recovery rate in a sample and the NO_3^- concentration in the injection water (Eq. 8.3). From the difference in the expected NO_3^- concentration in case of non-reactive transport and the measurement, we calculated the percentage of NO_3^- that must have been consumed along the flow path (Eq. 8.4). Calculated values $>$ 100 % were normalized to 100 %.

$$[\mathrm{NO_3^-}]_{\mathrm{expected}} = \mathrm{fA} \cdot [\mathrm{NO_3^-}]_{\mathrm{inj}} + (1 - \mathrm{fA}) \cdot [\mathrm{NO_3^-}]_{\mathrm{HZ}} \tag{8.3}$$

where $[NO_3^-]_{\mathrm{expected}}$ is the expected NO_3^- concentration in µmol L^{-1}, $[NO_3^-]_{\mathrm{inj}}$ and $[NO_3^-]_{\mathrm{HZ}}$ the end member NO_3^- concentrations in µmol L^{-1} of the injection liquid and undisturbed HZ, respectively, and fA the fraction of injection liquid in the sample (recovery rate) calculated from a conservative tracer (Eq. 8.2).

$$[NO_3^-]_{\text{consumed}}(\%) = \frac{[NO_3^-]_{\text{expected}} - [NO_3^-]_{\text{measured}}}{[NO_3^-]_{\text{expected}}} \cdot 100 \tag{8.4}$$

where $[NO_3^-]_{\text{consumed}}$ is the amount of NO_3^- consumed in percent, $[NO_3^-]_{\text{expected}}$ the expected NO_3^- concentration in µmol L^{-1} based on a conservative tracer, and $[NO_3^-]_{\text{measured}}$ the measured NO_3^- concentration in a sample in µmol L^{-1}.

8.3 Results and discussion

The new experimental concept was realized in June and July 2023. Constant injections over two phases of two weeks each were performed with one week in between. Fifteen times, O_2 profiles were measured and pore water was extracted from the five samplers around the injection ports and analyzed for R_{CH4}, R_{CO2}, and ions.

Up to 52 % of the injection liquid were recovered in the samples, as shown by the $H_2^{18}O$ data (Fig. 8.2). Samplers 4 and 6 received most of the tracer during the first part of the experiment, while in the second half most of the injection arrived at samplers 2, 6, and 7. In both injection periods, the liquid arrived approximately 2 days delayed at sampler 7 when compared to sampler 6, indicating a slow downwards-directed flux. This could also explain why no injection liquid arrived at sampler 1 during the entire experiment.

Prior to the experiment, anoxic conditions prevailed below 3 cm depth. It was not possible to keep the HZ fully anoxic during the injection. O_2 data show an increase of dissolved O_2 concentrations during both of the injection phases, elevating dissolved O_2 concentrations by 10-100 µmol L^{-1} (Fig. 8.2). Considering the very low pumping rates during the injection, it seems possible that atmospheric O_2 diffused through the teflon tubes, which have a low gas diffusivity but are not totally gas tight. Imperfections in the gas bags may also have lead to O_2 contamination of the injection fluid during the relatively long holding times of two weeks. The elevated O_2 concentrations during the injection periods complicate the separation of aerobic and anaerobic CH_4 oxidation.

All measured NO_3^- concentrations were much lower than the calculated expected value. The highest measured NO_3^- concentration was 12.5 µmol L^{-1} in sampler 6, only 4 % of the initial concentration in the injection liquid. Values for NO_3^- consumption were generally between 80-100 %, indicating that almost all NO_3^- was immediately consumed in the HZ, even far below the natural denitrification zone.

R_{CH4} values were between 0.0079 and 0.0223 of which values above 0.0127 (dotted horizontal line in Fig. 8.2) indicate labeling. This threshold represents the upper 95 % confidence interval of all R_{CH4} measurements taken before the injection (t_0). Several samples show ^{13}C labeling of CH_4, interestingly especially in the most shallow and in the deepest sampling points, but compared to the inital R_{CH4} of 0.15, these values seem quite low. Either dilution or consumption of the injected CH_4 could be responsible for the low recovery rates of $^{13}CH_4$. It is noteworthy that at sampler 6, where generally most of the tracers arrived, none of the CH_4 samples were labeled while at sampler 1, that did not receive any tracer, R_{CH4} values were highest. Thus, dilution alone cannot explain the loss of the ^{13}C label in CH_4.

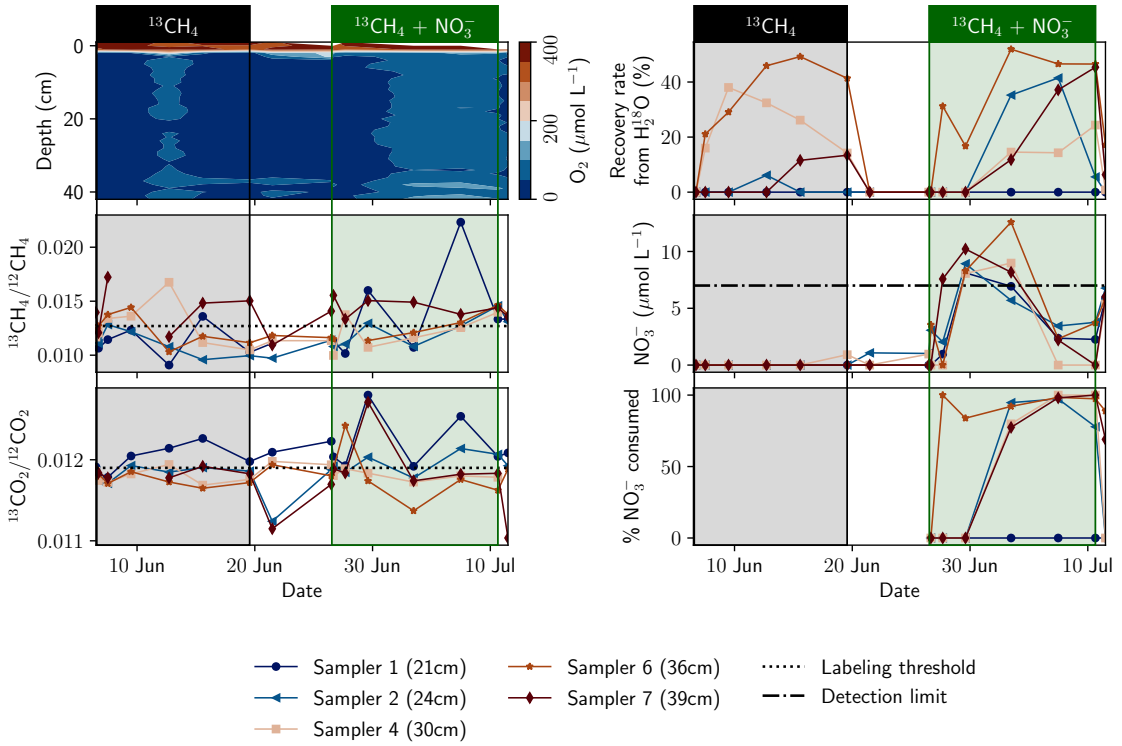

Figure 8.2: **Results of the in situ labeling experiment.** The dotted horizontal line in the stable isotope ratio plots indicates the threshold above which data points are considered to be labeled.

If CH_4 oxidation was responsible for the removal of the ^{13}C label, we would expect elevated R_{CO2} values. However, only very few data points were above the labeling threshold of 0.0119 (upper 95 % confidence interval of R_{CO2} at t_0), most of them measured at sampler 1. In addition, the overall spread of the measurements was very large which decreases the credibility of the few values above the labeling threshold. There was no discernible trend towards an enrichment of ^{13}C in CO_2 over time.

It seems that neither dilution nor consumption can fully explain the loss of the ^{13}C label. We suspect that, as previously discussed in Sec. 6.4, CH_4 and dissolved solutes behave differently in the pore space. While tracers like ^{18}O-enriched water and Cl^- can model the behavior of dissolved solutes, gases seem to exchange with bubbles in the pore space and travel differently through the HZ. The high ebullition fluxes measured at river Moosach (Ch. 7) reaffirm the large amounts of gas that must be stored in the sediment. While dissolved solutes and conservative tracers apparently traveled downwards, CH_4 seems to have moved upwards, as indicated by the more enriched R_{CH4} and R_{CO2} values at sampler 1. Partitioning of CH_4 between gas and water phase and upward movement of the gas bubbles could explain our observations, but measurements of a non-reactive gas tracer would be needed to obtain proof of these processes.

The microbial community structure changed during the experiment (Fig. 8.3). While Methylomirabilaceae decreased, *Crenothrix* and aerobic methanotrophs increased in relative abundance. However, results were not statistically significant ($p > 0.05$ for all groups). Growth of aerobic and facultative anaerobic methanotrophic groups during the experiment was likely

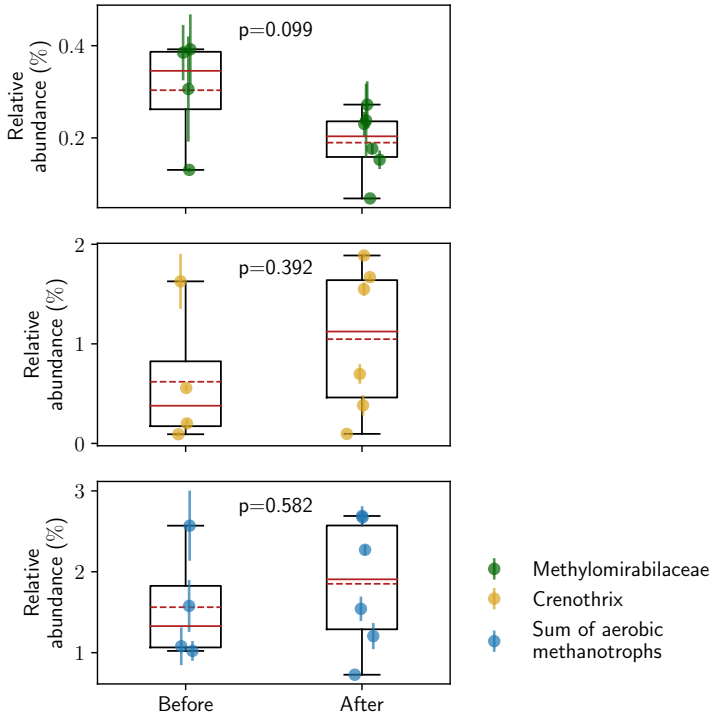

Figure 8.3: **Relative abundance of methanotrophs before and after the experiment.** Methanotrophs were grouped into strictly anaerobic (Methylomirabilaceae), facultative anaerobic (*Crenothrix*), and aerobic organisms (sum of the groups Methylophilaceae, Methylococcales, and Methylopilaceae). Error bars show minimum and maximum values obtained from duplicate measurements. Boxplots and p-values are based on the median for each sample. P-values were calculated with an independent *t* test and the python package scipy.stats (version 1.5.1).

stimulated by the input of CH_4 and electron acceptors, and is a sign for active CH_4 oxidation in the HZ. The reason for the observed decrease in the strictly anaerbic Methylomirabilaceae could well be the intrusion of dissolved O_2 during the injection periods. *Crenothrix* may have coupled CH_4 oxidation to the reduction of dissolved O_2 or NO_3^-, but due to the simultaneous presence of both electron acceptors it is not possible to quantify the contribution of each one. Therefore, it is necessary to improve the experimental set-up, repeat the experiment, and avoid O_2 contamination under all circumstances for a meaningful outcome.

8.4 Concluding remarks

The outcome of the in situ labeling experiment demonstrates a high denitrification potential in the HZ, even below the natural denitrification zone, but the data were insufficient for fully clarifying of the role of NO_3^- as an electron acceptor for CH_4 oxidation for three main reasons: (i) The injection resulted in oxygen input into the HZ, (ii) the ^{13}C label was severely diluted, and (iii) tracers dissolved in the pore water may not accurately represent the behavior of gases in the HZ. The open-system dilution was too large for quantifying the amount of CH_4 consumed. Large scatter in the R_{CH4} and R_{CO2} data and the absence of a clear trend reduced

the informative value of single labeled data points. It was surprising that neither CH_4 nor CO_2 received significant portions of the label although up to half of the sample volume was derived from the injection liquid according to tracer measurements. Potentially, different behaviors of water and gas phases in the pore space can explain these observations. Nevertheless, an increase in relative abundance of aerobic and facultative anaerobic methanotrophs indicated CH_4 oxidation in the HZ. It is promising that the composition of microbial groups in the sediment changed during the experiment because this demonstrates that the microbial community structure can be influenced with the introduced experimental set-up, even if the differences were not statistically significant this time.

This work is ongoing and the working group plans to repeat the experiment with an improved set-up to prohibit accidental O_2 infiltration. Increased CH_4 concentrations and R_{CH4} values in the injection liquid should be used to strengthen the labeling effect. A higher number of subsamples for 16S rRNA analyses could increase the statistical significance of data on microbial community changes. Further details on the planned experiments can be found in Ch. 10.

9 Synoptic discussion

9.1 The HZ of river Moosach is a hotspot of methane production

Our data clearly confirm that the HZ can be a hotspot of CH_4 production and CH_4 emissions. We found pore-water CH_4 concentrations of up to 1000 µmol L^{-1} at several sites in the HZ of river Moosach in combination with a high abundance of methanogens (Ch. 5). Only a single geochemical profile, measured in March 2021, showed low pore-water CH_4 concentrations throughout the HZ. When we monitored HZ geochemistry for five months, pore-water CH_4 concentrations remained high and we did not see a significant reduction in pore-water CH_4 concentrations during autumn (Ch. 6). In addition, extremely high CH_4 ebullition was observed throughout the year, at one site even with persistent high fluxes during winter (Ch. 7). These high emissions at low temperatures indicate that CH_4 is produced in the HZ throughout the year.

Unpublished experiments in which we incubated sediments from river Moosach together with autoclaved river water and an anoxic N_2 headspace support the high methanogenic potential (Fig. 9.1). Sediment for all incubations was collected from a single site and homogenized before filling the bottles. After a pre-incubation period of eight months, we monitored CH_4 production at 30 °C in fifteen 250 ml incubation bottles filled with 50 ml saturated sediment (20.1 $\pm$ 1.1 gDW (gram dry weight); mean $\pm$ standard deviation; n = 3) and 100 ml river water over a period of 5 weeks. Every week, the bottles were flushed with N_2 and headspace CH_4 concentrations were measured before and after flushing. Average CH_4 production rates of 1.56 $\pm$ 0.31 µmol CH_4 gDW^{-1} d^{-1} (n=70) were calculated from the difference in CH_4 concentrations before and after the 7-day incubation interval.

These rates of potential CH_4 production are in the upper range of what other researchers have measured in river sediments: Bednařík et al. (2019) found rates between $1.2 \cdot 10^{-4}$ and 0.64 µmol gDW^{-1} d^{-1}, Bodmer et al. (2020) reported a range of $3.1 \cdot 10^{-5}$ to 1.79 µmol gDW^{-1} d^{-1}, and Shelley et al. (2015) measured potential CH_4 production between 0.53 and 1.92 µmol gDW^{-1} d^{-1}. The values obtained in our incubation experiment are therefore comparable to other studies, yet rather high. In this context, it needs to be noted that the methanogenic potential of river sediments has been found to be temperature-dependent (Comer-Warner et al., 2018), and the studies mentioned above generally incubated at lower temperatures than 30 °C. Nevertheless, the data support our findings from in situ measurements and demonstrate a high methanogenic potential in river Moosach's sediment.

Factors identified in the literature to fuel methanogenesis, namely a high accumulation of fines in the HZ and a high organic carbon content (Bednařík et al., 2019; Bodmer et al., 2020;

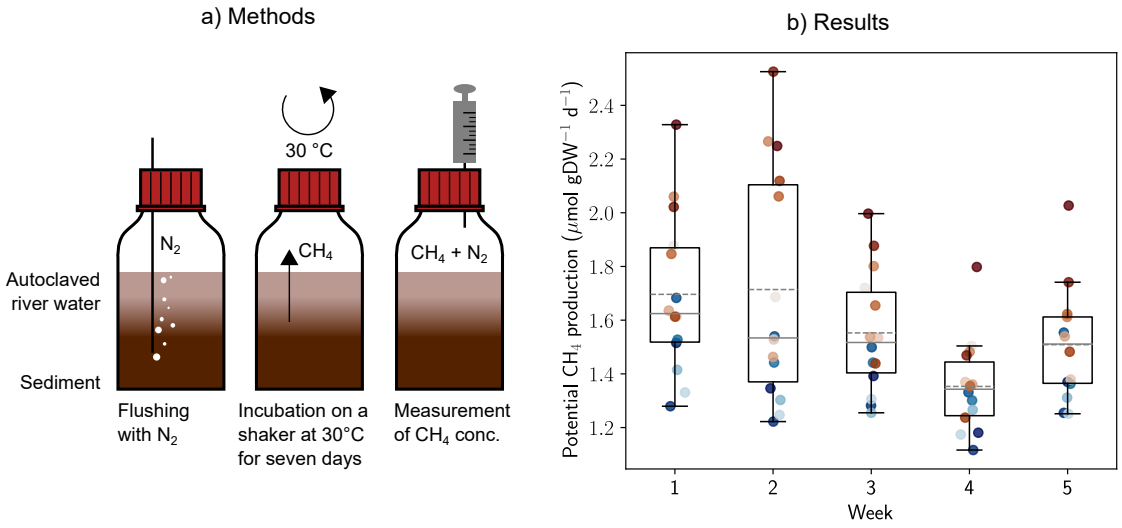

Figure 9.1: **Laboratory incubation experiments.** 50 ml (20.1 ± 1.1 gDW) hyporheic sediment were incubated at 30 °C with 100 ml autoclaved stream water for five weeks to measure CH_4 production rates as displayed in panel (a). Potential CH_4 production rates are shown in panel (b). Different colors of the data points refer to the 15 incubation bottles.

Zhu et al., 2022), are also likely to explain the high CH_4 production in river Moosach. These hydromorphic properties are connected to the river's low gradient and flow velocity, brought about by the high number of impoundments along the watercourse (Auerswald & Geist, 2018).

However, the relation between grain size of the river sediment and CH_4 emissions is not a linear one. We observed largest CH_4 ebullition centrally in the stream, connected to a sandy fraction atop the methanogenic zone, and not at the very fine-grained slip-off slope. Very fine bed substrate has been shown to hamper hyporheic exchange (Sunjidmaa et al., 2022). Slightly coarser grain sizes, in contrast, allow an intensified exchange with stream water and in addition, appear to be more permeable for gas bubbles. This is only true if the top of the streambed is not consolidated and as long as anoxic conditions prevail, which would be unlikely in gravelly river beds with rapid hyporheic exchange, very low residence times, and a reduced surface area for the attachment of biofilm. Thus, it seems that smaller grain size enhances CH_4 production up to a certain point where conditions are already anoxic and more fine material only hinders replenishment of carbon and nutrients. But grain size is only one of many interrelated factors determining the methanogenic potential of a specific site. River flow velocity above the riverbed, obstacles forcing hyporheic exchange, or inhomogeneities like roots, leaves or small branches can also enhance riverine CH_4 emissions by supplying nutrient-rich surface water, providing particulate organic carbon, and forming pathways for the escape of gas bubbles.

The amplifying effect of high organic matter contents in the HZ on CH_4 production was found to be more obvious. Leaf litter from around the stream and large in-stream macrophyte growth supplied organic carbon to the HZ of river Moosach. The sediment was often black, a sign of high organic carbon contents, and LOI values up to 27 % were measured. Ebullition was highest at the most organic-rich site. High NH_4^+ concentrations are a sign of high carbon decomposition rates, because NH_4^+ is released during ammonification of nitrogenous compounds (Ladd & Jackson, 1982). NH_4^+ concentrations in general correlated with CH_4 concentrations

in geochemical profiles (Sec. A.4), showing the relation of increasing biodegradation and methanogenesis.

The combination of δ^{13}C–CH_4 and 16S rRNA sequencing data allows the discussion of relevant CH_4 production pathways. The carbon stable isotope signature of pore water and ebullition samples was generally $<$ -60 ‰. Exceptions were samples extracted by peristaltic pumps through Rhizon samplers, some pore-water samples from the upper part of the methanotrophic zone, and dissolved CH_4 in the surface water. In the first case, the less negative δ^{13}C–CH_4 values could mainly be attributed to sampling effects, in the latter two cases oxidation clearly influenced the stable carbon isotope composition of CH_4. CH_4 deeper in the riverbed and in gas bubbles, representative of what is produced in the HZ of river Moosach, was highly depleted in ^{13}C.

In the context of CH_4 production pathways, the discrimination against ^{13}C is highest when CO_2 is reduced to CH_4 (hydrogenotrophic methaneogenesis). This pathway can lead to δ^{13}C–CH_4 values as low as -110 ‰ (Whiticar, 1999). Methylated substrates such as acetate or methyl amines generally lead to a lower fractionation, except for methanol which can produce similar δ^{13}C–CH_4 values as hydrogenotrophic methanogenesis (Whiticar, 1999). The values observed in river Moosach are expected to represent a mix of different production pathways, because they lie between what would be expected for hydrogenotrophic and acetoclastic methanogenesis. The generally depleted δ^{13}C–CH_4 values indicate a large contribution of hydrogenotrophic methanogenesis.

However, variations in the stable carbon isotope composition of CH_4 have been observed in time and space. δ^{13}C–CH_4 in gas bubbles at one site were more enriched during July 2022 compared to the rest of the year as well as compared to the other three sites. This effect is not expected to be caused by oxidation, because gas bubbles are generally assumed to escape oxidation due to their high transport velocity (Sawakuchi et al., 2016). In addition, we did not see a significant shift from high CH_4 to high CO_2 concentrations in the gas mixture during that period. The shift in δ^{13}C–CH_4 could be connected to a change in available substrates or a change in the stable isotope composition of the substrates due to increased macrophyte growth in July. Moreover, δ^{13}C–CH_4 values in the CH_4 zone varied in space, both for ebullition samples and in pore-water profiles. Hydrogeochemical site properties and local substrate availability appear to influence microbial communities and methanogenic pathways.

Although hydrogeneotrophic and acetoclastic methanogenesis are said to be the most prominent CH_4 production pathways in natural freshwater systems (Ferry, 2010), we found several indications that also methanol may be a substrate for methanogenesis in the HZ of river Moosach. First, the groups Methanomassiliicoccales and Methanomethyliales, both capable of catalyzing H_2-dependent methylotrophic methanogenesis (Berghuis et al., 2019; Vanwonterghem et al., 2016), dominated the methanogenic community in depths $>$ 15 cm. Methanomassiliicoccales were postulated to produce CH_4 from methanol in freshwater wetlands (Narrowe et al., 2019) and their high abundance could mean that methanol is also a substrate for methanogenesis in the HZ of river Moosach. Methanol is derived from pectin in terrestrial plants (Conrad, 2005), and large amounts of allochthonous plant material found in almost all sediment cores could deliver methanol to the methanogens. Second, as mentioned above, the carbon stable isotope fractionation during CH_4 production from methanol and CO_2 are comparable, thus δ^{13}C–CH_4 values as observed here support the possibility of this production pathway. Third,

high ebullition rates during winter were a sign for CH_4 production at temperatures of $< 8\,^{\circ}C$. Typically, methanogenesis is expected to decrease at low temperatures (Aben et al., 2017; Comer-Warner et al., 2018), but CH_4 production from methanol has been shown to be a cold-adapted pathway used by psychrophilic methanogens (Cao et al., 2014; Jia et al., 2021; Zhang et al., 2008).

9.2 There is a potential for aerobic and anaerobic methane oxidation in the HZ of river Moosach

We hypothesized that both aerobic and anaerobic CH_4 oxidation would reduce CH_4 emissions from the HZ. Indeed, the data showed clear indications for CH_4 oxidation. In four of the measured high-resolution geochemical profiles (site C in Ch. 5, site B in Ch. 7, and both peeper profiles in App. B), a strong enrichment in $\delta^{13}C$–CH_4 at the top of the streambed was detected. A similar shift was seen in most of the pore-water profiles extracted at the monitoring station (Sec. B.2). In saturated conditions, the kinetic isotope fractionation during microbial consumption is generally larger than isotope fractionation in the context of physical processes such as diffusion, sorption, or volatilization (Elsner, 2010) and thus, the observed change in slope between the lower and upper part of the $\delta^{13}C$–CH_4 profiles is a clear sign for microbial CH_4 oxidation in the mentioned cases.

A further indication of CH_4 oxidation was the enrichment of dissolved CH_4 in the surface water compared to pore water and gas bubbles. Based on the difference in $\delta^{13}C$–CH_4 of surface water and ebullition samples we calculated that 12-44 % of the CH_4 transported diffusively was oxidized. However, this range is quite uncertain, as fractionation factors can vary greatly. Adding to the uncertainty, dissolved CH_4 in the surface water can also be influenced by CH_4 transported through plants and by exchange with rising gas bubbles during ebullition. Plants may deliver more enriched CH_4 to the surface water because they favor CH_4 oxidation (Li et al., 2021). A more enriched CH_4 source in the mixture would mean that CH_4 from the HZ was less enriched, and thus, that less CH_4 is oxidized in the HZ than the $\delta^{13}C$–CH_4 value in the surface water suggests. On the other hand, gas exchanges between water and gas phase during bubble transport delivers less enriched CH_4 which would have an opposite effect.

Microbiological analyses revealed aerobic methanotrophs as well as bacteria capable of catalyzing the n-damo process in the HZ of river Moosach. Aerobic groups were more abundant in the upper 12 cm of the HZ. In the same zone, we found an increased abundance of anaerobic methanotrophs affiliated with *Candidatus* "Methylomirabilis", known to use NO_2^- as an electron acceptor for CH_4 oxidation, and with *Crenothrix*, a facultative anaerobe reducing NO_3^- in O_2 limited conditions. ANME archaea, which can perform AOM coupled to SO_4^{2-} or metal oxidation, were not abundant. The overlap in habitats of the O_2-sensitive *Candidatus* "Methylomirabilis" and aerobic methanotrophs is surprising, but there are other published examples (Vaksmaa et al., 2017).

O_2 was consumed in a narrow zone at the very top of river Moosach's sediment, and denitrification occurred just below, mostly in a similarly narrow zone. In many of the measured geochemical profiles, O_2 reduction and denitrification zones partly overlapped. Even a vertical resolution of 1 cm was insufficient to separate the two processes. Also modeling of the concen-

tration gradients revealed overlaps of these two zones. Aerobic methanotrophy and n-damo are therefore likely to occur in adjacent or even slightly overlapping narrow zones and with the applied methods it was not possible to quantify how much CH_4 was oxidized aerobically and how much via the n-damo process.

Modeling of concentration gradients showed overlaps of the CH_4 oxidation zone not only with O_2 reduction and denitification zones but repeatedly also with SO_4^{2-} reduction zones. Coupling of CH_4 and sulfur cycling at the location where microbial samples were taken seems unlikely due to the absence of ANME archaea. However, at other sites the microbial community may be different. It is noteworthy that river Moosach is atypically SO_4^{2-} rich; that SO_4^{2-} profiles were often complex, with an increase of SO_4^{2-} concentrations in the upper part of the HZ above the SO_4^{2-} reduction zone; and that CH_4 oxidation and SO_4^{2-} reduction zones overlapped in almost all profiles. Although out of scope for this thesis, the sulfur cycle in the HZ of river Mooosach seems an interesting topic of study and the available geochemical profiles could be of use for this in the future.

As described previously, an incubation experiment was set up to estimate potential CH_4 production of sediments from river Moosach (Fig. 9.1). We tried to use the same incubation bottles for separating aerobic and anaerobic CH_4 oxidation experimentally. Different electron acceptors were added to test their potential to catalyze CH_4 oxidation, but, despite the consumption of O_2, NO_3^-, and SO_4^{2-} within few hours or days, CH_4 oxidation could not be quantified nor could the effect of different electron acceptors on CH_4 consumption rates be compared. High CH_4 production rates superposed expected effects of CH_4 oxidation like a concentration reduction or an enrichment in δ^{13}C–CH_4. It was not possible to prevent CH_4 production with a chemical methanogenesis inhibitor such as 2-bromoethanesulfonate (BES), because this would have equally affected the pathway of reverse methanogenesis that many methanotrophs encode in their genomes (Liu et al., 2011). Thus, the incubation experiments could neither resolve the roles of aerobic versus anaerobic CH_4 oxidation quantitatively.

Although all our O_2 measurements strongly suggest anoxic conditions in the HZ of river Moosach below a few centimeters, trace amounts of O_2 in deeper layers may have gone undetected and have been said to be sufficient for aerobic CH_4 oxidation in sediments (Steinle et al., 2017). Furthermore, river Moosach has a high degree of plant cover (Braun et al., 2012) and macrophytes favor aerobic CH_4 oxidation for two reasons: plants can deliver dissolved O_2 through their roots into the HZ and aerobic methanotrophs can inhabit the surface of macrophytes (Li et al., 2021). Nevertheless, the abundance of organisms that couple CH_4 oxidation to NO_3^- or NO_2^- reduction combined with the overlap in CH_4 oxidation and denitrification zones are strong signs of the occurrence of n-damo in the HZ of river Moosach, even if they may not provide definite proof. It is likely that CH_4 diffusing upwards is first oxidized with available NO_3^- or NO_2^- and that most CH_4 does not reach the oxic layer, just like it was observed in deep lake sediments (Deutzmann et al., 2014).

To summarize, there were strong indications for both aerobic and anaerobic CH_4 oxidation, but the exact share of CH_4 oxidized by dissolved O_2 or other electron acceptors remains unresolved. AOM could be coupled to denitrification while the involvement of other electron acceptors is rather unlikely.

9.3 The relevance of methane oxidation coupled to denitrification for GHG emission reduction and nitrate removal was limited by methane availability

This thesis focused on the role of the n-damo process in the HZ for the reduction of CH_4 emissions and for NO_3^- removal from stream water. As discussed in Sec. 9.2, the combined data from river Moosach demonstrated a potential for CH_4 oxidation coupled to denitrification, however, could not quantify n-damo rates.

Nonetheless, our data suggest for several reasons that the n-damo process was only of minor importance as a CH_4 sink. An isotopic enrichment at the top of the HZ, indicative of CH_4 oxidation, was only found in four geochemical profiles. Six of the peeper profiles did not show an enrichment in δ^{13}C–CH_4 at the top of the streambed. This does not necessarily rule out the possibility that CH_4 is oxidized. CH_4 oxidation could either occur at rates too low to influence the stable carbon isotope composition or in the uppermost centimeters of the HZ, where CH_4 concentrations were too low for reliable δ^{13}C–CH_4 measurements. In both cases, CH_4 fluxes can only marginally be reduced by oxidation. Low oxidation rates were confirmed by modeling. All CH_4 consumption rates in Ch. 5 were below $2 \cdot 10^{-4}$ µmol L^{-1} s^{-1}, and in Ch. 7 below $3 \cdot 10^{-4}$ µmol L^{-1} s^{-1}.

CH_4 concentrations at the sediment–water interface were very low in all measured geochemical profiles. The decrease in concentrations at more or less constant δ^{13}C–CH_4 values could largely be explained by diffusion from CH_4-rich deeper zones to the highly diluted surface water, that is in constant exchange with the atmosphere. Low CH_4 availability presumably limited CH_4 oxidation. At low diffusion coefficients, CH_4 was transported only slowly into the methanotrophic zone. In addition, pore-water CH_4 is diluted with surface water at the top of the HZ due to hyporheic exchange fluxes. Even more importantly, most CH_4 was removed from the HZ via ebullition, as indicated by the reduced pore-water CH_4 concentrations at sites with higher ebullition compared to less active sites. In this way, most CH_4 produced in the HZ of river Moosach didn't reach the oxidative layer, but was rather transported directly to the surface water. Thus, CH_4 as a substrate was likely a limiting factor for the n-damo process.

The role of the n-damo process for NO_3^- removal from stream water seems to be similarly limited. Only if the availability of CH_4 as an electron donor is high, this process can become a relevant NO_3^- sink. Despite this, the HZ of river Moosach had a high denitrification potential, as demonstrated by steep NO_3^- gradients and quick NO_3^- removal from incubation bottles. Heterotrophic denitrification is expected to strongly contribute to NO_3^- reduction from the stream (Kim et al., 2016; Zhou et al., 2014). Other sources of organic carbon than CH_4, which are necessary for this respiration pathway (Trimmer et al., 2012), were readily available. The total number of microorganisms in the hyporheic sediments of river Moosach was high, and denitrification is a ubiquitous process encoded in the genomes of many microorganisms. The in situ labeling experiment described in Ch. 8 confirmed the very high denitrification potential of the HZ. NO_3^- was almost completely consumed within hours when injected into the riverbed. The experiment was performed between 20 cm and 40 cm depth and thus, far below the natural denitrification zone. Therefore, NO_3^- supply to the HZ seems to be more of a limiting factor for NO_3^- removal than carbon availability or microbial limitations.

Hydrologic connectivity has been shown to increase denitrification (Roley et al., 2012) and similar to what was found for O_2 uptake (Rutherford et al., 1993, 1995), NO_3^- reduction may be proportional to influx rates. Exchange between HZ and surface water was highest in the central section of the stream, whereas it was limited by consolidation, lower porosity, a more homogeneous bed substrate, and lower above-ground river flow velocities on the sides. In contrast, CH_4 oxidation was more pronounced at the sides, because CH_4 was transported slower and got more concentrated in the pore water compared to the center, where gas was removed quickly via ebullition. Thus, the middle of the river might be more important for overall denitrification (Fischer et al., 2005), while the n-damo process is probably more localized to the sides of the riverbed.

To summarize, factors limiting the n-damo process seem to be CH_4 availability and NO_3^- supply to deeper layers of the HZ. The first is mainly reduced by low diffusion coefficients and a high ebullitive transport which removes CH_4 quickly from the riverbed. The latter is hindered by low hyporeic exchange fluxes. Very fine deposits and consolidation reduce the supply of nutrients to the HZ and controlled discharge conditions prevent flood events which would foster periodic exchange due to sediment relocation.

9.4 Stream methane emissions are likely to increase in the future

Another initial hypothesis was that temperature sensitivity, fine-grained bed substrate and organic-rich sediments are methanogenesis-promoting factors that make a future increase in CH_4 emissions from rivers likely. To predict whether riverine CH_4 emissions will increase in the future, it is necessary to understand (i) which parameters enhance or hamper CH_4 emissions from streams and (ii) how these parameters will develop under climate change. Our data is suitable to discuss the first question, while literature is reviewed to assess the second.

As discussed above, our data suggest that CH_4 oxidation only plays a minor role in reducing GHG emissions from river Moosach because most of the gas was transported directly to the atmosphere via ebullition. In fact, ebullition rates were up to 30 times higher than estimated diffusive fluxes. This means that increased CH_4 production will directly translate to higher CH_4 emissions. Therefore, an increase in CH_4 production at warmer future temperatures cannot be counteracted by similar increases in CH_4 oxidation.

A rise in temperatures in the future is no longer probable, but inevitable (IPCC, 2021). An average global temperature increase of $+2.5$ to $+4\,^{\circ}C$ compared to pre-industrial levels has been classified as *very likely* (IPCC, 2021). The increase of CH_4 emissions at higher temperatures was not as clear as expected based on the literature review (Sec. 2.4). The amount of CH_4 found in pore-water concentration profiles could not be correlated with temperature. Site-specific differences were larger than differences between seasons, also when looking at CH_4 ebullition. When we tried to apply a non-linear regression model to our ebullition data, that has prior been used to describe ebullition from freshwater systems (Aben et al., 2017), we did not achieve a good fit. Only a few other studies have shown an ambiguous influence of temperature on CH_4 emissions. For example, Silvennoinen et al. (2008) discovered that the majority of CO_2 and CH_4 were released during winter from ice-free parts of a river in northern Finland. Similarly, more than 50 % of CH_4 emissions occurred during winter in the Arctic tundra (Zona et al., 2016).

The overall picture, however, still suggests increasing CH_4 production at higher temperatures. Looking at our own data, largest pore-water CH_4 concentrations were measured during summer, even if temperature alone could not explain all observed differences. And although one site kept emitting CH_4 via ebullition during winter, the other two sites with large summer CH_4 efflux were not at all active between mid January and late April. Spacial variance may be larger than seasonal, temperature-dependent variation in a certain area, but a system-wide increase of total CH_4 production and emissions at higher temperatures is still to be expected. This is also in line with the majority of research articles, of which only a subset can be cited here (Aben et al., 2017; Christensen et al., 2003; Comer-Warner et al., 2018; Dean et al., 2018; Wik et al., 2016; Yvon-Durocher et al., 2011, 2014, 2017; Zhu et al., 2020). Also the IPCC (2021) assessed that natural CH_4 and N_2O emissions will have a positive feedback to warming with $+0.04$ (0.02-0.06) W m^{-2} $^{\circ}C^{-1}$.

Site-specific factors that we identified to foster riverine CH_4 production and emissions were a high content of organic matter and a rather fine bed substrate, although with a good permeability for hyporheic exchange fluxes and gas bubbles. High contents of organic matter in combination with high microbial carbon turnover, inferred from NH_4^+ profiles, were related to highest pore-water CH_4 concentrations. The strongest CH_4 ebullition was observed at sites with a sandy top layer and very fine-grained, organic-rich material below. High permeability presumably facilitates the rise of gas bubbles and supposedly fostered microbial turnover due to inputs of organic carbon and nutrients. Nonetheless, the bed substrate needs to be fine enough to ensure anoxic conditions in the HZ. There are claims that CH_4 can be produced in oxic environments like lake water but expected rates would be negligible compared to what was observed in river Moosach's strongly reducing HZ (Bogard et al., 2014; DelSontro et al., 2018; Grossart et al., 2011).

The input of fines into streams has risen since the 1940s and was associated with a concurrent increase in organic matter as demonstrated by a study from 236 streams in the UK (Zhu et al., 2022). The combined impact of increased fine material and organic matter amplified streambed CH_4 emissions (Zhu et al., 2022). On a global scale, erosion is predicted to further increase in the future, mainly due to higher precipitation intensities (Borrelli et al., 2020). Future land-use changes are harder to foresee and scenarios vary in the development of crop lands but clearly, expansion of arable land would contribute to higher erosion rates (Borrelli et al., 2020).

Auerswald and Geist (2018) pointed out that it is not enough to look at the sources of fine material (at river Moosach mainly internal calcite precipitation and erosion in the catchment), but that factors controlling the deposition rate, such as the flow regime and the energetic gradient in a stream, must also be considered. In river Moosach, favorable conditions for high methanogenesis rates prevail not least because of human alterations to the river's course and hydrology. The construction of a series of weirs has led to a reduction in the longitudinal gradient and has reduced flow velocities and hydrologic extremes, favoring the deposition of fines. Sediments of these kind of anthropogenically altered, warm, and O_2-depleted streams were found to be a preferred habitat for highly efficient hydrogenotrophic methanogens (Nagler et al., 2021). Indeed, *Methanosarcinaceae* and *Methanobacteriaceaea*, two of the mentioned efficient CH_4 producing groups (Nagler et al., 2021), were very abundant in river Moosach.

In the EU, most dams for hydropower generation were built in 1970-1980 and although the pace of river development slowed down after 2000, partly due to the introduction of the European

Water Framework Directive (WFD), it has not stopped ever since (Quaranta et al., 2021). Of the world's longest rivers, only 37 % remain free-flowing (Grill et al., 2019) and more than 3700 new hydropower plants with a capacity of > 1 MW are either planned or under construction worldwide, mainly in low and low-middle income countries in Southeast Asia, South America, and Africa (Wasti et al., 2022; Zarfl et al., 2015). While hydropower is a renewable energy and therefore inherently climate-friendly, impoundments also have the potential to increase riverine CH_4 emissions, especially if valleys are not cleared before flooding and all plant material becomes available carbon for methanogenesis (Li & He, 2022). A dam affects not only the impounded river section directly upstream of the structure, but also the sections in between, where gradient and flow velocity are reduced (Auerswald & Geist, 2018). This phenomenon does by no means only occur with large water reservoirs, but, as demonstrated by this study, anthropogenically altered small watercourses can also contribute significant GHG emissions.

Combining the effects of growing fine sediment inputs due to increased erosion and a more efficient river sink due to the construction of new hydropower dams, a global future increase in CH_4 emissions from rivers is likely.

Extreme precipitation events will increase in frequency and magnitude in the future (IPCC, 2021) and this will not only impact erosion rates. Floods are expected to occur more often and earlier in the year than previously (Alfieri et al., 2015; Blöschl et al., 2017). These changes may affect riverine CH_4 emissions in various ways. Some of these effects may stimulate CH_4 emissions, for example the burial of particulate organic matter during a flood event. By displacing larger artifacts like branches, floods could also stir up bubbles and trigger sudden gas releases during the event. Further, the redistribution of sediments could regularly affect anaerobic microbes that are active close to the top of the HZ such as O_2-intolerant methanotrophs. Methanogens were more abundant in deeper sediment layers than metanotrophs and thus, they are less likely to be affected. If anaerobic methanotrophic communities are more affected by an increase in flood frequency than methanogens, the ratio of CH_4 production to consumption in the HZ could increase. On the other hand, floods could also prevent or mitigate riverine CH_4 emissions, for example if disturbances reach deeper layers and methanogens are affected. The sediment relocation could supply dissolved O_2 to the sediments and enhance aerobic methanotrophy in the aftermaths. Floods also have the potential to rinse clogged streambeds and restore oxic conditions for a while. Thus, the effect of increased flood frequency and intensity could go either way, stimulating or inhibiting stream CH_4 emissions.

Unfortunately, our data cannot support the discussion of the impacts of floods on riverine CH_4 emissions. We did design a monitoring station to study those dynamics but did not witness any major flood events while the monitoring station was in place. The controlled discharge conditions at river Moosach largely reduced the frequency of extreme events. This allowed establishment of large, stable methanogenic and methanotrophic communities. Organisms with a low tolerance to O_2 were found even at the top of the riverbed and we saw only slow changes in HZ geochemistry throughout the year.

Freshwater eutrophication is another factor that, if increased, has the potential to rise future CH_4 emissions from streams (Li et al., 2021). Climate change will alter inland aquatic ecosystems in terms of water quality and quantity, posing new risks for eutrophication through warming and nutrient inputs during extreme events (Dokulil & Teubner, 2010). Additionally, external drivers of eutrophication such as population growth, urbanization, intensive agricultural production,

and rising energy demands will increase in the near future (Dokulil & Teubner, 2010). Yet, the development of freshwater eutrophication very much depends on the implementation of mitigation schemes (Murray et al., 2019), making future predictions as difficult as for land-use changes. River Moosach is a rather nutrient-rich stream with average surface water NO_3^- concentrations of 20 mg L^{-1} (2010-2018) but the ecosystem is not eutrophic (Bavarian State Office of the Environment, 2023). The relatively high nitrogen loads may have fostered microbial turnover and hyporheic CH_4 production. However, we did not compare rivers with different trophic states and cannot deduce the effect of eutrophication on CH_4 emissions from our own data.

Overall, many interrelated factors define the amount of CH_4 produced and consumed in the HZ. Many of these, such as rising temperatures, increased erosion due to more intense precipitation events, further constructions of hydraulic barriers, and eutrophication are likely to amplify riverine CH_4 emissions in the future. At our study site, the role of oxidation for reducing CH_4 emissions was limited and it is unlikely that it will drastically increase in the future. Rivers and streams globally are therefore likely to fuel a positive climate feedback in the future.

9.5 Methodological advances and additional findings

Not only were we testing the hypotheses discussed above but this work also advanced methods for pore-water sampling from the HZ. We tested the suitability of Rhizon samplers for gas analyses and found a strong dependence of measured CH_4 concentrations and $\delta^{13}C$–CH_4 values on the pumping rate (Ch. 6). This information is important for research on GHG production in freshwater and marine sediments, and may even be of relevance in some soils. Rhizon samplers with larger pore diameters may not show the same dependence and the problem might also be less pronounced in coarser riverbeds. On the basis of our study, we hope that the suitability of a pore-water extraction technique will be evaluated before application in future biogeochemical research.

In the same study, we also combined pore-water extraction with in situ dissolved O_2 profiling and the estimation of vertical hyporheic exchange fluxes from distributed temperature measurements. Although these two methods had been described previously (Brandt et al., 2017; Gordon et al., 2012) the combination was new and may be very beneficial for future studies on hyporheic biogeochemistry. To the best of our knowledge, the sensor of Brandt et al. (2017) had not been rebuilt by other scientists and the proof of repeatability can be of value to the scientific community.

To target the potential of the n-damo process in the HZ we also conceptualized and tested a new in situ labeling experiment. Although improvements to set-up and execution are necessary in our case, the idea and experimental design have a great potential for studying microbial turnover processes in the HZ and other saturated sediments. Using in situ labeling, the disadvantages of incubating sediment samples in the laboratory such as necessary changes to environmental conditions and temperature or a potential contamination during sampling, transport, and sample distribution can be avoided.

Furthermore, the data gathered in this thesis stressed the very high small-scale spacial heterogeneity in streams. Geochemical gradients, as well as CH_4 ebullition, and also grain-size

distribution and organic carbon content of the sediment were highly location-specific. Finding representative sites for measurements in the HZ remains a challenge in experimental design and complicates the extrapolation from point measurements. Based on our data it seems necessary to cover and compare as many sites as possible in studies on the HZ.

In contrast, temporal variations were slower and less pronounced than expected. It may therefore be sufficient to measure only during a few weeks per season or during an interesting event as opposed to whole-year monitoring. There is potential here to save time and resources. In exchange, however, several locations should be sampled whenever the HZ is investigated because a single point measurement can never fully represent this complex system. We faced difficulties in the interpretation of geochemical profiles where we varied both location and time (Ch. 5). Interpretations can be much more robust if both dimensions, time and space, are separated in the data.

10 Outlook

Some questions remained unresolved in this work, for example the exact contributions of aerobic CH_4 oxidation versus n-damo, the relevance of methanogenesis during winter, and how results of river Moosach compare to other rivers. Possible future studies and experiments that could target these open questions are described and discussed below.

The exact contribution of aerobic CH_4 oxidation and AOM coupled to denitrification could not be quantitatively resolved with the methods applied in this thesis. Ongoing research for the first time uses in situ isotope labeling to try tracing labeled carbon in injected CH_4 and quantify how much CH_4 is oxidized to CO_2 in the HZ (Ch.8). The addition of different electron acceptors is expected to affect the amount of CH_4 that will be consumed as well as the microbial community. If successful, the experiment will provide first in situ evidence for the activity of specific anaerobic methanotrophic groups in the HZ. However, this far, strong dilution of the input signal made a quantification of CH_4 oxidation rates from stable carbon isotope ratios impossible. Further, the disadvantages of the installed Rhizon samplers reduced the quality of the gas measurements. When performing the experiment for the first time, it was not possible to carry out the injection completely in the absence of O_2. Microbiological analyses are still pending.

The working group plans to repeat the experiment with an improved setup. Completely gastight connectors and tubing should prevent O_2 contamination; the installation of Rhizon samplers with a larger pore diameter may improve the quality of gas measurements in extracted samples; and with a stronger label it should be possible to recover enough ^{13}C in CO_2 for a quantification of oxidation rates. For increasing the label, pure $^{13}CH_4$ has to be purchased in a sufficient quantity to allow a 100 % CH_4 headspace in the injection bottles and connected gasbags. Potentially, it will be necessary to apply pressure so that more CH_4 will dissolve in the injection water. If dilution still doesn't allow recovery of the label in the samples in a sufficient quantity, it may be necessary to shield the direct surroundings of the Rhizon samplers from the rest of the HZ, for example with a lengthwise-cut half tube. This would keep the conditions as close to the natural state of the system as possible while cutting off horizontal hyporheic exchange fluxes. A good idea could also be to compare results from lab incubations, in situ labeling with a cover, and in situ labeling in the open system.

If similar experiments are simultaneously conducted at sites with different substrate properties, observed differences can be related to site specific properties such as sediment composition and the magnitude of hyporheic exchange. Using again a combination of pore-water extraction with in situ O_2 measurements and reverse modeling of hyporheic exchange fluxes from temperature data, the influence of these exchange fluxes on methanotrophic processes in the HZ can

be studied. Using temperature as a tracer in this case is an effective way to quantify exchange fluxes without disturbing the sediment.

The improved set-up can not only be used for a repetition and expansion of the in situ labeling experiments but could also be highly beneficial for studying the effect of floods and droughts on the CH_4 cycle. Since river Moosach is subject only to minor discharge fluctuations, it could be interesting to compare these conditions to the HZ of a more variable and dynamic stream system. Villa et al. (2020) was one of the few who compared the distribution of GHGs in the pore space of river substratum during different flood stages. An interesting experiment could also be designed in an artificial channel where the discharge rate is adjustable. Then, alternating low-flow periods and flood events can be simulated.

This thesis had a strong focus on anaerobic CH_4 oxidation. However, some other interesting findings have opened new questions on the biogeochemistry of the HZ. One potential research topic are the observed CH_4 emissions during winter: How relevant is CH_4 production during winter, which organisms produce CH_4 at cold temperatures, and what factors favor this process? Was really CH_4 production from methanol responsible for the large ebullition during winter and why did one site behave so differently from neighboring sites during the cold season? Temperature-controlled laboratory incubation experiments could help to answer these questions. Addition of isotopically labeled substrates to incubations of different sediment types at cold and warm temperatures could reveal controls on cold-adapted methanogenesis. Such experiments could identify the substrates, that can be microbially converted to CH_4 at cold temperatures and the sediment properties, that favor this process. 16S rRNA sequencing of DNA extracted from the sediment samples before and after incubation could give insights on the responsible microorganisms. To relate the results obtained in laboratory incubations to the reality one could mark where sediment was taken from and perform in situ measurements during winter specifically at interesting locations.

Another interesting geochemical phenomenon we observed was the complexity of SO_4^{2-} profiles. Often, elevated SO_4^{2-} concentrations were measured below the sediment–water interface and above the SO_4^{2-} reduction zone. We speculated that this slightly convex part of the gradients could be caused by re-oxidation of reduced sulfur species from deeper zones or could be connected to cryptic sulfur cycling as suggested previously (Ng et al., 2020; Norði et al., 2013). It was out of scope for this thesis to study the sulfur cycle in depth but examining the proposed cryptic sulfur cycle in the HZ could be really interesting. For this, H_2S measurements may be a challenge due to the quick oxidation of H_2S to SO_4^{2-} in oxic conditions and the high probability of sample contamination with atmospheric O_2 during and after extraction from the HZ. Iron measurements would also be necessary since the involvement of Fe in the cryptic sulfur cycle has been suggested (Ng et al., 2020).

Choosing only one test site was a deliberate decision to achieve a high data resolution and good coverage of the study site and to allow deduction of general findings from these data. However, it would still be really interesting to see how results from river Moosach compare to other rivers, especially considering ebullition as a transport pathway. Our results showed that the contribution of ebullition to total CH_4 emissions was much larger than the share of diffusive fluxes. This contradicts what other researchers have found for streams in the UK (Robison et al., 2022). Therefore, there are still uncertainties in the relevance of CH_4 ebullition from rivers. Gathering a large-scale data set with ebullition measurements from several streams

with different hydrologic and geomorphic characteristics could be really beneficial for targeting these uncertainties. Results would surely improve global GHG budgets like the Global Methane Budget (Saunois et al., 2020) or the next Assessment Report of the IPCC.

However, installing gas traps and especially collecting and measuring the samples from too many sites over at least one year would exceed the capacity of most research institutes. The design and construction of a simple low-cost automated gas sampler for ebullition measurements would be the first necessary step in this advent. There have been examples of automated gas traps for ebullition monitoring previously (Maeck et al., 2014) and recent advances in the construction of low-cost sensors for CH_4 and CO_2 concentrations in flux chambers may be very helpful (Bastviken et al., 2020). Only such automated measurement techniques would allow the installation of a statistically representative number of gas samplers in different rivers. Combining this with sediment analyses and maybe 16S rRNA gene sequencing would largely contribute to the quantification of CH_4 ebullition from streams and to the understanding of the role of different CH_4 transport pathways.

Incorporation of both diffusive and ebullitive CH_4 fluxes from rivers and streams into climate models could be a long-term goal. For this, extrapolation from point measurements to regional CH_4 fluxes from complete river networks is necessary. This again requires large spatially and temporarily resolved data sets on ebullition on the one hand and on dissolved CH_4 concentrations in surface water for the quantification of total diffusive fluxes on the other hand. Cooperation with geomorphologists and hydraulic modelers will be needed to understand which type of sediment will be deposited where in a stream as a basis for the deduction of CH_4 fluxes.

Modeling was not a focus of this study. Neither extrapolation and modeling of river network-wide CH_4 emissions as mentioned above nor detailed transport-reaction modeling in the HZ. But surely, our understanding of the hyporheic CH_4 cycle could be hugely improved by a model combining diffusive and advective transport, geochemical reactions, and partitioning between gas and water phases. This means a three-phase model considering solid, gas, and water phase combined with a geochemical model such as PHREEQC (Parkhurst & Appelo, 2013). Design and implementation of such a model is a highly complex task. However, if attempted, our data could be valuable to test and calibrate these models with high-resolution geochemcial gradients of dissolved solutes and gases.

In general, for further advances in understanding hyporheic CH_4 production, consumption, and transport processes, the interdiscipinary work of geochemists, microbiologists, and modelers is needed. I am confident that this interaction of different specialists can produce much more detailed results than it could be achieved by a single field. In this work for example, the cooperation with microbiologists and ecologists largely facilitated the interpretation of our geochemical data.

11 Conclusions

This thesis contributed spatially and temporarily resolved data from a study site in southern Germany for a better description of the CH_4 cycle in the HZ. We measured high-resolution vertical geochemical profiles at different sites; designed, installed, and tested a monitoring station for repeated pore-water extraction, O_2 profiling, and automated temperature measurements; and monitored ebullition for a full year. Especially stable isotope measurements were helpful to trace hyporheic CH_4 cycling. Microbiological analyses and modeling of geochemical gradients were applied to gain a deeper understanding of the microbially catalyzed turnover processes in the HZ. The estimation of diffusive CH_4 fluxes across the sediment-water and water–air interfaces could be used to evaluate the scale of different transport processes.

Based on these data we would answer the initial hypotheses as follows:

- **The hyporheic zone of river Moosach is a hotspot of methane cycling, where methane is produced at significant rates as well as oxidized aerobically and anaerobically**: Our data clearly show that the HZ of river Moosach has a high methanogenic potential. Hydrogenotrophic methanogenesis probably contributed most of the biogenic CH_4 in the HZ, but there were also signs for CH_4 production from methanol. We found a potential for aerobic methanotrophy and CH_4 oxidation coupled to NO_3^- or NO_2^- reduction. Both processes occurred in narrow, adjacent zones, with overlaps in some places. AOM coupled to SO_4^{2-} or metal reduction seemed unlikely due to a lack of ANME archaea in the sediment.
- **Microbial methane oxidation coupled to nitrate or nitrite reduction (n-damo) not only reduces methane emissions but also enhances the removal of surplus nitrogen from stream ecosystems**: The n-damo process was of limited relevance as a CH_4 sink in the HZ of river Moosach. Main reasons were low CH_4 concentrations in the oxidative zone due to gas removal via ebullition, dilution with surface water, and limited diffusive transport. Most CH_4 was transported directly to the atmosphere and escaped oxidation. Heterotrophic denitrification presumably removed more NO_3^- from the stream than n-damo.
- **Most of the methane produced in the hyporheic zone is transported upwards by diffusion while ebullitive methane fluxes are of minor importance**: In contrast to this initial hypothesis, ebullition transported up to 30 times more CH_4 to the atmosphere than diffusion. The contribution of ebullition was highly site specific and gas fluxes were highest in the central section of the river. The overall reduction of CH_4 fluxes by oxidation was of minor importance because most CH_4 escaped the oxidative layer quickly in the form of gas bubbles.

- **Stream methane emissions are temperature-sensitive and enhanced by fine, organic-rich sediments, and are therefore likely to increase in the future**: Many interrelated factors control how much CH_4 is emitted at a specific site in a stream. Although local differences were more pronounced than seasonal, temperature-dependent changes we would expect whole-system increases in CH_4 emissions from rivers in a warmer climate. Several other factors such as increased erosion due to more intense precipitation, combined with high inputs of organic matter, further dam constructions, and potentially eutrophication are believed to synergetically lead to a positive climate feedback from rivers.

In addition to answering the hypotheses above, this thesis provided several methodological advances. We discovered a dependence of CH_4 concentration and $\delta^{13}C$–CH_4 measurements on the pumping rate in pore-water samples extracted with Rhizon samplers. This finding is of relevance for all future studies, that want to monitor gas concentrations in the HZ over time. Our data also highlights the large spatial heterogeneity of the HZ, leaving the impression that a coverage of many study sites is key in understanding hyporheic biogeochemical process.

An improved version of the monitoring station introduced in Ch. 6 could help the discovery of seasonal changes in hyporheic geochemistry and the CH_4 cycle, both through time-resolved observations and in situ (isotope) tracer experiments. Automated gas traps could be hugely beneficial for global CH_4 budgets because they would enable monitoring of a statistically relevant number of sites in diverse streams. A focus on modeling could help a better understanding of field data on the small scale and could also allow extrapolation from point measurements and incorporation of riverine CH_4 emissions into climate models on the large scale.

Bibliography

Aben, R. C. H., Barros, N., van Donk, E., Frenken, T., Hilt, S., Kazanjian, G., Lamers, L. P. M., Peeters, E. T. H. M., Roelofs, J. G. M., de Senerpont Domis, L. N., Stephan, S., Velthuis, M., Van de Waal, D. B., Wik, M., Thornton, B. F., Wilkinson, J., DelSontro, T., & Kosten, S. (2017). Cross continental increase in methane ebullition under climate change. *Nature Communications*, *8*(1), 1682. https://doi.org/10.1038/s41467-017-01535-y

Alfieri, L., Burek, P., Feyen, L., & Forzieri, G. (2015). Global warming increases the frequency of river floods in Europe. *Hydrology and Earth System Sciences*, *19*(5), 2247. https://doi.org/10.5194/hess-19-2247-2015

Alm, E. W., & Stahl, D. A. (2004). Extraction of microbial DNA from aquatic sediments. In G. A. Kowalchuk, F. J. de Bruijn, I. M. Head, A. D. L. Akkermans, & J. D. van Elsas (Eds.), *Molecular microbial ecology manual* (2nd Edition, pp. 61–88, Vol. 1). Kluwer Academic Publishers. https://doi.org/10.1007/978-1-4020-2177-0

Amos, R. T., Bekins, B. A., Cozzarelli, I. M., Voytek, M. A., Kirshtein, J. D., Jones, E. J. P., & Blowes, D. W. (2012). Evidence for iron-mediated anaerobic methane oxidation in a crude oil-contaminated aquifer. *Geobiology*, *10*(6), 506–517. https://doi.org/10.1111/j.1472-4669.2012.00341.x

Anderson, M. P. (2005). Heat as a ground water tracer. *Groundwater*, *43*(6), 951–968. https://doi.org/10.1111/j.1745-6584.2005.00052.x

Arshad, A., Speth, D. R., de Graaf, R. M., Op den Camp, H. J., Jetten, M. S., & Welte, C. U. (2015). A metagenomics-based metabolic model of nitrate-dependent anaerobic oxidation of methane by Methanoperedens-like archaea. *Frontiers in Microbiology*, *6*, 1423. https://doi.org/10.3389/fmicb.2015.01423

Auerswald, K., & Geist, J. (2018). Extent and causes of siltation in a headwater stream bed: Catchment soil erosion is less important than internal stream processes. *Land Degradation & Development*, *29*(3), 737–748. https://doi.org/10.1002/ldr.2779

Bange, H. W., Sim, C. H., Bastian, D., Kallert, J., Kock, A., Mujahid, A., & Müller, M. (2019). Nitrous oxide (N_2O) and methane (CH_4) in rivers and estuaries of northwestern Borneo. *Biogeosciences*, *16*(22), 4321–4335. https://doi.org/10.5194/bg-16-4321-2019

Bardini, L., Boano, F., Cardenas, M. B., Revelli, R., & Ridolfi, L. (2012). Nutrient cycling in bedform induced hyporheic zones. *Geochimica et Cosmochimica Acta*, *84*, 47–61. https://doi.org/10.1016/j.gca.2012.01.025

Bardini, L., Boano, F., Cardenas, M. B., Sawyer, A. H., Revelli, R., & Ridolfi, L. (2013). Small-scale permeability heterogeneity has negligible effects on nutrient cycling in streambeds. *Geophysical Research Letters*, *40*(6), 1118–1122. https://doi.org/10.1002/grl.50224

Barnes, R. O., & Goldberg, E. D. (1976). Methane production and consumption in anoxic marine sediments. *Geology*, *4*(5), 297–300.

Barret, M., Gandois, L., Thalasso, F., Martinez Cruz, K., Sepulveda Jauregui, A., Lavergne, C., Teisserenc, R., Aguilar, P., Gerardo Nieto, O., & Etchebehere, C. (2022). A combined microbial and biogeochemical dataset from high-latitude ecosystems with respect to methane cycle. *Scientific Data*, *9*(1), 674. https://doi.org/10.1038/s41597-022-01759-8

Bastviken, D., Nygren, J., Schenk, J., Parellada Massana, R., & Duc, N. T. (2020). Technical note: Facilitating the use of low-cost methane (CH_4) sensors in flux chambers – calibration, data processing, and an open-source make-it-yourself logger. *Biogeosciences*, *17*(13), 3659–3667. https://doi.org/10.5194/bg-17-3659-2020

Bastviken, D., Cole, J. J., Pace, M. L., & Van de Bogert, M. C. (2008). Fates of methane from different lake habitats: Connecting whole-lake budgets and CH_4 emissions. *Journal of Geophysical Research: Biogeosciences*, *113*(G2). https://doi.org/10.1029/2007JG000608

Bavarian State Office of the Environment. (2023). Gewässerkundlicher Dienst Bayern. Data and information [https://www.gkd.bayern.de/en/; Accessed: 2023-06-13].

Beal, E. J., House, C. H., & Orphan, V. J. (2009). Manganese-and iron-dependent marine methane oxidation. *Science*, *325*(5937), 184–187. https://doi.org/10.1126/science.1169984

Bednařík, A., Blaser, M., Matoušů, A., Tušer, M., Chaudhary, P. P., Šimek, K., & Rulík, M. (2019). Sediment methane dynamics along the Elbe River. *Limnologica*, *79*, 125716. https://doi.org/10.1016/j.limno.2019.125716

Bender, M., Martin, W., Hess, J., Sayles, F., Ball, L., & Lambert, C. (1987). A whole-core squeezer for interfacial pore-water sampling. *Limnology and Oceanography*, *32*(6), 1214–1225. https://doi.org/10.4319/lo.1987.32.6.1214

Berg, P., Risgaard-Petersen, N., & Rysgaard, S. (1998). Interpretation of measured concentration profiles in sediment pore water. *Limnology and Oceanography*, *43*(7), 1500–1510. https://doi.org/10.4319/lo.1998.43.7.1500

Berghuis, B. A., Yu, F. B., Schulz, F., Blainey, P. C., Woyke, T., & Quake, S. R. (2019). Hydrogenotrophic methanogenesis in archaeal phylum Verstraetearchaeota reveals the shared ancestry of all methanogens. *Proceedings of the National Academy of Sciences*, *116*(11), 5037–5044. https://doi.org/10.1073/pnas.1815631116

Beyer, W. (1964). Zur Bestimmung der Wasserdurchlässigkeit von Kiesen und Sanden aus der Kornverteilungskurve. *Wasserwirtschaft Wassertechnik (WWT)*, *14*(6), 165–168.

Bhaskar, A. S., Harvey, J. W., & Henry, E. J. (2012). Resolving hyporheic and groundwater components of streambed water flux using heat as a tracer. *Water Resources Research*, *48*(8). https://doi.org/10.1029/2011WR011784

Bishop, K., Buffam, I., Erlandsson, M., Folster, J., Laudon, H., Seibert, J., & Temnerud, J. (2008). Aqua Incognita: The unknown headwaters. *Hydrological Processes*, *22*(8), 1239. https://doi.org/10.1002/hyp.7049

Blair, N., Leu, A., Muñoz, E., Olsen, J., Kwong, E., & Des Marais, D. (1985). Carbon isotopic fractionation in heterotrophic microbial metabolism. *Applied and Environmental Microbiology*, *50*(4), 996–1001. https://doi.org/10.1128/aem.50.4.996-1001.1985

Blöschl, G., Hall, J., Parajka, J., Perdigão, R. A., Merz, B., Arheimer, B., Aronica, G. T., Bilibashi, A., Bonacci, O., & Borga, M. (2017). Changing climate shifts timing of European floods. *Science*, *357*(6351), 588–590. https://doi.org/10.1126/science.aan2506

Boano, F., Harvey, J. W., Marion, A., Packman, A. I., Revelli, R., Ridolfi, L., & Wörman, A. (2014). Hyporheic flow and transport processes: Mechanisms, models, and biogeochemical implications. *Reviews of Geophysics*, *52*(4), 603–679. https://doi.org/10.1002/2012RG000417

Bodelier, P. L. E., & Steenbergh, A. K. (2014). Interactions between methane and the nitrogen cycle in light of climate change. *Current Opinion in Environmental Sustainability*, *9*, 26–36. https://doi.org/10.1016/j.cosust.2014.07.004

Bodmer, P., Wilkinson, J., & Lorke, A. (2020). Sediment properties drive spatial variability of potential methane production and oxidation in small streams. *Journal of Geophysical Research: Biogeosciences*, *125*(1), e2019JG005213. https://doi.org/10.1029/2019JG005213

Boetius, A., Ravenschlag, K., Schubert, C. J., Rickert, D., Widdel, F., Gieseke, A., Amann, R., Jørgensen, B. B., Witte, U., & Pfannkuche, O. (2000). A marine microbial consortium apparently mediating anaerobic oxidation of methane. *Nature*, *407*(6804), 623–626. https://doi.org/10.1038/35036572

Boetius, A., & Wenzhöfer, F. (2009). In situ technologies for studying deep-sea hotspot ecosystems. *Oceanography*, *22*(1 Sp. Iss. Sp. Iss. SI), 177–177. https://doi.org/10013/epic.35367

Bogard, M. J., Del Giorgio, P. A., Boutet, L., Chaves, M. C. G., Prairie, Y. T., Merante, A., & Derry, A. M. (2014). Oxic water column methanogenesis as a major component of aquatic CH_4 fluxes. *Nature Communications*, *5*(1), 1–9. https://doi.org/10.1038/ncomms6350

Borges, A. V., Darchambeau, F., Teodoru, C. R., Marwick, T. R., Tamooh, F., Geeraert, N., Omengo, F. O., Guérin, F., Lambert, T., & Morana, C. (2015). Globally significant greenhouse-gas emissions from African inland waters. *Nature Geoscience*, *8*(8), 637–642. https://doi.org/10.1038/ngeo2486

Borrel, G., Parisot, N., Harris, H. M., Peyretaillade, E., Gaci, N., Tottey, W., Bardot, O., Raymann, K., Gribaldo, S., & Peyret, P. (2014). Comparative genomics highlights the unique biology of Methanomassiliicoccales, a Thermoplasmatales-related seventh order of methanogenic archaea that encodes pyrrolysine. *BMC Genomics*, *15*(1), 1–24. https://doi.org/10.1186/1471-2164-15-679

Borrelli, P., Robinson, D. A., Panagos, P., Lugato, E., Yang, J. E., Alewell, C., Wuepper, D., Montanarella, L., & Ballabio, C. (2020). Land use and climate change impacts on global soil erosion by water (2015-2070). *Proceedings of the National Academy of Sciences*, *117*(36), 21994–22001. https://doi.org/10.1073/pnas.2001403117

Boudreau, B. P. (1997). *Diagenetic models and their implementation* (Vol. 410). Springer, Berlin. https://doi.org/10.1007/978-3-642-60421-8

Boulton, A. J., Findlay, S., Marmonier, P., Stanley, E. H., & Valett, H. M. (1998). The functional significance of the hyporheic zone in streams and rivers. *Annual Review of Ecology and Systematics*, *29*(1), 59–81. https://doi.org/10.1146/annurev.ecolsys.29.1.59

Brandt, T., Vieweg, M., Laube, G., Schima, R., Goblirsch, T., Fleckenstein, J. H., & Schmidt, C. (2017). Automated in situ oxygen profiling at aquatic–terrestrial interfaces. *Environmental Science & Technology*, *51*(17), 9970–9978. https://doi.org/10.1021/acs.est.7b01482

Braun, A., Auerswald, K., & Geist, J. (2012). Drivers and spatio-temporal extent of hyporheic patch variation: Implications for sampling. *PLoS ONE*, *7*(7), 1–10. https://doi.org/10.1371/journal.pone.0042046

Briggs, M. A., Lautz, L. K., McKenzie, J. M., Gordon, R. P., & Hare, D. K. (2012). Using high-resolution distributed temperature sensing to quantify spatial and temporal variability in vertical hyporheic flux. *Water Resources Research*, *48*(2). https://doi.org/10.1029/2011WR011227

Brownlow, R., Lowry, D., Fisher, R., France, J., Lanoisellé, M., White, B., Wooster, M., Zhang, T., & Nisbet, E. (2017). Isotopic ratios of tropical methane emissions by atmospheric measurement. *Global Biogeochemical Cycles*, *31*(9), 1408–1419. https://doi.org/10.1002/2017GB005689

Cai, C., Leu, A. O., Xie, G.-J., Guo, J., Feng, Y., Zhao, J.-X., Tyson, G. W., Yuan, Z., & Hu, S. (2018). A methanotrophic archaeon couples anaerobic oxidation of methane to Fe(III) reduction. *The ISME Journal*, *12*(8), 1929–1939. https://doi.org/10.1038/s41396-018-0109-x

Campeau, A., & Del Giorgio, P. A. (2014). Patterns in CH_4 and CO_2 concentrations across boreal rivers: Major drivers and implications for fluvial greenhouse emissions under climate change scenarios. *Global Change Biology*, *20*(4), 1075–1088. https://doi.org/10.1111/gcb.12479

Canfield, D. E., & Thamdrup, B. (2009). Towards a consistent classification scheme for geochemical environments, or, why we wish the term 'suboxic' would go away. *Geobiology*, *7*(4), 385–392. https://doi.org/10.1111/j.1472-4669.2009.00214.x

Cao, Y., Li, J., Jiang, N., & Dong, X. (2014). Mechanism for stabilizing mRNAs involved in methanol-dependent methanogenesis of cold-adaptive methanosarcina mazei zm-15. *Applied and Environmental Microbiology*, *80*(4), 1291–1298. https://doi.org/http://doi.org/10.1128/AEM.03495-13

Capone, D. G., & Kiene, R. P. (1988). Comparison of microbial dynamics in marine and freshwater sediments: Contrasts in anaerobic carbon catabolism. *Limnology and Oceanography*, *33*(4part2), 725–749. https://doi.org/10.4319/lo.1988.33.4part2.0725

Carraway, E. R., Demas, J. N., DeGraff, B. A., & Bacon, J. R. (1991). Photophysics and photochemistry of oxygen sensors based on luminescent transition-metal complexes. *Analytical Chemistry*, *63*(4), 337–342. https://doi.org/10.1021/ac00004a007

Casagrande, D. J., Siefert, K., Berschinski, C., & Sutton, N. (1977). Sulfur in peat-forming systems of the Okefenokee Swamp and Florida Everglades: Origins of sulfur in coal. *Geochimica et Cosmochimica Acta*, *41*(1), 161–167. https://doi.org/10.1016/0016-7037(77)90196-X

Casas-Mulet, R., Pander, J., Prietzel, M., & Geist, J. (2021). The HydroEcoSedimentary tool: An integrated approach to characterise interstitial hydro-sedimentary and associated ecological processes. *River Research and Applications*, *37*(7), 988–1002. https://doi.org/10.1002/rra.3819

Case, R. J., Boucher, Y., Dahllöf, I., Holmström, C., Doolittle, W. F., & Kjelleberg, S. (2007). Use of 16S rRNA and rpoB genes as molecular markers for microbial ecology studies. *Applied and Environmental Microbiology*, *73*(1), 278–288. https://doi.org/10.1128/AEM.01177-06

Castro-Morales, K., Canning, A., Arzberger, S., Overholt, W. A., Küsel, K., Kolle, O., Göckede, M., Zimov, N., & Körtzinger, A. (2022). The highest methane concentrations in an arctic river are linked to local terrestrial inputs. *Biogeosciences*, 1–36. https://doi.org/10.5194/bg-19-5059-2022

Cavicchioli, R., Ripple, W. J., Timmis, K. N., Azam, F., Bakken, L. R., Baylis, M., Behrenfeld, M. J., Boetius, A., Boyd, P. W., & Classen, A. T. (2019). Scientists' warning to humanity: Microorganisms and climate change. *Nature Reviews Microbiology*, *17*(9), 569–586. https://doi.org/10.1038/s41579-019-0222-5

Cech, T. R. (2000). The ribosome is a ribozyme. *Science*, *289*(5481), 878–879. https://doi.org/10.1126/science.289.5481.878

Chanton, J. P., Martens, C. S., & Kelley, C. A. (1989). Gas transport from methane-saturated, tidal freshwater and wetland sediments. *Limnology and Oceanography*, *34*(5), 807–819. https://doi.org/10.4319/lo.1989.34.5.0807

Chanton, J. P., Powelson, D. K., Abichou, T., Fields, D., & Green, R. (2008). Effect of temperature and oxidation rate on carbon-isotope fractionation during methane oxidation by landfill cover materials. *Environmental Science & Technology*, *42*(21), 7818–7823. https://doi.org/10.1021/es801221y

Christensen, T. R., Ekberg, A., Ström, L., Mastepanov, M., Panikov, N., Öquist, M., Svensson, B. H., Nykänen, H., Martikainen, P. J., & Oskarsson, H. (2003). Factors controlling large scale variations in methane emissions from wetlands. *Geophysical Research Letters*, *30*(7). https://doi.org/10.1029/2002GL016848

Clark, I. D., & Fritz, P. (1997). *Environmental isotopes in hydrogeology*. CRC press.

Coenye, T., & Vandamme, P. (2003). Intragenomic heterogeneity between multiple 16S ribosomal RNA operons in sequenced bacterial genomes. *FEMS Microbiology Letters*, *228*(1), 45–49. https://doi.org/10.1016/S0378-1097(03)00717-1

Coleman, D. D., Risatti, J. B., & Schoell, M. (1981). Fractionation of carbon and hydrogen isotopes by methane-oxidizing bacteria. *Geochimica et Cosmochimica Acta*, *45*(7), 1033–1037. https://doi.org/10.1016/0016-7037(81)90129-0

Comer-Warner, S. A., Romeijn, P., Gooddy, D. C., Ullah, S., Kettridge, N., Marchant, B., Hannah, D. M., & Krause, S. (2018). Thermal sensitivity of CO_2 and CH_4 emissions varies with streambed sediment properties. *Nature Communications*, *9*(1), 1–9. https://doi.org/10.1038/s41467-018-04756-x

Conrad, R. (2005). Quantification of methanogenic pathways using stable carbon isotopic signatures: A review and a proposal. *Organic Geochemistry*, *36*(5), 739–752. https://doi.org/10.1016/j.orggeochem.2004.09.006

Conrad, R. (2009). The global methane cycle: Recent advances in understanding the microbial processes involved. *Environmental Microbiology Reports*, *1*(5), 285–292. https://doi.org/10.1111/j.1758-2229.2009.00038.x

Conrad, R. (2020). Importance of hydrogenotrophic, aceticlastic and methylotrophic methanogenesis for methane production in terrestrial, aquatic and other anoxic environments: A mini review. *Pedosphere*, *30*(1), 25–39. https://doi.org/10.1016/S1002-0160(18)60052-9

Constantz, J. (2008). Heat as a tracer to determine streambed water exchanges. *Water Resources Research*, *44*(4). https://doi.org/10.1029/2008WR006996

Coskun, Ö. K., Özen, V., Wankel, S. D., & Orsi, W. D. (2019). Quantifying population-specific growth in benthic bacterial communities under low oxygen using $H_2^{18}O$. *The ISME Journal*, *13*(6), 1546–1559. https://doi.org/10.1038/s41396-019-0373-4

Covino, T. (2017). Hydrologic connectivity as a framework for understanding biogeochemical flux through watersheds and along fluvial networks. *Geomorphology*, *277*, 133–144. https://doi.org/10.1016/j.geomorph.2016.09.030

Crowe, S., Katsev, S., Leslie, K., Sturm, A., Magen, C., Nomosatryo, S., Pack, M., Kessler, J., Reeburgh, W., & Roberts, J. (2011). The methane cycle in ferruginous Lake Matano. *Geobiology*, *9*(1), 61–78. https://doi.org/10.1111/j.1472-4669.2010.00257.x

Cui, M., Ma, A., Qi, H., Zhuang, X., & Zhuang, G. (2015). Anaerobic oxidation of methane: An "active" microbial process. *Microbiology Open*, *4*(1), 1–11. https://doi.org/10.1002/mbo3.232

Dalla Santa, G., Galgaro, A., Sassi, R., Cultrera, M., Scotton, P., Mueller, J., Bertermann, D., Mendrinos, D., Pasquali, R., & Perego, R. (2020). An updated ground thermal properties database for GSHP applications. *Geothermics*, *85*, 101758. https://doi.org/10.1016/j.geothermics.2019.101758

Danczak, R. E., Sawyer, A. H., Williams, K. H., Stegen, J. C., Hobson, C., & Wilkins, M. J. (2016). Seasonal hyporheic dynamics control coupled microbiology and geochemistry in Colorado River sediments. *Journal of Geophysical Research: Biogeosciences*, *121*(12), 2976–2987. https://doi.org/10.1002/2016JG003527

Dansgaard, W. (1964). Stable isotopes in precipitation. *Tellus*, *16*(4), 436–468. https://doi.org/10.1111/j.2153-3490.1964.tb00181.x

Dean, J. F., Middelburg, J. J., Röckmann, T., Aerts, R., Blauw, L. G., Egger, M., Jetten, M. S. M., de Jong, A. E. E., Meisel, O. H., & Rasigraf, O. (2018). Methane feedbacks to the global climate system in a warmer world. *Reviews of Geophysics*, *56*(1), 207–250. https://doi.org/10.1002/2017RG000559

Dedysh, S. N., & Knief, C. (2018). Diversity and phylogeny of described aerobic methanotrophs. In *Methane biocatalysis: Paving the way to sustainability* (pp. 17–42). Springer. https://doi.org/10.1007/978-3-319-74866-5_2

DelSontro, T., Del Giorgio, P. A., & Prairie, Y. T. (2018). No longer a paradox: The interaction between physical transport and biological processes explains the spatial distribution of surface water methane within and across lakes. *Ecosystems*, *21*, 1073–1087. https://doi.org/10.1007/s10021-017-0205-1

DelSontro, T., McGinnis, D. F., Sobek, S., Ostrovsky, I., & Wehrli, B. (2010). Extreme methane emissions from a Swiss hydropower reservoir: Contribution from bubbling sediments. *Environmental Science & Technology*, *44*(7), 2419–2425. https://doi.org/10.1021/es9031369

Denic, M., & Geist, J. (2015). Linking stream sediment deposition and aquatic habitat quality in pearl mussel streams: Implications for conservation. *River Research and Applications*, *31*(8), 943–952. https://doi.org/10.1002/rra.2794

Deppenmeier, U. (2002). The unique biochemistry of methanogenesis. *Progress in Nucleic Acid Research and Molecular Biology*, *71*, 223–283. https://doi.org/10.1016/S0079-6603(02)71045-3

Deutzmann, J. S. (2020). Anaerobic methane oxidation in freshwater environments. *Anaerobic Utilization of Hydrocarbons, Oils, and Lipids*, 391–404. https://doi.org/10.1007/978-3-319-50391-2_21

Deutzmann, J. S., Stief, P., Brandes, J., & Schink, B. (2014). Anaerobic methane oxidation coupled to denitrification is the dominant methane sink in a deep lake. *Proceedings of the National Academy of Sciences*, *111*(51), 18273–18278. https://doi.org/10.1073/pnas.1411617111

Devereux, R., & Wilkinson, S. S. (2004). Amplification of ribosomal RNA sequences. In G. A. Kowalchuk, F. J. de Bruijn, I. M. Head, A. D. L. Akkermans, & J. D. van Elsas (Eds.), *Molecular microbial ecology manual* (2nd Edition, pp. 509–521, Vol. 1). Kluwer Academic Publishers. https://doi.org/10.1007/978-1-4020-2177-0

Dokulil, M. T., & Teubner, K. (2010). Eutrophication and climate change: Present situation and future scenarios. In A. Ansari, S. Singh Gill, G. Lanza, & W. Rast (Eds.), *Eutrophication: Causes, consequences and control* (pp. 1–16). Springer. https://doi.org/10.1007/978-90-481-9625-8_1

Dridi, B., Fardeau, M.-L., Ollivier, B., Raoult, D., & Drancourt, M. (2012). Methanomassiliicoccus luminyensis gen. nov., sp. nov., a methanogenic archaeon isolated from human faeces. *International Journal of Systematic and Evolutionary Microbiology*, *62*(8), 1902–1907. https://doi.org/10.1099/ijs.0.033712-0

Duff, J. H., Murphy, F., Fuller, C. C., Triska, F. J., Harvey, J. W., & Jackman, A. P. (1998). A mini drivepoint sampler for measuring pore water solute concentrations in the hyporheic zone of sand-bottom streams. *Limnology and Oceanography*, *43*(6), 1378–1383. https://doi.org/10.4319/lo.1998.43.6.1378

DWD. (2023). Deutscher Wetterdienst [https://opendata.dwd.de/climate_environment/; Accessed: 2023-06-13].

Edgar, R. C. (2013). UPARSE: highly accurate OTU sequences from microbial amplicon reads. *Nature Methods*, *10*(10), 996–998. https://doi.org/10.1038/nmeth.2604

Egger, M., Rasigraf, O., Sapart, C. J., Jilbert, T., Jetten, M. S. M., Röckmann, T., Van der Veen, C., Banda, N., Kartal, B., & Ettwig, K. F. (2015). Iron-mediated anaerobic oxidation of methane in brackish coastal sediments. *Environmental Science & Technology*, *49*(1), 277–283. https://doi.org/10.1021/es503663z

Einsiedl, F., Wunderlich, A., Sebilo, M., Coskun, Ö. K., Orsi, W. D., & Mayer, B. (2020). Biogeochemical evidence of anaerobic methane oxidation and anaerobic ammonium oxidation in a stratified lake using stable isotopes. *Biogeosciences*, *17*(20), 5149–5161. https://doi.org/10.5194/bg-17-5149-2020

Eller, G., Känel, L., & Krüger, M. (2005). Cooccurrence of aerobic and anaerobic methane oxidation in the water column of Lake Plußsee. *Applied and Environmental Microbiology*, *71*(12), 8925–8928. https://doi.org/10.1128/AEM.71.12.89258928.2005

Elsner, M. (2010). Stable isotope fractionation to investigate natural transformation mechanisms of organic contaminants: Principles, prospects and limitations. *Journal of Environmental Monitoring*, *12*(11), 2005–2031. https://doi.org/10.1039/C0EM00277A

Emerson, S., Jahnke, R., Bender, M., Froelich, P., Klinkhammer, G., Bowser, C., & Setlock, G. (1980). Early diagenesis in sediments from the eastern equatorial Pacific, I. Pore water nutrient and carbonate results. *Earth and Planetary Science Letters*, *49*(1), 57–80. https://doi.org/10.1016/0012-821X(80)90150-8

EPA, U. (2001). *Technical guidance for the natural attenuation indicators: Methane, ethane, and ethene* (Report).

Ettwig, K. F., Butler, M. K., Le Paslier, D., Pelletier, E., Mangenot, S., Kuypers, M. M., Schreiber, F., Dutilh, B. E., Zedelius, J., & de Beer, D. (2010). Nitrite-driven anaerobic methane oxidation by oxygenic bacteria. *Nature*, *464*(7288), 543–548. https://doi.org/10.1038/nature08883

Ettwig, K. F., Zhu, B., Speth, D., Keltjens, J. T., Jetten, M. S., & Kartal, B. (2016). Archaea catalyze iron-dependent anaerobic oxidation of methane. *Proceedings of the National Academy of Sciences*, *113*(45), 12792–12796. https://doi.org/10.1073/pnas.1609534113

European Commission and United States of America. (2021). *Global Methane Pledge* (Report). Climate and Clean Air Coalition.

Feisthauer, S., Vogt, C., Modrzynski, J., Szlenkier, M., Krüger, M., Siegert, M., & Richnow, H.-H. (2011). Different types of methane monooxygenases produce similar carbon and hydrogen isotope fractionation patterns during methane oxidation. *Geochimica et Cosmochimica Acta*, *75*(5), 1173–1184. https://doi.org/10.1016/j.gca.2010.12.006

Ferry, J. G. (2010). How to make a living by exhaling methane. *Annual Review of Microbiology*, *64*, 453–473. https://doi.org/10.1146/annurev.micro.112408.134051

Findlay, S. (1995). Importance of surface-subsurface exchange in stream ecosystems: The hyporheic zone. *Limnology and Oceanography*, *40*(1), 159–164. https://doi.org/10.4319/lo.1995.40.1.0159

Fischer, H., Kloep, F., Wilzcek, S., & Pusch, M. T. (2005). A river's liver – microbial processes within the hyporheic zone of a large lowland river. *Biogeochemistry*, *76*(2), 349–371. https://doi.org/10.1007/s10533-005-6896-y

Fowler, D., Coyle, M., Skiba, U., Sutton, M. A., Cape, J. N., Reis, S., Sheppard, L. J., Jenkins, A., Grizzetti, B., & Galloway, J. N. (2013). The global nitrogen cycle in the twenty-first century. *Philosophical Transactions of the Royal Society B: Biological Sciences*, *368*(1621), 20130164. https://doi.org/10.1098/rstb.2013.0164

Fu, L., Li, S.-W., Ding, Z.-W., Ding, J., Lu, Y.-Z., & Zeng, R. J. (2016). Iron reduction in the DAMO/Shewanella oneidensis MR-1 coculture system and the fate of Fe(II). *Water Research*, *88*, 808–815. https://doi.org/10.1016/j.watres.2015.11.011

Galloway, J. N., Townsend, A. R., Erisman, J. W., Bekunda, M., Cai, Z., Freney, J. R., Martinelli, L. A., Seitzinger, S. P., & Sutton, M. A. (2008). Transformation of the nitrogen cycle: Recent trends, questions, and potential solutions. *Science*, *320*(5878), 889–892. https://doi.org/10.1126/science.1136674

Geist, J., & Auerswald, K. (2007). Physicochemical stream bed characteristics and recruitment of the freshwater pearl mussel (Margaritifera margaritifera). *Freshwater Biology*, *52*(12), 2299–2316. https://doi.org/10.1111/j.1365-2427.2007.01812.x

Gordon, R. P., Lautz, L. K., Briggs, M. A., & McKenzie, J. M. (2012). Automated calculation of vertical pore-water flux from field temperature time series using the VFLUX method and computer program. *Journal of Hydrology*, *420*, 142–158. https://doi.org/10.1016/j.jhydrol.2011.11.053

Graf, J. S., Mayr, M. J., Marchant, H. K., Tienken, D., Hach, P. F., Brand, A., Schubert, C. J., Kuypers, M. M., & Milucka, J. (2018). Bloom of a denitrifying methanotroph, 'Candidatus Methylomirabilis limnetica', in a deep stratified lake. *Environmental Microbiology*, *20*(7), 2598–2614. https://doi.org/10.1111/1462-2920.14285

Greinert, J., & McGinnis, D. F. (2009). Single bubble dissolution model: The graphical user interface SiBu-GUI. *Environmental Modelling & Software*, *24*(8), 1012–1013. https://doi.org/10.1016/j.envsoft.2008.12.011

Grill, G., Lehner, B., Thieme, M., Geenen, B., Tickner, D., Antonelli, F., Babu, S., Borrelli, P., Cheng, L., & Crochetiere, H. (2019). Mapping the world's free-flowing rivers. *Nature*, *569*(7755), 215–221. https://doi.org/10.1038/s41586-019-1111-9

Grossart, H.-P., Frindte, K., Dziallas, C., Eckert, W., & Tang, K. W. (2011). Microbial methane production in oxygenated water column of an oligotrophic lake. *Proceedings of the National Academy of Sciences*, *108*(49), 19657–19661. https://doi.org/10.1073/pnas.1110716108

Günthel, M., Donis, D., Kirillin, G., Ionescu, D., Bizic, M., McGinnis, D. F., Grossart, H.-P., & Tang, K. W. (2019). Contribution of oxic methane production to surface methane emission in lakes and its global importance. *Nature Communications*, *10*(1), 5497. https://doi.org/10.1038/s41467-019-13320-0

Hakemian, A. S., & Rosenzweig, A. C. (2007). The biochemistry of methane oxidation. *Annual Review of Biochemistry*, *76*, 223–241. https://doi.org/10.1146/annurev.biochem.76.061505.175355

Hancock, P. J. (2002). Human impacts on the stream–groundwater exchange zone. *Environmental Management*, *29*(6), 763–781. https://doi.org/10.1007/s00267-001-0064-5

Hancock, P. J., Boulton, A. J., & Humphreys, W. F. (2005). Aquifers and hyporheic zones: Towards an ecological understanding of groundwater. *Hydrogeology Journal*, *13*(1), 98–111. https://doi.org/10.1007/s10040-004-0421-6

Hanson, R. S., & Hanson, T. E. (1996). Methanotrophic bacteria. *Microbiological Reviews*, *60*(2), 439–471. https://doi.org/10.1128/mr.60.2.439-471.1996

Happell, J. D., Chanton, J. P., & Showers, W. S. (1994). The influence of methane oxidation on the stable isotopic composition of methane emitted from Florida swamp forests. *Geochimica et Cosmochimica Acta*, *58*(20), 4377–4388. https://doi.org/10.1016/0016-7037(94)90341-7

Haroon, M. F., Hu, S., Shi, Y., Imelfort, M., Keller, J., Hugenholtz, P., Yuan, Z., & Tyson, G. W. (2013). Anaerobic oxidation of methane coupled to nitrate reduction in a novel archaeal lineage. *Nature*, *500*(7464), 567–570. https://doi.org/10.1038/nature12375

Hatch, C. E., Fisher, A. T., Revenaugh, J. S., Constantz, J., & Ruehl, C. (2006). Quantifying surface water–groundwater interactions using time series analysis of streambed thermal records: Method development. *Water Resources Research*, *42*(10). https://doi.org/10.1029/2005WR004787

He, Z., Cai, C., Wang, J., Xu, X., Zheng, P., Jetten, M. S., & Hu, B. (2016). A novel denitrifying methanotroph of the NC10 phylum and its microcolony. *Scientific Reports*, *6*(1), 1–10. https://doi.org/10.1038/s41598-016-0001-8

He, Z., Zhang, Q., Feng, Y., Luo, H., Pan, X., & Gadd, G. M. (2018). Microbiological and environmental significance of metal-dependent anaerobic oxidation of methane. *Science of the Total Environment*, *610*, 759–768. https://doi.org/10.1016/j.scitotenv.2017.08.140

Hendricks, S. P. (1993). Microbial ecology of the hyporheic zone: A perspective integrating hydrology and biology. *Journal of the North American Benthological Society*, *12*(1), 70–78. https://doi.org/10.2307/1467687

Hesslein, R. H. (1976). An in situ sampler for close interval pore water studies. *Limnology and Oceanography*, *21*(6), 912–914. https://doi.org/10.4319/lo.1976.21.6.0912

Holmer, M., & Storkholm, P. (2001). Sulphate reduction and sulphur cycling in lake sediments: A review. *Freshwater Biology*, *46*(4), 431–451. https://doi.org/10.1046/j.1365-2427.2001.00687.x

Hu, B.-l., Shen, L.-d., Lian, X., Zhu, Q., Liu, S., Huang, Q., He, Z.-f., Geng, S., Cheng, D.-q., Lou, L.-p., Xu, X.-y., Zheng, P., & He, Y.-f. (2014). Evidence for nitrite-dependent anaerobic methane oxidation as a previously overlooked microbial methane sink in wetlands. *Proceedings of the National Academy of Sciences*, *111*(12), 4495–4500. https://doi.org/10.1073/pnas.1318393111

Illumina. (2023). Illumina sequencing platforms [https://www.illumina.com/systems/sequencing-platforms.html; Accessed: 2023-10-15].

Imig, A., Shajari, F., Augustin, L., Einsiedl, F., & Rein, A. (2023). Improved lumped-parameter and numerical modeling of unsaturated water flow and stable water isotopes. *Groundwater*, *61*(3), 389–401. https://doi.org/10.1111/gwat.13244

IPCC. (2013). *Climate Change 2013: The physical science basis. Working Group I Contribution to the Fifth Assessment Report of the Intergovernmental Panel on Climate Change* (T. F. Stocker, D. Qin, G.-K. Plattner, M. M. Tignor, S. K. Allen, J. Boschung, A. Nauels, Y. Xia, V. Bex, & P. M. Midgley, Eds.; Report). Intergovernmental Panel of Climate Change. Cambridge, United Kingdom, New York, NY, USA, Cambridge University Press.

IPCC. (2021). *Climate Change 2021: The physical science basis. Working Group I Contribution to the Sixth Assessment Report of the Intergovernmental Panel on Climate Change* (V. Masson-Delmotte, P. Zhai, A. Pirani, S. L. Connors, C. Péan, S. Berger, N. Caud, Y. Chen, L. Goldfarb, M. I. Gomis, M. Huang, K. Leitzell, E. Lonnoy, J. R. Matthews, T. K. Maycock, T. Waterfield, O. Yelekçi, R. Yu, & B. Zhou, Eds.; Report). Intergovernmental Panel of Climate Change. Cambridge, United Kingdom, New York, NY, USA, Cambridge University Press. https://doi.org/10.1017/9781009157896

Iversen, N., & Jørgensen, B. B. (1993). Diffusion coefficients of sulfate and methane in marine sediments: Influence of porosity. *Geochimica et Cosmochimica Acta*, *57*(3), 571–578. https://doi.org/10.1016/0016-7037(93)90368-7

Jahnke, R. A. (1988). A simple, reliable, and inexpensive pore-water sampler. *Limnology and Oceanography*, *33*(3), 483–487. https://doi.org/10.4319/lo.1988.33.3.0483

Jansson, J. K., & Leser, T. (2004). Quantitative PCR of environmental samples. In G. A. Kowalchuk, F. J. de Bruijn, I. M. Head, A. D. L. Akkermans, & J. D. van Elsas (Eds.), *Molecular microbial ecology manual* (2nd Edition, pp. 445–463, Vol. 1). Kluwer Academic Publishers. https://doi.org/10.1007/978-1-4020-2177-0

Jia, J., Li, J., Qi, L., Li, L., Yue, L., & Dong, X. (2021). Post-transcriptional regulation is involved in the cold-active methanol-based methanogenic pathway of a psychrophilic methanogen. *Environmental Microbiology*, *23*(7), 3773–3788. https://doi.org/10.1111/1462-2920.15420

Johnson, J. S., Spakowicz, D. J., Hong, B.-Y., Petersen, L. M., Demkowicz, P., Chen, L., Leopold, S. R., Hanson, B. M., Agresta, H. O., & Gerstein, M. (2019). Evaluation of 16S rRNA gene sequencing for species and strain-level microbiome analysis. *Nature Communications*, *10*(1), 5029. https://doi.org/10.1038/s41467-019-13036-1

Jørgensen, B. B., Böttcher, M. E., Lüschen, H., Neretin, L. N., & Volkov, I. I. (2004). Anaerobic methane oxidation and a deep H_2S sink generate isotopically heavy sulfides in Black Sea sediments. *Geochimica et Cosmochimica Acta*, *68*(9), 2095–2118. https://doi.org/10.1016/j.gca.2003.07.017

Jørgensen, B. B., Weber, A., & Zopfi, J. (2001). Sulfate reduction and anaerobic methane oxidation in black sea sediments. *Deep Sea Research Part I: Oceanographic Research Papers*, *48*(9), 2097–2120. https://doi.org/10.1016/S0967-0637(01)00007-3

Kadlec, R. H., & Reddy, K. (2001). Temperature effects in treatment wetlands. *Water Environment Research*, *73*(5), 543–557. https://doi.org/10.2175/106143001X139614

Kampbell, D. H., & Vandegrift, S. A. (1998). Analysis of dissolved methane, ethane, and ethylene in groundwater by a standard gas chromatographic technique. *Journal of Chromatographic Science*, *36*(5), 253–256. https://doi.org/10.1093/chromsci/36.5.253

Keery, J., Binley, A., Crook, N., & Smith, J. W. (2007). Temporal and spatial variability of groundwater–surface water fluxes: Development and application of an analytical method using temperature time series. *Journal of Hydrology*, *336*(1-2), 1–16. https://doi.org/10.1016/j.jhydrol.2006.12.003

Kendall, C., & Caldwell, E. A. (1998). Fundamentals of isotope geochemistry. In *Isotope tracers in catchment hydrology* (pp. 51–86). Elsevier. https://doi.org/10.1016/B978-0-444-81546-0.50009-4

Kestin, J., Sokolov, M., & Wakeham, W. A. (1978). Viscosity of liquid water in the range -8℃ to 150℃. *Journal of Physical and Chemical Reference Data*, *7*(3), 941–948. https://doi.org/10.1063/1.555581

Kim, H., Bae, H.-S., Reddy, K. R., & Ogram, A. (2016). Distributions, abundances and activities of microbes associated with the nitrogen cycle in riparian and stream sediments of a river tributary. *Water Research*, *106*, 51–61. https://doi.org/10.1016/j.watres.2016.09.048

Kinnaman, F. S., Valentine, D. L., & Tyler, S. C. (2007). Carbon and hydrogen isotope fractionation associated with the aerobic microbial oxidation of methane, ethane, propane and butane. *Geochimica et Cosmochimica Acta*, *71*(2), 271–283. https://doi.org/10.1016/j.gca.2006.09.007

Kirschke, S., Bousquet, P., Ciais, P., Saunois, M., Canadell, J. G., Dlugokencky, E. J., Bergamaschi, P., Bergmann, D., Blake, D. R., & Bruhwiler, L. (2013). Three decades of global methane sources and sinks. *Nature Geoscience*, *6*(10), 813–823. https://doi.org/10.1038/ngeo1955

Kits, K. D., Klotz, M. G., & Stein, L. Y. (2015). Methane oxidation coupled to nitrate reduction under hypoxia by the Gammaproteobacterium Methylomonas denitrificans, sp. nov. type strain FJG1. *Environmental Microbiology*, *17*(9), 3219–3232. https://doi.org/10.1111/1462-2920.12772

Knapp, J. L., González-Pinzón, R., Drummond, J. D., Larsen, L. G., Cirpka, O. A., & Harvey, J. W. (2017). Tracer-based characterization of hyporheic exchange and benthic biolayers in streams. *Water Resources Research*, *53*(2), 1575–1594. https://doi.org/10.1002/2016WR019393

Koeniger, P., Gaj, M., Beyer, M., & Himmelsbach, T. (2016). Review on soil water isotope-based groundwater recharge estimations. *Hydrological Processes*, *30*(16), 2817–2834. https://doi.org/10.1002/hyp.10775

Kohler, A., Zeller, M., & Zeltner, G. (1987). Veränderungen von Flora und Vegetation im Fließgewässersystem der Moosach (Münchener Ebene) 1970-1985. *Berichte der Bayerischen Botanischen Gesellschaft zur Erforschung der Flora*, *58*, 115–137.

Komura, S., & Colby, B. R. (1963). Sediment transportation mechanics: Introduction and properties of sediment. *Journal of the Hydraulics Division*, *89*(1), 263–268. https://doi.org/10.1061/JYCEAJ.0000768

Koschorreck, M., Kamjunke, N., Koedel, U., Rode, M., Schuetze, C., & Bussmann, I. (2023). Diurnal versus spatial variability of greenhouse gas emissions from an anthropogenic modified german lowland river. *Biogeosciences Discussions*, *2023*, 1–22. https://doi.org/10.5194/bg-2023-176

Krause, S., Blume, T., & Cassidy, N. (2012). Investigating patterns and controls of groundwater up-welling in a lowland river by combining fibre-optic distributed temperature sensing with observations of vertical hydraulic gradients. *Hydrology and Earth System Sciences*, *16*(6), 1775–1792. https://doi.org/10.5194/hess-16-1775-2012

Krause, S., Hannah, D. M., Fleckenstein, J., Heppell, C., Kaeser, D., Pickup, R., Pinay, G., Robertson, A. L., & Wood, P. J. (2011). Inter-disciplinary perspectives on processes in the hyporheic zone. *Ecohydrology*, *4*(4), 481–499. https://doi.org/10.1002/eco.176

Krzycki, J., Kenealy, W., DeNiro, M., & Zeikus, J. (1987). Stable carbon isotope fractionation by Methanosarcina barkeri during methanogenesis from acetate, methanol, or carbon dioxide-hydrogen. *Applied and Environmental Microbiology*, *53*(10), 2597–2599. https://doi.org/10.1128/aem.53.10.2597-2599.1987

Ladd, J., & Jackson, R. (1982). Biochemistry of ammonification. *Nitrogen in Agricultural Soils*, *22*, 173–228. https://doi.org/10.2134/agronmonogr22.c5

Langenegger, T., Vachon, D., Donis, D., & McGinnis, D. (2019). What the bubble knows: Lake methane dynamics revealed by sediment gas bubble composition. *Limnology and Oceanography*, *64*(4), 1526–1544. https://doi.org/10.1002/lno.11133

Lewandowski, J., Arnon, S., Banks, E., Batelaan, O., Betterle, A., Broecker, T., Coll, C., Drummond, J. D., Gaona Garcia, J., & Galloway, J. (2019). Is the hyporheic zone relevant beyond the scientific community? *Water*, *11*(11), 2230. https://doi.org/10.3390/w11112230

Li, M., & He, N. (2022). Carbon intensity of global existing and future hydropower reservoirs. *Renewable and Sustainable Energy Reviews*, *162*, 112433. https://doi.org/10.1016/j.rser.2022.112433

Li, W., Lu, S., Li, J., Feng, W., Zhang, P., Wang, J., Wang, Z., & Li, X. (2022). Concentration loss and diffusive fractionation of methane during storage: Implications for gas sampling and isotopic analysis. *Journal of Natural Gas Science and Engineering*, *101*, 104562. https://doi.org/10.1016/j.jngse.2022.104562

Li, Y., Shang, J., Zhang, C., Zhang, W., Niu, L., Wang, L., & Zhang, H. (2021). The role of freshwater eutrophication in greenhouse gas emissions: A review. *Science of the Total Environment*, *768*, 144582. https://doi.org/10.1016/j.scitotenv.2020.144582

Linkhorst, A., Hiller, C., DelSontro, T., M. Azevedo, G., Barros, N., Mendonça, R., & Sobek, S. (2020). Comparing methane ebullition variability across space and time in a Brazilian reservoir. *Limnology and Oceanography*, *65*(7), 1623–1634. https://doi.org/10.1002/lno.11410

Linkhorst, A., Paranaíba, J. R., Mendonça, R., Rudberg, D., DelSontro, T., Barros, N., & Sobek, S. (2021). Spatially resolved measurements in tropical reservoirs reveal elevated methane ebullition at river inflows and at high productivity. *Global Biogeochemical Cycles*, *35*(5), e2020GB006717. https://doi.org/10.1029/2020GB006717

Liu, H., Wang, J., Wang, A., & Chen, J. (2011). Chemical inhibitors of methanogenesis and putative applications. *Applied Microbiology and Biotechnology*, *89*(5), 1333–1340. https://doi.org/10.1007/s00253-010-3066-5

Liu, L., De Kock, T., Wilkinson, J., Cnudde, V., Xiao, S., Buchmann, C., Uteau, D., Peth, S., & Lorke, A. (2018). Methane bubble growth and migration in aquatic sediments observed by X-ray µCT. *Environmental Science & Technology*, *52*(4), 2007–2015. https://doi.org/10.1021/acs.est.7b06061

Lubetkin, S. (2003). Why is it much easier to nucleate gas bubbles than theory predicts? *Langmuir*, *19*(7), 2575–2587. https://doi.org/10.1021/la0266381

Luesken, F. A., Wu, M. L., Op den Camp, H. J., Keltjens, J. T., Stunnenberg, H., Francoijs, K.-J., Strous, M., & Jetten, M. S. (2012). Effect of oxygen on the anaerobic methanotroph 'Candidatus Methylomirabilis oxyfera': Kinetic and transcriptional analysis. *Environmental Microbiology*, *14*(4), 1024–1034. https://doi.org/10.1111/j.1462-2920.2011.02682.x

Lyu, Z., Shao, N., Akinyemi, T., & Whitman, W. B. (2018). Methanogenesis. *Current Biology*, *28*(13), R727–R732. https://doi.org/10.1016/j.cub.2018.05.021

Mach, V., Blaser, M. B., Claus, P., Chaudhary, P. P., & Rulík, M. (2015). Methane production potentials, pathways, and communities of methanogens in vertical sediment profiles of river Sitka. *Frontiers in Microbiology*, *6*, 506. https://doi.org/10.3389/fmicb.2015.00506

Maeck, A., DelSontro, T., McGinnis, D. F., Fischer, H., Flury, S., Schmidt, M., Fietzek, P., & Lorke, A. (2013). Sediment trapping by dams creates methane emission hot spots. *Environmental Science & Technology*, *47*(15), 8130–8137. https://doi.org/10.1021/es4003907

Maeck, A., Hofmann, H., & Lorke, A. (2014). Pumping methane out of aquatic sediments: Ebullition forcing mechanisms in an impounded river. *Biogeosciences*, *11*(11), 2925–2938. https://doi.org/10.5194/bg-11-2925-2014

Malcolm, I., Soulsby, C., Youngson, A., & Hannah, D. (2005). Catchment-scale controls on groundwater–surface water interactions in the hyporheic zone: Implications for salmon embryo survival. *River Research and Applications*, *21*(9), 977–989. https://doi.org/10.1002/rra.861

Martin, W., & Banta, G. (1992). The measurement of sediment irrigation rates: A comparison of the Br^- tracer and $^{222}Rn/^{226}Ra$ disequilibrium techniques. *Journal of Marine Research*, *50*(1), 125–154. https://doi.org/10.1357/002224092784797737

Martin, W., & Sayles, F. (1987). Seasonal cycles of particle and solute transport processes in nearshore sediments: $^{222}Rn^{226}Ra$ and $^{234}Th^{238}U$ disequilibrium at a site in buzzards bay, MA. *Geochimica et Cosmochimica Acta*, *51*(4), 927–943. https://doi.org/10.1016/0016-7037(87)90106-2

Marzadri, A., Tonina, D., & Bellin, A. (2012). Morphodynamic controls on redox conditions and on nitrogen dynamics within the hyporheic zone: Application to gravel bed rivers with alternate-bar morphology. *Journal of Geophysical Research: Biogeosciences*, *117*(G3). https://doi.org/10.1029/2012JG001966

Mattson, M. D., & Likens, G. E. (1990). Air pressure and methane fluxes. *Nature*, *347*(6295), 718–719. https://doi.org/10.1038/347718b0

McGinnis, D. F., Bilsley, N., Schmidt, M., Fietzek, P., Bodmer, P., Premke, K., Lorke, A., & Flury, S. (2016). Deconstructing methane emissions from a small Northern European river: Hydrodynamics and temperature as key drivers. *Environmental Science & Technology*, *50*(21), 11680–11687. https://doi.org/10.1021/acs.est.6b03268

Michaelis, T., Wunderlich, A., Baumann, T., Geist, J., & Einsiedl, F. (2023). Technical note: Testing the effect of different pumping rates on pore-water sampling for ions, stable isotopes, and gas concentrations in the hyporheic zone. *Hydrology and Earth System Sciences*, *27*(20), 3769–3782. https://doi.org/10.5194/hess-27-3769-2023

Michaelis, T., Wunderlich, A., Coskun, Ö. K., Orsi, W., Baumann, T., & Einsiedl, F. (2022). High-resolution vertical biogeochemical profiles in the hyporheic zone reveal insights into microbial methane cycling. *Biogeosciences*, *19*(18), 4551–4569. https://doi.org/10.5194/bg-19-4551-2022

Michaelis, T., Kaplar, F., Baumann, T., Wunderlich, A., & Einsiedl, F. (2024). High methane ebullition throughout one year in a regulated central European stream. *Scientific Reports*, *14*(1), 5359. https://doi.org/10.1038/s41598-024-54760-z

Miller, B. L., Arntzen, E. V., Goldman, A. E., & Richmond, M. C. (2017). Methane ebullition in temperate hydropower reservoirs and implications for US policy on greenhouse gas emissions. *Environmental Management*, *60*(4), 615–629. https://doi.org/10.1007/s00267-017-0909-1

Murray, C. J., Müller-Karulis, B., Carstensen, J., Conley, D. J., Gustafsson, B. G., & Andersen, J. H. (2019). Past, present and future eutrophication status of the baltic sea. *Frontiers in Marine Science*, *6*, 2. https://doi.org/10.3389/fmars.2019.00002

Nagler, M., Praeg, N., Niedrist, G. H., Attermeyer, K., Catalán, N., Pilotto, F., Gutmann Roberts, C., Bors, C., Fenoglio, S., & Colls, M. (2021). Abundance and biogeography of methanogenic and methanotrophic microorganisms across European streams. *Journal of Biogeography*, *48*(4), 947–960. https://doi.org/10.1111/jbi.14052

Naqvi, S. W. A., Lam, P., Narvenkar, G., Sarkar, A., Naik, H., Pratihary, A., Shenoy, D. M., Gauns, M., Kurian, S., & Damare, S. (2018). Methane stimulates massive nitrogen loss from freshwater reservoirs in India. *Nature Communications*, *9*(1), 1–10. https://doi.org/10.1038/s41467-018-03607-z

Narrowe, A. B., Borton, M. A., Hoyt, D. W., Smith, G. J., Daly, R. A., Angle, J. C., Eder, E. K., Wong, A. R., Wolfe, R. A., & Pappas, A. (2019). Uncovering the diversity and activity of methylotrophic methanogens in freshwater wetland soils. *Msystems*, *4*(6), e00320–19. https://doi.org/10.1128/mSystems.00320-19

Natchimuthu, S., Sundgren, I., Gålfalk, M., Klemedtsson, L., Crill, P., Danielsson, Å., & Bastviken, D. (2016). Spatio-temporal variability of lake CH_4 fluxes and its influence on annual whole lake emission estimates. *Limnology and Oceanography*, *61*(S1), S13–S26. https://doi.org/10.1002/lno.10222

Nazaries, L., Murrell, J. C., Millard, P., Baggs, L., & Singh, B. K. (2013). Methane, microbes and models: Fundamental understanding of the soil methane cycle for future predictions. *Environmental Microbiology*, *15*(9), 2395–2417. https://doi.org/10.1111/1462-2920.12149

Ng, G.-H. C., Rosenfeld, C. E., Santelli, C. M., Yourd, A. R., Lange, J., Duhn, K., & Johnson, N. W. (2020). Microbial and reactive transport modeling evidence for hyporheic flux-driven cryptic sulfur cycling and anaerobic methane oxidation in a sulfate-impacted wetland-stream system. *Journal of Geophysical Research: Biogeosciences*, *125*(2). https://doi.org/10.1029/2019JG005185

Nisbet, E. G., Dlugokencky, E. J., & Bousquet, P. (2014). Methane on the rise — again. *Science*, *343*(6170), 493–495. https://doi.org/10.1126/science.1247828

Nisbet, E. G., Manning, M., Dlugokencky, E., Fisher, R., Lowry, D., Michel, S., Myhre, C. L., Platt, S. M., Allen, G., & Bousquet, P. (2019). Very strong atmospheric methane growth in the 4 years 2014–2017: Implications for the Paris Agreement. *Global Biogeochemical Cycles*, *33*(3), 318–342. https://doi.org/10.1029/2018GB006009

NOAA. (2023). Global monitoring laboratory [https://www.gml.noaa.gov/; Accessed: 2023-06-13].

Norði, K. á., & Thamdrup, B. (2014). Nitrate-dependent anaerobic methane oxidation in a freshwater sediment. *Geochimica et Cosmochimica Acta*, *132*, 141–150. https://doi.org/10.1016/j.gca.2014.01.032

Norði, K. á., Thamdrup, B., & Schubert, C. J. (2013). Anaerobic oxidation of methane in an iron-rich Danish freshwater lake sediment. *Limnology and Oceanography*, *58*(2), 546–554. https://doi.org/10.4319/lo.2013.58.2.0546

Offre, P., Spang, A., & Schleper, C. (2013). Archaea in biogeochemical cycles. *Annual Review of Microbiology*, *67*, 437–457. https://doi.org/10.1146/annurev-micro-092412-155614

Op den Camp, H. J., Islam, T., Stott, M. B., Harhangi, H. R., Hynes, A., Schouten, S., Jetten, M. S., Birkeland, N.-K., Pol, A., & Dunfield, P. F. (2009). Environmental, genomic and taxonomic perspectives on methanotrophic Verrucomicrobia. *Environmental Microbiology Reports*, *1*(5), 293–306. https://doi.org/10.1111/j.1758-2229.2009.00022.x

Oswald, K., Graf, J. S., Littmann, S., Tienken, D., Brand, A., Wehrli, B., Albertsen, M., Daims, H., Wagner, M., & Kuypers, M. M. (2017). Crenothrix are major methane consumers in stratified lakes. *The ISME journal*, *11*(9), 2124–2140. https://doi.org/10.1038/ismej.2017.77

Parkhurst, D. L., & Appelo, C. (2013). Description of input and examples for PHREEQC version 3: A computer program for speciation, batch-reaction, one-dimensional transport, and inverse geochemical calculations. *US Geological Survey Techniques and Methods*, *6*(A43), 497.

Paul, K., Nonoh, J. O., Mikulski, L., & Brune, A. (2012). "Methanoplasmatales," Thermoplasmatales-related archaea in termite guts and other environments, are the seventh order of methanogens. *Applied and Environmental Microbiology*, *78*(23), 8245–8253. https://doi.org/10.1128/AEM.02193-12

Peeters, F., & Hofmann, H. (2021). Oxic methanogenesis is only a minor source of lake-wide diffusive CH_4 emissions from lakes. *Nature Communications*, *12*(1), 1206. https://doi.org/10.1038/s41467-019-13320-0

Peña Sanchez, A., Duffner, C., Wunderlich, A., Mayer, B., Schulz, S., Schloter, M., & Einsiedl, F. (2022a). Seasonal dynamics of anaerobic oxidation of ammonium and denitrification in a dimictic lake during the stratified spring–summer period. *Limnology and Oceanography*, *67*(5), 1194–1210. https://doi.org/10.1002/lno.12067

Peña Sanchez, A., Mayer, B., Wunderlich, A., Rein, A., & Einsiedl, F. (2022b). Analysing seasonal variations of methane oxidation processes coupled with denitrification in a stratified lake using stable isotopes and numerical modeling. *Geochimica et Cosmochimica Acta*, *323*, 242–257. https://doi.org/10.1016/j.gca.2022.01.022

Peng, S., Lin, X., Thompson, R. L., Xi, Y., Liu, G., Hauglustaine, D., Lan, X., Poulter, B., Ramonet, M., & Saunois, M. (2022). Wetland emission and atmospheric sink changes explain methane growth in 2020. *Nature*, *612*(7940), 477–482. https://doi.org/https://doi.org/10.1038/s41586-022-05447-w

Peralta-Maraver, I., Reiss, J., & Robertson, A. L. (2018). Interplay of hydrology, community ecology and pollutant attenuation in the hyporheic zone. *Science of the Total Environment*, *610*, 267–275. https://doi.org/10.1016/j.scitotenv.2017.08.036

Phillips, D. L., & Gregg, J. W. (2001). Uncertainty in source partitioning using stable isotopes. *Oecologia*, *127*, 171–179. https://doi.org/10.1007/s004420000578

Pichler, M., Coskun, Ö. K., Ortega-Arbulú, A.-S., Conci, N., Wörheide, G., Vargas, S., & Orsi, W. D. (2018). A 16S rRNA gene sequencing and analysis protocol for the Illumina MiniSeq platform. *Microbiologyopen*, *7*(6), e00611. https://doi.org/10.1002/mbo3.611

Plante, A. F., Stone, M. M., & McGill, W. B. (2015). The metabolic physiology of soil microorganisms. In E. A. Paul (Ed.), *Soil microbiology, ecology and biochemistry (fourth edition)* (pp. 245–272). Academic Press. https://doi.org/10.1016/B978-0-12-415955-6.00009-8

Preuss, I., Knoblauch, C., Gebert, J., & Pfeiffer, E.-M. (2013). Improved quantification of microbial CH_4 oxidation efficiency in arctic wetland soils using carbon isotope fractionation. *Biogeosciences*, *10*(4), 2539–2552. https://doi.org/10.5194/bg-10-2539-2013

Pulg, U., Barlaup, B. T., Sternecker, K., Trepl, L., & Unfer, G. (2013). Restoration of spawning habitats of brown trout (Salmo trutta) in a regulated chalk stream. *River Research and Applications*, *29*(2), 172–182. https://doi.org/10.1002/rra.1594

Quaranta, E., Aggidis, G., Boes, R. M., Comoglio, C., De Michele, C., Patro, E. R., Georgievskaia, E., Harby, A., Kougias, I., & Muntean, S. (2021). Assessing the energy potential of modernizing the European hydropower fleet. *Energy Conversion and Management*, *246*, 114655. https://doi.org/10.1016/j.enconman.2021.114655

Quast, C., Pruesse, E., Yilmaz, P., Gerken, J., Schweer, T., Yarza, P., Peplies, J., & Glöckner, F. O. (2012). The SILVA ribosomal RNA gene database project: Improved data processing and web-based tools. *Nucleic Acids Research*, *41*(D1), D590–D596. https://doi.org/10.1093/nar/gks1219

Raghoebarsing, A. A., Pol, A., van de Pas-Schoonen, K. T., Smolders, A. J. P., Ettwig, K. F., Rijpstra, W. I. C., Schouten, S., Damsté, J. S. S., Op den Camp, H. J. M., Jetten, M. S. M., & Strous, M. (2006). A microbial consortium couples anaerobic methane oxidation to denitrification. *Nature*, *440*(7086), 918–921. https://doi.org/10.1038/nature04617

Rayleigh, L. (1896). Theoretical considerations respecting the separation of gases by diffusion and similar processes. *The London, Edinburgh, and Dublin Philosophical Magazine and Journal of Science*, *42*(259), 493–498. https://doi.org/10.1080/14786449608620944

Raymond, P. A., Zappa, C. J., Butman, D., Bott, T. L., Potter, J., Mulholland, P., Laursen, A. E., McDowell, W. H., & Newbold, D. (2012). Scaling the gas transfer velocity and hydraulic geometry in streams and small rivers. *Limnology and Oceanography: Fluids and Environments*, *2*(1), 41–53. https://doi.org/10.1215/21573689-1597669

Reckerth, A., Stichler, W., Schmidt, A., & Stumpp, C. (2017). Long-term data set analysis of stable isotopic composition in German rivers. *Journal of Hydrology*, *552*, 718–731. https://doi.org/10.1016/j.jhydrol.2017.07.022

Reeburgh, W. S. (1976). Methane consumption in Cariaco Trench waters and sediments. *Earth and Planetary Science Letters*, *28*(3), 337–344. https://doi.org/10.1016/0012-821X(76)90195-3

Reeburgh, W. S. (2007). Oceanic methane biogeochemistry. *Chemical Reviews*, *107*(2), 486–513. https://doi.org/10.1021/cr050362v

Revsbech, N. P. (1989). An oxygen microsensor with a guard cathode. *Limnology and Oceanography*, *34*(2), 474–478. https://doi.org/10.4319/lo.1989.34.2.0474

Ripple, W. J., Wolf, C., Gregg, J. W., Levin, K., Rockström, J., Newsome, T. M., Betts, M. G., Huq, S., Law, B. E., & Kemp, L. (2022). World scientists' warning of a climate emergency 2022. *BioScience*, *72*(12), 1149–1155. https://doi.org/10.1093/biosci/biac083

Ripple, W. J., Wolf, C., Newsome, T. M., Barnard, P., & Moomaw, W. R. (2019). World scientists' warning of a climate emergency [https://www.jstor.org/stable/26891410]. *BioScience*, *70*(1).

Rivett, M., Ellis, P., Greswell, R., Ward, R., Roche, R., Cleverly, M., Walker, C., Conran, D., Fitzgerald, P., & Willcox, T. (2008). Cost-effective mini drive-point piezometers and multilevel samplers for monitoring the hyporheic zone. *Quarterly Journal of Engineering Geology and Hydrogeology*, *41*(1), 49–60. https://doi.org/10.1144/1470-9236/07-012

Robertson, A., & Wood, P. (2010). Ecology of the hyporheic zone: Origins, current knowledge and future directions. *Fundamental and Applied Limnology*, *176*(4), 279–289. https://doi.org/10.1127/1863-9135/2010/0176-0279

Robison, A. L., Wollheim, W. M., Perryman, C. R., Cotter, A. R., Mackay, J. E., Varner, R. K., Clarizia, P., & Ernakovich, J. G. (2022). Dominance of diffusive methane emissions from lowland headwater streams promotes oxidation and isotopic enrichment. *Frontiers in Environmental Science*, *9*, 760. https://doi.org/10.3389/fenvs.2021.791305

Robison, A. L., Wollheim, W. M., Turek, B., Bova, C., Snay, C., & Varner, R. K. (2021). Spatial and temporal heterogeneity of methane ebullition in lowland headwater streams and the impact on sampling design. *Limnology and Oceanography*, *66*(12), 4063–4076. https://doi.org/10.1002/lno.11943

Rocher-Ros, G., Stanley, E. H., Loken, L. C., Casson, N. J., Raymond, P. A., Liu, S., Amatulli, G., & Sponseller, R. A. (2023). Global methane emissions from rivers and streams. *Nature*, *621*(7979), 530–535. https://doi.org/10.1038/s41586-023-06344-6

Rode, M., Hartwig, M., Wagenschein, D., Kebede, T., & Borchardt, D. (2015). The importance of hyporheic zone processes on ecological functioning and solute transport of streams and rivers. In L. Chicharo, F. Müller, & N. Fohrer (Eds.), *Ecosystem services and river basin ecohydrology* (pp. 57–82). Springer. https://doi.org/10.1007/978-94-017-9846-4_4

Roley, S. S., Tank, J. L., & Williams, M. A. (2012). Hydrologic connectivity increases denitrification in the hyporheic zone and restored floodplains of an agricultural stream. *Journal of Geophysical Research: Biogeosciences*, *117*(G3). https://doi.org/10.1029/2012JG001950

Romeijn, P., Comer-Warner, S. A., Ullah, S., Hannah, D. M., & Krause, S. (2019). Streambed organic matter controls on carbon dioxide and methane emissions from streams. *Environmental Science & Technology*, *53*(5), 2364–2374. https://doi.org/10.1021/acs.est.8b04243

Rosas, J., Lopez, O., Missimer, T. M., Coulibaly, K. M., Dehwah, A. H., Sesler, K., Lujan, L. R., & Mantilla, D. (2014). Determination of hydraulic conductivity from grain-size distribution for different depositional environments. *Groundwater*, *52*(3), 399–413. https://doi.org/10.1111/gwat.12078

Rosentreter, J. A., Borges, A. V., Deemer, B. R., Holgerson, M. A., Liu, S., Song, C., Melack, J., Raymond, P. A., Duarte, C. M., & Allen, G. H. (2021). Half of global methane emissions come from highly variable aquatic ecosystem sources. *Nature Geoscience*, *14*(4), 225–230. https://doi.org/10.1038/s41561-021-00715-2

Rutherford, J. C., Boyle, J. D., Elliott, A. H., Hatherell, T. V. J., & Chiu, T. W. (1995). Modeling benthic oxygen uptake by pumping. *Journal of Environmental Engineering*, *121*(1), 84–95. https://doi.org/10.1061/(ASCE)0733-9372(1995)121:1(84)

Rutherford, J. C., Latimer, G. J., & Smith, R. K. (1993). Bedform mobility and benthic oxygen uptake. *Water Research*, *27*(10), 1545–1558. https://doi.org/10.1016/0043-1354(93)90099-4

Sanders, I., Heppell, C., Cotton, J., Wharton, G., Hildrew, A., Flowers, E., & Trimmer, M. (2007). Emission of methane from chalk streams has potential implications for agricultural practices. *Freshwater Biology*, *52*(6), 1176–1186. https://doi.org/10.1111/j.1365-2427.2007.01745.x

Saunois, M., Stavert, A. R., Poulter, B., Bousquet, P., Canadell, J. G., Jackson, R. B., Raymond, P. A., Dlugokencky, E. J., Houweling, S., & Patra, P. K. (2020). The global methane budget 2000–2017. *Earth System Science Data*, *12*(3), 1561–1623. https://doi.org/10.5194/essd-12-1561-2020

Sawakuchi, H. O., Bastviken, D., Sawakuchi, A. O., Ward, N. D., Borges, C. D., Tsai, S. M., Richey, J. E., Ballester, M. V. R., & Krusche, A. V. (2016). Oxidative mitigation of aquatic methane emissions in large Amazonian rivers. *Global Change Biology*, *22*(3), 1075–1085. https://doi.org/10.1111/gcb.13169

Schaefer, H., Fletcher, S. E. M., Veidt, C., Lassey, K. R., Brailsford, G. W., Bromley, T. M., Dlugokencky, E. J., Michel, S. E., Miller, J. B., & Levin, I. (2016). A 21st-century shift from fossil-fuel to biogenic methane emissions indicated by $^{13}CH_4$. *Science*, *352*(6281), 80–84. https://doi.org/10.1126/science.aad2705

Schaper, J. L., Posselt, M., McCallum, J. L., Banks, E. W., Hoehne, A., Meinikmann, K., Shanafield, M. A., Batelaan, O., & Lewandowski, J. (2018). Hyporheic exchange controls fate of trace organic compounds in an urban stream. *Environmental Science & Technology*, *52*(21), 12285–12294. https://doi.org/10.1021/acs.est.8b03117

Scheller, S., Ermler, U., & Shima, S. (2020). Catabolic pathways and enzymes involved in anaerobic methane oxidation. *Anaerobic Utilization of Hydrocarbons, Oils, and Lipids*, 31–59. https://doi.org/10.1007/978-3-319-50391-2_3

Scheller, S., Yu, H., Chadwick, G. L., McGlynn, S. E., & Orphan, V. J. (2016). Artificial electron acceptors decouple archaeal methane oxidation from sulfate reduction. *Science*, *351*(6274), 703–707. https://doi.org/10.1126/science.aad7154

Schmidt, C., Büttner, O., Musolff, A., & Fleckenstein, J. H. (2014). A method for automated, daily, temperature-based vertical streambed water-fluxes. *Fundamental and Applied Limnology/Archiv für Hydrobiologie*, *184*(3), 173–181. https://doi.org/10.1127/1863-9135/2014/0548

Schubert, C. J., Vazquez, F., Lösekann-Behrens, T., Knittel, K., Tonolla, M., & Boetius, A. (2011). Evidence for anaerobic oxidation of methane in sediments of a freshwater system (Lago di Cadagno). *FEMS Microbiology Ecology*, *76*(1), 26–38. https://doi.org/10.1111/j.1574-6941.2010.01036.x

Seeberg-Elverfeldt, J., Schlüter, M., Feseker, T., & Kölling, M. (2005). Rhizon sampling of porewaters near the sediment-water interface of aquatic systems. *Limnology and Oceanography: Methods*, *3*(8), 361–371. https://doi.org/10.4319/lom.2005.3.361

Segarra, K., Schubotz, F., Samarkin, V., Yoshinaga, M., Hinrichs, K., & Joye, S. (2015). High rates of anaerobic methane oxidation in freshwater wetlands reduce potential atmospheric methane emissions. *Nature Communications*, *6*(1), 1–8. https://doi.org/10.1038/ncomms8477

Seitzinger, S., Harrison, J. A., Böhlke, J., Bouwman, A., Lowrance, R., Peterson, B., Tobias, C., & Drecht, G. V. (2006). Denitrification across landscapes and waterscapes: A synthesis. *Ecological applications*, *16*(6), 2064–2090. https://doi.org/10.1890/1051-0761(2006)016[2064:DALAWA]2.0.CO;2

Shelley, F., Abdullahi, F., Grey, J., & Trimmer, M. (2015). Microbial methane cycling in the bed of a chalk river: Oxidation has the potential to match methanogenesis enhanced by warming. *Freshwater Biology*, *60*(1), 150–160. https://doi.org/10.1111/fwb.12480

Shelley, F., Ings, N., Hildrew, A. G., Trimmer, M., & Grey, J. (2017). Bringing methanotrophy in rivers out of the shadows. *Limnology and Oceanography*, *62*(6), 2345–2359. https://doi.org/10.1002/lno.10569

Shen, L.-d., Ouyang, L., Zhu, Y., & Trimmer, M. (2019a). Active pathways of anaerobic methane oxidation across contrasting riverbeds. *The ISME journal*, *13*(3), 752–766. https://doi.org/10.1038/s41396-018-0302-y

Shen, L.-d., Ouyang, L., Zhu, Y., & Trimmer, M. (2019b). Spatial separation of anaerobic ammonium oxidation and nitrite-dependent anaerobic methane oxidation in permeable riverbeds. *Environmental Microbiology*, *21*(4), 1185–1195. https://doi.org/10.1111/1462-2920.14554

Shen, L.-d., Tian, M.-h., Cheng, H.-x., Liu, X., Yang, Y.-l., Liu, J.-q., Xu, J.-b., Kong, Y., Li, J.-h., & Liu, Y. (2020). Different responses of nitrite- and nitrate-dependent anaerobic methanotrophs to increasing nitrogen loading in a freshwater reservoir. *Environmental Pollution*, 114623. https://doi.org/10.1016/j.envpol.2020.114623

Shen, L.-d., Wu, H.-s., Liu, X., & Li, J. (2017). Cooccurrence and potential role of nitrite- and nitrate-dependent methanotrophs in freshwater marsh sediments. *Water Research*, *123*, 162–172. https://doi.org/10.1016/j.watres.2017.06.075

Shotbolt, L. (2010). Pore water sampling from lake and estuary sediments using Rhizon samplers. *Journal of Paleolimnology*, *44*(2), 695–700. https://doi.org/10.1007/s10933-008-9301-8

Sidle, W. C. (1998). Environmental isotopes for resolution of hydrology problems. *Environmental Monitoring and Assessment*, *52*(3), 389–410. https://doi.org/10.1023/A:1005922029958

Silvennoinen, H., Liikanen, A., Rintala, J., & Martikainen, P. J. (2008). Greenhouse gas fluxes from the eutrophic Temmesjoki River and its estuary in the Liminganlahti Bay (the Baltic Sea). *Biogeochemistry*, *90*(2), 193–208. https://doi.org/10.1007/s10533-008-9244-1

Sivan, O., Adler, M., Pearson, A., Gelman, F., Bar-Or, I., John, S. G., & Eckert, W. (2011). Geochemical evidence for iron-mediated anaerobic oxidation of methane. *Limnology and Oceanography*, *56*(4), 1536–1544. https://doi.org/10.4319/lo.2011.56.4.1536

Smialek, N., Pander, J., & Geist, J. (2021). Environmental threats and conservation implications for atlantic salmon and brown trout during their critical freshwater phases of spawning, egg development and juvenile emergence. *Fisheries Management and Ecology*, *28*(5), 437–467. https://doi.org/10.1111/fme.12507

Snover, A. K., & Quay, P. D. (2000). Hydrogen and carbon kinetic isotope effects during soil uptake of atmospheric methane. *Global Biogeochemical Cycles*, *14*(1), 25–39. https://doi.org/10.1029/1999GB900089

Song, J., Luo, Y., Zhao, Q., & Christie, P. (2003). Novel use of soil moisture samplers for studies on anaerobic ammonium fluxes across lake sediment–water interfaces. *Chemosphere*, *50*(6), 711–715. https://doi.org/10.1016/S0045-6535(02)00210-2

Sophocleous, M. (2002). Interactions between groundwater and surface water: The state of the science. *Hydrogeology Journal*, *10*(1), 52–67. https://doi.org/10.1007/s10040-001-0170-8

Spoelstra, J., Leal, K. A., Senger, N. D., Schiff, S. L., & Post, R. (2021). Isotopic characterization of sulfate in a shallow aquifer impacted by agricultural fertilizer. *Groundwater*, *59*(5), 658–670. https://doi.org/10.1111/gwat.13093

Spratt Jr, H. G., Morgan, M. D., & Good, R. E. (1987). Sulfate reduction in peat from a New Jersey pinelands cedar swamp. *Applied and Environmental Microbiology*, *53*(7), 1406–1411. https://doi.org/10.1128/aem.53.7.1406-1411.1987

Stallman, R. (1965). Steady one-dimensional fluid flow in a semi-infinite porous medium with sinusoidal surface temperature. *Journal of Geophysical Research*, *70*(12), 2821–2827. https://doi.org/10.1029/JZ070i012p02821

Stanley, E. H., Casson, N. J., Christel, S. T., Crawford, J. T., Loken, L. C., & Oliver, S. K. (2016). The ecology of methane in streams and rivers: Patterns, controls, and global significance. *Ecological Monographs*, *86*(2), 146–171. https://doi.org/10.1890/15-1027

Stein, H. (1987). *Die Auswirkungen von Besatzmaßnahmen auf den Fischbestand der Moosach* (Report). Bayerische Landesanstalt für Wasserforschung.

Steinle, L., Maltby, J., Treude, T., Kock, A., Bange, H. W., Engbersen, N., Zopfi, J., Lehmann, M. F., & Niemann, H. (2017). Effects of low oxygen concentrations on aerobic methane oxidation in seasonally hypoxic coastal waters. *Biogeosciences*, *14*(6), 1631–1645. https://doi.org/10.5194/bg-14-1631-2017

Stern, O., & Volmer, M. (1919). Über die Abklingzeit der Fluoreszenz. *Physikalische Zeitschrift*, *20*, 183–188. https://doi.org/10.1007/978-3-662-46962-0_5

Sternecker, K., & Geist, J. (2010). The effects of stream substratum composition on the emergence of salmonid fry. *Ecology of Freshwater Fish*, *19*(4), 537–544. https://doi.org/10.1111/j.1600-0633.2010.00432.x

Stoewer, M., Knöller, K., & Stumpp, C. (2015). Tracing freshwater nitrate sources in pre-alpine groundwater catchments using environmental tracers. *Journal of Hydrology*, *524*, 753–767.

Storey, R. G., Fulthorpe, R. R., & Williams, D. D. (1999). Perspectives and predictions on the microbial ecology of the hyporheic zone. *Freshwater Biology*, *41*(1), 119–130. https://doi.org/10.1046/j.1365-2427.1999.00377.x

Storey, R. G., Williams, D. D., & Fulthorpe, R. R. (2004). Nitrogen processing in the hyporheic zone of a pastoral stream. *Biogeochemistry*, *69*(3), 285–313. https://doi.org/10.1023/B:BIOG.0000031049.95805.ec

Stumpp, C., Klaus, J., & Stichler, W. (2014). Analysis of long-term stable isotopic composition in German precipitation. *Journal of Hydrology*, *517*, 351–361. https://doi.org/10.1016/j.jhydrol.2014.05.034

Sunjidmaa, N., Mendoza-Lera, C., Hille, S., Schmidt, C., Borchardt, D., & Graeber, D. (2022). Carbon limitation may override fine-sediment induced alterations of hyporheic nitrogen and phosphorus dynamics. *Science of The Total Environment*, *837*, 155689. https://doi.org/10.1016/j.scitotenv.2022.155689

Sutton, M. A., Howard, C. M., Erisman, J. W., Billen, G., Bleeker, A., Grennfelt, P., Van Grinsven, H., & Grizzetti, B. (2011). *The European nitrogen assessment: Sources, effects and policy perspectives* (Report). Cambridge University Press.

Takeuchi, M., Ozaki, H., Hiraoka, S., Kamagata, Y., Sakata, S., Yoshioka, H., & Iwasaki, W. (2019). Possible cross-feeding pathway of facultative methylotroph Methyloceanibacter caenitepidi Gela4 on methanotroph Methylocaldum marinum S8. *PloS One*, *14*(3), e0213535. https://doi.org/10.1371/journal.pone.0213535

Teasdale, P. R., Batley, G. E., Apte, S. C., & Webster, I. T. (1995). Pore water sampling with sediment peepers. *TrAC Trends in Analytical Chemistry*, *14*(6), 250–256. https://doi.org/10.1016/0165-9936(95)91617-2

Templeton, A. S., Chu, K.-H., Alvarez-Cohen, L., & Conrad, M. E. (2006). Variable carbon isotope fractionation expressed by aerobic CH_4-oxidizing bacteria. *Geochimica et Cosmochimica Acta*, *70*(7), 1739–1752. https://doi.org/10.1016/j.gca.2005.12.002

Timmers, P. H., Suarez-Zuluaga, D. A., van Rossem, M., Diender, M., Stams, A. J., & Plugge, C. M. (2016). Anaerobic oxidation of methane associated with sulfate reduction in a natural freshwater gas source. *The ISME Journal*, *10*(6), 1400–1412. https://doi.org/10.1038/ismej.2015.213

Torres, N. T., Och, L. M., Hauser, P. C., Furrer, G., Brandl, H., Vologina, E., Sturm, M., Bürgmann, H., & Müller, B. (2014). Early diagenetic processes generate iron and manganese oxide layers in the sediments of Lake Baikal, Siberia. *Environmental Science: Processes & Impacts*, *16*(4), 879–889. https://doi.org/10.1039/C3EM00676J

Trauth, N., & Fleckenstein, J. H. (2017). Single discharge events increase reactive efficiency of the hyporheic zone. *Water Resources Research*, *53*(1), 779–798. https://doi.org/10.1002/2016WR019488

Trimmer, M., Grey, J., Heppell, C. M., Hildrew, A. G., Lansdown, K., Stahl, H., & Yvon-Durocher, G. (2012). River bed carbon and nitrogen cycling: State of play and some new directions. *Science of the Total Environment*, *434*, 143–158. https://doi.org/10.1016/j.scitotenv.2011.10.074

Triska, F. J., Duff, J. H., & Avanzino, R. J. (1993). The role of water exchange between a stream channel and its hyporheic zone in nitrogen cycling at the terrestrial—aquatic interface. In A. Hillbricht-Ilkowska & E. Pieczyńska (Eds.), *Nutrient dynamics and retention in land/water ecotones of lowland, temperate lakes and rivers* (pp. 167–184). Springer. https://doi.org/10.1007/978-94-011-1602-2_20

Trotsenko, Y. A., & Murrell, J. C. (2008). Metabolic aspects of aerobic obligate methanotrophy. *Advances in Applied Microbiology*, *63*, 183–229. https://doi.org/10.1016/S0065-2164(07)00005-6

Vaksmaa, A., van Alen, T. A., Ettwig, K. F., Lupotto, E., Valè, G., Jetten, M. S., & Lüke, C. (2017). Stratification of diversity and activity of methanogenic and methanotrophic microorganisms in a nitrogen-fertilized Italian paddy soil. *Frontiers in Microbiology*, *8*, 2127. https://doi.org/10.3389/fmicb.2017.02127

van Grinsven, S., Sinninghe Damsté, J. S., Abdala Asbun, A., Engelmann, J. C., Harrison, J., & Villanueva, L. (2020). Methane oxidation in anoxic lake water stimulated by nitrate and sulfate addition. *Environmental Microbiology*, *22*(2), 766–782. https://doi.org/10.1111/1462-2920.14886

Vanwonterghem, I., Evans, P. N., Parks, D. H., Jensen, P. D., Woodcroft, B. J., Hugenholtz, P., & Tyson, G. W. (2016). Methylotrophic methanogenesis discovered in the archaeal phylum Verstraetearchaeota. *Nature Microbiology*, *1*(12), 1–9. https://doi.org/10.1038/NMICROBIOL.2016.170

Vermaat, J. E., Harmsen, J., Hellmann, F. A., van der Geest, H. G., de Klein, J. J., Kosten, S., Smolders, A. J., Verhoeven, J. T., Mes, R. G., & Ouboter, M. (2016). Annual sulfate budgets for Dutch lowland peat polders: The soil is a major sulfate source through peat and pyrite oxidation. *Journal of Hydrology*, *533*, 515–522.

Versantvoort, W., Guerrero-Cruz, S., Speth, D. R., Frank, J., Gambelli, L., Cremers, G., van Alen, T., Jetten, M. S., Kartal, B., & Op den Camp, H. J. (2018). Comparative genomics of Candidatus Methylomirabilis species and description of Ca. Methylomirabilis lanthanidiphila. *Frontiers in Microbiology*, *9*, 1672. https://doi.org/10.3389/fmicb.2018.01672

Větrovský, T., & Baldrian, P. (2013). The variability of the 16S rRNA gene in bacterial genomes and its consequences for bacterial community analyses. *PloS One*, *8*(2), e57923. https://doi.org/10.1371/journal.pone.0057923

Vieweg, M., Trauth, N., Fleckenstein, J. H., & Schmidt, C. (2013). Robust optode-based method for measuring in situ oxygen profiles in gravelly streambeds. *Environmental Science & Technology*, *47*(17), 9858–9865. https://doi.org/10.1021/es401040w

Villa, J. A., Smith, G. J., Ju, Y., Renteria, L., Angle, J. C., Arntzen, E., Harding, S. F., Ren, H., Chen, X., & Sawyer, A. H. (2020). Methane and nitrous oxide porewater concentrations and surface fluxes of a regulated river. *Science of The Total Environment*, *715*, 136920. https://doi.org/10.1016/j.scitotenv.2020.136920

Vitousek, P. M., Naylor, R., Crews, T., David, M., Drinkwater, L., Holland, E., Johnes, P., Katzenberger, J., Martinelli, L., & Matson, P. (2009). Nutrient imbalances in agricultural development. *Science*, *324*(5934), 1519–1520. https://doi.org/10.1126/science.1170261

Vonnahme, T. R., Molari, M., Janssen, F., Wenzhöfer, F., Haeckel, M., Titschack, J., & Boetius, A. (2020). Effects of a deep-sea mining experiment on seafloor microbial communities and functions after 26 years. *Science Advances*, *6*(18), eaaz5922. https://doi.org/10.1126/sciadv.aaz5922

Voorhees, R. M., & Ramakrishnan, V. (2013). Structural basis of the translational elongation cycle. *Annual Review of Biochemistry*, *82*, 203–236. https://doi.org/10.1146/annurev-biochem-113009-092313

Vuillemin, A., Wankel, S. D., Coskun, Ö. K., Magritsch, T., Vargas, S., Estes, E. R., Spivack, A. J., Smith, D. C., Pockalny, R., & Murray, R. W. (2019). Archaea dominate oxic subseafloor communities over multimillion-year time scales. *Science Advances*, *5*(6), eaaw4108. https://doi.org/10.1126/sciadv.aaw4108

Wanninkhof, R., Asher, W. E., Ho, D. T., Sweeney, C., & McGillis, W. R. (2009). Advances in quantifying air-sea gas exchange and environmental forcing. *Annual Review of Marine Science*, *1*, 213–244. https://doi.org/10.1146/annurev.marine.010908.163742

Wasti, A., Ray, P., Wi, S., Folch, C., Ubierna, M., & Karki, P. (2022). Climate change and the hydropower sector: A global review. *Wiley Interdisciplinary Reviews: Climate Change*, *13*(2), e757. https://doi.org/10.1002/wcc.757

Weisburg, W. G., Barns, S. M., Pelletier, D. A., & Lane, D. J. (1991). 16S ribosomal DNA amplification for phylogenetic study. *Journal of Bacteriology*, *173*(2), 697–703. https://doi.org/10.1128/jb.173.2.697-703.1991

Wheeler, M. D., Newman, S. M., Orr-Ewing, A. J., & Ashfold, M. N. (1998). Cavity ring-down spectroscopy. *Journal of the Chemical Society, Faraday Transactions*, *94*(3), 337–351. https://doi.org/10.1039/A707686J

Whiticar, M. J. (1999). Carbon and hydrogen isotope systematics of bacterial formation and oxidation of methane. *Chemical Geology*, *161*(1-3), 291–314. https://doi.org/10.1016/S0009-2541(99)00092-3

Whiticar, M. J., Faber, E., & Schoell, M. (1986). Biogenic methane formation in marine and freshwater environments: CO_2 reduction vs. acetate fermentation – isotope evidence. *Geochimica et Cosmochimica Acta*, *50*(5), 693–709. https://doi.org/10.1016/0016-7037(86)90346-7

Whiticar, M. J., & Faber, E. (1986). Methane oxidation in sediment and water column environments – isotope evidence. *Organic Geochemistry*, *10*(4-6), 759–768. https://doi.org/10.1016/S0146-6380(86)80013-4

Wik, M., Varner, R. K., Anthony, K. W., MacIntyre, S., & Bastviken, D. (2016). Climate-sensitive northern lakes and ponds are critical components of methane release. *Nature Geoscience*, *9*(2), 99–105. https://doi.org/10.1038/ngeo2578

Wild, R., Nagel, C., & Geist, J. (2023). Climate change effects on hatching success and embryonic development of fish: Assessing multiple stressor responses in a large-scale mesocosm study. *Science of The Total Environment*, 164834. https://doi.org/10.1016/j.scitotenv.2023.164834

Wilkinson, J., Bodmer, P., & Lorke, A. (2019). Methane dynamics and thermal response in impoundments of the Rhine River, Germany. *Science of the Total Environment*, *659*, 1045–1057. https://doi.org/10.1016/j.scitotenv.2018.12.424

Wilkinson, J., Maeck, A., Alshboul, Z., & Lorke, A. (2015). Continuous seasonal river ebullition measurements linked to sediment methane formation. *Environmental Science & Technology*, *49*(22), 13121–13129. https://doi.org/10.1021/acs.est.5b01525

Winter, T., & Einsiedl, F. (2022). Combining $^{14}C_{DOC}$ and ^{81}Kr with hydrochemical data to identify recharge processes in the South German Molasse Basin. *Journal of Hydrology*, *612*, 128020. https://doi.org/10.1016/j.jhydrol.2022.128020

Winter, T. C., Harvey, J. W., Franke, L. O., & Alley, W. M. (1998). *Ground water and surface water: A single resource* (Report). U.S. Geological Survey.

Woese, C. R., & Fox, G. E. (1977). Phylogenetic structure of the prokaryotic domain: The primary kingdoms. *Proceedings of the National Academy of Sciences*, *74*(11), 5088–5090. https://doi.org/10.1073/pnas.74.11.5088

Worden, R. H. (2005). Analytical methods: Geochemical analysis (including X-ray). In R. C. Selley, L. R. M. Cocks, I. R. Pilmer, & J. McCall (Eds.), *Encyclopedia of geology* (pp. 54–76). Elsevier Academic. https://doi.org/10.1016/B0-12-369396-9/00096-4

Wu, G., Zhang, T., Gu, M., Chen, Z., & Yin, Q. (2020). Review of characteristics of anammox bacteria and strategies for anammox start-up for sustainable wastewater resource management. *Water Science and Technology*, *82*(9), 1742–1757. https://doi.org/10.2166/wst.2020.443

Wu, W., & Wang, S. S. (2006). Formulas for sediment porosity and settling velocity. *Journal of Hydraulic Engineering*, *132*(8), 858–862. https://doi.org/10.1061/(ASCE)0733-9429(2006)132:8(858)

Yang, B., Wang, Y., & Qian, P.-Y. (2016). Sensitivity and correlation of hypervariable regions in 16S rRNA genes in phylogenetic analysis. *BMC Bioinformatics*, *17*(1), 1–8. https://doi.org/10.1186/s12859-016-0992-y

Young, P. C., Pedregal, D. J., & Tych, W. (1999). Dynamic harmonic regression. *Journal of Forecasting*, *18*(6), 369–394.

Yvon-Durocher, G., Allen, A. P., Bastviken, D., Conrad, R., Gudasz, C., St-Pierre, A., Thanh-Duc, N., & Del Giorgio, P. A. (2014). Methane fluxes show consistent temperature dependence across microbial to ecosystem scales. *Nature*, *507*(7493), 488–491. https://doi.org/10.1038/nature13164

Yvon-Durocher, G., Hulatt, C. J., Woodward, G., & Trimmer, M. (2017). Long-term warming amplifies shifts in the carbon cycle of experimental ponds. *Nature Climate Change*, *7*(3), 209–213. https://doi.org/10.1038/nclimate3229

Yvon-Durocher, G., Montoya, J. M., Woodward, G., Jones, J. I., & Trimmer, M. (2011). Warming increases the proportion of primary production emitted as methane from freshwater mesocosms. *Global Change Biology*, *17*(2), 1225–1234. https://doi.org/10.1111/j.1365-2486.2010.02289.x

Zarfl, C., Lumsdon, A. E., Berlekamp, J., Tydecks, L., & Tockner, K. (2015). A global boom in hydropower dam construction. *Aquatic Sciences*, *77*, 161–170. https://doi.org/10.1007/s00027-014-0377-0

Zarnetske, J. P., Haggerty, R., Wondzell, S. M., & Baker, M. A. (2011). Dynamics of nitrate production and removal as a function of residence time in the hyporheic zone. *Journal of Geophysical Research: Biogeosciences*, *116*(G1). https://doi.org/10.1029/2010JG001356

Zehlius-Eckert, W., Schwaiger, H., & Beckmann, A. (2003). Monitoring und Erfolgskontrolle im Freisinger Moos. In N. Mallach & C. Stettmer (Eds.). Bayerische Akademie für Naturschutz und Landschaftspflege.

Zhang, G., Jiang, N., Liu, X., & Dong, X. (2008). Methanogenesis from methanol at low temperatures by a novel psychrophilic methanogen, "Methanolobus psychrophilus" sp. nov., prevalent in Zoige wetland of the Tibetan plateau. *Applied and Environmental Microbiology*, *74*(19), 6114–6120. https://doi.org/10.1128/AEM.01146-08

Zhang, L., Xia, X., Liu, S., Zhang, S., Li, S., Wang, J., Wang, G., Gao, H., Zhang, Z., Wang, Q., Wen, W., Liu, R., Yang, Z., Stanley, E. H., & Raymond, P. A. (2020). Significant methane ebullition from alpine permafrost rivers on the East Qinghai–Tibet Plateau. *Nature Geoscience*, *13*(5), 349–354. https://doi.org/10.1038/s41561-020-0571-8

Zhang, M., Luo, Y., Lin, X., Hetharua, B., Zhao, W., Zhou, M., Zhan, Q., Xu, H., Zheng, T., & Tian, Y. (2018). Molecular and stable isotopic evidence for the occurrence of nitrite-dependent anaerobic methane-oxidizing bacteria in the mangrove sediment of Zhangjiang Estuary, China. *Applied Microbiology and Biotechnology*, *102*(5), 2441–2454. https://doi.org/10.1007/s00253-017-8718-2

Zhou, N., Zhao, S., & Shen, X. (2014). Nitrogen cycle in the hyporheic zone of natural wetlands. *Chinese Science Bulletin*, *59*, 2945–2956. https://doi.org/10.1007/s11434-014-0224-7

Zhu, G., Zhou, L., Wang, Y., Wang, S., Guo, J., Long, X.-E., Sun, X., Jiang, B., Hou, Q., & Jetten, M. S. (2015). Biogeographical distribution of denitrifying anaerobic methane oxidizing bacteria in Chinese wetland ecosystems. *Environmental Microbiology Reports*, *7*(1), 128–138. https://doi.org/10.1111/1758-2229.12214

Zhu, Y., Jones, J. I., Collins, A. L., Zhang, Y., Olde, L., Rovelli, L., Murphy, J. F., Heppell, C. M., & Trimmer, M. (2022). Separating natural from human enhanced methane emissions in headwater streams. *Nature Communications*, *13*(1), 1–11. https://doi.org/10.1038/s41467-022-31559-y

Zhu, Y., Purdy, K. J., Eyice, Ö., Shen, L., Harpenslager, S. F., Yvon-Durocher, G., Dumbrell, A. J., & Trimmer, M. (2020). Disproportionate increase in freshwater methane emissions induced by experimental warming. *Nature Climate Change*, *10*(7), 685–690. https://doi.org/10.1038/s41558-020-0824-y

Zimmer, M. A., & Lautz, L. K. (2014). Temporal and spatial response of hyporheic zone geochemistry to a storm event. *Hydrological Processes*, *28*(4), 2324–2337. https://doi.org/10.1002/hyp.9778

Zona, D., Gioli, B., Commane, R., Lindaas, J., Wofsy, S. C., Miller, C. E., Dinardo, S. J., Dengel, S., Sweeney, C., & Karion, A. (2016). Cold season emissions dominate the Arctic tundra methane budget. *Proceedings of the National Academy of Sciences*, *113*(1), 40–45. https://doi.org/10.1073/pnas.1516017113

A Supplement to ”High-resolution vertical biogeochemical profiles in the hyporheic zone reveal insights into microbial methane cycling”

A.1 Hydrology, surface water chemistry, sampling details and sediment characteristics

Table A.1 shows the surface water chemistry of the Moosach river. The water is of calcium-magnesium-bicarbonate type with elevated Cl^- concentrations.

Table A.1: Surface water chemistry. Concentrations represent mean values of data recorded between 2010-2018. Data retreived from the Bavarian State Office of the Environment (2023).

Component	**Concentration** ($mg\,L^{-1}$)
Na^+	30.9
Ca^{2+}	100
Mg^{2+}	20.7
Cl^-	54
NO_3^-	20.4
SO_4^{2-}	30.4
HCO_3^-	340
Dissolved O_2	8.7
TOC	3.5
DOC	2.8

Table A.2 summarizes information on sampling intervals and measured basic chemical parameters of the surface water as measured on the days of sampling. Further, average discharge and temperature during equilibration period are given. Stream discharge and surface water temperature during the sampling periods is shown in Fig. A.1.

Sediment cores were taken at each sampling site by manually pushing a coring tube (inner diameter 42 mm) into the sediment. In the laboratory, each core was divided into homogeneous layers. Sieve-slurry analyses were performed to obtain sediment grain size distributions according to DIN EN ISO 17892-4. Sedimentation experiments failed for location B (11-22 cm) due to the high content of organic matter which induced coagulation at an unexpectedly high rate. Sedimentation experiments were not performed for location E 0-7 cm. The grain size

Table A.2: Background information on the five sampling periods, basic chemical parameters of the surface water on the days of sampling and mean discharge and surface water temperature during the sampling period.

Profile	**Placement**	**Sampling**	**Days**	**Basic chemical parameters of the surface water on the days of sampling**				**Mean discharge & temperature during equilibration***	
				T_{SW} (°C)	O_2 (mg L^{-1})	pH	el. C. (µS cm^{-1})	Q_M (m^3 s^{-1})	T_M (°C)
A	2021-03-02	2021-03-22	36	7.0	no measurements			2.33	7.5
B	2021-05-04	2021-05-26	22	11.3	9.9	7.9	819	2.51	12.0
C	2021-06-16	2021-07-06	20	15.3	10.5	8.1	806	2.93	16.6
D	2020-07-15	2020-08-20	20	16.2	10.2	7.6	756	1.46	17.1
E	2021-07-21	2021-08-18	28	14.5	10.9	8.1	797	2.48	15.8

* Data retrieved from the Bavarian State Office of the Environment (2023)

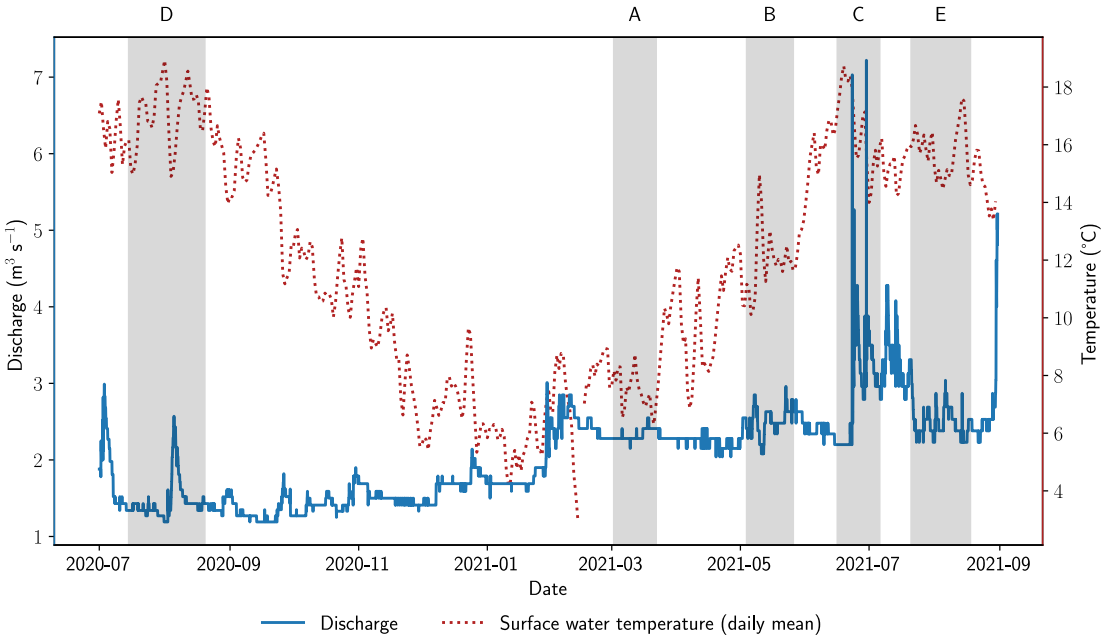

Figure A.1: **Stream water temperature (daily mean) and discharge.** Data was recorded at gauging station Freising Moosach (river chainage: 9.45 km, 4.5 km downstream of the sampling sites), as retrieved from the Bavarian State Office of the Environment (2023).

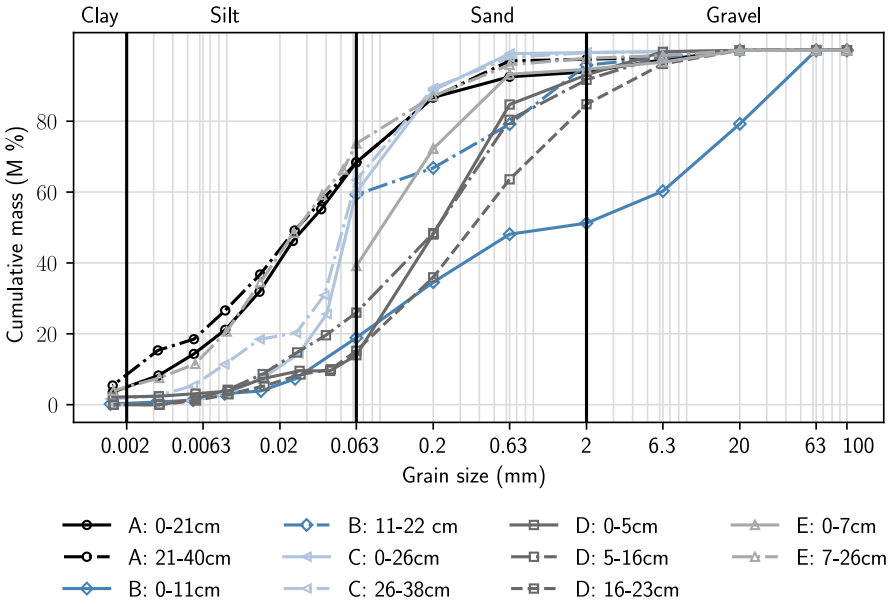

Figure A.2: **Grain size distribution curves**

Table A.3: Sediment characteristics and calculated porosity φ

Profile	**Sampling date**	**Depth** (cm)	**Silt/Clay** (%)	**Sand** (%)	**Gravel** (%)	$\mathbf{d_{50}}$ (mm)	φ
A	2021-03-22	0-21	65	29	6	0.030	0.56
		21-40	68	29	3	0.026	0.57
B	2021-05-26	0-11	19	32	49	1.46	0.32
		11-22	59	37	4	*0.040*	*0.54*
C	2021-07-06	0-26	60	39	1	0.030	0.51
		26-38	63	36	1	0.019	0.51
D	2020-08-20	0-5	14	79	7	0.22	0.42
		5-16	26	66	8	0.22	0.42
		16-23	15	70	15	0.42	0.38
E	2021-08-18	0-7	39	56	5	0.11	0.46
		7-26	74	24	2	0.027	0.57

distribution curves for each sampling site are displayed in Fig. A.2 and characteristic values listed in Tab. A.3.

Porosity φ was calculated as a function of the median grain diameter d_{50} as suggested by Wu and Wang (2006) who modified the formula for initial porosity of sediment deposits (less than one year after deposition) proposed by Komura and Colby (1963). Values for d_{50} and φ are also given in Tab. A.3. For location B (11-22 cm), the given d_{50} is an estimation based exclusively on the sieving analysis.

$$\varphi = 0.13 + \frac{0.21}{(d_{50} + 0.002)^{0.21}} \tag{A.1}$$

Hydraulic conductivity K was roughly estimated using the formula introduced by Beyer (1964) (Eq. A.2).

Table A.4: Hydraulic conductivities estimated using the Beyer equation.

Profile	**Sampling date**	**Depth** (cm)	$\mathbf{d}_{10}$ (mm)	$\mathbf{d}_{60}$ (mm)	$\mathbf{C}_\mathrm{U}$	**K** ($\mathrm{m\,s^{-1}}$)
A	2021-03-22	0-21	0.0039	0.047	12.0	$2.4 \cdot 10^{-6}$
		21-40	0.0023	0.043	18.7	$7.4 \cdot 10^{-7}$
B	2021-05-26	0-11	0.041	6.2	150.5	$8.6 \cdot 10^{-5}$
		11-22	*0.010*	0.076	*7.6*	$1.8 \cdot 10^{-5}$
C	2021-07-06	0-26	0.0019	0.063	33.2	$4.1 \cdot 10^{-7}$
		26-38	0.008	0.062	7.8	$1.1 \cdot 10^{-5}$
D	2020-08-20	0-5	0.048	0.34	7.1	$4.2 \cdot 10^{-4}$
		5-16	0.018	0.36	20.0	$4.4 \cdot 10^{-5}$
		16-23	0.043	0.57	13.3	$2.8 \cdot 10^{-4}$
E	2021-08-18	0-7	*0.020*	0.15	*7.5*	$7.1 \cdot 10^{-5}$
		7-26	0.0047	0.039	8.3	$3.8 \cdot 10^{-6}$

$$\mathrm{K} = \beta \frac{\mathrm{g}}{\nu} \log\left(\frac{500}{\mathrm{C_U}}\right) \mathrm{d}_{10}^2 \tag{A.2}$$

with the coefficient β = $1.30 \cdot 10^{-5}$ as recommended by Rosas et al. (2014) for river sediments, the gravitational constant g = 9.81 $\mathrm{m\,s^{-2}}$, the kinematic viscosity ν = 1.307 $\mathrm{mm^2\,s^{-1}}$ for 10 °C (Kestin et al., 1978), the uniformity coefficient $\mathrm{C_U}$ = $\mathrm{d_{60}/d_{10}}$ and the grain diameters $\mathrm{d_{10}}$ and $\mathrm{d_{60}}$ at 10 % and 60 % of the cumulative grain size distribution curve, respectively. For location B (11-22 cm) and location E (0-7 cm) the $\mathrm{d_{10}}$ was estimated only based on the sieving analysis. Results are given in Tab. A.4.

A.2 Determination of a cut-off threshold concentration for isotope measurements

Measurements of $\delta^{13}C$–CH_4 at low headspace CH_4 concentrations in the sample vials showed large standard deviations between repeated measurements. Thus, an experiment was conducted to find an appropriate cut-off value above which reliable isotopic data could be obtained. Two standards with -21.1 ‰ and -69.0 ‰ were diluted to obtain different concentrations and measured repeatedly. A cut-off value of 30 ppm was chosen based on the results displayed in Fig. A.3.

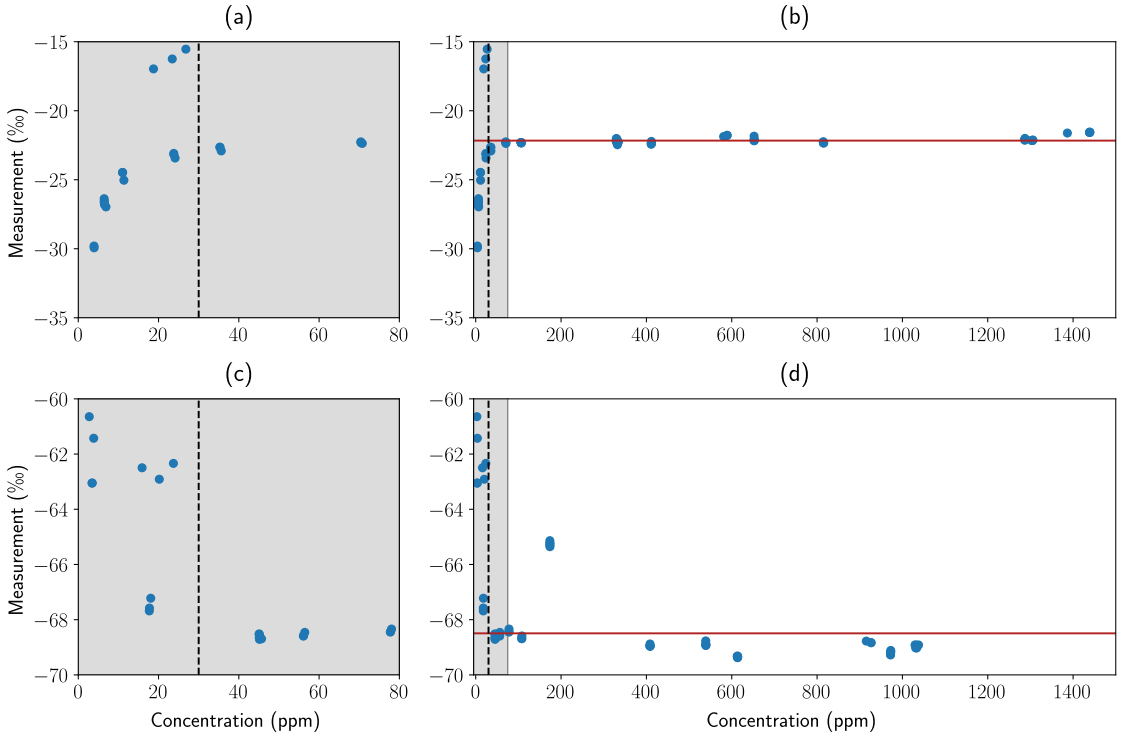

Figure A.3: **Repeated measurements of standards with $\delta^{13}C$–CH_4 values of -21.1 ‰ (panels (a) and (b)) and -69.0 ‰ (panels (c) and (d))**. The red line in panels (b) and (d) represents the average value of all measurements above the cut-off threshold.

A.3 Calculation of sediment diffusion coefficients

Diffusion coefficients were calculated based on Boudreau (1997). Equations A.3 and A.4 have been used for the diffusion coefficients in water D^0 of gases and ions, respectively. The mean surface water temperature during the equilibration period of the peeper T_M (Tab. A.2) was used for temperatures in Eq. A.3 and A.4.

$$D^0 = 4.72 \cdot 10^{-9} \frac{T}{\mu V_b^{0.6}} \tag{A.3}$$

where μ is the dynamic viscosity of water in units of poise, T the absolute temperature (°K) and V_b the molar volume of the solute. Values for V_b are given in Tab. A.5.

$$D^0 = (m_0 + m_1 T) \cdot 10^{-6} \tag{A.4}$$

where m_0 and m_1 are parameters listed in Tab. A.6 and T is temperature in (°C).

Table A.7 shows diffusion coefficients for the different solutes and sampling dates in water and Tab. A.8 the calculated sediment diffusion coefficients based on Eq. A.5 (Iversen & Jørgensen, 1993).

$$D_S = \frac{D^0}{1 + 3(1 - \varphi)} \tag{A.5}$$

where D_S is the diffusion coefficient in the sediment, D^0 the temperature-dependent diffusion coefficient in water and φ the porosity.

Table A.5: Parameters for the calculation of D^0 for relevant gases

Species	$\mathbf{V_b}$
O_2	27.9
CH_4	37.7

Table A.6: Parameters for the calculation of D^0 for relevant ions

Ion	$\mathbf{m_0}$	$\mathbf{m_1}$
NO_3^-	9.50	0.388
SO_4^{2-}	4.88	0.232

Table A.7: Calculated values for D^0 for mean surface water temperature during the sampling period T_M

Profile	**Sampling date**	$\mathbf{T_M}$ (°C)	$\mathbf{D^0_{CH_4}}$ $(\cdot 10^{-5} cm^2 s^{-1})$	$\mathbf{D^0_{O2}}$ $(\cdot 10^{-5} cm^2 s^{-1})$	$\mathbf{D^0_{NO3}}$ $(\cdot 10^{-5} cm^2 s^{-1})$	$\mathbf{D^0_{SO4}}$ $(\cdot 10^{-6} cm^2 s^{-1})$
A	2021-03-22	7.4	1.04	1.25	1.22	6.50
B	2021-05-26	11.3	1.20	1.44	1.39	7.50
C	2021-07-06	15.3	1.36	1.63	1.54	8.43
D	2020-08-20	16.2	1.40	1.67	1.58	8.64
E	2021-08-18	14.5	1.33	1.59	1.51	8.24

Table A.8: Calculated values for D_S for sampling days and sedimentary layers

Profile	**Sampling date**	**Sediment depth** (cm)	φ	$\mathbf{D}_{S,CH4}$ ($\cdot 10^{-6} cm^2 s^{-1}$)	$\mathbf{D}_{S,O2}$ ($\cdot 10^{-6} cm^2 s^{-1}$)	$\mathbf{D}_{S,NO3}$ ($\cdot 10^{-6} cm^2 s^{-1}$)	$\mathbf{D}_{S,SO4}$ ($\cdot 10^{-6} cm^2 s^{-1}$)
A	2021-03-22	0-21	0.56	4.50	5.39	5.27	2.80
		21-40	0.57	4.56	5.46	5.33	2.84
B	2021-05-26	0-11	0.32	3.99	4.75	4.57	2.47
		11-22	0.54	5.09	6.06	5.83	3.15
C	2021-07-06	0-26	0.51	5.53	6.62	6.25	3.41
D	2020-08-20	0-16	0.42	5.10	6.12	5.76	3.15
		16-23	0.38	4.89	5.86	5.52	3.02
E	2021-08-18	0-7	0.46	5.08	6.09	5.77	3.15
		7-26	0.57	5.81	6.97	6.61	3.60

A.4 Correlation between CH_4 and NH_4^+ data

Figure A.4 shows the correlation between CH_4 and NH_4^+ concentrations. In profile A, no NH_4^+ could be detected, therefore only data for profiles B-E is displayed. A clear positive linear correlation can be observed for profiles C and D. In profile B, NH_4^+ was mostly below the detection limit of 0.005 mmol L^{-1}. Higher concentrations were only found between 6-14 cm depth, above the zone where CH_4 concentrations peaked (increased CH_4 concentrations between 5-23 cm depth with a peak at 15 cm depth). A negative correlation between CH_4 and NH_4^+ concentrations appears to exist between 6-14 cm depth. In profile E, no correlation can be observed, NH_4^+ concentrations are generally very low compared to the other profiles.

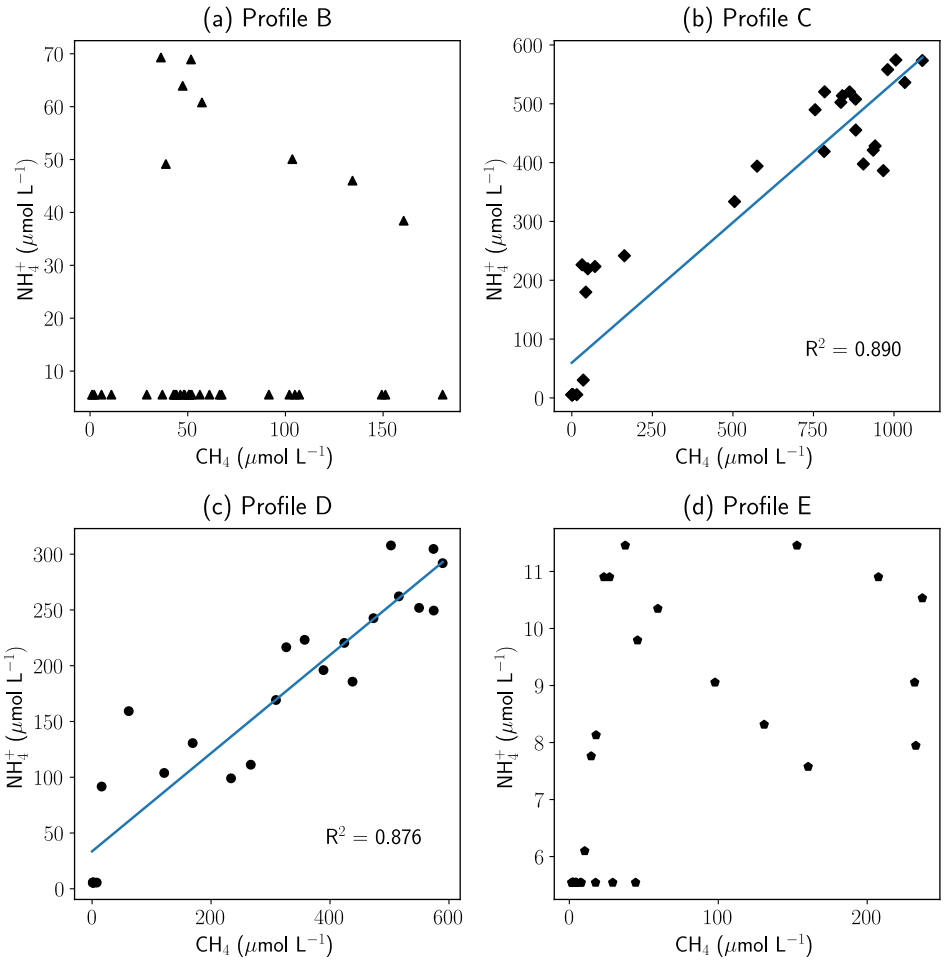

Figure A.4: **Correlation between CH_4 and NH_4^+. Each panel corresponds to one measured profile.** Axes are scaled in the range of the data. For profiles C and D, a linear regression was performed and R^2 values are given in the respective plots. Panels (a) to (d) correspond to profiles B-E, respectively.

B Supplement to "Technical note: Testing the effect of different pumping rates on pore-water sampling for ions, stable isotopes, and gas concentrations in the hyporheic zone"

B.1 Sediment properties

For sediment characterization, cores were taken by manually pushing a liner with 6 cm inner diameter into the sediment. In September 2021 and August 2022 sieve–slurry analyses were performed, each time for two homogeneous layers, according to the German norm DIN 17892-4. Resulting grain-size distribution curves are displayed in Fig. B.1. Porosity was measured from two separate liners by weighting a known volume of sediment before and after drying at 105 °C. The same samples were later used for the determination of organic carbon content as Loss On Ignition (LOI) according to the German DIN 18128. After grinding and weighting, samples were annealed in a furnace at 550 °C to constant mass, cooled to room temperature in a desiccator, and weighted again. Results showed that the sediment at the sampling site consisted of 3 % gravel, 27 % sand and 70 % silt with a porosity of 81.5 % and an LOI of 21 %.

Three additional cores were used for measurements of thermal conductivity with the TCi-3-A Thermal Conductivity Analyzer and a Transient Line Source (TLS) (C-Therm, Fredericton, Canada). The sediment cores were taken in liners with 42 cm diameter and sample heights between 25 and 30 cm. Measurements were conducted at a constant temperature of 8 ± 1 °C, close to true sediment temperatures, in a cooling room, and samples were pre-tempered for > 12 hours. The line source with a sensor length of 15 cm was inserted vertically in the center of the sediment core and heated with 0.1 W. In most measurements, small deviations from the expected linear relation between the logarithm of time and the change in measured temperature were observed. Linear regression reached R^2 = 0.972 to 0.984. Most likely, this was caused by inhomogeneities in the sample or small rates of water drainage and consolidation during the measurement. Values for thermal conductivity λ between 0.56 and 0.64 $W\,m^{-1}\,K^{-1}$ were found. In this study, we used the median λ = 0.60 $W\,m^{-1}\,K^{-1}$. This value lies well in the range of 0.20 to 0.70 $W\,m^{-1}\,K^{-1}$ (mean: 0.51 $W\,m^{-1}\,K^{-1}$) found by Dalla Santa et al. (2020) for unconsolidated material with an organic matter content of > 5%.

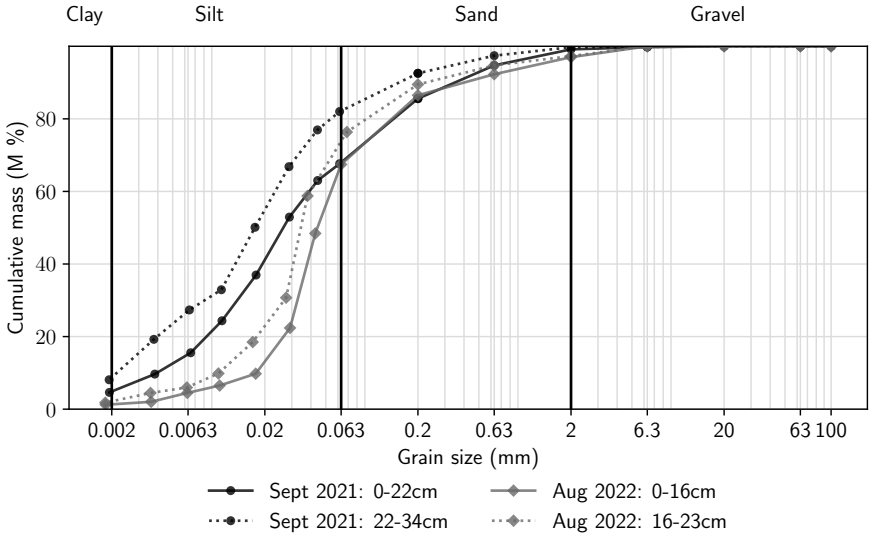

Figure B.1: **Grain-size distribution curves from sediment cores taken in September 2021 and August 2022.**

B.2 Geochemistry of the sampling site

Dates, sampling method, and pumping rate for all sampling campaigns are summarized in Tab. B.1. During 11 sampling campaigns between April and September 2021, samples were withdrawn with two LA-110 High Pressure syringe pumps (HLL Landgraf Laborsysteme, Langenhausen, Deutschland) at a pumping rate of 0.15 mL min^{-1}. The syringe pumps were equipped with 3D printed racks to hold 5 syringes each. Thus, up to 10 samples could be withdrawn simultaneously. Samples were collected in the syringes and then transferred to the respective vials for gas, sulfide, anion, or cation analyses. However, several disadvantages became obvious during sampling: not all 15 Rhizon samplers could be sampled simultaneously, thus making cross-contamination of samples from different depths more likely; syringes filled at different speeds, potentially due to sediment heterogeneities and gas intrusions; long stay of the sample in the syringes during collection made gas losses more likely. Therefore, the sampling technique was improved in 2022 as described in the main text.

Sample collection was carried out as described in Sec. 6.2.1. For gas sampling with syringe pumps, two needles were pierced through the rubber stoppers for sample injection, one connected to the syringe and one for pressure exchange. Samples were injected slowly along the side of the vial to prohibit degassing. Both needles were removed directly after sampling.

Table B.1: Summary of sampling dates, measurement technique, and pumping rate.

Date	Sampling technique	Pumping rate
2021-04-19	Rhizon samplers + syringe pumps with space for max. 10 plastic syringes	0.15 mL min^{-1}
2021-05-10		
2021-05-26		
2021-06-09		
2021-06-23		
2021-07-06		
2021-07-20		
2021-08-03		
2021-08-17		
2021-09-01		
2021-09-23		
2021-09-23	Peeper	-
2022-05-03		
2022-05-03	Rhizon samplers + peristaltic pumps (15 ports) and gastight tubing	0.19 mL min^{-1}
2022-05-30		0.09 mL min^{-1}
2022-05-31		0.38 mL min^{-1}

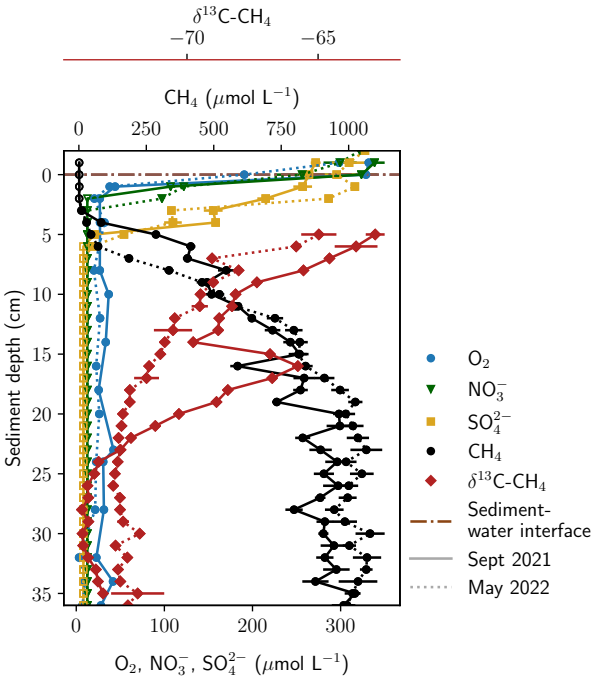

Figure B.2: **Comparison of two depth-profiles measured with pore-water dialysis samplers (peepers) in September 2021 and May 2022.**

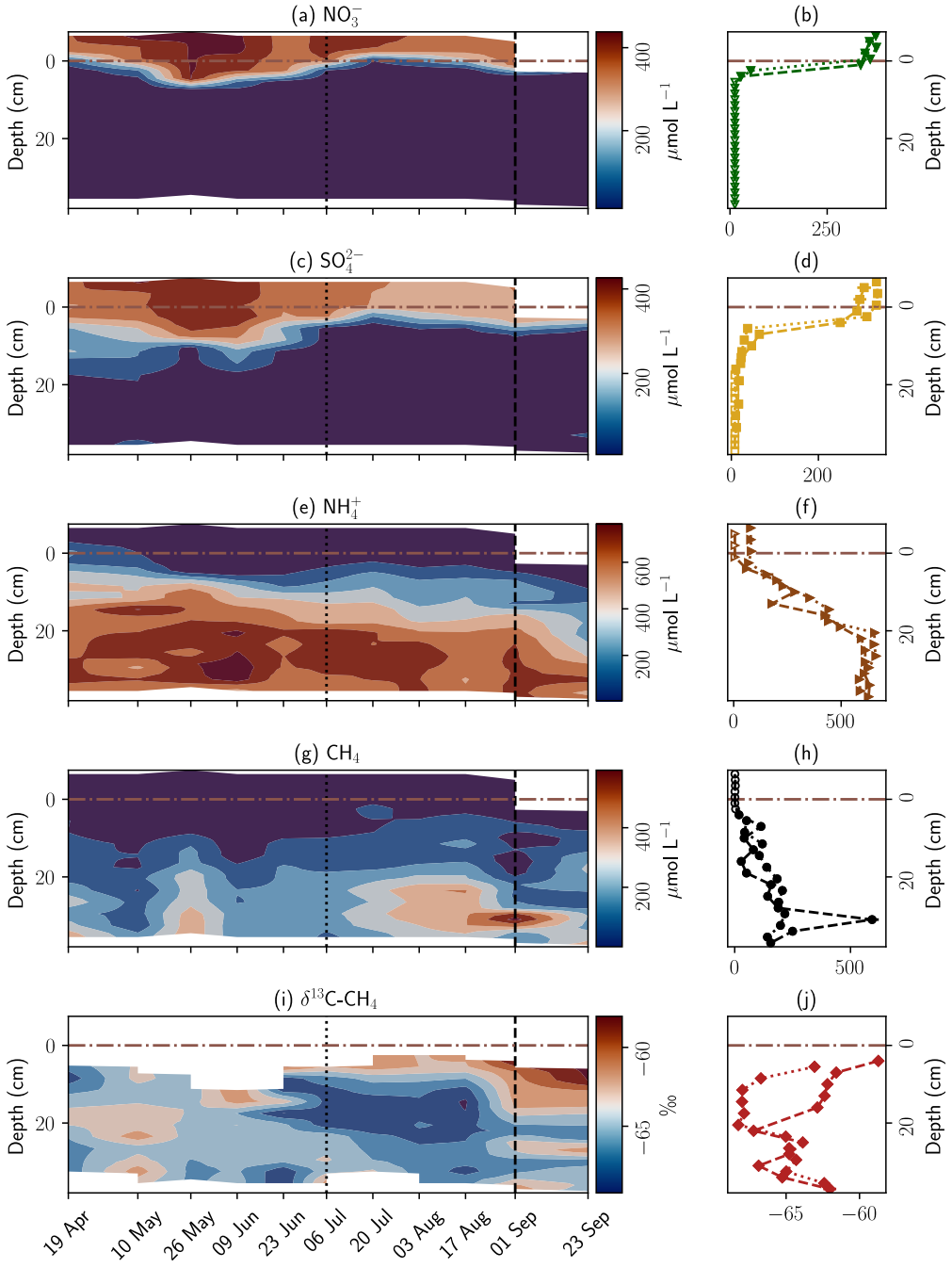

Figure B.3: **Concentration- and stable isotope measurements conducted at the monitoring station during spring and summer 2021.** Panels on the left show concentrations over time as contour plots. Panels on the right show two selected depth-profiles.

B.3 Oxygen sensor calibration

Calculation of dissolved O_2 concentrations from measured phase angles was based on the two-site quenching model of the Stern-Volmer equation (Eq. B.1) (Carraway et al., 1991; Vieweg et al., 2013).

$$\frac{\tan(\phi)}{\tan(\phi_0)} = \frac{\mathrm{f}}{1+\mathrm{K_{SV}}[\mathrm{O_2}]} + \frac{1-\mathrm{f}}{1+\mathrm{mK_{SV}}[\mathrm{O_2}]} \tag{B.1}$$

with ϕ being the measured phase angle, ϕ_0 the phase angle at 0% a.s., K_{SV} the quenching constant as a function of saturation O_2 concentration, and f and m fit paramters. The parameters f, m, and K_{SV} (20 °C, lab air pressure) were estimated as best fit for calibration measurements conducted at 7 different dissolved O_2 concentrations at 20 °C (Fig. B.4a).

Measured phase angles are temperature-dependent, thus compensation for field temperatures was necessary (Vieweg et al., 2013). For this, measurements were conducted at 0 % a.s. and 100 % a.s. at five and four environmentally relevant temperatures between 5 and 25 °C. The change of measured phase angle per Kelvin $\Delta\phi \mathrm{K}_{\phi_0}^{-1}$ and $\Delta\phi \mathrm{K}_{\phi_{100}}^{-1}$ at 0 % a.s. and 100 % a.s., respectively, was estimated with linear regression (Eq. B.2, B.3 and Fig. B.4b).

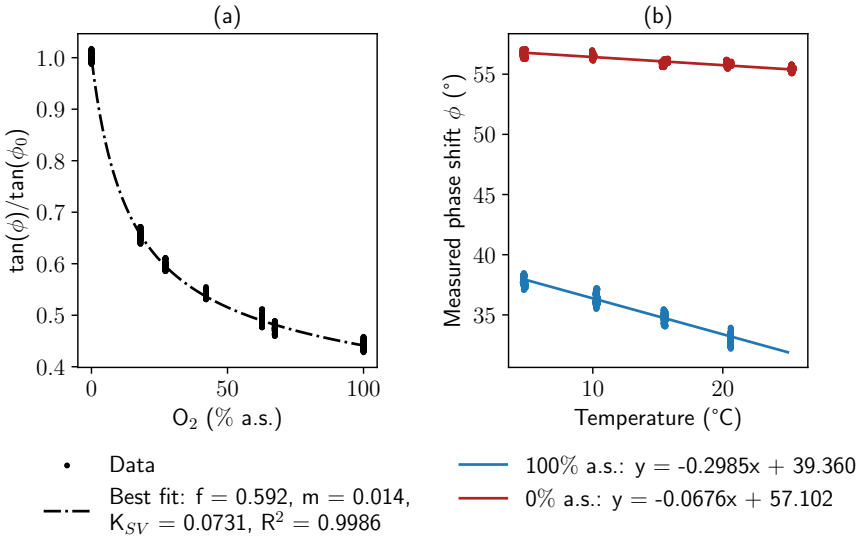

Figure B.4: **Calibration of the custom-made fiber-optic oxygen sensor.** Panel (a) shows the Stern-Volmer Plot with best-fit parameters for the model and panel (b) the temperature dependence at 0 % and 100 % a.s.

$$\tan(\phi_0)[\mathrm{T_m}] = \tan(\phi_0 + \Delta\phi \mathrm{K}_{\phi_0}^{-1}(\mathrm{T_m} - \mathrm{T_0})) \tag{B.2}$$

$$\tan(\phi_{100})[\mathrm{T_m}] = \tan(\phi_{100} + \Delta\phi \mathrm{K}_{\phi_{100}}^{-1}(\mathrm{T_m} - \mathrm{T_{100}})) \tag{B.3}$$

For the calculation of O_2 concentrations from phase angles measured in the field, first a fourth order polynomial was fit to temperature data recorded at the time of measurement to gain a continuous temperature depth-distribution (Fig. 6.4b). Above the sediment–water interface,

average temperature of all sensors was assumed to be constant. For each depth, K_{SV} was re-calculated based on O_2 saturation concentration, a function of water temperature and pressure at the specific depth. Then, O_2 concentrations were calculated with the Stern-Volmer equation (Eq. B.1) in % a.s. and converted to µmol L^{-1} based on depth-dependent saturation concentrations.

Due to the flat shape of the calibration model in saturated and near-saturated conditions (Fig. B.4a), small errors in measured phase angles partly led to extremely high concentrations. To avoid these unrealistic values, all concentrations of >100 % a.s. were normalized such that the maximal concentration was 120 % a.s. (Eq. B.4).

$$O_{2,\mathrm{nomalized}} = \frac{20}{(O_{2,\mathrm{max}} - 100)} \cdot (O_{2,\mathrm{original}} - 100) + 100 \tag{B.4}$$

where $O_{2,\mathrm{nomalized}}$ is the normalized concentration value between 100 % and 120 % a.s., $O_{2,\mathrm{max}}$ the maximally measured concentration considering all values of a profile, and $O_{2,\mathrm{original}}$ the originally calculated concentration with an original value of $>$100 % a.s.

B.4 Additional pore-water analyses

This section includes additional information on pore-water sampling and analyses. The equilibration period of the peeper was between April 6$^{\mathrm{th}}$ 2022 and May 3$^{\mathrm{rd}}$ 2022. Rhizon sampling at 0.19 ml min^{-1} was conducted on May 3$^{\mathrm{rd}}$ right before sampling of the peeper. Pumping rates of 0.09 ml min^{-1} and 0.38 ml min^{-1} were tested on May 30$^{\mathrm{th}}$ and 31$^{\mathrm{st}}$, respectively.

Box plots in Fig. B.6 show that differences in Ca^{2+}, Mg^{2+}, and Cl^{-} concentrations were significant between samples withdrawn with the peeper and Rhizons. This difference may have been caused directly by the sampling technique or by small-scale chemical heterogeneities, because the peeper was placed approx. 15 cm away from the monitoring station to avoid mutual disturbances. Box plots are also provided for CH_4 concentrations and δ^{13}C–CH_4 in Fig. B.5, as well as δ^{18}O and δ^{2}H in Fig. B.7. Data sets of δ^{18}O and δ^{2}H were not significantly different for high and low pumping rates.

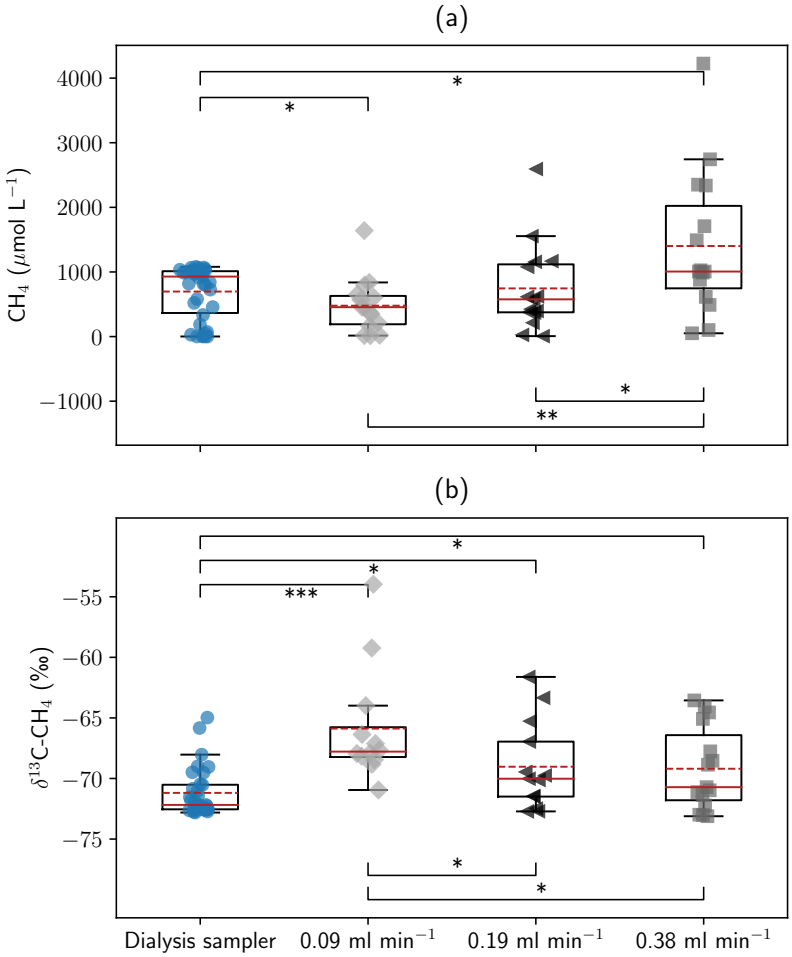

Figure B.5: **Box plots of (a) CH_4 concentration and (b) stable isotope measurements.** The box indicates the inter-quartile range (IQR) between first and third quartile. Whiskers show 1.5 times the IQR. Median is displayed as solid, mean as dashed line. Where pairwise comparisons (Mann Whitney U test) showed significant differences, this is marked as follows: *($0.05 > p > 0.01$), **($0.01 > p > 0.001$), ***($p < 0.001$).

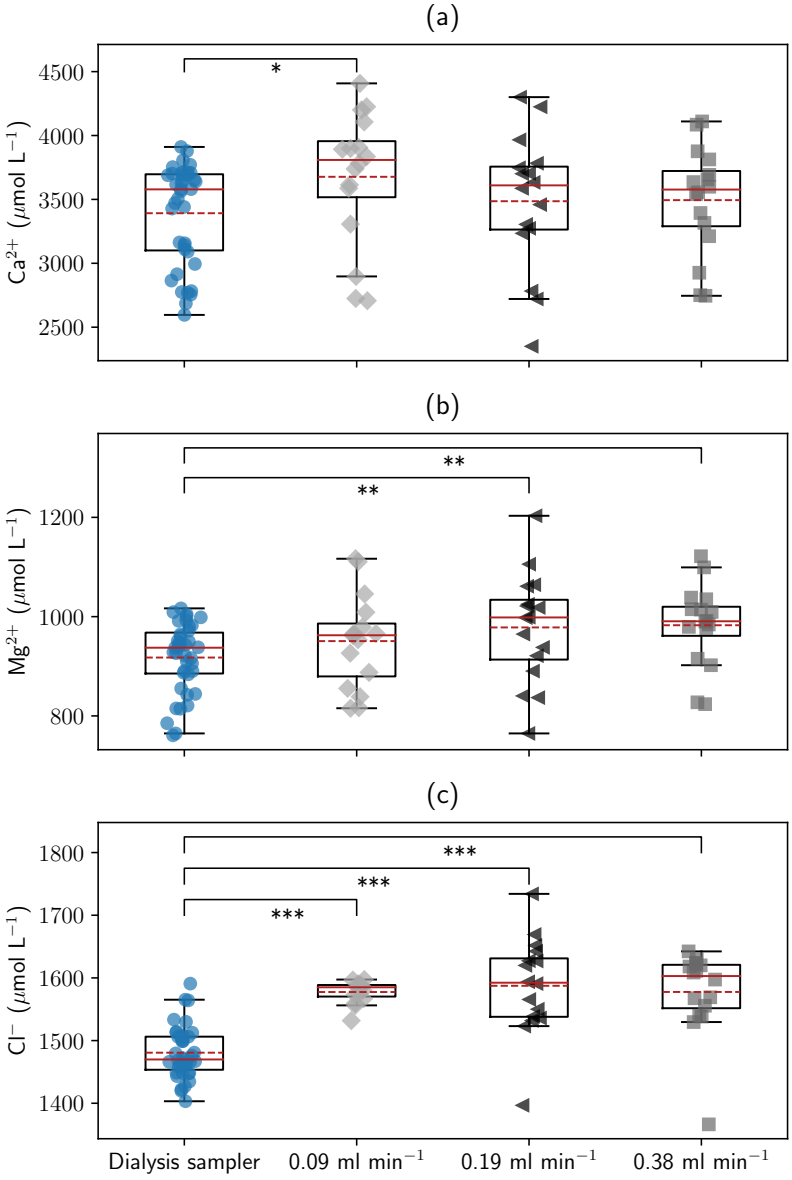

Figure B.6: **Box plots of (a) Ca^{2+}, (b) Mg^{2+}, and (c) Cl^{-} concentration data.** The box indicates the IQR between first and third quartile. Whiskers show 1.5 times the IQR. Median is displayed as solid, mean as dashed line. Where pairwise comparisons (Mann Whitney U test) showed significant differences, this is marked as follows: *($0.05 > p > 0.01$), **($0.01 > p > 0.001$), ***($p < 0.001$).

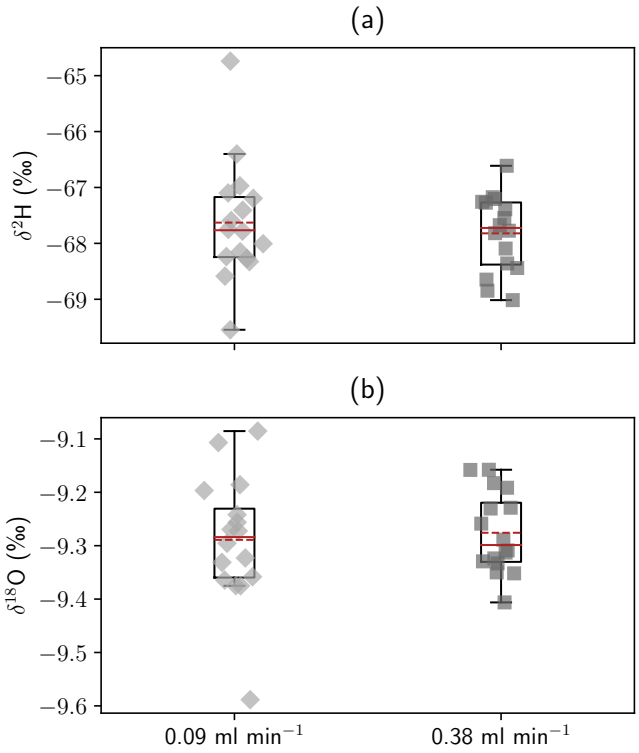

Figure B.7: **Box plots of (a) δ^2H, and (b) δ^{18}O data.** The box indicates the IQR between first and third quartile. Whiskers show 1.5 times the IQR. Median is displayed as solid, mean as dashed line. Differences between the data sets were not significant.

B.5 Detailed temperature modeling results

Flux rates calculated with both amplitude and phase methods by Hatch et al. (2006) and Keery et al. (2007) from the deepest 6 sensors in 6 cm, 8 cm, 10 cm, 12 cm, 14 cm, and 24 cm depth are given in Fig. B.8. Fluxes were calculated between overlapping sensor pairs. For example, the flux calculated for 8 cm depth was calculated from the sensors in 6 cm and 10 cm depth. Mean, mean of absolute values, range, and the percentage of negative values for each simulated time series are summarized in Tab. B.2. Based on the amplitude method, the majority of values was negative when considering sensors at 8 cm depth and deeper, indicating upwards directed flow. Values calculated for shallower depths were mainly positive, showing large peaks when considering sensors placed in less than 6 cm depth. These peaks are assumed to be caused by sediment dynamics like sedimentation and erosion (see main paper). With the phase method, only absolute flux rates could be calculated.

Fluxes calculated based on phase change were 4-18 times larger than fluxes based on amplitude dampening. Amplitude dampening was pronounced in the data while phase differences between the sensor pairs were only very small. In fact, it was not possible to get flux estimates from neighboring sensors with the phase method due to the minimal time lag which was smaller than the temporal resolution of the time series. Therefore, we hypothesize that for our data set estimates based on the amplitude method are much more reliable and have chosen not to display results based on the phase method in the main paper. The data is still displayed here to allow a comparison and for transparency by showing all results.

Table B.2: Summary of results from VFLUX modeling from sensors in 6 cm, 8 cm, 10 cm, 12 cm, 14 cm, and 24 cm depths. Fluxes were calculated between each other sensor. For example, the flux calculated for 8 cm depth was calculated from the sensors in 6 cm and 10 cm depth. Lower sensors were not included due a strong influence of sedimentation and erosion events. All values are given in m s^{-1}.

Depth		Hatch amplitude	Keery amplitude	Hatch phase	Keery phase
8 cm	mean	$6.3 \cdot 10^{-8}$	$6.3 \cdot 10^{-8}$		
	mean (abs)	$1.7 \cdot 10^{-7}$	$1.7 \cdot 10^{-7}$	$3.0 \cdot 10^{-6}$	$3.1 \cdot 10^{-6}$
	range	-5.6 to $6.0 \cdot 10^{-7}$	-5.7 to $6.0 \cdot 10^{-7}$	1.2 to $5.7 \cdot 10^{-6}$	1.3 to $5.7 \cdot 10^{-6}$
	$\% < 0$	34%	34%	-	-
10 cm	mean	$-1.6 \cdot 10^{-7}$	$-1.6 \cdot 10^{-7}$		
	mean (abs)	$2.1 \cdot 10^{-7}$	$2.1 \cdot 10^{-7}$	$2.4 \cdot 10^{-6}$	$2.5 \cdot 10^{-6}$
	range	-7.2 to $4.5 \cdot 10^{-7}$	-7.3 to $4.6 \cdot 10^{-7}$	0.44 to $5.8 \cdot 10^{-6}$	0.15 to $5.9 \cdot 10^{-6}$
	$\% < 0$	85%	85%	-	-
12 cm	mean	$-2.6 \cdot 10^{-7}$	$-2.6 \cdot 10^{-7}$		
	mean (abs)	$2.8 \cdot 10^{-7}$	$2.8 \cdot 10^{-7}$	$1.8 \cdot 10^{-6}$	$1.9 \cdot 10^{-6}$
	range	-7.9 to $3.4 \cdot 10^{-7}$	-8.1 to $3.5 \cdot 10^{-7}$	0.43 to $4.4 \cdot 10^{-6}$	0.17 to $4.4 \cdot 10^{-6}$
	$\% < 0$	90%	90%	-	-
18 cm	mean	$-4.9 \cdot 10^{-7}$	$-5.0 \cdot 10^{-7}$		
	mean (abs)	$4.9 \cdot 10^{-7}$	$5.0 \cdot 10^{-7}$	$2.1 \cdot 10^{-6}$	$2.1 \cdot 10^{-6}$
	range	-1.2 to $-0.035 \cdot 10^{-6}$	-1.2 to $-0.035 \cdot 10^{-6}$	0.43 to $5.0 \cdot 10^{-6}$	0.024 to $5.1 \cdot 10^{-6}$
	$\% < 0$	100%	100%	-	-

The influence of the thermal dispersivity parameter β was tested with a Monte Carlo analysis on a reduced data set, including data from April and May 2022 and the sensor pair in 8 cm

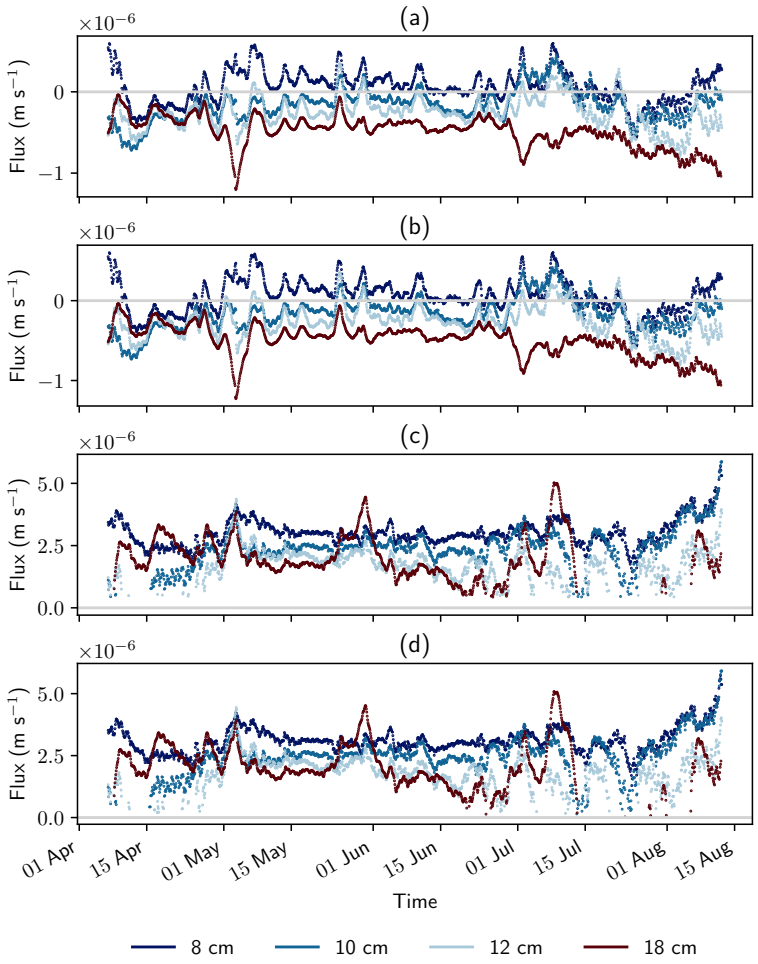

Figure B.8: **Detailed results of VFLUX modeling.** Calculated fluxes are based on (a) amplitude method by Hatch et al. (2006), (b) amplitude method by Keery et al. (2007), (c) phase method by Hatch et al. (2006), and (d) phase method by Keery et al. (2007). Positive flow in (a) and (b) is downwards directed. The phase method in (c) and (d) only gives absolute values and no direction of flow.

and 12 cm depth. A normal distribution was assumed for the parameter β, with different means and standard deviations. For each scenario, 100 runs of VFLUX were performed with the random variations of β according to the respective distribution. The results show that higher thermal dispersion would lead to lower absolute flux values and less intense fluctuations (Fig. B.9). Considering that β was changed by two orders of magnitude, the sensitivity of the model to changes in dispersivity appear to be limited. Nevertheless, further investigations on thermal dispersivity could help to improve the use of temperature measurements for hyporheic exchange flux modeling.

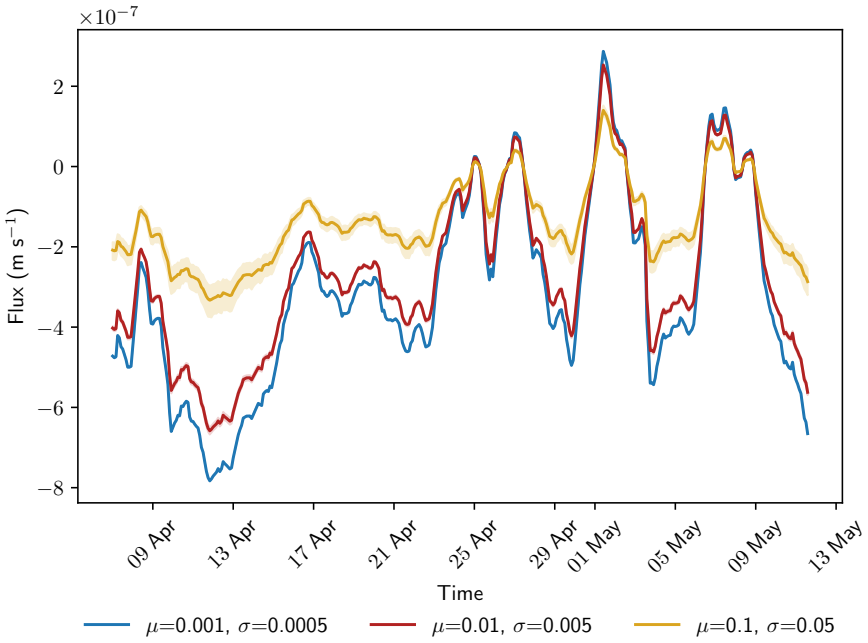

Figure B.9: **Monte Carlo analysis for thermal dispersivity.** Three scenarios were tested for mean μ and standard deviation σ of the thermal dispersivity parameter β in m. Results were generated with n=100 runs for each scenario. Shading indicates 95 % confidence intervals for each scenario. The results were calculated with the software package VFLUX and the Hatch amplitude method.

C Supplement to ”High methane ebullition throughout one year in a regulated central European stream”

C.1 Photographs of the gas traps and sampling procedure

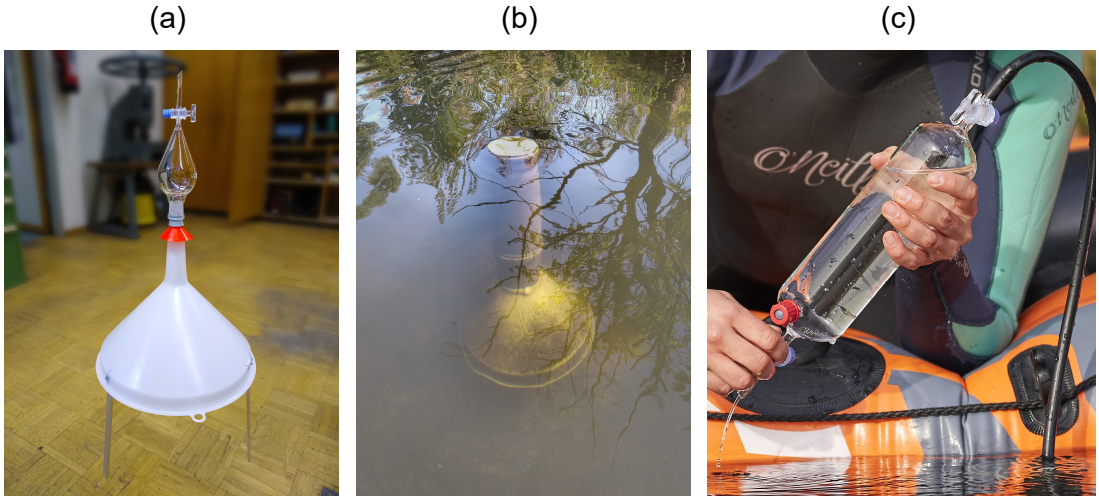

Figure C.1: **Photographs of the gas traps and sampling procedure.** Panel (a) displays a gas trap in the workshop. Legs were later extended to at least 60 cm. Panel (b) shows a sampler after installation in river Moosach. The distance between the bottom of the gas trap and the streambed was at least 10 cm at the day of installation. The sampling procedure is illutrated in panel (c). Pictures were taken by Felicitas Kaplar and Julia Bergmeister.

C.2 Additional values and descriptive statistics

Quantitative information on the sediment characteristics is given in Tab. C.1. Descriptive statistics of ebullition data for each season are summarized in Tab. C.2.

Table C.1: Sediment characteristics at the four sampling sites. Grain size distribution is given in percent gravel, sand, and silt/clay fractions. Porosity n and loss on ignition (LOI) are also given in percent.

Site	**Depth** (cm)	**Gravel** (%)	**Sand** (%)	**Silt & Clay** (%)	**n** (%)	**LOI** (%)
A	0-30	0.4	61.3	38.3	78.0	14.6
B	0-10	1.7	86.6	11.7	76.5	6.0
	10-23	1.5	53.1	45.4		13.3
C	0-11	14.1	63.5	22.4	81.0	26.6
	11-20	0.8	65.3	33.9		
D	0-9	40.6	32.8	26.6	59.9	5.0
	9-30	0.2	54.2	45.6		9.9

Table C.2: Summary of ebullition data grouped by season.

Parameter	Site	Summer					Autumn					Winter					Spring				
		n	min	max	mean	SD	n	min	max	mean	SD	n	min	max	mean	SD	n	min	max	mean	SD
Volume flux ($mL\,m^{-2}\,d^{-1}$)	A	20	66.8	319.4	187.1	63.9	8	10.9	367.4	150.9	110.7	5	5.9	34.0	22.8	11.2	9	3.8	158.6	72.6	54.8
	B	22	116.2	591.9	378.4	120.5	8	235.9	1004.7	650.7	269.1	8	2.8	284.6	93.5	101.9	14	28.9	1068.4	470.2	386.1
	C	12	420.3	994.4	801.7	164.5	7	181.4	496.7	374.1	111.7	13	223.7	790.8	464.4	185.9	18	403.8	996.0	608.1	167.1
	D	2	0.4	4.1	2.3	2.7	2	1.0	1.3	1.1	0.2	3	0.0	7.6	4.2	3.9	1	-	-	2.7	-
CH_4 content (%)	A	20	3.1	40.0	23.0	12.4	8	15.3	41.3	32.7	10.2	5	0.4	28.5	14.4	12.4	9	8.0	29.8	20.1	6.8
	B	22	25.4	58.5	43.9	7.8	8	49.5	72.7	63.1	8.2	8	10.0	70.3	38.2	21.8	14	7.7	63.5	38.3	19.2
	C	12	67.1	78.7	73.2	3.7	7	50.6	78.9	65.5	10.3	13	54.1	76.4	67.7	7.3	18	41.4	80.9	61.6	11.4
	D	1	-	-	0.02	-	0	-	-	-	-	1	-	-	0.02	-	1	-	-	0.01	-
CH_4 flux ($mmol\,m^{-2}\,d^{-1}$)	A	20	0.2	5.3	1.9	1.4	8	0.07	3.5	2.2	1.3	5	0.004	0.4	0.2	0.2	9	0.03	1.7	0.7	0.6
	B	22	1.9	12.7	7.1	2.9	8	5.7	31.2	17.9	8.2	8	0.03	8.7	2.1	2.9	14	0.1	28.5	10.4	10.4
	C	12	14.1	29.4	24.6	4.3	7	4.4	14.3	10.7	3.9	13	6.4	27.7	13.8	6.0	18	8.1	26.5	16.3	6.1
	D	1	-	-	$3 \cdot 10^{-5}$	-	0	-	-	-	-	1	-	-	$5 \cdot 10^{-5}$	-	1	-	-	$1 \cdot 10^{-5}$	-
$\delta^{13}C$–CH_4 (‰)	A	15	-70.6	-47.9	-64.1	6.4	7	-72.0	-68.0	-70.2	1.3	4	-73.4	-66.8	-69.7	2.8	8	-73.9	-69.0	-72.2	1.4
	B	17	-70.9	-66.4	-68.6	1.2	6	-70.1	-67.2	-68.5	0.9	7	-72.8	-68.8	-70.9	1.4	14	-72.2	-70.4	-71.1	0.6
	C	10	-66.5	-63.7	-64.6	0.8	6	-68.4	-63.3	-66.6	1.7	11	-67.7	-65.0	-66.8	0.7	18	-67.8	-66.5	-67.4	0.4
	D	0	-	-	-	-	0	-	-	-	-	1	-	-	-52.5	-	0	-	-	-	-

C.3 Complete geochemical profiles

In addition to CH_4 concentrations and $\delta^{13}C$–CH_4, dissolved O_2, anion, and cation concentrations were measured in pore-water samples (Fig. C.2). Dissolved O_2 concentrations were measured with a Clark-type microsensor (Unisense, Aarhus, Denmark) by piercing the membrane of the peeper chambers immediately upon retrieval from the streambed and cleaning with deionized water. Samples for anion and cation concentration measurements were taken in 1.5 ml glass vials and analyzed with a system of two ICS-1100 ion chromatographs (Thermo Fisher Scientific) with Dionex IonPac^{TM} columns AS9-HC for anions and CS12A for cations.

C.4 Cross correlations between variables

The relation between CH_4 content and volume flux, CH_4 content and $\delta^{13}C$–CH_4, and CH_4 and CO_2 contents were tested by calculating the Pearson correlation coefficient. A statistically significant correlation was detected between CH_4 content and volume flux, whereas neither CH_4 content and $\delta^{13}C$–CH_4 nor CH_4 and CO_2 contents were linearly correlated. Figure C.3 displays both scatter plots twice, once highlighting the site and once the season.

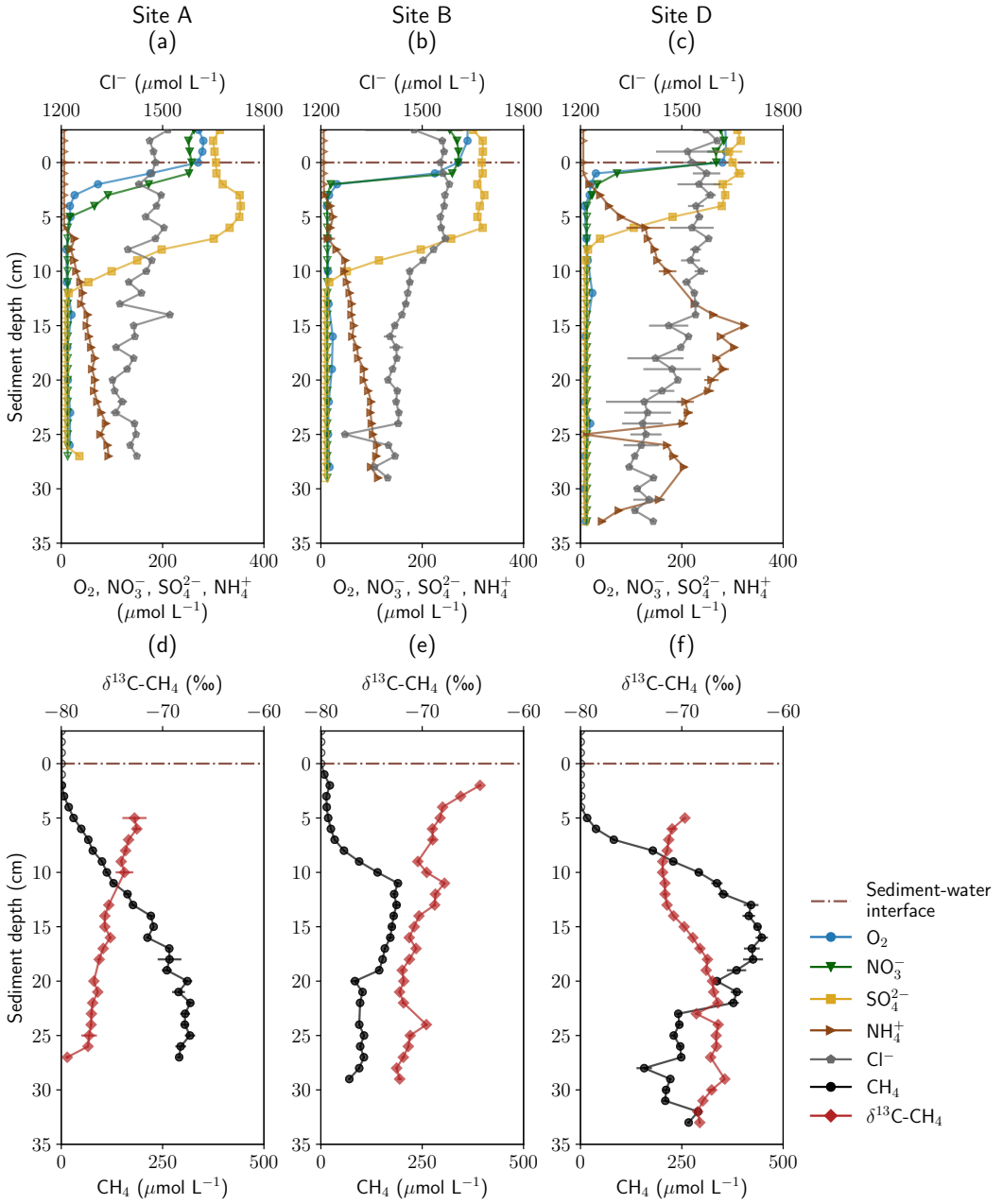

Figure C.2: **Additional data on geochemical profiles.** Error bars indicate standard deviations of triplicate measurements. Markers of measurements below the limit of detection are not filled.

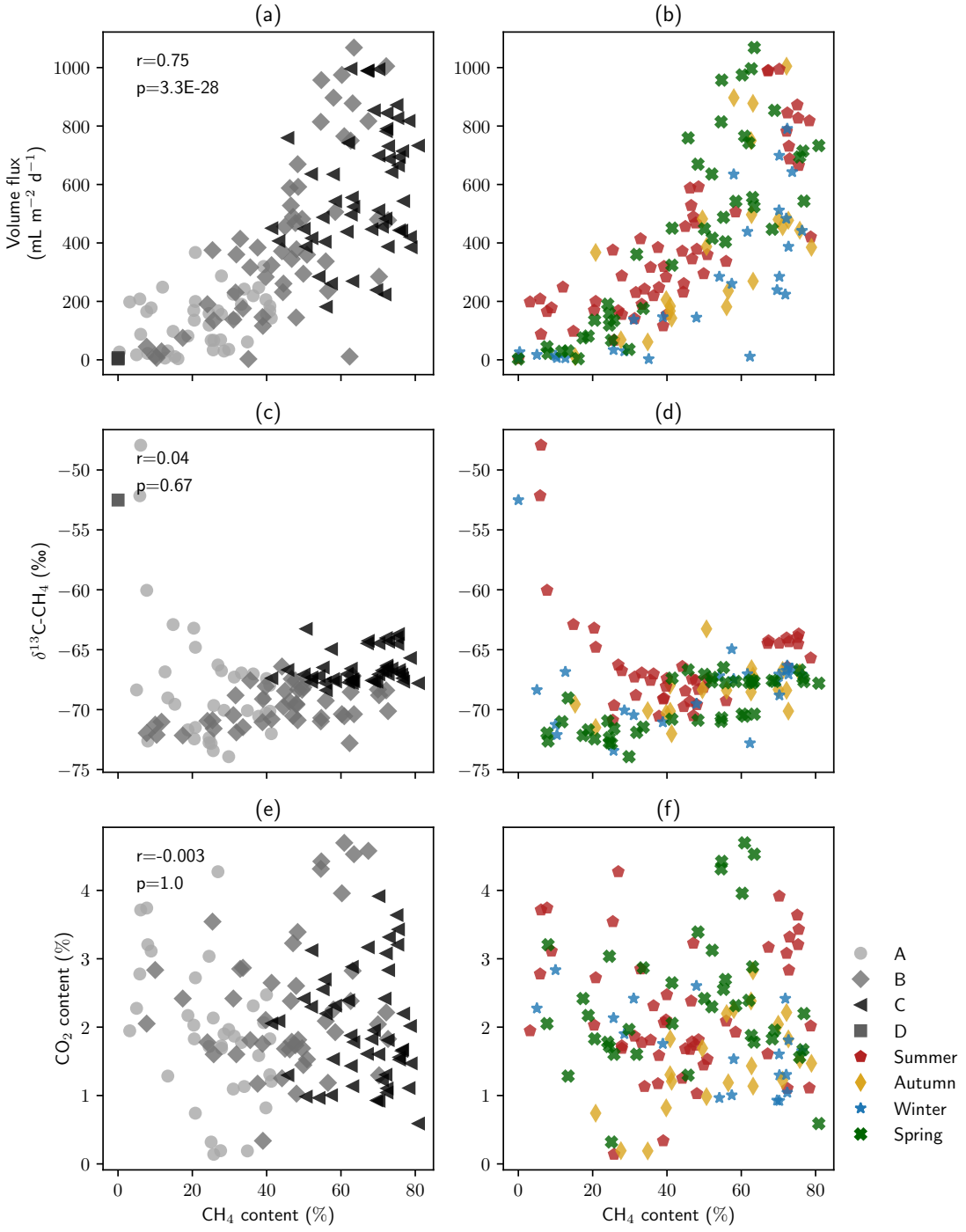

Figure C.3: **Cross correlations between measurements.** Panels (a), (c), and (e) are colored by site, panels (b), (d), and (f) by season. Panels (a) and (b) display CH_4 content and volume flux, panels (c) and (d) CH_4 content and $\delta^{13}C$–CH_4, and panels (e) and (f) CH_4 and CO_2 contents. Pearson correlation coefficients and p-values are shown for all data. A statistically significant correlation ($p < 0.05$) was found for CH_4 content and volume flux.